

**Initial Fouling Rate and Delay Time Studies of Aqueous Calcium Sulphate  
Scaling under Sensible Heating Conditions**

by

Feridoun Fahiminia

B. Sc., Tehran University, Iran, 1990

M. Sc., Tehran University, Iran, 1993

A DISSERTATION SUBMITTED IN PARTIAL FULFILLMENT OF  
THE REQUIREMENT FOR THE DEGREE OF  
DOCTOR OF PHILOSOPHY

in

THE FACULTY OF GRADUATE STUDIES  
CHEMICAL AND BIOLOGICAL ENGINEERING

THE UNIVERSITY OF BRITISH COLUMBIA

March 2007

© Feridoun Fahiminia, 2007

**Abstract**

Calcium sulphate scaling can give rise to operating problems and additional costs in industrial systems and desalination units. In order to control scale formation it is desirable to understand the mechanisms of its inception and growth. The present study focuses on understanding how process variables such as fluid velocity and temperature affect the initial fouling rate and delay time. For initial fouling rate, previous studies of calcium sulphate scaling have demonstrated conflicting behaviour with respect to fluid velocity: some investigations report an increase, others a decrease, and still others no change of initial fouling rate with increasing fluid velocity. For the delay time, most researchers have focused on bulk precipitation rather than on wall surface crystallization. For wall surface crystallization, no values have been reported for calcium sulphate delay time activation energies.

In this work a theoretical model for initial crystallization fouling rate in turbulent flow, where attachment is treated as a physico-chemical rate process in series with mass transfer (Epstein, 1994), was examined. According to the model, mass transfer is directly proportional to the friction velocity, and attachment is inversely proportional to the square of this velocity. Therefore, at a given wall temperature, it follows that if the initial fouling rate is mass transfer controlled (low fluid velocity), the deposition flux increases as the fluid velocity increases. If, however, the initial fouling rate is attachment controlled (high fluid velocity), the deposition flux will decrease as the fluid velocity increases. Therefore as the fluid velocity is lowered the initial fouling rate goes through a maximum at a given wall temperature. In addition, this maximum initial fouling rate can be expected to increase and move towards higher critical velocities as the wall temperature increases.

Fouling experiments were performed in a Tube Fouling Unit (TFU) (Wilson and Watkinson, 1996; Rose et al., 2000) using aqueous calcium sulphate solutions as recirculating

fluid. To meet the required operating conditions, some modifications were made on the TFU. Mainly two different sets of experiments were performed, one using a concentration of 3400 ppm of calcium sulphate in solution, and the other in which a range of concentrations from 3100 to 3600 ppm was covered. The first set of experiments was performed over film Reynolds numbers of 2100 – 36000, clean inside wall temperatures of 66 - 87°C and bulk temperatures of 50°C, to observe the effect of velocity on both initial fouling rate and delay time. In the second set, performed to extract crystal surface energies, the Reynolds number and bulk temperature were kept constant at 20000 and 50°C, respectively. Also, some extra experiments were performed to investigate deposit removal occurrence and the filter pore size effect on the fouling behaviour. All the experiments were performed in a 9.02 mm i.d. electrically heated, stainless steel tube.

The main features of the model were qualitatively demonstrated with calcium sulphate solutions, i.e. a maximum in experimental initial fouling rate at a given wall temperature over a range of fluid velocities, and an increase in the maximum rate and in the corresponding critical velocity as the wall temperature was increased.

Calcium sulphate scaling results showed that as the velocity increased from 0.1 to 1.6 m/s, the fouling activation energy,  $\Delta E_f$ , increased from 66 to 620 kJ/mol. This observation was consistent with the model, but the maximum fouling activation energy was significantly larger than the kinetic activation energy,  $\Delta E$ , reported by other investigators. Modeling results showed an optimal solution, with an average absolute percent deviation in initial fouling rates of 67.4 % from the fit of the model.  $\Delta E$  was evaluated as 262.5 kJ/mol. To reduce the deviations between the model predictions and experimental results, the model was refined by nominally taking the number of nucleation sites into account. This was done by inserting a simple function of wall

temperature in the surface integration term. The results of the refined model indicated a substantial reduction in the average absolute percent deviation.

From classical nucleation theory and delay time measurements the effective surface energy values were determined as 7.5 to 9.9 mJ/m<sup>2</sup> over a range of wall temperatures from 73 to 82°C. These values are close to the values of 7.9 and 14.6 mJ/m<sup>2</sup> that have been reported by Linnikov (1999) for surface nucleation on a metal surface and by Hasson et al. (2003) on a polymeric membrane surface under laminar flow conditions, respectively.

Also, from delay time measurements it was possible to use Branch's (1991) approach, applied by him to black liquor fouling, for generating delay time activation energies. Calcium sulphate delay time activation energies for wall surface crystallization were determined for the first time over a range of fluid velocities. It was shown that as the velocity increased, delay time activation energies increased and approached a value around 172 kJ/mol.

In order to separate the contribution of surface reaction (integration) from that of mass transfer, purely chemical activation energy values were generated through kinetic studies of calcium sulphate precipitation in a jacketed-glass reactor. The activation energies were determined as 210 and 254 kJ/mol for initial concentrations of 3400 and 3100 ppm, respectively. These values were smaller than the maximum fouling activation energy of 620 kJ/mol extracted from fouling experiments. This observation again suggested that the number of surface nucleation sites plays an important role in the wall surface crystallization process.

Removal effects were studied by increasing the fluid velocity while simultaneously eliminating the concentration driving force. No continuous deposit removal was detected at a velocity of 0.7 m/s. Finally, at higher wall temperatures filter pore size had no impact on the delay time and the initial fouling rate. However, at lower wall temperatures the initial fouling

rate increased with filter pore size, indicating the occurrence of bulk precipitation and particulate fouling at these temperatures.

## Table of Contents

|  |           |
|--|-----------|
| Abstract.....  | ii        |
| Table of Contents.....   | vi        |
| List of Tables.....  | x         |
| List of Figures.....   | xii       |
| Acknowledgements.....  | xvi       |
| <b>Chapter 1 Introduction.....</b>                                   | <b>1</b>  |
| 1.1 Measurement of Fouling.....                                      | 2         |
| 1.2 Fouling Classification.....                                      | 5         |
| 1.2.1 Heat exchanger fouling variables.....                          | 9         |
| <b>Chapter 2 Literature Review.....</b>                              | <b>11</b> |
| 2.1 Crystallization Fouling .....                                    | 11        |
| 2.2 Nucleation and Surface Energy.....                               | 12        |
| 2.3 Delay Time and Classical Nucleation Theory.....                  | 15        |
| 2.4 Previous Delay Time Studies.....                                 | 16        |
| 2.5 Precipitation Kinetic Models.....                                | 23        |
| 2.5.1 Calcium Sulphate Kinetic Models.....                           | 24        |
| 2.6 Crystallization Fouling Complexities and Simplifications.....    | 27        |
| 2.7 Previous Crystal Growth and Crystallization Fouling Studies..... | 31        |
| 2.8 Theoretical Fouling Model.....                                   | 51        |
| 2.8.1 Mathematical Model Development for Precipitation Fouling.....  | 51        |
| 2.9 Calcium Sulphate Solubility and Its Crystallization Forms.....   | 55        |
| 2.10 Objectives.....   | 60        |

|   |           |
|---|-----------|
| <b>Chapter 3 Experimental Materials and Methods</b> .....             | <b>62</b> |
| 3.1 Tube Fouling Unit (TFU).....                                      | 62        |
| 3.1.1 TFU Apparatus (Wilson, 1994).....                               | 62        |
| 3.1.2 Wall Temperature Measurements.....                              | 69        |
| 3.2 Modifications Made to Improve the TFU Performance.....            | 70        |
| 3.2.1 Initial TFU Operating Problems.....                             | 70        |
| 3.2.2 Filter.....   | 70        |
| 3.2.3 Concentration Equalizer.....                                    | 71        |
| 3.2.4 Cooling System Valve Modification.....                          | 73        |
| 3.2.5 New Thermocouple Holder Design.....                             | 73        |
| 3.3 Data Acquisition System.....                                      | 75        |
| 3.4 TFU Experimental Procedures.....                                  | 78        |
| 3.4.1 TFU Cleaning Procedure.....                                     | 81        |
| 3.5 Solution Preparation for TFU Experiments.....                     | 81        |
| 3.6 Jacketed Glass Reactor (JGR) Experiments.....                     | 83        |
| 3.6.1 Jacketed Glass Reactor (JGR) Constituents.....                  | 83        |
| 3.6.2 JGR Operating Procedures.....                                   | 85        |
| 3.7 Physical Properties.....  | 87        |
| 3.8 Deposit Property Estimation Procedures.....                       | 89        |
| <b>Chapter 4 Experimental Results and Discussions</b> .....           | <b>92</b> |
| 4.1 Data Processing Steps for Fouling Experiments.....                | 92        |
| 4.2 Fouling Experiments.....  | 98        |
| 4.2.1 Effect of Concentration and Wall Temperature on Delay Time..... | 99        |
| 4.2.2 Surface Energy and Delay Time Activation Energies.....          | 100       |
| 4.2.3 Effect of Velocity on the Delay Time.....                       | 103       |

|       |  |            |
|-------|--|------------|
| 4.3   | Initial Fouling Rate Analysis.....   | 103        |
| 4.3.1 | Initial Fouling Rate measurement.....  | 103        |
| 4.3.2 | Effect of Velocity on the Initial Fouling Rate.....                          | 107        |
| 4.4   | Deposit Distribution along the Test Section and its Physical Properties..... | 111        |
| 4.4.1 | Deposit Coverage Analysis.....   | 111        |
| 4.4.2 | Deposit Physical Properties.....   | 119        |
| 4.5   | Deposit Removal.....   | 133        |
| 4.6   | Filter Pore Size Effect.....   | 137        |
| 4.7   | Kinetic Studies.....   | 140        |
| 4.7.1 | A General Approach to Kinetics of Calcium Sulphate Precipitation.....        | 141        |
| 4.7.2 | A Modified Kinetic Approach.....   | 145        |
|       | <b>Chapter 5 Mathematical Modeling and Discussions.....</b>                  | <b>150</b> |
| 5.1   | Initial Fouling Rate Model.....  | 150        |
| 5.2   | Input Data.....  | 156        |
| 5.3   | Physical Properties and Temperature Effect.....                              | 156        |
| 5.4   | Model Predictions.....   | 159        |
| 5.5   | Estimation of Constants from Model Solutions.....                            | 165        |
| 5.6   | Problems Associated with Surface Crystallization Modeling.....               | 169        |
| 5.7   | Considering Nucleation Sites in a Crude Model.....                           | 170        |
|       | <b>Chapter 6 Summary.....</b>  | <b>175</b> |
|       | <b>Chapter 7 Conclusions.....</b>  | <b>181</b> |
|       | <b>Chapter 8 Recommendations for Future Studies.....</b>                     | <b>183</b> |
|       | <b>Nomenclature.....</b>   | <b>185</b> |
|       | <b>References.....</b>   | <b>193</b> |
|       | <b>Appendix 1 Calibration.....</b>   | <b>202</b> |

|            |                                       |     |
|------------|---------------------------------------|-----|
| Appendix 2 | Solubility Measurements.....          | 208 |
| Appendix 3 | Modified Kinetic Plots.....           | 209 |
| Appendix 4 | Numerical Integration.....            | 211 |
| Appendix 5 | Matlab Program for Curve Fitting..... | 212 |
| Appendix 6 | Solution Physical Properties.....     | 214 |

## List of Tables

|         |   |     |
|---------|---|-----|
| 2.4.1   | Surface Energy and Delay Time Activation Energy Results Reported in the Literature...                     | 22  |
| 2.5.1.1 | Calcium Sulphate Crystallization (mainly in bulk fluid) Growth Characteristics.....                       | 29  |
| 2.7.1   | Fouling Rate and Asymptotic Fouling Resistance Values (Mwaba et al., 2001).....                           | 41  |
| 2.7.2   | Activation Energy Values for Different Regions (Bansal et al. , 2005).....                                | 45  |
| 2.7.3   | Summary of Calcium Sulphate Scaling Mainly under Non-boiling Conditions.....                              | 47  |
| 2.9.1   | Phase and Thermal Conductivity of the Deposit (Fand, 1969).....   | 59  |
| 3.1.1.1 | Three Rotameters with Corresponding Ranges of Reynolds Numbers.....                                       | 65  |
| 3.1.1.2 | Different TFU Hazard Situations with Relevant Proper Actions.....   | 66  |
| 3.7.1   | Property Measurement Results for Different Concentrations as a Function of.....<br>Temperature            | 89  |
| 3.8.1   | Experiments Used for Deposit Analysis.....  | 90  |
| 3.8.2   | TFU Thermocouple Locations.....   | 91  |
| 4.2.1.1 | Delay Time Values for Different Operating Conditions (V=1.2 m/s).....                                     | 100 |
| 4.2.2.1 | Surface Energy Values for Different Wall Temperatures.....  | 102 |
| 4.2.2.2 | Delay Time Activation Energies.....   | 102 |
| 4.3.2.1 | Arrhenius parameters for Calcium Sulphate Fouling Experiments (C = 3400 ppm).....                         | 109 |
| 4.4.1.1 | EDX Analysis of the Fouling Deposits for TFU 809.....   | 117 |
| 4.4.2.1 | Deposit Coverage and Thickness Results.....   | 121 |
| 4.4.2.2 | Summary of Deposit Coverage and Thickness Results.....  | 127 |
| 4.5.1   | Comparison of Local Reciprocal Heat Transfer Coefficients Before and .....<br>After the Velocity Increase | 136 |
| 4.6.1   | The Effect of Filtration on the Delay Time and Initial Fouling Rate.....                                  | 138 |
| 4.7.1.1 | Kinetic Results for Individual Crystallization Stages (Stirring Rate = 300 RPM).....                      | 144 |
| 4.7.2.1 | Kinetic Results Based on the New Kinetic Model .....  | 148 |
| 5.1.1   | Spreadsheet for Initial Fouling Rate Modelling.....   | 153 |

|        |  |     |
|--------|--|-----|
| 5.4.1  | Adjusted Parameters at the Optimal Solution.....                                       | 159 |
| 5.4.1a | Statistical Analysis of the Results.....   | 161 |
| 5.5.1  | Diffusivities of Calcium Sulphate in Water at Different Temperatures (Bohnet, 1987)... | 166 |
| 5.5.2  | Summary of Transport and Attachment Properties used in or Evaluated from Model.....    | 167 |
| 5.7.1  | Adjusted Parameters for Refined Model.....   | 171 |
| 5.7.2  | Comparing Original Model with Refined Model.....                                       | 172 |

## List of Figures

|         |   |    |
|---------|---|----|
| 1.1.1   | Heat Transfer Resistances and Temperature Distribution Through a Flat Heat Exchanger Wall (a) without and (b) with a Fouling Deposit .....                                      | 3  |
| 1.1.2   | Different Types of Fouling Curves.....  | 5  |
| 2.4.1   | Illustration of homogeneous and Heterogeneous Nucleation Regions at Different Temperatures (Alimi et al., 2003).....  | 21 |
| 2.7.1   | Effect of Solution Velocity on the Face Growth Rate of Potash Alum Crystals at 32°C... and $\Delta C = 0.003 - 0.015$ kg of Hydrate / kg of Solution (Mullin and Garside, 1967) | 32 |
| 2.7.2   | Effect of Velocity on Fouling Resistance (Bohnet et al. , 1997).....  | 34 |
| 2.7.3   | Calcium Sulphate Fouling Curve (Bridgwater & Loo, 1984).....  | 37 |
| 2.7.4   | Effect of Velocity on Initial Fouling Rate in Plate Heat Exchangers..... (Bansal and Muller-Steinhagen , 1993)  | 37 |
| 2.7.5   | Effect of Filtration on Fouling Resistance (Bansal et al. , 1997).....  | 39 |
| 2.7.6   | Fouling Rate as a Function of Reynolds number (Najibi et al., 1997).....  | 39 |
| 2.7.7   | Effect of Bulk Temperature on the Fouling Resistance (Najibi et al., 1997).....   | 40 |
| 2.7.8   | Effect of Velocity on Calcium Sulphate Fouling Resistance (Middis et al. , 1998).....   | 42 |
| 2.7.9   | Effect of Velocity on Calcium Sulphate Fouling Resistance (curve 3 at 0.4 m/s..... and curve 4 at 0.6 m/s) (Kazi et al. , 2002)   | 43 |
| 2.7.10  | Experimental vs. Predicted Fouling Resistances (Bansal et al. , 2005).....  | 44 |
| 2.7.11  | Different Growth Rate Regions (Bansal et al. , 2005).....   | 45 |
| 2.9.1   | Calcium Sulphate Solubility in Water (Mwaba et al., 2001).....  | 57 |
| 2.9.2   | Calcium Sulphate Phase Transition Stages (Glater, 1980).....  | 59 |
| 3.1.1.1 | Schematic of Tube Fouling Unit (TFU) apparatus (Wilson, 1994).....  | 63 |
| 3.2.3.1 | Schematic of the Concentration Equalizer Assembled on the Holding Tank.....   | 72 |
| 3.2.4.1 | New Cooling Water Valve Configuration Setup.....  | 74 |
| 3.2.5.1 | Schematic Diagram of the New Thermocouple Holder Construction, Showing Tufnol Blocks Drilled for Set Screws .....   | 75 |
| 3.6.1.1 | Schematic Diagram of the Jacketed Glass Reactor (JGR).....  | 84 |
| 3.7.1   | Densities of Solutions with Different Concentrations.....   | 88 |
| 3.7.2   | Kinematic Viscosities of Solutions with Different Concentrations.....   | 88 |

|         |   |     |
|---------|---|-----|
| 4.1.1   | Temperature Profile for Clean Condition (TFU 703).....  | 94  |
| 4.1.2   | Initial and Final Wall Temperature Profiles (TFU 703).....  | 94  |
| 4.1.3   | Initial Fouling Stages at $x = 715$ mm for TFU 703 ( $V = 1.2$ m/s), Showing .....<br>Heat-up, Nucleation and Roughness Stages                | 96  |
| 4.1.4   | Different Fouling Stages at $x = 715$ mm for TFU 703 ( $V = 1.2$ m/s, $C = 3128$ ppm).....  | 97  |
| 4.1.5   | Delay Time Evaluation at $x = 715$ mm for TFU 703 ( $V = 1.2$ m/s, $C = 3128$ ppm).....   | 97  |
| 4.2.2.1 | Plot of Delay Time versus Supersaturation According Classical Nucleation.....<br>Theory ( $V = 1.2$ m/s, $T_{w,c} = 82^\circ\text{C}$ )       | 101 |
| 4.2.2.2 | Arrhenius Type Plot of Delay Time versus Local Inside Wall Temperature for.....<br>TFU 804 ( $C=3400$ ppm, $V = 0.5$ m/s)                     | 101 |
| 4.2.3.1 | Effect of Velocity on the Delay Time ( $T_{w,c} = 82^\circ\text{C}$ , $C = 3400$ ppm).....  | 104 |
| 4.2.3.2 | Effect of Velocity on the Delay Time ( $T_{w,c} = 74^\circ\text{C}$ , $C = 3400$ ppm).....  | 104 |
| 4.3.1.1 | Inside Wall Temperature Profiles for Different Thermocouple Locations.....<br>(TFU 703, $V = 1.2$ m/s, $C = 3128$ ppm)                        | 106 |
| 4.3.1.2 | Initial Fouling Rate Determination for the Top Thermocouple.....<br>(TFU 703, $V = 1.2$ m/s, $T_{w,c} = 82^\circ\text{C}$ , $C = 3128$ ppm)   | 106 |
| 4.3.2.1 | Linear Least Squares Regression for TFU 809.....  | 108 |
| 4.3.2.2 | Non-linear Least Squares Regression for TFU 809.....  | 108 |
| 4.3.2.3 | Effect of Velocity on Initial Fouling Rate .....<br>( $C = 3400$ ppm, $(T_{w,i})_c = 77 - 83^\circ\text{C}$ , $T_b = 50 - 61^\circ\text{C}$ ) | 109 |
| 4.4.1.1 | Photograph of Fouled Tube Sections from TFU ( $V = 1.2$ m/s).....   | 112 |
| 4.4.1.2 | SEM of TFU 809, $x \approx 48$ mm, Magnification 600x.....  | 115 |
| 4.4.1.3 | SEM of TFU 809, $x \approx 710$ mm, Magnification 60x.....  | 115 |
| 4.4.1.4 | SEM of TFU 809, $x \approx 710$ mm, Magnification 90x.....  | 116 |
| 4.4.1.5 | EDX Analysis of the Fouling Deposits for TFU 809.....   | 116 |
| 4.4.1.6 | Weight Loss Profile for Dry Sample in TFU 809, $x \approx 710$ mm.....  | 118 |
| 4.4.2.1 | Deposit distribution along length of tube for TFU 809.....  | 119 |
| 4.4.2.2 | Deposit Coverage for Each Experiment.....   | 126 |

|         |   |     |
|---------|---|-----|
| 4.4.2.3 | Dependence of Physical Properties on Temperature for All Data.....  | 127 |
| 4.4.2.4 | Comparison of Different Deposit Thermal Conductivity Measurement Methods.....   | 128 |
| 4.4.2.5 | Estimation of an Average Deposit Density for TFU 800 Experiments.....   | 130 |
| 4.4.2.6 | Estimation of Low and High Deposit Density for TFU 800 Experiments.....   | 130 |
| 4.5.1   | Local Reciprocal Heat Transfer Coefficient Before and After the.....<br>Velocity Increase for $T_{10}$  | 135 |
| 4.5.2   | Local Reciprocal Heat Transfer Coefficient Before and After the velocity Increase.....<br>for $T_5$   | 135 |
| 4.5.3   | Local Reciprocal Heat Transfer Coefficient Before and After the velocity Increase for...<br>$T_1$   | 135 |
| 4.6.1   | The Effect of Filtration on Fouling Behavior at Thermocouple $T_{10}$ .....   | 139 |
| 4.6.2   | The Effect of Filtration on Fouling Behavior at Thermocouple $T_5$ .....  | 139 |
| 4.6.3   | The Effect of Filtration on Fouling Behavior at Thermocouple $T_1$ .....  | 140 |
| 4.7.1.1 | Plot of Calcium Sulphate Concentration vs. time ( $T_b = 80^\circ\text{C}$ , $C_{A0} = 3100$ ppm).....  | 141 |
| 4.7.1.2 | Reaction Rate Constants for Different Reaction Steps $T_b = 80^\circ\text{C}$ , $C_{A0} = 3100$ ppm).....   | 143 |
| 4.7.1.3 | Arrhenius plot for three different stages ( $C_{A0} = 3100$ ppm).....   | 144 |
| 4.7.2.1 | Reaction Rate Constant Evaluation Based on the Modified.....<br>Kinetic Model ( $T_b = 65^\circ\text{C}$ , $C_{A0} = 3400$ ppm)   | 147 |
| 4.7.2.2 | Arrhenius plot for Modified Kinetic Approach ( $C_{A0} = 3400$ ppm).....  | 147 |
| 5.2.1   | Experimental Data Used for Modeling ( $C = 3400$ ppm).....  | 157 |
| 5.3.1   | Friction Factor Correlations.....   | 158 |
| 5.4.1   | Sum of the Squares of the Residuals Over a Range of Activation Energies.....  | 160 |
| 5.4.2   | Comparing Experimental and Model Initial Fouling Rate Results Listed in.....<br>Table 5.4.1.a (Run numbers are identified in legend)  | 160 |
| 5.4.3   | Effect of Wall and Bulk Temperatures on Model Prediction.....   | 163 |
| 5.4.4   | Comparison of Model Predictions to Experimental Data Obtained from the Arrhenius...<br>Type Equations. Points above $\dot{R}_{fo} = 8 \times 10^{-8} \text{ m}^2\text{K/J}$ Are Extrapolations. | 165 |
| 5.5.1   | Extracting Best Value of $D_o$ Based on the Data of Bohnet (1987), with $T_f = \text{Absolute...}$<br>Film Temperature  | 167 |

5.7.1 Comparing Experimental and Model Initial Fouling Rate Results for the Refined..... 171  
Model

5.7.2 Comparison of Model Predictions to Experimental Data for Refined Model..... 172

## **Acknowledgements**

I would like to thank all members of the Department of Chemical Engineering for their friendship and encouragement throughout the duration of this study. In particular, I wish to express sincere gratitude to my research supervisors, Dr. Norman Epstein and Dr. Paul Watkinson, for the support, patience and guidance that they have shown over the past five and a half years.

Valuable information concerning operation of the Tube Fouling Unit, provided by both Dr. Ian Wilson and Dr. Ian Rose, is truly appreciated.

Support from the Chemical Engineering office, stores, and technical advice from the workshop is also appreciated. In addition, I would like to thank the staff of the Department of Metals and Materials for the use of the scanning electron microscope.

Financial support of the University of British Columbia (University Graduate Fellowships) and the Natural Sciences and Engineering Research Council of Canada are gratefully acknowledged.

Finally, special thanks are due to my family for all of the extended hours I spent in the lab instead of being with them, and to other relatives and friends for their encouragement and support.

## **1. Introduction**

The accumulation of unwanted material on a heat transfer surface is usually referred to as fouling (Taborek et al., 1972). Fouling is a very complicated phenomenon, involving heat, mass, and momentum transfer that may be accompanied by chemical reactions and phase changes. It has been recognized as a nearly universal problem in design and operation of heat exchangers. It affects the operation of thermal equipment either by decreasing thermal efficiency due to extra thermal resistance or by increasing pressure drop across the equipment due to reduced cross-sectional area and / or enhanced surface roughness. In general, fouling is a very challenging and time-consuming issue for industries to overcome. In some industries periodic cleaning of heat transfer surfaces is routinely practiced, leading to high operating costs. The total fouling-related cost for industries (capital expenditure, extra fuel costs, cleaning and production losses) is increasing rapidly. Based on the cost factors suggested by Müller-Steinhagen (1993), total heat exchanger fouling costs for highly industrialised countries such as the US and the UK are about 0.25% of the countries' gross national product (GNP).

The process of deposit buildup can be treated by introducing an additional thermal resistance, termed the fouling factor,  $R_f$ . In reality, its value depends on the operating bulk and surface temperatures, fluid velocity, fluid concentration, tube surface roughness and material, the presence of particles, and the length of service of the heat exchanger. Industrially, it is difficult to get accurate and reliable fouling data from real full-scale plants, and hence lab and pilot scale units offer a better environment to study this phenomenon. The main goal of much fouling research is to understand the mechanisms

of fouling and to develop models of the fouling process to move towards minimizing industrial fouling problems.

### 1.1 Measurement of Fouling

In thermal processes, fouling is usually monitored by either measuring the mass of deposit per unit heat transfer surface area, or the deposit thickness, or the thermal fouling resistance, as a function of time. The relationship between the terms deposit coverage ( $m_f$ ), deposit thickness ( $x_f$ ), fouling resistance ( $R_f$ ), and the deposit physical properties ( $\rho_f, \lambda_f$ ) is given by

$$dR_f = \frac{dx_f}{\lambda_f} = \frac{dm_f}{\rho_f \lambda_f} \quad (1.1.1)$$

Equation (1.1.1) is written in differential form to allow for the possible variation of both deposit density and deposit thermal conductivity with distance from the heat transfer surface. For a given fluid, the fouling resistance in any heat exchanger is usually a function of heat exchanger geometry, surface material, surface and bulk temperatures, fluid velocity and deposit properties. The fouling resistance is usually obtained by subtracting the total thermal resistance at time zero, when the surface is assumed to be clean, from the corresponding value at time  $t$ . Figure 1.1.1 illustrates the various thermal resistances in a heat exchanger, in which one side of a flat wall is subjected to a constant heat flux, and a fluid is flowing on the other side parallel to the surface. If the deposit forms on the fluid-side surface and two thermocouples measure the wall temperature,  $T_w$ , and the bulk temperature,  $T_b$ , respectively, then for the clean condition,

$$\frac{1}{U_o} = R_w + R_1 \quad (1.1.2)$$

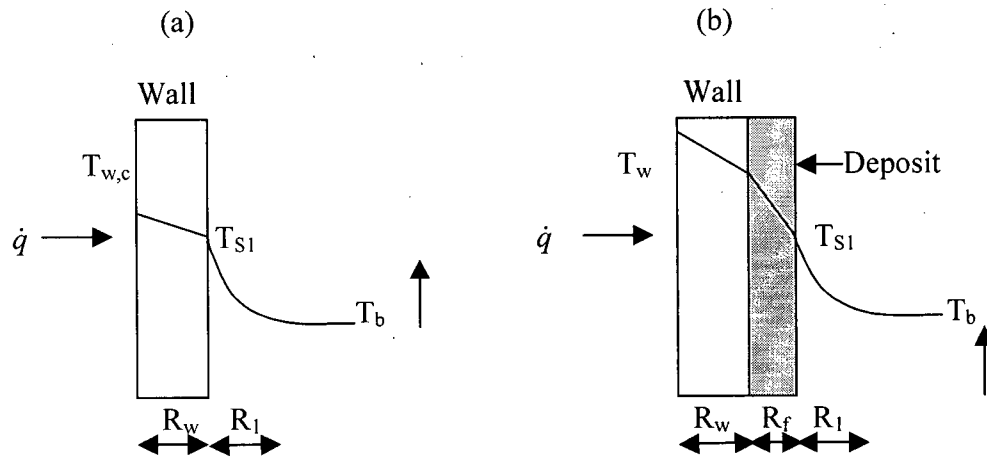


**Figure 1.1.1: Heat Transfer Resistances and Temperature Distributions through a Flat Heat Exchanger Wall (a) without and (b) with a Fouling Deposit**

$$\dot{q} = U_o(T_{w,c} - T_b) \quad (1.1.3)$$

where  $U_o$  is the clean overall heat transfer coefficient. As time goes by, deposit builds up on the surface; if the constant heat flux is maintained, the surface temperature increases due to the thermal resistance associated with the deposit, and the wall temperature increases correspondingly. At this condition, which is called a fouled condition,

$$\frac{1}{U} = R_w + R_f + R_l \quad (1.1.4)$$

$$\dot{q} = U(T_w - T_b) \quad (1.1.5)$$

and the fouling resistance, which changes with time, can be calculated from:

$$R_f = \frac{1}{U} - \frac{1}{U_o} \quad (1.1.6)$$

$$R_f = \frac{(T_w - T_b)}{\dot{q}} - \frac{(T_{w,c} - T_b)}{\dot{q}}$$

$$R_f = \frac{T_w - T_{w,c}}{\dot{q}} \quad (1.1.7)$$

Increasing fouling resistance is an indication of decline in heat transfer performance. When it comes to heat exchanger design, selection of an appropriate fouling resistance is usually based upon the fluid velocity, temperature and fluid properties, but its representation with a simple listing of time-invariant fouling factors such as those of the Tubular Exchangers Manufacturers Association (TEMA, 1978) is highly questionable; nevertheless, in industrial practice, TEMA's constant values are still commonly used. Using a constant value of  $R_f$  implies that rapid asymptotic fouling is assumed, despite the fact that in some cases, fouling curves do not even approach an asymptotic value. Therefore, it is important to consider the effect of variables such as velocity, temperature, and concentration on the *rate* of fouling.

Fouling curves are constructed by plotting fouling resistance vs. time. Generally they show, after a delay time followed by a roughness control period, one of four types of curves illustrated in Figure 1.1.2. The top curve is a constant rate fouling curve, in which there is a linear increase in fouling resistance with time, which implies that there is no removal or that the difference between deposition rate and removal rate is constant. In a non-asymptotic falling rate fouling curve, the net deposition rate slows down as the deposit thickness gets larger, without attaining a maximum. This behavior is due to auto-retardation mechanisms with or without removal. Asymptotic fouling is often assumed to arise from a constant deposition rate with a progressive removal rate that is proportional to the deposit thickness. This behavior forces the fouling curve to approach an asymptotic fouling resistance. The removal term is related to the fluid shear force exerted on the deposit layer, and is more effective at higher deposit thicknesses. Finally a saw-tooth fouling curve is characterized by an increase in fouling resistance with time, interrupted

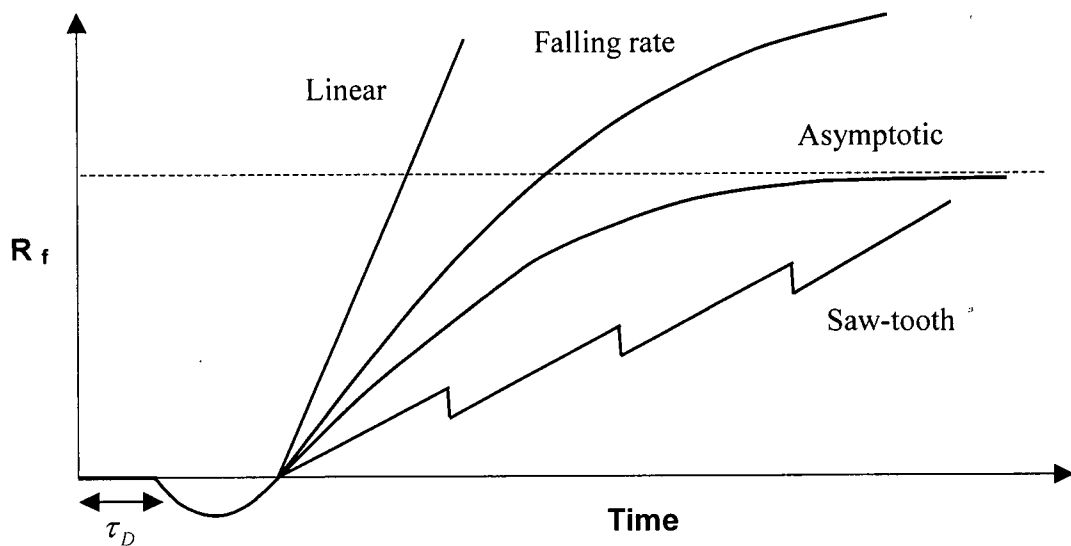


**Figure 1.1.2: Different Types of Fouling Curves**

by periodic shedding of deposit due to deposit weakening caused by thermal stresses or changes in operating conditions.

## 1.2 Fouling Classification

Generally there are five types of fouling as outlined by Epstein (1983): crystallization, particulate, chemical reaction, corrosion, and biological fouling.

### 1. Crystallization Fouling

Crystallization fouling has been subdivided into two categories (Hewitt et al., 1994):

#### a. Precipitation Fouling

In this type of fouling, sometimes called *scaling*, dissolved substances crystallize from solution onto the heat transfer surface. Normal solubility salts precipitate on cooled surfaces, while the more troublesome inverse solubility salts precipitate on heated surfaces.

**b. Solidification Fouling**

In this category, pure liquid or the higher melting point constituents of a multi-component solution freeze onto a sub-cooled surface.

**2. Particulate Fouling**

This is the accumulation of finely divided solids suspended in the process fluid onto the heat transfer surface. In a minority of instances settling by gravity prevails, and the process may then be referred to as sedimentation fouling.

**3. Chemical Reaction Fouling**

In this type of fouling, deposit builds up at the heat transfer surface by chemical reactions in which the surface material itself is not a reactant (e.g., in petroleum refining, polymer production and food processing).

**4. Corrosion Fouling**

In this category, deposit formation is due to the accumulation of indigenous corrosion products on the heat transfer surface.

**5. Biological Fouling**

This is the attachment of macro-organisms (macrobiofouling) and/or micro-organisms (microbiofouling or microbial fouling) to a heat transfer surface.

For all the aforementioned categories the progression of fouling has been broken down into five sequential events giving rise to the 5 x 5 matrix (Epstein, 1983).

**A. Initiation**

This event is associated with an induction or delay period ( $\tau_d$ ) before any measurable fouling has occurred. For all modes of fouling other than

particulate, many investigators have reported that  $\tau_d$  decreases as the surface roughness increases. The roughness projections provide additional sites for nucleation, adsorption and chemical surface activity. Surface roughness also decreases the thickness of the viscous sublayer and hence increases eddy transport to the wall. It has also been shown that an increase in the surface temperature decreases the delay time for scaling (Troup and Richardson, 1978), while no clear effect of fluid velocity has been determined.

### **B. Transport**

The fouling material (or its precursor) must be transported from the bulk fluid to the wall, where its concentration decreases. This process is therefore a mass transfer phenomenon, where the concentration difference is the driving force.

### **C. Attachment**

Attachment of the fouling species to the wall follows the transport of the foulant or the key component to the wall region, where the deposit is actually formed. Depending on the fouling category, different mechanisms can contribute to the attachment process. In particulate fouling the important factors responsible for attachment have been identified (Bott, 1995) as:

- Van der Waals forces of attraction
- Electrostatic forces in systems having charged surfaces
- The contact area between particle and surface

For crystallization fouling, attachment occurs by a process known as surface integration. The deposition process can be characterized by a mass transfer coefficient at low velocities, where the deposition is controlled by mass

transfer, or by an attachment rate constant at higher velocities, where the deposition process is surface reaction (integration) controlled, or by a combination of both at intermediate velocities.

#### D. Removal

Removal of deposit, a result of force imbalance between fluid shear and deposit bond resistance, may or may not begin right after deposition has started. That it does is an assumption implicit in the following model originally proposed by Kern and Seaton (1959) and further developed by Taborek et al. (1972):

$$\dot{m}_r = \frac{b\tau_w m_f}{\Psi} \quad (1.2.1)$$

The removal flux,  $\dot{m}_r$ , is assumed to be directly proportional to the mass of deposit per unit surface area ( $m_f$ ) and the fluid shear stress at the wall ( $\tau_w$ ), and inversely proportional to the deposit strength ( $\Psi$ ).

#### E. Aging

Aging of the deposit may start as soon as it has been laid down on the heat transfer surface. The aging process depends on operating conditions such as the presence of suspended particles. In crystallization fouling, it may include changes in crystal or chemical structure by dehydration. During a particulate fouling study, Turner et al. (2001) introduced a new concept for aging, called consolidation. It was defined as the process whereby particles become chemically bonded to either the heat-transfer surface or pre-existing deposit. It was stated that deposit consolidation exerts a strong influence on the fouling behaviour by controlling the fraction of the deposit that is available to be re-entrained.

### **1.2.1 Heat exchanger fouling variables**

Fluid velocity, wall (and fluid) temperature, foulant (or precursor) concentration, and surface roughness and material are the main variables that affect the rate at which deposit builds up on the heat transfer surface. Fluid velocity is perhaps the most influential variable and fortunately it is the one variable over which the designers have the most control. In general, as velocity is increased, heat transfer is enhanced but in addition there is an increase in pressure drop (in turbulent flow, heat transfer rate is roughly proportional to velocity whereas pressure drop is a function of velocity squared). By analogy with heat transfer, the mass transfer rate is also increased, thereby facilitating the transport of foulant materials towards the surface. At the same time, an increase in velocity results in increased shear effects at the wall, so that with respect to fouling, it is likely that there is a critical velocity at which the auto-retardation and/or removal effects of shear start to counteract the associated mass transfer and thus reduce the accumulation of deposit.

The wall temperature in a heat exchanger can have a marked influence on the deposition rate onto the heat exchange surface. Under conditions where deposition is controlled by mass transfer, the effect of wall temperature is felt only through the diffusivity of the foulant or its precursor, and therefore its contribution is small. However, when the deposition process is controlled by chemical reaction at the wall and therefore by an attachment mechanism, the fouling rate is strongly dependent on the surface temperature as displayed by an Arrhenius relationship. Under these conditions the fouling rate increases exponentially with wall temperature.

Concentration of foulant (or precursor) and the heat exchanger surface roughness are also important variables affecting the deposition rate. With increasing concentration, the driving force for both mass transfer and surface reaction increases, resulting in a higher deposition rate. The surface roughness provides additional sites for nucleation, adsorption and chemical surface activity so that, in general, the higher the surface roughness, the greater the potential for fouling.

The present thesis is concerned with calcium sulphate precipitation fouling from aqueous solution, particularly in its initial stages, and the following literature review will therefore be primarily restricted to this topic. The reported influence of each of the important fouling variables will be included in the review.

## 2. Literature Review

### 2.1 Crystallization Fouling

Precipitation fouling may be defined as solid layer deposition on a surface that arises primarily from the presence of dissolved inorganic salts in the flowing solution which exhibit supersaturation under the process conditions. It presents one of the major fouling problems in almost all chemical industries such as paper mills, food processing plants, electricity generation plants, etc. Water hardness salts like calcium sulphate and calcium carbonate are the main fouling species during water cooling applications. In saline water distillation units, precipitation of calcium sulphate present in sea water is very common (Lu and Fabuss, 1968). During water desalination by reverse osmosis membranes (Brusilovsky et al., 1992), calcium sulphate blocks the membranes. Even small quantities of these salts in the boiler feed water can cause a significant increase in power consumption.

Mechanical properties of deposits depend strongly on the operating conditions. Hasson (1981) defined the term 'scale' as the formation of a dense crystalline deposit well bonded to the metal surface, which is often associated with the crystallization of salts of inverse solubilities under heat-transfer conditions. But terms such as soft scale, powdery deposit, or sludge are used when the deposited layer is porous and loosely adherent. In general, sludge formation is a result of the accumulation of hardness salts combined with suspended matter, which often occurs in steam boilers. In practice, the ideal situation is to prevent scale formation; but if it forms within the boiler, it should be chemically altered into suspended solids, or sludge, which can be removed easily by periodic boiler blowdown.

Calcium sulphate scaling is a major problem for several industrial processes and for that reason it has been a focus of attention for various researchers around the world. To study the mechanisms of its formation, different experimental setups have been employed. Some researchers have used electrical heaters for heat transfer (Hasson and Zahavi, 1970; Loo, 1979; Ritter, 1983; Bohnet, 1987; Augustin, 1992; Krause, 1993; Middis, 1994; Brahim et al., 2001; Mwaba et al., 2001; Fahiminia et al., 2003), while others have used either water heated surfaces (Bansal and Müller-Steinhagen 1993, Bansal et al. 1993, 1997, 2000) or steam heated surfaces (Gonionskiy et al. 1970). Depending on the operating conditions, heat exchanger characteristics, and deposit strength, different kinds of fouling behaviour such as linear, falling rate, asymptotic, and saw-tooth have been observed for calcium sulphate scaling. The observed deposition patterns on heat transfer surfaces also varied significantly, with some investigators reporting uneven deposit formation at any cross-section as well as along the surfaces. In contrast, others reported uniform deposit formation at any cross-section. A number of researchers have investigated cases where calcium sulphate fouling is affected either by another type of fouling occurring simultaneously or by the presence of particles in the process solution (Bramson et al., 1995; Bansal et al., 1997; Gill and Sheikholeslami, 1997; Andritsos and Karabelas, 1999; Chong and Sheikholeslami, 2001; Li et al., 2001; Yu et al., 2002).

## 2.2 Nucleation and Surface Energy

The state of supersaturation is the first prerequisite of crystal nucleation in all crystallization processes, including crystallization fouling. Several expressions have been used to quantify the extent of supersaturation, but the most common are the concentration

driving force,  $\Delta C$ , the supersaturation ratio,  $S$ , and a quantity sometimes referred to as the relative supersaturation,  $\sigma$ . These quantities are defined by:

$$\Delta C = C - C_s \quad (2.2.1)$$

$$S = \frac{C}{C_s} \quad (2.2.2)$$

$$\sigma = \frac{\Delta C}{C_s} = S - 1 \quad (2.2.3)$$

where  $C$  is the solute concentration and  $C_s$  is the solute saturation concentration at the given temperature. The condition of supersaturation is not sufficient cause for a system to begin to crystallize. Before crystals can develop there must exist on the surface a number of minute solid bodies, embryos, nuclei or seeds, that act as centers of crystallization. In general, crystallographers divide crystal nucleation into three main categories: homogeneous nucleation, primary heterogeneous nucleation, and secondary heterogeneous nucleation.

In homogeneous nucleation, crystal nucleation occurs spontaneously (without the aid of any foreign bodies or particles). According to classical nucleation theory (Mullin, 2001), it is assumed that a primary nucleus (i.e., a critical size of the smallest stable crystallite) is formed by a series of bimolecular collisions. The Gibbs free energy change that must be overcome to obtain a stable crystallite (assumed spherical) is given by:

$$\Delta G_{crit} = \frac{16\pi}{3} \frac{\gamma^3 v_m^2}{(zRT \ln S)^2} = \frac{4}{3} \pi \gamma r_c^2 \quad (2.2.4)$$

where  $r_c$  is the radius of the nucleated crystallite,  $\gamma$  the surface energy ( $\text{J/m}^2$ ),  $v_m$  the molar volume of the crystalline phase ( $7.445 \times 10^{-5} \text{ m}^3/\text{mol}$  for  $\text{CaSO}_4 \cdot 2\text{H}_2\text{O}$ ),  $z$  the number of ions of a crystallizing salt molecule ( $z = 2$  for  $\text{CaSO}_4 \cdot 2\text{H}_2\text{O}$ ),  $R$  the gas

constant,  $T$  the absolute temperature (K), and  $S$  the supersaturation ratio. Assuming that the embryos (unstable molecular clusters preceding nucleation) achieve an immediate steady state distribution, the rate of nucleation,  $J$ , i.e. the number of nuclei formed per unit time per unit volume (for bulk crystallization) or unit surface area (for surface crystallization) can be expressed as:

$$J = A \exp(-\Delta G_{crit} / k_B T) = A \exp \left[ - \frac{\beta \gamma^3 v_m^2}{z^2 N_A^2 k_B^3 T^3 (\ln S)^2} \right] \quad (2.2.5)$$

where  $A$  is a frequency factor,  $\beta$  is a shape factor ( $=16\pi/3$  for spheres),  $N_A$  is Avogadro's number ( $6.025 \times 10^{23} \text{ mol}^{-1}$ ), and  $k_B$  is the Boltzmann constant ( $1.38 \times 10^{-23} \text{ J/K}$ ). Equation (2.2.5) indicates that three main variables govern the rate of nucleation: temperature,  $T$ ; degree of supersaturation,  $S$ ; and surface energy,  $\gamma$ .

Nucleation is more readily achieved in the presence of trace impurities, i.e. crystals form with the aid of foreign bodies and surfaces, which is what characterizes primary heterogeneous nucleation. This is closer to industrial situations in which particles exist in the process fluid that accelerate the crystallization fouling. It is assumed that the nucleus then requires less interfacial energy for its formation due to contact with a wetted solid surface. Equations (2.2.4) and (2.2.5) retain the same general form for primary heterogeneous nucleation but are corrected for the reduced activation energy according to:

$$\Delta G'_{crit} = \phi \Delta G_{crit} \quad (2.2.6)$$

where  $\phi < 1$  depends on the contact angle between the crystallite and the solid surface. Randolph and Larson (1965) showed that a supersaturated solution nucleates much more

readily, i.e. at a lower supersaturation, when the crystals of the solute are already present or deliberately added, which is what is meant by secondary heterogeneous nucleation.

### 2.3 Delay Time and Classical Nucleation Theory

Initiation is the first step of the successive events that commonly occur in crystallization fouling (Epstein, 1983). In order to mitigate fouling, it would be better to start with understanding its initiation mechanism, rather than focusing only on the crystal growth period. To do so it is important to quantify the relationship between the relevant variables in the initiation step. In general, initiation is associated with the delay time, the period of time that elapses between the achievement of supersaturation at a given surface and the first detection of a fouling deposit on that surface. The duration of the delay time for a given system is affected by the degree of supersaturation, the temperature level, the fluid velocity and the presence of impurities. The occurrence of a delay time is undoubtedly related to the kinetics of nucleation, but its duration is difficult to predict. It has been shown that  $\text{CaSO}_4$  nucleation on the heat transfer surface of a non-boiling flow exchanger is a transient nucleation phenomenon (Hasson and Zahavi, 1970). Also, Branch (1991) correlated the reciprocal of the delay time as if it were independent of solute concentration but with an Arrhenius dependence on wall temperature, but Najibi et al. (1997) showed that the delay time is a strong function of the degree of supersaturation and, therefore, cannot be expressed by a zero-order model.

Mullin (2001) developed a model for delay time by assuming that it is inversely proportional to the nucleation rate:

$$\tau_D = \frac{B}{J} \quad (2.3.1)$$

where B is the proportionality constant. Combining Eqs. (2.2.5) and (2.3.1), we arrive at:

$$\ln \tau_D = \ln \frac{B}{A} + \frac{K}{(\ln S)^2} \quad (2.3.2)$$

where

$$K = \frac{\beta \gamma_{eff}^3 v_m^2}{z^2 N_A^2 (k_B T)^3} \quad (2.3.3)$$

In Equation (2.3.3), the surface energy  $\gamma$  has been replaced by an effective surface energy  $\gamma_{eff}$ , which, according to Hasson et al. (2003), is given by

$$\gamma_{eff} = \gamma \phi^{1/3} \quad (2.3.4)$$

where the parameter  $\phi=1$  for homogeneous nucleation and  $\phi < 1$  (but usually unknown) for heterogeneous nucleation (Sohnel and Mullin, 1988). For a given temperature, a plot of  $\ln \tau_D$  vs.  $(\ln S)^{-2}$  should yield a straight line, from the slope of which  $\gamma_{eff}$ , which plays an important role in crystallization fouling, can be determined.

Several researchers (Walton, 1967; Mullin, 2001; Sohnel and Mullin; 1988) have employed classical nucleation theory to characterize bulk crystallization, whereas others (Hasson and Zahavi., 1970; Linnikov, 1999; Sheikholeslami, 2003) have focused mainly on surface crystallization. A variety of techniques have been employed to measure delay times in both bulk and surface crystallization, in order to understand the effect of operating variables such as fluid velocity, fluid temperature, concentration, and surface properties.

#### 2.4 Previous Delay Time Studies

Banchero and Gorden (1960) measured the time for scale appearance from solutions flowing in a semicircular transport passage, 37 ft long. Pressurized hot water was used for heating. Aqueous solutions of inverse solubility scaling salts were examined

under both boiling and non-boiling conditions. Scale formation always occurred first at the exit end and propagated toward the inlet region. The time for the first scale observation was empirically correlated against percentage supersaturation, with solution concentration as parameter. Trends were as qualitatively expected from nucleation theory for the effect of supersaturation and wall temperature. However, the time for scale formation was found to be insensitive to velocity, contrary to the results observed in other studies. Also, there was little difference between boiling and non-boiling conditions, possibly due to vapour bubbles obscuring observation of earlier scale formation. They found that the greater the surface temperature, the less time required for scale formation, and the time for scale formation (delay time) was found to be independent of velocity between 0.61 m/s and 3.05 m/s ( $Re=10000-50000$ ).

Hasson and Zahavi (1970) studied the mechanism of calcium sulphate nucleation in an annular test section using a saturated solution of calcium sulphate. They found that the first appearance of a fine scale coating could be visually detected at the downstream edge of the tube some 10 to 30 minutes from initial operation. This nucleate layer then propagated toward the upstream edge of the tube, initially at a fast rate and subsequently at a rapidly diminishing rate which became very slow as the upstream edge of the tube was approached. In the initial rapid period, as much as 50 to 70 % of the tube length was covered by a nuclear layer within the first two hours of operation at surface temperatures of 80°C and 87°C. A further advance of the nucleate front of only 10 to 20% of the tube length required more than 20 hours of operation. The above phenomenon showed that nucleation is a transient process, and it was successfully interpreted using a transient nucleation rate model. Also, they found that an increase of surface temperature at

constant flow velocity augmented both the propagation rate of the nucleation front and the amount of scale formed. Decreasing the flow velocity had the same effect as an increase in temperature. Moreover, they observed that solution filtration (25 micron pore size) decreased the propagation rate of the nucleation front and the total amount of deposit formation decreased by a factor of three or four. For example, the amount of deposit formed in 49 hours with filtration was 5.7 grams, compared to 15.3 grams without filtration at  $T_w = 80^\circ\text{C}$  and a flow velocity of 22.3 cm/s.

Liu and Nancollas (1975) proposed an empirical relationship for the effect of temperature on the delay time which is similar to the Arrhenius equation for the temperature dependence of the rate constant,

$$\ln(1/\tau_D) = \ln \Omega - E_D/RT \quad (2.4.1)$$

where  $E_D$  is the delay time activation energy and  $\Omega$  is a constant. It has been employed by many researchers in bulk crystallization studies for experiments performed at the same concentration without considering stirring effects. Branch (1997) employed Equation (2.4.1) for evaporators operating with kraft pulp black liquor. To date some delay time activation energy values have been reported for calcium sulphate bulk crystallization, but no values have been reported for calcium sulphate crystallization fouling.

Ritter (1983) proposed different criteria for delay time determination. To analyze experimental results, the delay time was defined as the time to reach a fouling resistance of  $0.00018 \text{ m}^2\text{K/W}$ . The experimental results showed that after the horizontal line representing the initiation period, the measured thermal resistance started increasing without recording any roughness effect. The following empirical equation was developed

for delay time as a function of the solution supersaturation and the mass transfer coefficient  $k_l$ :

$$\tau_D = \frac{2.1 \times 10^{-4}}{k_l \left( \frac{C_b - C_{sat}}{C_{sat}} \right)^2} \quad (2.4.2)$$

During the analysis of experimental results, the surface energy was not considered as an important parameter. Equation (2.4.2) illustrates that increasing the fluid velocity will decrease the delay time. For all the performed experiments, a range of 0.15 to 50 hours was observed for delay time.

Linnikov (1999) investigated the kinetics and mechanism of calcium sulphate nucleation on a heat-exchange surface. The test section was a rectangular channel and made of stainless steel. The nucleation process was observed by photographing the crystallization section on the heated surface through a glass installed in one side of the test section. The experiments were carried out at a velocity range of 8.3 to 9.7 mm/s under laminar flow conditions. Significant crystal removal was observed when the velocity was increased by a factor of 2-3 under laminar flow conditions. The surface energy value, based on the classical nucleation theory, was found to be 8 mJ/m<sup>2</sup>.

Hasson et al. (2003) studied the effect of antiscalants on calcium sulphate induction time on a polymeric substrate in a membrane system at a temperature of about 30°C. For pure calcium sulphate solutions, based on the classical nucleation theory, a value of 14.7 mJ/m<sup>2</sup> was reported for surface energy. Also, they pointed out that antiscalant dosage acts to extend the induction period, i.e. the presence of an antiscalant would enhance the crystallization surface energy. Their experimental data showed that in most cases the antiscalant increased the surface energy from about 15 to 29 mJ/m<sup>2</sup>.

Alimi et al. (2003) used a new technique called the quartz microbalance (QMC) to study delay times of calcium sulphate dihydrate precipitation over a range of 20 to 70°C. The QMC technique uses a quartz electrode placed in a jacketed reactor, under well-controlled hydrodynamic and temperature conditions, to measure the mass of deposit layer forming on the electrode surface. This technique is useful for detecting small amounts of deposit buildup, as low as  $5 \times 10^{-3}$  mg, on its surface. The quartz electrode had the same temperature as the solution in the jacketed reactor and as the crystals formed on the electrode surface. Values of delay times were measured and reported for the supersaturation range between 2.5 and 11. Surface energy values were found to be 48.5 and 46.2 mJ/m<sup>2</sup> at 20 and 70°C, respectively. The dependence of the delay time on temperature determined the delay time activation energy, which ranged from 71 to 51 kJ/mol for the supersaturation range between 2.5 and 11. According to a constructed plot of  $\ln \tau_D$  versus  $(\ln S)^{-2}$ , Figure 2.4.1, they pointed out that homogeneous nucleation was dominant, and heterogeneous nucleation was estimated to occur at supersaturations less than four. The critical supersaturation, which according to their plot occurs at a value of 2, corresponds to the limit between the heterogeneous and homogeneous nucleation. Figure 2.4.1 illustrates two different slopes at each temperature, corresponding to the different nucleation mechanisms. The flatter slope results from the fact that at low supersaturation, the nucleation is predominantly heterogeneous, whereas at high supersaturation, homogeneous nucleation prevails.

Important calcium sulphate nucleation parameters such as delay time activation energy (for bulk precipitation) and surface energy values (for both bulk and surface crystallization), reported in the literature, have been summarized in Table 2.4.1. The

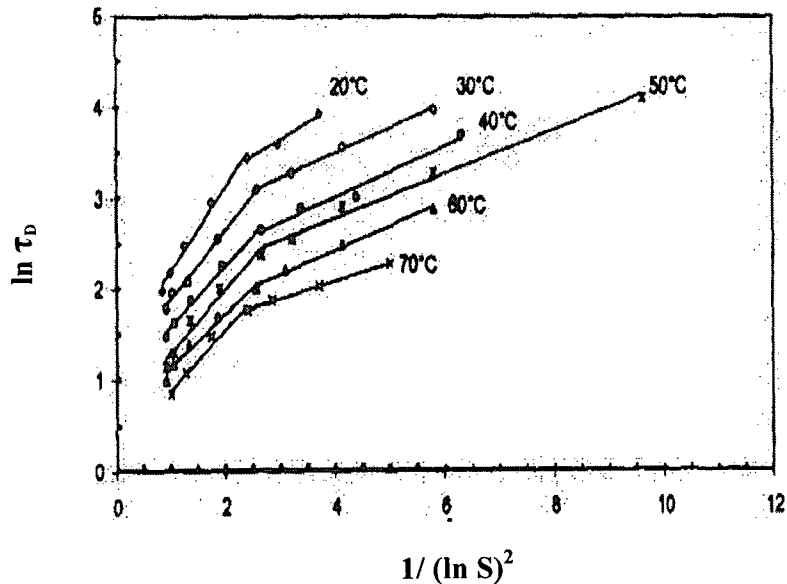


**Figure 2.4.1: Illustration of Homogeneous and Heterogeneous Nucleation Regions at Different Temperatures (Alimi et al. , 2003)**

surface energy values in Table 2.4.1 illustrate that:

- Surface energy values for bulk crystallization are higher than those for surface crystallization, and that is because of the heterogeneity of surface nucleation.
- The lowest surface energy is reported for nucleation on a metal surface which has been under laminar flow condition.
- In spite of the large number of reported data for bulk crystallization delay time activation energies, no value has been reported for surface crystallization under sensible heat transfer.
- No specific trend can be made between temperature and reported surface energies.
- No surface energy value has been reported for surface crystallization on a metal surface in turbulent flow under sensible heating conditions.

**Table 2.4.1: Surface Energy and Delay Time Activation Energy Results Reported in the Literature**

| $T_b$<br>(°C) | Nucleation<br>location        | $\gamma_{eff}$<br>(mJ/m <sup>2</sup> ) | $E_D$<br>(kJ/mol) | Reference                  | Comments  |
|---------------|-------------------------------|--|-------------------|----------------------------|---|
| 25-70         | Metal<br>surface<br>reported* | 14-50                                  | 51-71             | Alimi et al.<br>2003       | No temperature difference<br>between bulk and<br>surface temperature          |
| 28            | Polymeric<br>substrate        | 15                                     | –                 | Hasson et al.<br>2003      | –   |
| 69-75         | Metal<br>surface              | 8                                      | –                 | Linnikov<br>1999           | Under laminar flow  |
| 25-80         | Solution<br>bulk              | 18-13                                  | –                 | Klepetsanis et al.<br>1999 | No specific trend between<br>surface energy and<br>temperature was recognized |
| 25-70         | Solution<br>bulk              | 37                                     | 30                | Lancia et al.<br>1999      | No specific trend between<br>surface energy and<br>temperature was recognized |
| 50-90         | Metal<br>surface              | 11-12                                  | –                 | Vasina et al.<br>1996      | Under film evaporation  |
| 25-90         | Solution<br>bulk              | 32-53                                  | 53                | He et al.<br>1994          | Surface energy increases<br>with temperature                                  |
| 22-40         | Solution<br>bulk              | 34-38                                  | –                 | Keller et al.<br>1978      | Surface energy mainly<br>increases with temperature                           |

\*However, due to absence of temperature gradient between bulk fluid and metal surface, crystallization probably occurred in bulk.

## 2.5 Precipitation Kinetic Models

To study crystallization fouling, it is desirable to have proper kinetic models. The nature of crystallization kinetics is complicated and that is the reason why a variety of models have been proposed. Rigorous analysis of precipitation kinetics is not possible; however, useful models have been developed by considering two limiting conditions, reaction controlled and mass transfer controlled precipitation. Several researchers have studied kinetics of calcium sulphate precipitation and proposed different models. In general, for simple reactions considering component A as reactant, the rate of reaction can be given as:

$$-r_A = f(C_A, T) \quad (2.5.1)$$

where  $C_A$  and  $T$  are the concentration and temperature, respectively. However, for crystallization precipitation the rate equation is much more complicated and can be expressed as:

$$-r_A = f(C_A, T, A_c, N_s) \quad (2.5.2)$$

where  $A_c$  and  $N_s$  are crystal surface area and number of nucleation sites, respectively.

Basically the form of the kinetic model depends strongly on the experimental techniques and operating conditions employed during the experiment. In general, batch precipitation experiments provide a basis for calcium sulphate precipitation fouling studies. Two different methods of performing experiments have been utilized:

- Spontaneous precipitation in which both nucleation and crystal growth occur.
- Seeded precipitation in which crystal growth kinetics are studied in the absence of significant nucleation.

Data obtained from the first type of experiment are obviously more difficult to interpret by kinetic models since it is necessary to distinguish between nucleation and crystal growth processes, and since the crystallization surface depends on the nucleation stage. Seeded precipitation on a controlled crystal surface produces more interpretable information on crystal growth kinetics. Most researchers consider batch precipitation as a surface reaction controlled process. This is often justified by testing for the effect of increasing stirrer speed and showing that it has a negligibly small effect at the mixing rate used to gather the kinetic data. However, Garside (1971) showed that a significant diffusional resistance may be sometimes present even when the mixing rate has a very small effect on the overall crystallization rate. Conflicting results in the literature could be due to the above uncertainty. There is no universal model that may be confidently used for all precipitates, and even for calcium sulphate a variety of models have been proposed to describe the kinetics of its precipitation.

### 2.5.1 Calcium Sulphate Kinetic Models

Earlier work on unseeded crystallization of calcium sulphate by Schierholtz (1958) suggested that the kinetics was first-order at 25°C, but the plot of his experimental results showed considerable deviations from linearity. McCartney and Alexander's results (1958) gave second-order plots for part of the crystallization range. In neither of these earlier studies was allowance made for the changing surface area which occurred during the growth. Smith and Sweett (1971) pointed out that in general, whenever the surface area of the crystals changes significantly during growth, it is necessary to incorporate its effect. They adopted a model to consider the crystal surface area changes during the crystallization process. The model starts with the following equation:

$$A_c = A_o (m / m_o)^{2/3} \quad (2.5.1.1)$$

where  $A_c$  is the surface area of crystals at any time  $t$ ,  $A_o$  and  $m_o$  are the surface area and the mass of crystals at time  $t_o$  and  $m$  is the mass of crystals at any time  $t$ . It was assumed that the shape of the growing crystals remains invariant during the growth process. They incorporated Equation (2.5.1.1) into a variety of kinetic models.

Nancollas (1968) proposed a geometric mean model which is based on the geometric mean of the concentrations of the ions:

$$-r_A = A_c k_R \{ [Ca^{2+}]^{1/2} [SO_4^{2-}]^{1/2} - K'_s \}^2 \quad (2.5.1.2)$$

where  $A_c$  and  $k_R$  are the total crystal surface area and reaction rate constant, respectively.

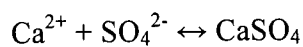
$K'_s$ , the ionic solubility product based on concentration rather than activity, can be written as:

$$K'_s = [Ca^{2+}]_s \cdot [SO_4^{2-}]_s \quad (2.5.1.3)$$

For the conditions where depositing species are in stoichiometric proportions, then:

$$-r_A = A_c k_R (C_A - C_s)^2 \quad (2.5.1.4)$$

Hasson (1981) discussed an ionic product model for calcium sulphate precipitation. The model treats the following crystallization reaction:



by analogy to an elementary reversible chemical reaction, which can be expressed as:

$$-r_A = A_c k_R \{ [Ca^{2+}] \cdot [SO_4^{2-}] - K'_s \} \quad (2.5.1.5)$$

When the depositing species are in stoichiometric proportions, then:

$$-r_A = A_c k_R (C_A^2 - C_s^2) \quad (2.5.1.6)$$

Konak (1974) proposed a different model for surface reaction-controlled growth of crystals from solution. He concluded that the growth rate is a function of supersaturation,  $(C_A - C_s)$ , rather than of supersaturation concentration,  $C_A$ , itself, and in almost all cases measured growth rates can be satisfactorily correlated by an equation of the form:

$$\text{Rate} = K(C_A - C_s)^n \quad (2.5.1.7)$$

where  $n$  lies between 1 (for the case of complete mass transfer control) and  $z$ , the number of ionic species obtained from the dissociation of one solute molecule, (for surface reaction controlled growth). In another study, Konak (1974) used a power law model in the form of:

$$-r_A = A_c k_R [C_A - C_s]^P \quad (2.5.1.8)$$

where  $P$  is an experimentally fitted parameter, which seems to coincide with  $z$  for surface reaction control. For calcium sulphate precipitation, it can be written as:

$$-r_A = A_c k_R (C_A - C_s)^2 \quad (2.5.1.9)$$

in agreement with Nancollas (1968). Many researchers have integrated the above expression for batch systems, which yields a simple linear relationship between  $(C_A - C_s)^{-1}$  and time  $t$ , and is useful for kinetic parameter evaluation.

Smith and Sweett (1971) studied the bulk crystallization of calcium sulphate dihydrate from aqueous solutions at 30°C in the absence of added seed crystals and indicated that nucleation was heterogeneous. They pointed out that the occurrence of crystal nucleation makes the kinetics of precipitation more complicated. It was observed that nucleation is complete in a very short time after solution preparation, which suggests heterogeneous rather than homogeneous nucleation. They found that the rate of

crystallization was slightly dependent on the stirring conditions. As the rate of stirring was increased, the growth rate approached a constant value, suggesting that the growth rate was not diffusion controlled at high stirring rates and that the rate-determining step was then a surface reaction process. They performed seeded experiments at a range of temperatures from 50 to 90°C, and based on the extracted reaction rate constant results, a value of 63 kJ/mol was reported for the activation energy of the crystallization process. Also, they discussed further models in which activities are employed in rate expressions instead of concentrations.

In general, to establish the validity of each kinetic model it is necessary to show that the experimentally measured  $k_R$  is indeed constant under conditions specified by the model. In the above models, it is taken that the kinetic coefficient  $k_R$  depends on temperature as given by the Arrhenius relationship:

$$k_R = A_1 \exp(-E / RT) \quad (2.5.1.10)$$

where  $E$  is the activation energy for the crystallization surface reaction. Activation energy values for calcium sulphate precipitation, reported in the literature, are presented in Table 2.5.1.1. These values are mainly for bulk precipitation, except the values in the last row, which are for surface crystallization (Bansal et al., 2005), as explained with more details in section 2.7.

## 2.6 Crystallization Fouling Complexities and Simplifications

After the initiation period, crystals start growing on the heated surface and this process affects the flow hydrodynamics, making the fouling behaviour more complex. To understand the crystal growth mechanisms, a comprehensive knowledge of hydrodynamics of local flow, thermodynamics of solutions, and kinetics of crystal

growth is essential. In order to illustrate the complexity of any kind of crystallization process, Konak (1974) listed different physico-chemical steps taking place for an ionizing solute crystallizing from aqueous solution as follows:

- Transfer of ions from the bulk to the immediate vicinity of the crystals by eddy and molecular diffusion;
- Adsorption of ions on the surface;
- Surface migration of ions to the kinks;
- Dehydration of ions and kinks; the latter probably occurs through exchanges of water molecules occupying the kinks with already (partially or fully) dehydrated ions in the immediate vicinity of the kinks;
- Incorporation of ions into the crystal lattice;
- Counter-diffusion of water to the bulk of the solution.

Due to the occurrence of the aforementioned steps, adequate mathematical models for describing crystallization fouling are difficult to formulate. Bott (1995) pointed out that in order to avoid the problems of taking into account the details of the micro-phenomena by which new material may be incorporated into the crystal lattice, it is possible to lump these effects together in terms of a chemical reaction. The rate of reaction under these circumstances will depend upon the concentration distribution of ions in the region of the interface between liquid and heat transfer surface.

To date a number of models have been proposed for crystallization fouling and most of them are highly simplified because they are based on assumptions such as:

1. No crystal nucleation occurs during crystal growth period.
2. Deposit formation is uniform circumferentially.

**Table 2.5.1.1: Calcium Sulphate Crystallization (mainly in bulk fluid) Growth Characteristics**

| Reaction order | $T_b$ (°C) | E (kJ/mol) | Crystallization condition | Reference                   |
|----------------|------------|------------|---------------------------|-----------------------------|
| 1              | 25         | 44         | Unseeded                  | Schierholtz, 1958           |
| 2              | –          | –          | Unseeded                  | McCartney & Alexander, 1958 |
| 1.8            | 70-98      | –          | Single crystal growth     | Turner, 1965                |
| 2              | 15-45      | 65         | Seeded                    | Liu and Nancollas, 1970     |
| 2              | 25-40      | 44         | Seeded                    | Konak, 1971                 |
| 2              | 30-90      | 63         | Seeded and unseeded       | Smith and Sweett, 1971      |
| 2              | 25-90      | 53         | Seeded                    | He et al., 1994             |
| 2              | 50-55      | 105-219    | Surface crystallization   | Bansal et al., 2005         |

3. Only one type of fouling occurs.
4. The fouling layer is homogeneous.
5. The deposit surface roughness is neglected.
6. Changes in physical properties of the streams are neglected.
7. The initial condition of the surface is not considered.
8. The aging effect in the deposit layer is neglected.
9. Heat transfer through the deposit is one-dimensional.
10. The presence of nanometer sized particles in the bulk fluid is neglected.

Furthermore, most models only consider some of the variables, such as velocity, time, concentration, and temperature, whereas other parameters which are more difficult to evaluate are neglected, e.g. effect of simultaneous action of different fouling mechanisms, nature and condition of the initial surface, design of the equipment and fluctuations in operating conditions. In this section some of the important calcium sulphate fouling models are briefly discussed.

In general, the following expression stemming from a material balance is the basis for fouling studies such as those on calcium sulphate scaling:

$$\begin{aligned} \text{Net rate of deposition} &= \text{Rate of crystallization} + \text{Rate of particulate fouling} \\ &\quad - \text{Rate of deposit removal} \end{aligned}$$

or

$$\frac{dR_f}{dt}(\rho_f \lambda_f) = \dot{m}_c + \dot{m}_p - \dot{m}_r \quad (2.6.1)$$

where  $\frac{dR_f}{dt}$  is the fouling rate ( $\text{m}^2 \cdot \text{K}/\text{J}$ ),  $\dot{m}_c$  the crystallization deposition rate ( $\text{kg}/\text{m}^2 \cdot \text{s}$ ),

$\dot{m}_p$  the particulate fouling rate ( $\text{kg}/\text{m}^2 \cdot \text{s}$ ), and  $\dot{m}_r$  the removal rate ( $\text{kg}/\text{m}^2 \cdot \text{s}$ ).

Although some researchers have developed mathematical models considering crystallization and particulate fouling simultaneously (Sheikholeslami, 2000), there are unanswered questions about their individual fouling mechanisms, and this is a motivation for continuing research on crystallization and particulate fouling separately. In terms of experiment, the operating conditions are changed so as to approach purely crystallization or particulate fouling and as a result of that Equation (2.6.1) becomes simpler. For instance, if the system is essentially free of particles, e.g. by employing an in-line filter, then:

$$\frac{dR_f}{dt}(\rho_f \lambda_f) = \dot{m}_c - \dot{m}_r \quad (2.6.2)$$

The removal rate depends on both the cohesive and adhesive forces of the deposit layer and the shear stress, which is a result of the fluid velocity. For calcium sulphate crystallization there is still a debate about the presence of deposit removal.

## 2.7 Previous Crystal Growth and Crystallization Fouling Studies

Mullin and Garside (1967) studied the effect of fluid velocity on the face growth rate of potash alum crystals at 32°C over a range of concentration driving forces,  $\Delta C$ , from 0.003 to 0.015 kg of hydrate / kg of solution. In their measurements, a small crystal was mounted on a 1 mm tungsten wire in a chosen orientation. Solution of known temperature, supersaturation, and velocity was pumped through the cell containing the crystal, and the growth rate of the chosen crystal face was observed through a traveling microscope. Three important conclusions were made from their experimental results (Figure 2.7.1): firstly, the growth rate was not first order with respect to the supersaturation; secondly, the solution velocity had a significant effect on the growth rate; and thirdly, significant crystal growth did not appear to commence until a certain

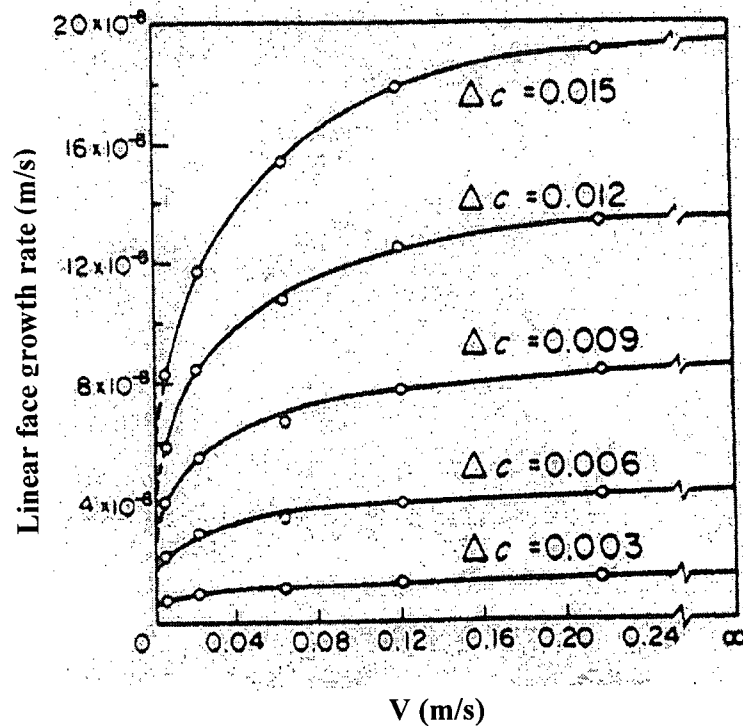


**Figure 2.7.1: Effect of Solution Velocity on the Face Growth Rate of Potash Alum Crystals at 32°C and  $\Delta C = 0.003 - 0.015$  kg of hydrate / kg of solution (Mullin and Garside, 1967)**

level of supersaturation was exceeded.

Using an electrically heated test tube, Ritter (1983) studied fouling of calcium sulphate and lithium sulphate during forced convective heat transfer under constant heat flux conditions. Based on the experimental results, he concluded that pure crystallization fouling is characterized by a linear fouling behaviour. An empirical equation was developed for fouling rate as a function of the solution supersaturation and the mass transfer coefficient. The final expression for fouling rate was as follows:

$$\frac{dR_f}{dt} = 1.9 \times 10^{-9} k_l \left( \frac{C_b - C_{sat}}{C_{sat}} \right)^2 \quad (2.7.1)$$

The exact operating conditions such as the filter pore size and system pressure were not described. According to Equation (2.7.1) the fouling rate increases with the mass transfer

coefficient  $k_1$  and therefore with velocity, i.e. calcium sulphate crystallization is mass transfer controlled. Other important results of the aforementioned study along with a summary of calcium sulphate scaling results, mainly under non-boiling conditions, from other investigators are presented in Table 2.7.3 at the end of section 2.7.

Nancollas (1983) studied crystallization in a stirred tank of the inverse solubility salts such as calcium sulphate and calcium carbonate and suggested that, for both, the deposition rate is controlled by surface reaction. In his model, activation energies for crystal growth are higher than those for diffusion controlled rates. He also mentioned that the fluid velocity had a negligible effect on the surface crystallization rate. He developed the following expression for the fouling rate of a salt with the formula  $M_aX_b$ :

$$\text{Rate} = \frac{d(C_{M_aX_b})}{dt} = -k_r S K_{SP}'^{(n/v)} \sigma^n \quad (2.7.2)$$

where

$K_{SP}'$  is the solubility product,  $n$  is the reaction order,  $v = a+b$ ,  $S$  is some function of surface area, and

$$\sigma = \left[ (M^{m+})^a (X^{x-})^b \right]^{1/v} - K_{SP}'^{1/v} \quad (2.7.3)$$

In Equation (2.7.2), activities of the lattice ions may be used as well. In this model, the rate of calcium sulphate crystallization follows a parabolic relationship with supersaturation which is characteristic of second order reactions.

Krause (1993) developed a model for calcium sulphate crystallization, similar to Hasson's model (1981), based on ion transport from the bulk to the crystal surface and second order integration of the ions into the surface. The final expression for the deposition rate is as follows:

$$\dot{m}_d = k_m \left[ \frac{1}{2} \left( \frac{k_m}{k_r} \right) + (C_b - C_{sat}) - \sqrt{\frac{1}{4} \left( \frac{k_m}{k_r} \right)^2 + \left( \frac{k_m}{k_r} \right) (C_b - C_{sat})} \right] \quad (2.7.4)$$

where both mass transfer coefficient,  $k_l$ , and surface reaction rate constant,  $k_r$ , are important. Equation (2.7.4) is the exact solution of the following equation, introduced by Hasson (1981), without considering the changes in crystal surface area  $A_c$ :

$$\frac{\dot{m}}{A_c k_r} = \left( [Ca^{2+}] - [Ca^{2+}]_s - \frac{\dot{m}}{A_c k_m} \right)^2 \quad (2.7.5)$$

where  $\dot{m}/A_c = \dot{m}_d$ ,  $[Ca^{2+}] = C_b$  and  $[Ca^{2+}]_s = C_{sat}$ .

Some years later, Bohnet et al. (1997) performed some experiments with an annular test section using calcium sulphate as the model solution. At high velocities, an asymptotic fouling behaviour was observed, whereas at low velocities it followed almost

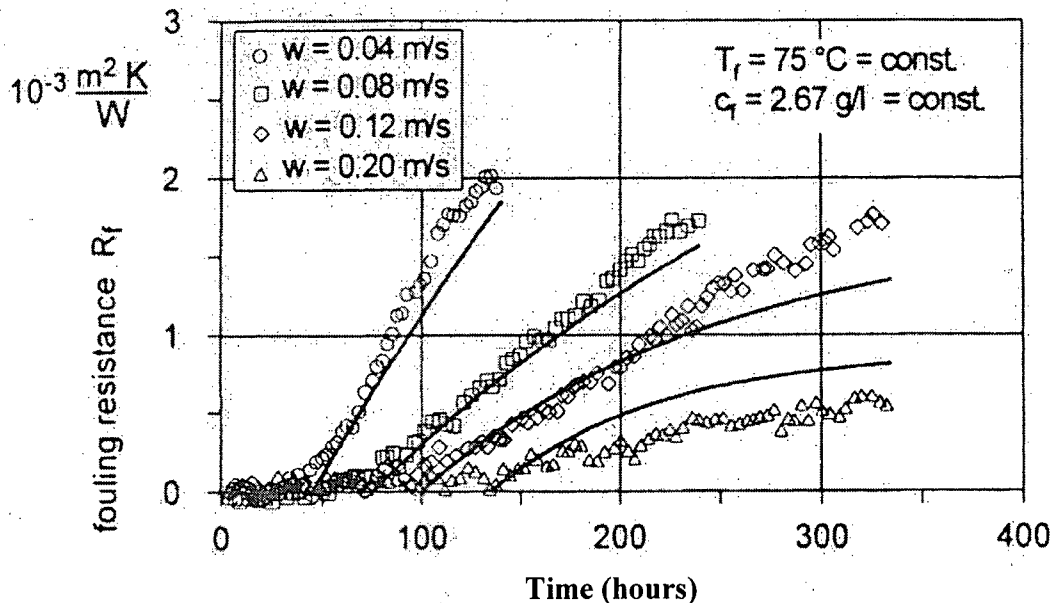


Figure 2.7.2: Effect of Velocity on Fouling Resistance (Bohnet et al. , 1997)

a linear trend as illustrated in Figure 2.7.2. In these experiments the surface temperature and concentration were kept constant at 75°C and 2670 ppm respectively. The fluid velocity was varied from 0.04 to 0.2 m/s and no in-line filter was employed to remove particles in the system. It is seen that as the velocity increases the initial fouling rate decreases. It was argued that the asymptotic behaviour is related to the action of a removal term which is directly proportional to the fluid shear stress, and inversely proportional to the deposit shear strength. The following expression was developed for shear strength of the scale layer:

$$\sigma_f = K_1 \frac{P}{N_f x_f (1 + \delta \Delta T) d_p} \quad (2.7.6)$$

Based on the above expression, the shear strength  $\sigma_f$  of the deposit layer depends on deposit thickness  $x_f$ , inter-crystalline adhesion force  $P$ , linear expansion coefficient of deposit  $\delta$ , number of fault points in the deposit layer  $N_f$ , temperature drop in the fouling layer  $\Delta T$ , and equivalent crystal diameter  $d_p$  ( $K_1$  is the proportionality constant). The following expression was developed for the removal rate:

$$\dot{m}_r = 52.5 \rho_f (1 + \delta \Delta T) d_p (\rho^2 \eta g)^{\frac{1}{3}} x_f v^{2.82} \quad (2.7.7)$$

Finally, combining Equations (2.7.4) and (2.7.7) and comparing the final result with the general asymptotic fouling equation,

$$R_f = R_f^* (1 - e^{-bt}) \quad (2.7.8)$$

yielded expressions for  $R_f^*$  and  $b$ :

$$R_f^* = \frac{k_m}{52.5 \rho_f \lambda_f (1 + \delta \Delta T) d_p (\rho^2 \eta g)^{\frac{1}{3}} v^{2.82}} \times \quad (2.7.9)$$

$$\left[ \frac{1}{2} \left( \frac{k_m}{k_r} \right) + (C_b - C_{sat}) - \sqrt{\frac{1}{4} \left( \frac{k_m}{k_r} \right)^2 + \left( \frac{k_m}{k_r} \right) (C_b - C_{sat})} \right]$$

$$b = 52.5 (1 + \delta \Delta T) d_p (\rho^2 \eta g)^{\frac{1}{3}} v^{2.82} \quad (2.7.10)$$

Bridgwater and Loo (1984) carried out experiments similar to those of Hasson and Zahavi (1970). They pointed out that the fouling curve showed repeated steady growth in  $T_w$  as scale develops followed by sudden drops due to spalling (Figure 2.7.3). Moreover, they observed that deposition did not occur at the tube wall temperatures of 80-87°C, and scale could only be formed if the wall temperature was raised to the boiling temperature at the system pressure.

Bansal and Müller-Steinhagen (1993) investigated crystallization fouling of calcium sulphate in a plate and frame heat exchanger and they observed that the formation of crystalline deposits in plate and frame heat exchangers is widely different from the fouling in conventional tubular heat exchangers. They explained that, because of the narrow flow channels, the formation of deposits significantly increases the local flow velocity, causing deposit removal and lower local interface temperatures. Also, they pointed out that crystallization of gypsum is surface reaction controlled and that the rate of deposition increases with increasing wall temperature and bulk concentration, and with decreasing velocity. They concluded that, with increasing flow velocity, both the initial fouling rate (Figure 2.7.4) and the absolute value of fouling resistance decrease. Their stated reason for the rate effect was the lower wall temperature at higher flow

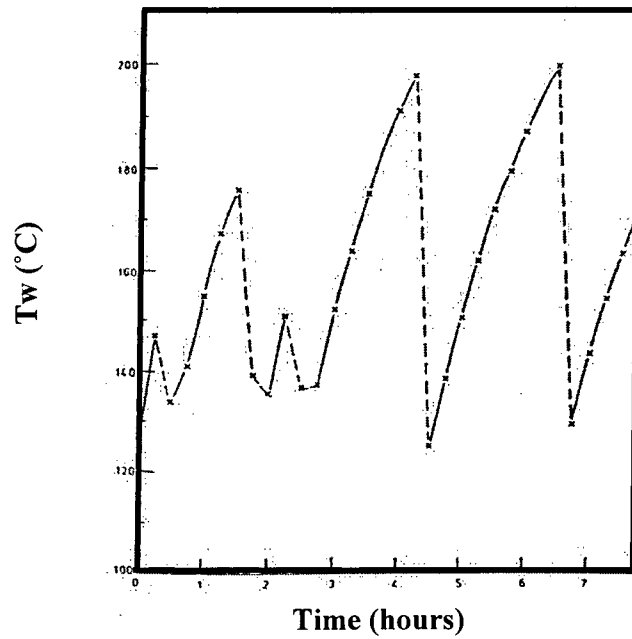


Figure 2.7.3: Calcium Sulphate Fouling Curve (Bridgwater & Loo, 1984)

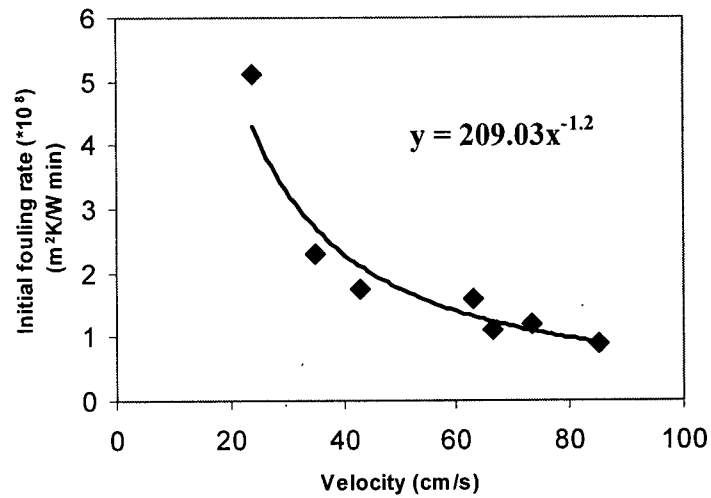


Figure 2.7.4: Effect of Velocity on Initial Fouling Rate in Plate Heat Exchangers (Bansal and Muller-Steinhagen, 1993)

velocities, whereas the decrease in absolute value of the fouling resistance was explained by a higher removal rate at a lower interface temperature. This conclusion was based only on the bulk temperature measurements, i.e. without surface temperature measurement. Also, they found that concentration is an important factor only in the initial stages of the fouling process whereas its changes, from 2622 to 2945 ppm, did not affect the fouling rate once the initial deposition had occurred. They carried out other experiments (Bansal and Müller-Steinhagen, 1997, 2000, and 2001) and found that no crystal formation occurred in the bulk fluid under their operating conditions of  $T_b$  from 50 to 55°C, their stated reason for which was the low bulk temperature (low surface reaction rate constant). Also, they found that solution filtration decreased the fouling rate (Figure 2.7.5), and recycling part of the outlet flow directly to the plate heat exchanger increased the initial fouling rate. Moreover, using 1  $\mu\text{m}$  alumina particles (inert particles) at a concentration of 82 ppm decreased the initial fouling rate by 50 %.

Najibi et al. (1997) studied calcium sulphate scale formation during subcooled flow boiling. To find the controlling fouling mechanism, they performed experiments over a range of fluid velocities under a constant degree of supersaturation and constant bulk and surface temperatures. They concluded that at low fluid velocities the fouling process was mass transfer controlled. However, as the velocity was increased to  $Re \geq 35000$ , mass transfer no longer affected the fouling rate, which meant that the fouling process was then controlled by chemical reaction. Since the reaction rate constant depends only on the surface temperature, the curves shown in Figure 2.7.6 level off for higher velocities. Also, they concluded that the bulk temperature did not substantially affect the fouling behaviour (Figure 2.7.7).

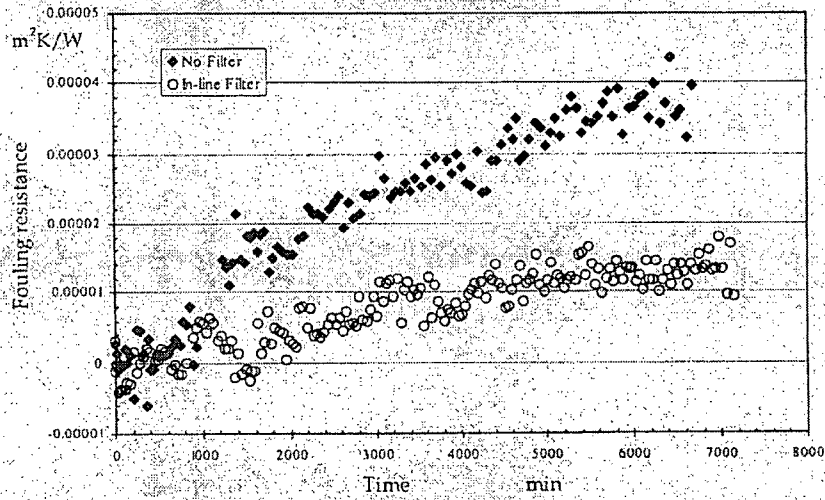


Figure 2.7.5: Effect of Filtration on Fouling Resistance (Bansal et al. , 1997)

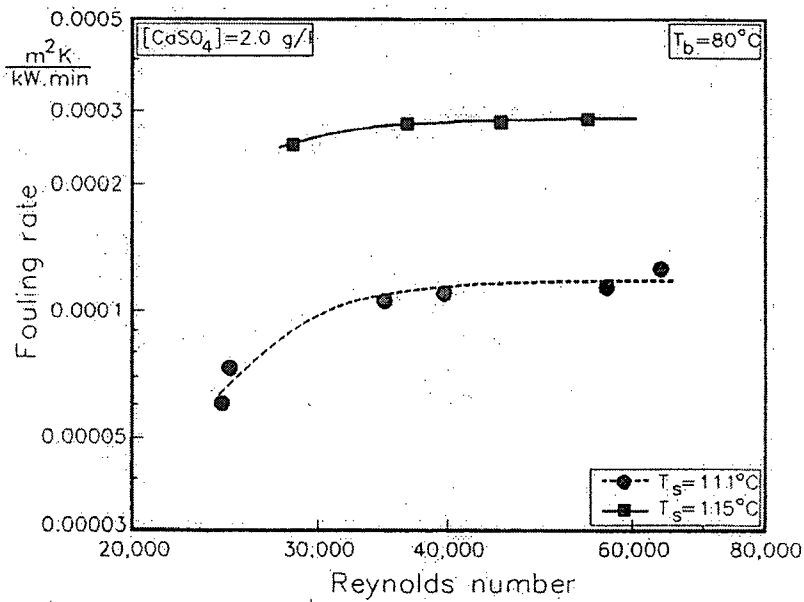
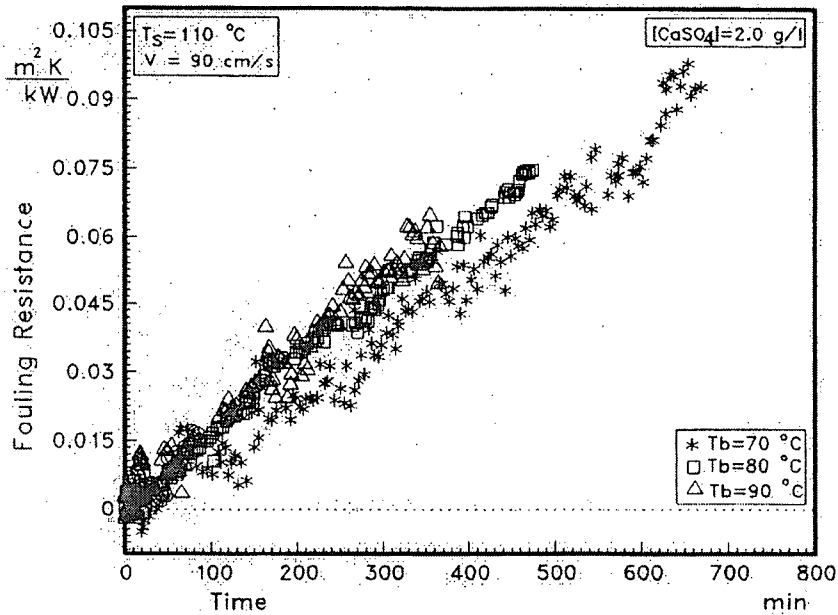


Figure 2.7.6: Fouling Rate as a Function of Reynolds Number (Najibi et al., 1997)



**Figure 2.7.7: Effect of Bulk Temperature on the Fouling Resistance (Najibi et al., 1997)**

Mori et al. (1996) used an electrically heated annular heat exchanger to study calcium sulphate scaling. They showed that both the asymptotic fouling resistance and deposition rate decrease with increasing fluid velocity at constant surface temperature. Also, conductivity of the deposit layer was estimated to be 2.2 W/m·K. They reported that the activation energy is 62 kJ/mol based on the following equation:

$$R_f^* = A \exp(-E / RT_s) \quad (2.7.11)$$

Epstein (1995) criticized this approach for activation energy evaluation on the grounds that it is the initial fouling rate,  $\dot{R}_{fo}$ , from Equation (2.7.8), namely

$$\dot{R}_{fo} = (dR_f / dt)_{t=0} = bR_f^* \quad (2.7.12)$$

that should be correlated in the Arrhenius manner rather than  $R_f^*$  alone. He described different methods of deriving an asymptotic fouling equation involving

**Table 2.7.1: Fouling Rate and Asymptotic Fouling Resistance Values (Mwaba et al., 2001)**

| V (m/s) | $\Delta R_f / \Delta t$ ( $m^2K/J$ ) | $R_f^*$ ( $m^2K/W$ )                              |
|---------|--------------------------------------|---|
| 0.3     | $3.75 \times 10^{-9}$                | $5.0 \times 10^{-4}$                              |
| 0.6     | $3.99 \times 10^{-9}$                | $3.8 \times 10^{-4}$                              |
| 1.0     | $3.59 \times 10^{-9}$                | Experiment was terminated before reaching $R_f^*$ |

autoretardation and removal mechanisms. He concluded that if  $b$ , which is a proportionality constant and is a function of velocity, does not change significantly with surface temperature, the approximate applicability of Equation (2.7.11) is then acceptable.

Mwaba et al. (2001) investigated the influence of surface temperature and fluid velocity on the calcium sulphate scaling on a heated plate. Their experimental results for fouling rate and asymptotic fouling resistance under different fluid velocities are presented in Table 2.7.1. Although, based on the values in Table 2.7.1, they concluded that the fouling rate was independent of fluid velocity, the data give some indication of a maximum value of fouling rate in the vicinity of 0.6 m/s (which corresponds to  $Re = 30500$ ). They noted that the asymptotic fouling resistance decreased with fluid velocity, which they believed was due to removal effects.

Kazi et al. (1999, 2001) carried out some experiments using two types of equipment (a tubular heat exchanger heated electrically and a pipe cooled in an agitated tank). They observed that at constant heat flux the fouling buildup was asymptotic and

that the fouling resistance at any given time, and thus the fouling rate, decreased with increasing bulk velocity. Moreover, they concluded that increasing the surface roughness from 0.22 to 0.47  $\mu\text{mRa}$  (Ra is the arithmetic average roughness) increased fouling by providing more sites for nucleation; the polycarbonate pipe exhibited lower fouling than the stainless steel surface under the same conditions of foulant concentration and mixing conditions.

Middis et al. (1998) used a tube with an external electrical heater as the test section. Their experimental results (Figure 2.7.8), performed at a clean surface temperature of  $55^\circ\text{C}$  ( $\Delta T_o = T_s - T_b = 15^\circ\text{C}$ ) over a range of Reynolds number from 18000 to 36000, showed that the initial fouling rate decreased with increasing velocity.

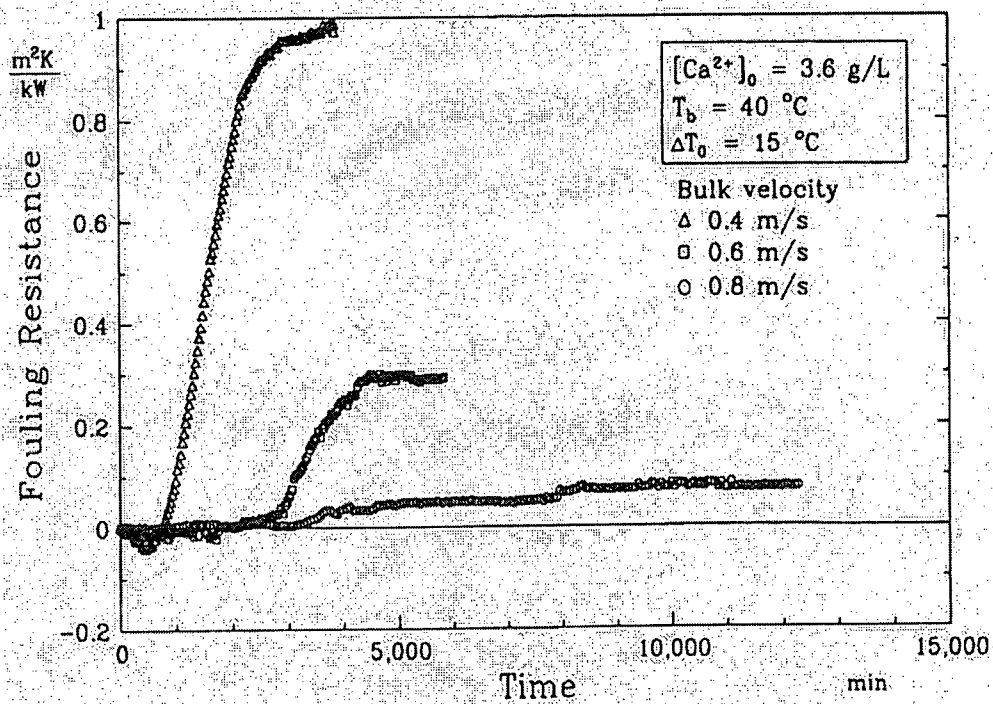
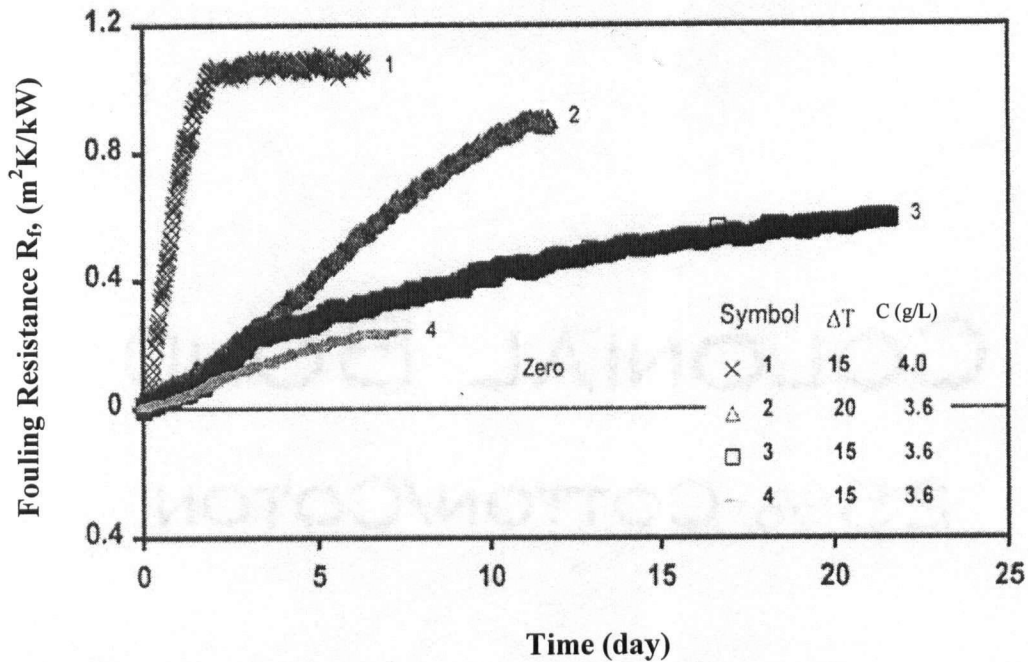


Figure 2.7.8: Effect of Velocity on Calcium Sulphate Fouling Resistance (Middis et al. , 1998)



**Figure 2.7.9: Effect of Velocity on Calcium Sulphate Fouling Resistance (Curve 3 at 0.4 m/s and Curve 4 at 0.6 m/s) (Kazi et al. , 2002)**

They argued that the asymptotic fouling behaviour confirms that a combination of particulate and crystallization fouling occurs. The particles could have been formed either by crystallization in the bulk or by reentrainment of the deposit from the fouling layer.

Kazi et al. (2002) used the same apparatus as Middis et al. (1998) and observed almost the same trend. Their experimental results are shown in Figure 2.7.9, which indicates a decrease in the initial fouling rate with an increase in velocity, a conclusion arrived at by comparing fouling curve 3 with that of curve 4 at 0.4 and 0.6 m/s, respectively. The clean surface temperature and concentration for both of the velocities were 55°C and 3600 ppm, respectively, and no in-line filter was employed to remove particles.

Recently, Bansal et al. (2005) reviewed their previous studies, discussed several aspects of calcium sulphate scaling, and developed a model for calcium sulphate deposition in a plate heat exchanger. In one section of the paper they discussed several mechanisms for deposit removal, i.e. spalling (thermal shock), erosion (hydrodynamic forces), and dissolution (chemical). They pointed out that, according to the experimental setup, only erosion could contribute to the deposit removal, and they determined numerical values of the removal rates from turbulent burst theory, which indicated that they were negligible, so they neglected the deposit removal in their model. To see whether or not the deposit removal occurred experimentally, two experiments, with and without an in-line 1  $\mu\text{m}$  filter, were performed, and based on these results, they concluded that there was some removal of calcium sulphate deposits. Figure 2.7.10 shows the experimental results vs. model predictions. Also, they discussed the kinetics of calcium sulphate scaling, and from their fouling experimental results, Figure 2.7.11, the entire

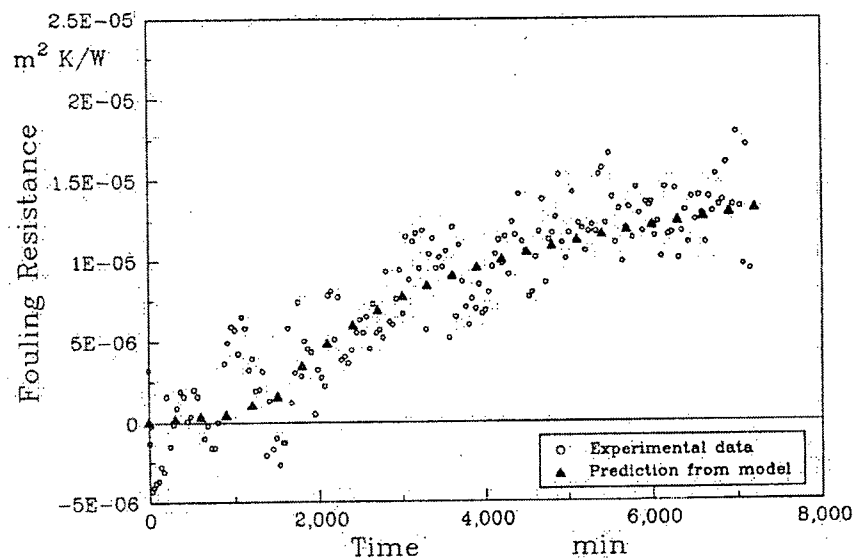


**Figure 2.7.10: Experimental vs. Predicted Fouling Resistances (Bansal et al. , 2005)**

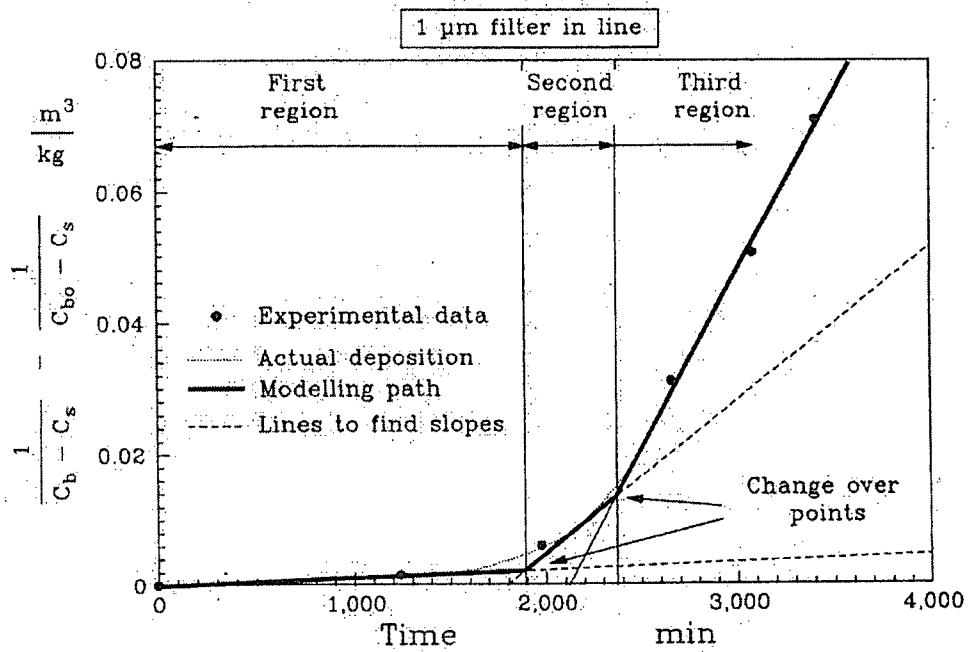


**Figure 2.7.11: Different Growth Rate Regions (Bansal et al., 2005)**

**Table 2.7.2: Activation Energy Values for Different Regions (Bansal et al., 2005)**

| Presence of in-line filter | Region number               | E (kJ/mol) |
|----------------------------|-----------------------------|------------|
| None                       | Three (growth)              | 108        |
| 1 $\mu\text{m}$            | One (nucleation)            | 219        |
| 1 $\mu\text{m}$            | Two (nucleation and growth) | 105        |
| 1 $\mu\text{m}$            | Three (growth)              | 134        |

fouling process was divided into three different stages. The first stage represents mainly crystal nucleation, while in the second stage further nucleation takes place and some nuclei grow into crystals, and finally the third stage represents primarily crystal growth. Only the third stage could be identified when faster fouling rates were observed in the absence of the in-line filter. Different activation energies corresponding to different regions were evaluated and are presented in Table 2.7.2. All investigation results on calcium sulphate scaling are presented in Table 2.7.3.

## 2: Literature Review

**Table 2.7.3: Summary of Calcium Sulphate Scaling Studies Mainly under Non-boiling Conditions**

| Reference            | Solution Preparation Method | Velocity (m/s) | T <sub>s</sub> (C) | Heating Section            | Delay Time(hr) | R <sub>f</sub> (m <sup>2</sup> K/k·W) | When Velocity increases initial fouling rate | Solution Filtration | Comments   |
|----------------------|-----------------------------|----------------|--------------------|----------------------------|----------------|---------------------------------------|--|---------------------|--|
|                      | Concentration (ppm)         | Re             | T <sub>b</sub> (C) | Power Supply               | Run Time (hr)  | Behavior                              |  |                     |  |
| Bansal et al. 2001 b | By Reaction                 | 0.22-0.435     | <88                | Double pipe heat exchanger | 4              | 0.1                                   |  | Yes                 | Heat flux was not constant   |
|                      | 2500-3000                   | 9000           | >60                | Hot water                  | 58             | Asymptotic                            |  |                     | No surface temperature measurement   |
|                      |                             |                |                    |                            |                |                                       |  |                     | Shear force is low in pipe heat exchangers   |
|                      |                             |                |                    |                            |                |                                       |  |                     | Fouling resistance is higher in pipe heat exchangers   |
| Bansal et al. 2001 a | By Reaction                 | 0.35           | <88                | Plate Heat exchanger       | 8              | 0.015                                 |  | Yes                 | Heat flux was not constant   |
|                      | 2500-3000                   | 4000           | >50                | Hot water                  | 58             | Asymptotic                            |  |                     | No surface temperature measurement   |
|                      |                             |                |                    |                            |                |                                       |  |                     | Turbulence level is higher in plate heat exchangers  |
|                      |                             |                |                    |                            |                |                                       |  |                     | Fouling is reaction controlled   |
| Mwaba et al. 2001    | By Reaction                 | 0.3-1          | 65-82              | Flat plate                 | 5 to 38        | 0.38-0.5                              | does not change                              | No                  | The delay time increases with increasing velocity while the maximum fouling resistance decreases |
|                      | 3200                        | 16000-53000    | 40                 | Electricity 800 W          | 96             | Asymptotic                            |  |                     | The rate of deposition is independent of velocity  |
| Kazi et al. 2001     | By Reaction                 | 0.05-0.1       | 55-63              | Pipe in a tank             | 16             | 150-300                               |  | No                  | Surface effect on the fouling is as follows:<br>Cu > Aluminium > Brass > Stainless steel         |
|                      | 3000-4000                   | 1500-3000      | 40                 |                            | Hot water      | 67                                    |  |                     | Asymptotic   |
| Bansal et al. 2001 a | By Reaction                 | 0.35-0.71      | 68-75              | Plate Heat exchanger       | 10 to 18       | 0.032 (Max)                           |  | Yes                 | The series flow arrangement has much more severe fouling than parallel arrangement               |
|                      | 2985                        | -              | 50-75.5            | Hot water                  | -              | Linear                                |  |                     |  |
| Bansal et al. 2000   | By Reaction                 | 0.183-0.667    | <88                | Plate Heat exchanger       | 4              | 0.0075                                |  | Yes                 | Heat flux was not constant during the experiments  |
|                      | 2826-3192                   | 4000-9000      | >50                | Hot water                  | 116            | Asymptotic                            |  |                     | No surface temperature measurement   |
| Kazi et al. 1999     | By Reaction                 | 0.4-0.6        | 60                 | Tubular                    | -              | 0.6                                   | Decreases                                    | No                  | Fouling process was a combination of crystallization and particulate fouling                     |
|                      | 3000-4000                   | 40000-60000    | 40                 | Electricity                | 16-50          | Asymptotic                            |  |                     |  |

## 2: Literature Review

**Table 2.7.3: Summary of Calcium Sulphate Scaling Studies Mainly under Non-boiling Conditions (cont'd)**

| Reference                       | Solution Preparation Method | Velocity (m/s) | T <sub>s</sub> (C)       | Heating Section        | Delay Time(hr) | R <sub>f</sub> (m <sup>2</sup> K/k-W) (Ranges) Behavior | When Velocity increases initial fouling rate | Solution Filtration | Comments  |
|---------------------------------|-----------------------------|----------------|--------------------------|------------------------|----------------|---|--|---------------------|---|
|                                 | Concentration (ppm)         | Re             | T <sub>b</sub> (C)       | Power Supply           | Run Time (hr)  |   |  |                     |   |
| Mwaba et al. 1999               | By Reaction                 | 0.11           | 70                       | Flat plate             | -              | -   |  | No                  | Al <sub>2</sub> O <sub>3</sub> (40 ppm, 30-200 μm) was used as inert particles  |
|                                 | 3400                        | 3400           | 40                       | Electricity 400 W      | 36             | Asymptotic  |  |                     | Inert particles decrease the final fouling resistance up to 70%   |
| Middis et al. 1998              | By Reaction                 | 0.4-0.8        | 55                       | Tubular                | 12             | 1   | Decreases                                    | No                  | Fouling was a combination of particulate and scaling  |
|                                 | 3600                        | 18000-36000    | 40                       | Electricity            | 67-100         | Asymptotic  |  |                     | EDX shows that the deposit is CaSO <sub>4</sub>   |
| Bansal et al. 1997              | By Reaction                 | 0.35-0.7       | <88                      | Plate heat exchanger   | 10             | 0.015   |  | Yes                 | Presence of CaSO <sub>4</sub> particles increases initial fouling rate  |
|                                 | 2985                        | -              | 50-52                    | Hot water              | 92-108         | Asymptotic  |  |                     | Presence of Al <sub>2</sub> O <sub>3</sub> particles (1 micron, 82.4 ppm) decreases the initial fouling rate                |
| Najibi et al. 1997              | By Reaction                 | 0.5-2          | 95-140                   | Annular                | 0-45           | 0.1   | Increase                                     | Yes                 | Experiment was under subcooled flow boiling conditions  |
|                                 | 1600-2700                   | 33000-215000   | 65-95                    | Electricity 0.5-1 kW   | 2.6-60         | (Max) Linear  |  |                     | Activation energy is 112.5 kJ/mol<br>Deposit density is 2.16 g/cm <sup>3</sup><br>Deposit thermal conductivity is 2.2 W/m-K |
| Mori et al. 1996                | Without Reaction            | 1-1.3          | 64-70                    | Annular                | 30             | 0.05  | Decreases                                    | No                  | The micrograph shows that the deposit is gypsum   |
|                                 | Saturated                   | 48000-52000    | 36-46                    | Electricity 2.2-4.5 kW | 90             | Asymptotic  |  |                     | Fouling mechanism is surface process controlled<br>Activation energy is 62 kJ/mol   |
| Bramson et al. 1995             | Without Reaction            | 3 gr/cm·s      | 110(T <sub>steam</sub> ) | Falling film           | -              |   |  | Yes                 | Scale adherence was very poor<br>Average deposition rate was 1 EXP(-5) m/hr<br>Nucleate boiling increases the fouling rate  |
|                                 | Saturated                   | 3400           | 65                       | Steam                  | 3.5            |   |  |                     | Particulate fouling is the dominant mechanism in CaSO <sub>4</sub> crystallization  |
| Bansal & Muller-Steinhagen 1993 |                             |                |                          | Plate Heat exchanger   |                | 0.03  | Decreases                                    | No                  | Heat flux was not constant  |
|                                 | By Reaction                 | 0.24-0.9       | <88                      | Hot water              | 5              | (Max) Decreasing Fouling                                |  |                     | No surface temperature measurement<br>Fouling is reaction controlled<br>Quick fouling happens at the outlet                 |
|                                 | 2500-3000                   | 2400-10500     | >50.5                    |                        | 50-91          |   |  |                     |   |

## 2: Literature Review

**Table 2.7.3: Summary of Calcium Sulphate Scaling Studies Mainly under Non-boiling Conditions (cont'd)**

| Reference              | Solution Preparation Method | Velocity (m/s) | T <sub>s</sub> (C) | Heating Section         | Delay Time(hr) | R <sub>f</sub> (m <sup>2</sup> K/k-W) (Ranges) Behavior | When Velocity increases initial fouling rate | Solution Filtration | Comments  |
|------------------------|-----------------------------|----------------|--------------------|-------------------------|----------------|---|--|---------------------|---|
|                        | Concentration (ppm)         | Re             | T <sub>b</sub> (C) | Power Supply            | Run Time (hr)  |   |  |                     |   |
| S.Krause 1993          | Without Reaction            | 0.5 to 1.3     | 75-88              | Annular                 | 20             | 0.05-0.6  |  | No                  | Wilson plot was employed to get wall temperature  |
|                        | Saturated                   | 12000-33000    | 42.7-45.1          | Electricity 8 kW        | 210-300        | Asymptotic  |  |                     | Activation energy is 37.1 kJ/mol  |
| M.Bohnet 1987          | Without Reaction            | 0.5 to 1.3     | 75-88              | Annular                 | 12.3-58.1      | 0.05-0.6  | Decreases                                    | No                  | Deposit thermal conductivity is 1.15 W/m-K  |
|                        | Saturated                   | 12000-33000    | 42.8-45            | Electricity 8 kW        | 210-730        | Asymptotic  |  |                     | Deposit density = 2.013 to 2.16 g/cm <sup>3</sup>                                       |
| Bridgwater & Loo 1984  | Without Reaction            | 0.3-0.6        | 125                | Annular                 | -              | -   |  | Yes                 | Activation energy is 40.4 kJ/mol  |
|                        | Saturated                   | 12700-23000    | 55                 | Electricity 12 kW       | 8              | Saw-tooth   |  |                     | The intercrystalline adhesion forces increase with fluid velocity                       |
| R.B. Ritter 1983       | Without Reaction            | 0.3-3          | 93-141             | Annular                 | 1 to 53        | -   | Increases                                    |                     | No observation of propagation front during the deposition process                       |
|                        | Saturated                   | 17000-160000   | -                  | Electricity 3.0-86.0 kW | 0-2.6          | Linear  |  |                     | Spalling occurred frequently  |
| Hasson and Zahavi 1970 | Without Reaction            | 0.165 or 0.223 | 80&87              | Annular                 | 0.2-1          |   |  | Yes                 | Scaling occurs only when the temperature increases to the boiling temperature           |
|                        | 2020-2050                   | 11000-15000    | 50&55              | Electricity 3 kW        | 48             |   |  |                     | Fouling rate is inversely proportional to the square root of the induction period       |
| R. M.Fand 1969         | Without Reaction            | 0.2-0.46       | 111-139            | circular cylinder       | -              | not   | Increases                                    |                     | No surface temperature measurement  |
|                        | 2044                        | -              | 65.5               | Electricity 500W        | 30-120         | monotonic   |  |                     | 0.58 W/m-K was used for thermal conductivity  |
|                        |                             |                |                    |                         |                |   |  |                     | Deposit density = 2.7- 3 g/cm <sup>3</sup>  |
|                        |                             |                |                    |                         |                |   |  |                     | Boiling happens during the experiment   |
|                        |                             |                |                    |                         |                |   |  |                     | Fouling starts rapidly in the aft of the heating section and develops to the front part |
|                        |                             |                |                    |                         |                |   |  |                     | Deposit thermal conductivity is 1.12 - 1.56 W/m-K                                       |

**2: Literature Review**

**Table 2.7.3: Summary of Calcium Sulphate Scaling Studies Mainly under Non-boiling Conditions (cont'd)**

| Reference              | Solution Preparation Method | Velocity (m/s) | T <sub>s</sub> ( C ) | Heating Section     | Delay Time(hr) | R <sub>f</sub> (m <sup>2</sup> K/k-W) (Ranges) | When Velocity increases initial fouling rate | Solution Filtration | Comments  |
|------------------------|-----------------------------|----------------|----------------------|---------------------|----------------|--|--|---------------------|---|
|                        | Concentration (ppm)         | Re             | T <sub>b</sub> ( C ) | Power Supply        | Run Time (hr)  | Behavior                                       |  |                     |   |
| Banchemo & Gordon 1960 | Without Reaction            | 0.61-3.05      | 97-140               | Helical coil        |                |  |  | Yes                 | The higher the surface temperature, the smaller the induction period            |
|                        | 1160-2160                   | 10000-50000    | -                    | Hot water           |                |  |  |                     | Induction period is independent of velocity between 0.61 and 3.05 m/s           |
| Knudsen & McCluer 1959 | Without Reaction            | 1.03-1.24      | 83-89                | Annular finned tube |                | 0.58 (Max)                                     | Increases                                    | Yes                 | Corner between the fin and the main tube showed more deposits                   |
|                        | Saturated                   | -              | 56-63                | Hot water           |                | Different trends                               |  |                     | Fin-spacing ratio is an important parameter for controlling the deposition rate |

## 2.8 Theoretical Fouling Model

A theoretical model for the initial fouling rate in turbulent flow, where surface attachment is treated as a physico-chemical rate process in series with mass transfer, has been proposed (Epstein, 1994) and applied successfully to styrene polymerization fouling. The model focuses on initial fouling rate,  $\dot{R}_{fo}$ , where time zero is taken as the time when measurable fouling can first be detected. It has been tested for colloidal particle deposition (Vasak et al., 1995) and chemical reaction fouling (Rose, 1999), but it has not been tested for precipitation fouling. In this study, the model will be tested using experimental data for calcium sulphate scaling under non-boiling conditions.

### 2.8.1 Mathematical Model Development for Precipitation Fouling

Crystallization may be divided into two major steps: (1) the transport of ions to the crystal-growth in the boundary layer which can be given by

$$\phi_{do} = k_m (C_b - C_w) \quad (2.8.1.1)$$

and (2) the integration of ions into the crystal surface which can be given by

$$\phi_{do} = k_a (C_w - C_{sat})^n \quad (2.8.1.2)$$

where  $n$ , the surface reaction order was retained in Epstein's derivation. In the present case, for calcium sulphate, based on several research studies, it is equal to 2 and the derivation is simplified, i.e.,

$$\phi_{do} = k_a (C_w - C_{sat})^2 \quad (2.8.1.3)$$

By combining Equations (2.8.1.1) and (2.8.1.3) we obtain:

$$\frac{\phi_{do}^2}{k_m^2} - \left( \frac{2\Delta C}{k_m} + \frac{1}{k_a} \right) \phi_{do} + (\Delta C)^2 = 0 \quad (2.8.1.4)$$

$$\text{where } \Delta C = C_b - C_{sat} \quad (2.8.1.5)$$

Solving Equation (2.8.1.4), which is a second order equation with respect to  $\phi_{do}$ , and considering the fact that always  $\phi_{do} < k_m \Delta C$ :

$$\phi_{do} = k_m \left( \frac{k_m}{2k_a} + \Delta C - \sqrt{\frac{1}{4} \left( \frac{k_m}{k_a} \right)^2 + \frac{k_m}{k_a} \Delta C} \right) \quad (2.8.1.6)$$

which is mathematically identical to Equation (2.7.4) by Krause (1993). The fouling resistance,  $R_f$ , is given by the following equation, assuming constant average foulant physical properties:

$$R_f = \frac{x_f}{\lambda_f} = \frac{m_f}{\rho_f \lambda_f} \quad (2.8.1.7)$$

From this it follows that the fouling rate,  $\dot{R}_f (= dR_f/dt)$ , is dependent on the rate of precursor converted to foulant and deposited on the heat transfer surface. Therefore initial fouling rate,  $\dot{R}_{fo}$ , can be related to initial mass flux,  $\phi_{do}$ , by

$$\dot{R}_{fo} = \frac{r \phi_{do}}{\lambda_f \rho_f} \quad (2.8.1.8)$$

where the stoichiometric ratio,  $r$ , is the mass of fouling deposit per mass of precursor required to produce it.

For turbulent liquid solution flow parallel to a heat transfer surface, and assuming fully developed velocity and concentration boundary layers, then in good approximation (Treybal, 1980),

$$k_m = v_* / k' Sc^{2/3} \quad (2.8.1.9)$$

Equation (2.8.1.9) can be written as:

$$k_m = v_* / k_1 \quad (2.8.1.10)$$

where

$$k_1 = k' Sc^{2/3} \quad (2.8.1.11)$$

Metzner and Friend (1958) reported a value of 11.8 for  $k'$  under isothermal fluid flow conditions.

A new feature of the present model which distinguishes it from prior work is introduction of the term  $\nu/v_*^2$  that is associated with periodic shedding and renewal of the viscous sublayer (Meek, 1972). It can alternately be rationalized as follows:

For a fluid flowing through a pipe, a very thin viscous sublayer exists near the wall with a linear relationship between  $v$  and  $y$  given by the universal velocity distribution equation (Knudsen and Katz, 1958),

$$\frac{v}{v_*} = \frac{v_*}{\nu} y \quad (2.8.1.12)$$

Near the heat transfer surface, the fluid residence time  $\theta$  is inversely proportional to velocity  $v$  within the viscous sublayer, and therefore

$$\theta \propto \frac{\nu}{yv_*^2}$$

The attachment coefficient,  $k_a$ , at the surface may be written as being proportional to the product of the kinetic rate constant, which bears the usual Arrhenius relationship to the surface temperature, and the fluid residence time in the vicinity of the surface (Epstein, 1994). The Arrhenius term describes the strong dependence of the reaction rate constant,  $k_r$ , on surface temperature, while the fluid residence time allows for the fact the longer the fouling material spends at the heat transfer surface, the greater the probability that it will deposit, i.e.,

$$k_a \propto k_r \theta \propto e^{-\Delta E / RT_w} \theta$$

Consequently, for an arbitrary, small but fixed value of  $y$ ,

$$k_a \propto \frac{v}{v_*^2} e^{-\Delta E / RT_w}$$

Therefore

$$k_a = \frac{v e^{-\Delta E / RT_w}}{k'' v_*^2} \quad (2.8.1.13)$$

The attachment constant  $k''$  includes both the Arrhenius pre-exponential factor and the residence time proportionality factor. Examination of Equation (2.8.1.13) shows that for a given fluid with constant concentration, and fixed tube wall temperature,

$$k_a = \frac{1}{k_2 v_*^2} \quad (2.8.1.14)$$

where

$$k_2 = \frac{k'' e^{\Delta E / RT_w}}{v}$$

Substitution of Equations (2.8.1.8), (2.8.1.10), and (2.8.1.14) into Equation (2.8.1.6) leads to:

$$\dot{R}_{f_0} = \frac{rv_*}{k_1 \rho_f \lambda_f} \left( \Delta C + \frac{k_2 v_*^3}{2k_1} - \sqrt{\frac{1}{4} \left( \frac{k_2 v_*^3}{k_1} \right)^2 + \frac{k_2 v_*^3}{k_1} \Delta C} \right) \quad (2.8.1.15)$$

Equation (2.8.1.15) can be rearranged by introducing new terms:

$$k_3 = \frac{r}{k_1 \rho_f \lambda_f}$$

$$k_4 = \frac{k_2}{k_1}$$

and then Equation (2.8.1.15) becomes

$$\dot{R}_{fo} = k_3 v_* \left( \Delta C + \frac{k_4 v_*^3}{2} - \sqrt{\frac{1}{4} (k_4 v_*^3)^2 + k_4 v_*^3 \Delta C} \right) \quad (2.8.1.16)$$

Equation (2.8.1.16) correlates the initial fouling rate explicitly as a function of important variables such as fluid velocity, wall temperature, and concentration. It also reflects the bulk temperature effect through variations in bulk fluid properties.

## 2.9 Calcium Sulphate Solubility and Its Crystallization Forms

Calcium sulphate solubility in pure water and multicomponent solutions has been the topic of many studies. Temperature, pressure, and concentration of other species are the important factors affecting calcium sulphate solubility.

Despite the large volume of experimental data for calcium sulphate solubility, there is still disagreement about its behaviour in solution and how to best model this behaviour. The transition temperature of gypsum to anhydrite has been reported with values ranging from 38°C (Toriumi and Hara, 1938) to 97°C (Ostroff, 1964). Several thermodynamic approaches have been made to the problem of solubility predictions in multicomponent aqueous salt solutions. In electrolyte solutions, the activity of component  $i$ ,  $a_i$ , is customarily used instead of the concentration,  $C_i$ , which is correlated with activity by means of the activity coefficient,  $\gamma_i$ :

$$a_i = C_i \gamma_i \quad (2.9.1)$$

The Debye-Hückel theory of electrolytes is the basis of any solubility studies of sparingly soluble salts including calcium sulphate. The theory, for the limiting (infinite dilution) law, gives the mean activity coefficient of the ion as:

$$\log \gamma_{\pm} = -A |z_+ z_-| I^{1/2} \quad (2.9.2)$$

where  $\gamma_{\pm}$  is the mean activity coefficient,  $A$  is the Debye-Hückel constant and is a function of temperature,  $z_+$  and  $z_-$  are the valencies of the cation and anion, respectively, and finally  $I$  is the ionic strength that can be defined as:

$$I = \frac{1}{2} \sum C_i z_i^2 \quad (2.9.3)$$

where  $C_i$  is the concentration of the  $i$ th ionic species and  $z_i$  is the corresponding valency. For calcium sulphate solubilities, some researchers such as Davies (1955) and Nancollas (1966) have modified the Debye-Hückel equation to account for deviations from infinite dilution, i.e. higher values of  $I$ . Marshall and Slusher (1966) made a detailed evaluation of the solubility of calcium sulphate in aqueous sodium chloride solution, and suggested that variations in ion solubility product could be described, for ionic strengths up to around 2 M at temperatures from 0 to 100°C, by adding another term in an extended Debye-Hückel expression. Above 2 M, Barba et al. (1982) developed a thermodynamic model in which the solubility of calcium sulphate in saline water was described. In their studies, a system of equations based on the Debye-Hückel and other models was used to describe isothermal activity coefficients of partially or completely dissociated electrolytes. Using binary parameters, good agreement was claimed between experimental and predicted values of calcium sulphate solubility in sea water and brackish brines, including those with a magnesium content.

Calcium sulphate crystallizing from an aqueous solution appears in three forms: gypsum ( $CaSO_4 \cdot 2H_2O$ ), hemihydrate ( $CaSO_4 \cdot 1/2H_2O$ ), and anhydrite ( $CaSO_4$ ). All three varieties (except for gypsum at lower temperatures) have solubilities which decrease with increasing temperature (Figure 2.9.1). Although gypsum behaves like a normal solubility salt at lower temperatures (less than 42°C), industrially it is considered

an inverse solubility salt because it is a serious problem in thermal units operating at high temperatures. In crystallization fouling, it is very important to determine which variety forms first and whether or not any phase transformation between varieties occurs during the deposit buildup. Answers to these questions enable us to estimate the physical and mechanical properties of the deposit layer.

Furby et al. (1968) discussed the conditions under which calcium sulphate and its hydrates crystallize from aqueous solutions. It was pointed out that above about 45°C the dihydrate  $\text{CaSO}_4 \cdot 2\text{H}_2\text{O}$  (gypsum) is thermodynamically unstable with respect to  $\text{CaSO}_4$  (anhydrite), whereas above about 93°C the metastable hemihydrate can be precipitated from supersaturated solutions. However, it appears that nucleation of anhydrite from solution does not take place spontaneously and its rate of formation from the hemihydrate is very slow. The products of crystallizations at 50°C, 70°C, and 90°C, performed under the conditions used in his work, were examined by X-ray diffraction and shown to be the

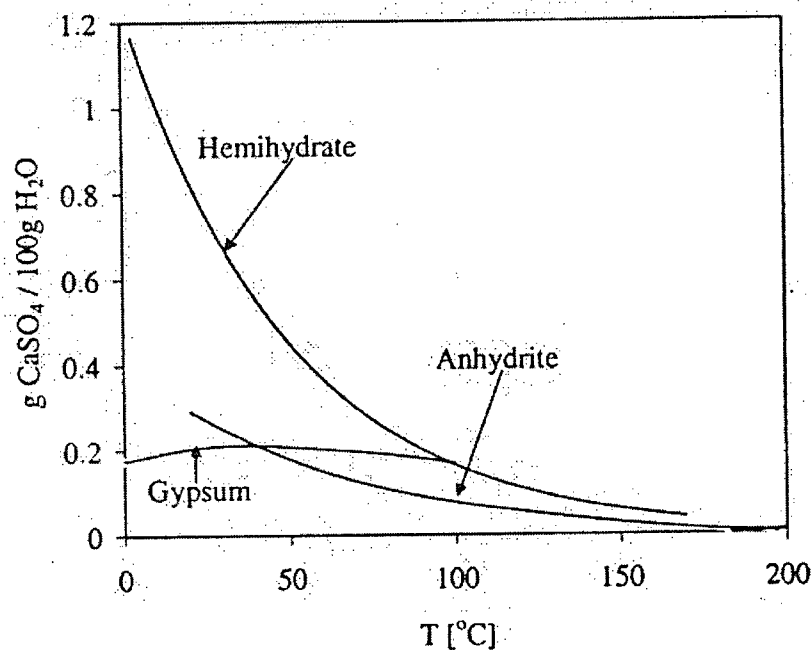


Figure 2.9.1: Calcium Sulphate Solubility in Water (Mwaba et al., 2001)

dihydrate with no sign of anhydrite or hemihydrate, despite the adverse thermodynamics.

Hasson and Zahavi (1970) reported that under their experimental conditions (surface temperature of 87°C), generally supersaturation conditions on the heat-transfer surface existed only with respect to the  $\text{CaSO}_4 \cdot 2\text{H}_2\text{O}$  and insoluble anhydrite. However, based on the work done by Langelier et al. (1950), and Partridge and White (1929), it is known that anhydrite nucleation is an extremely slow process. Hence only  $\text{CaSO}_4 \cdot 2\text{H}_2\text{O}$  can crystallize out of solution, so that in a constant-heat flux exchanger all crystal elements of a given deposit originally form as  $\text{CaSO}_4 \cdot 2\text{H}_2\text{O}$ , and as the temperature increases each element subsequently experiences an increasingly higher temperature due to the thermal-resistance increase of the thickening deposit. The eventual equilibration of the  $\text{CaSO}_4 \cdot 2\text{H}_2\text{O}$  crystals to the stable insoluble anhydrite phase begins with transformation to the metastable hemihydrate form. Accordingly, phase changes in deposited  $\text{CaSO}_4 \cdot 2\text{H}_2\text{O}$  crystals could be expected only for layers exposed to temperatures above 99°C, the  $\text{CaSO}_4 \cdot 2\text{H}_2\text{O} - \text{CaSO}_4 \cdot 1/2\text{H}_2\text{O}$  transition temperature.

Glater (1980) summarized the conditions of calcium sulphate phase transformation as illustrated in Figure 2.9.2. It shows that below 98°C the deposit is mainly gypsum. At 98°C it starts transforming to hemihydrate as a fast reaction, and finally as the temperature exceeds 98°C, it transforms to anhydrite as a slow irreversible process. Hasson and Zahavi (1970), above, gave 99°C as the transition temperature.

Mwaba et al. (2001) categorized the deposit layer based on its contact condition, i.e. the solution-side deposit was porous, consisting of needle-like crystals similar in structural characteristics to gypsum, and the metal-side deposit had higher density due to phase transformation at higher temperatures.

Figure 2.9.2: Calcium Sulphate Phase Transition Stages (Glater, 1980)

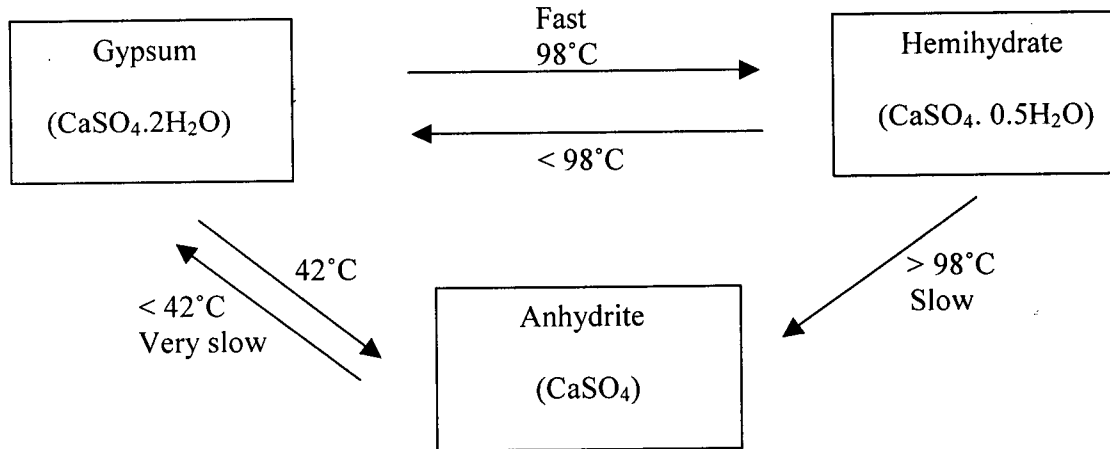


Table 2.9.1: Phase and Thermal Conductivity of the Deposit (Fand, 1969)

| $T_s$ ( $^\circ\text{C}$ ) | $\text{CaSO}_4 \cdot 2\text{H}_2\text{O}$<br>% | $\text{CaSO}_4 \cdot 1/2\text{H}_2\text{O}$<br>% | $\lambda_f$<br>( $\text{W/m}\cdot\text{K}$ ) |
|----------------------------|--|--|--|
| 106                        | 25   | 75   | 1.12   |
| 115                        | 5  | 95   | —  |
| 139                        | 0  | 100  | 1.56   |

Fand (1969) determined the thermal conductivity of calcium sulphate deposits by using deposit thickness measurements along with knowledge of the thermal operating conditions. The resulting values are presented in Table 2.9.1, which illustrates that as the surface temperature increases the crystal phase changes to hemihydrate and the deposit thermal conductivity becomes larger. Thermal conductivity values, reported in Table 2.9.1, are close to the value of  $1.15 \text{ W/m}\cdot\text{K}$  reported by Krause (1993), lower than the

value of 2.2 W/m·K reported by Najibi et al. (1997), and higher than the value of 0.58 W/m·K reported by Hasson and Zahavi (1970).

### 2.10 Objectives

This study focuses on the understanding of calcium sulphate scaling mechanisms by examining and testing both a model for predicting initial fouling rates over a range of fluid velocities and temperatures, and a classical nucleation-based model for delay time prediction.

The objectives of this study are to:

1. Investigate the effect of surface temperature, fluid velocity, concentration, and filter pore size on the initial fouling rate and to determine fouling activation energies.
2. Execute fouling experiments under sufficiently different conditions that both mass transfer and surface reaction controlling regions are encountered.
3. Determine ranges of fluid velocity and temperature under which calcium sulphate scaling is controlled by mass transfer, surface reaction or both.
4. Investigate, whenever deposition has occurred, whether or not the velocity increase causes any deposit removal.
5. Perform a deposit coverage analysis to estimate values of the deposit thermal conductivity and density, and then determine whether they change with wall temperature and fluid velocity.

6. Perform deposit Thermal Gravimetric Analysis and Scanning Electron Microscopy to see whether or not a deposit aging effect over the duration of an experiment is observed.
7. Measure the delay time for calcium sulphate scaling under different operating conditions, and then evaluate calcium sulphate surface energies and delay time activation energies from the tube fouling experiments.
8. Evaluate chemical activation energies and calcium sulphate solubilities from the Jacketed Glass Reactor experiments, and compare the chemical activation energies with the reported values in the literature as well as with the fouling activation energies.

### 3. Experimental Materials and Methods

This section describes experimental materials, apparatus, and procedures used in the current study of calcium sulphate scaling. Also, the major modifications made to the Tube Fouling Unit (TFU) (Wilson and Watkinson, 1996; Rose et al., 2000) are described. The model fluid used in the fouling and kinetic experiments is an aqueous calcium sulphate solution at a concentrations range of 3100 to 3600 ppm by weight as  $\text{CaSO}_4$ . This range of concentration was sufficient for successful experiments covering a wide range of fluid velocities, bulk and surface temperatures.

#### 3.1 Tube Fouling Unit (TFU)

##### 3.1.1 TFU Apparatus (Wilson, 1994)

The apparatus shown in Figure 3.1.1.1, originally designed by Wilson in 1994, was modified somewhat during this study. The apparatus consists of a flow loop in which the calcium sulphate solution is continuously recirculated from a holding tank, through the heated test section, a series of double pipe coolers and back to the holding tank. The test section consists of a drawn T304 stainless steel (ASTM A269-80A) tube 1.83 m (6 ft) long, an outside diameter of 9.525 mm, an inside diameter of 9.017 mm, and a wall thickness of 0.254 mm. The heated length of 0.771 m is subjected to electrical resistance heating by alternating current at a constant and uniform heat flux. The power to the heated section was kept essentially constant during a run so that it could be operated at a constant heat flux, such that as scaling proceeded, assuming a smooth deposit, the deposit-fluid interface temperature would remain constant while the temperature increased. For each experiment, the heat flux applied to the test section was adjusted to achieve a range of wall temperatures in approximate agreement with those obtained for experiments of differing fluid velocities. All

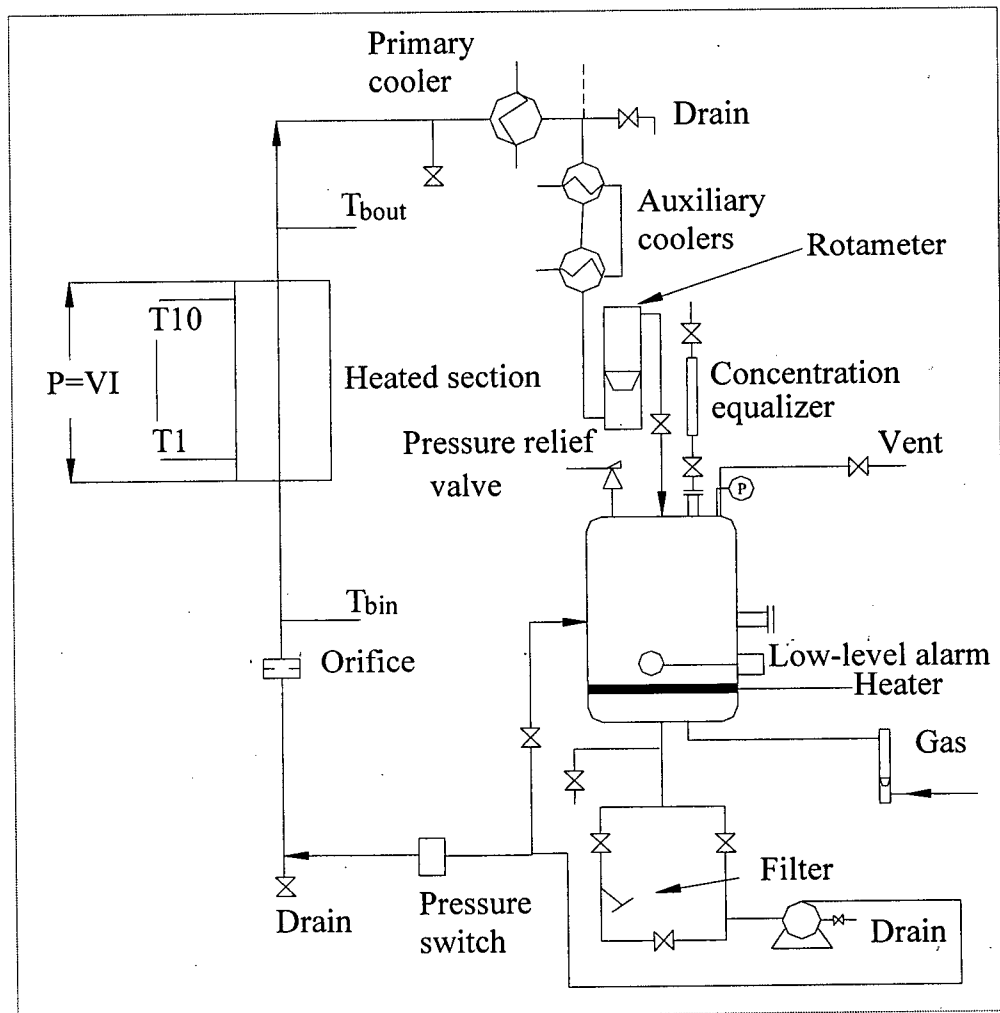


**Figure 3.1.1.1: Schematic of Tube Fouling Unit (TFU) apparatus (Wilson, 1994)**

materials in contact with the fluid are made from stainless steel. The process fluid was stored at the required bulk temperature in a 65 L holding tank, then passed through a pump, an orifice plate, the heated test section, a number of cold water coolers, one of the three rotameters, and finally returned to the tank through a small diameter orifice, to aid mixing. Hoke globe valves were used to split the flow between the test section and the bypass line, which ensured good mixing in the feed tank, especially when low flow rates were used in the

test section. The returned lines both terminated well below the liquid level in the tank, thus ensuring minimum gas entrainment.

The tank is equipped with filling and draining ports. A 20-foot by 2-inch, 2-kW band heating tape rated to a surface temperature of 260°C (500°F) is wrapped around its lower half. The tank contents could be maintained at temperatures of 100°C ± 2°C by an Omega CN 911 controller. The system was capable of being pressurized to 790 kPa (100 psig) using either nitrogen or building compressed air. The gas flow was monitored by the rotameter at the control panel, and gas flowed up from the bottom of the tank through the liquid into the available head space until the desired pressure was achieved, after which the gas was shut off. Pressure was primarily used to eliminate the possibility of boiling as the wall temperature rose. The tank was also fitted with a pressure relief valve set to 859 kPa (110 psig), in a vent line which led outside the laboratory. Along with the piping, the tank was insulated with aluminum backed fiberglass insulation.

For all of the experiments, the system was pressurized to 653 kPa (80 psig) using nitrogen, and the fiberglass insulation along the piping was fitted to minimize heat losses and maintain bulk temperatures in the holding tank constant (covering a range of 50 to 65°C for all of the performed experiments).

Liquid flow rates were monitored using one of three calibrated (with water) rotameters, shown in Table 3.1.1.1 with the corresponding inlet Reynolds numbers.

The temperature of the bulk liquid entering and exiting the heated section were monitored by thermocouples mounted in T-pieces as close to the entrance and exit of the heated section as practicable. The pressure drop across the heated section was monitored by a differential pressure transducer, again connected as close as possible to the entrance and exit

**Table 3.1.1.1: Three Rotameters with Corresponding Ranges of Reynolds Numbers**

| Rotameter              | Range of inlet Reynolds Number |
|------------------------|--------------------------------|
| Low Flow Rate (LFR)    | 1500 – 4500                    |
| Medium Flow Rate (MFR) | 3000 – 20000                   |
| High Flow Rate (HFR)   | 16000 – 40000                  |

of the heated section, with a length of 203 cm for the  $\Delta p$  section.

The coolers removed the heat supplied to the fluid in the test section. The primary double-pipe cooler consisted of a 2.44 m long x 25.4 mm diameter copper outer tube and a 12.7 mm diameter stainless steel tube carrying the process fluid. Cold water was passed counter-current to the process fluid and was controlled using a rotameter located at the control panel. Two auxiliary coolers downstream of the primary cooler were operated independently of the primary cooler and were used intermittently. An additional co-current water cooler was, however, inserted on the bypass line to remove any additional heat added to the fluid from the pump. This cooler was critical in maintaining bulk temperatures of the process fluid in the holding tank at the required value when it was flowing at a very low flow rate.

Several safety features are incorporated in the TFU to protect the system from hazardous situations through circuit breakers, fuses, relays, and trips for enhanced safety. Table 3.1.1.2 highlights the safety features installed into the TFU apparatus to enable safe operation of the equipment.

Despite these safety features it was still possible for tube burnout to occur at the electrical connections, causing fluid to leak across these connections (which resulted in large

**Table 3.1.1.2: Different TFU Hazard Situations with Relevant Proper Actions**

| Hazard  | Cause                  | Trip                 | Action           |
|---|------------------------|----------------------|------------------|
| Overpressure  | Blockage/Explosion     | PSW/PRV              | System Shut Down |
| Fluid Leaks/Runs Dry  | Leakage/Rupture        | LAL                  | System Shut Down |
| Overheated Liquid   | Cooling Water Failure  | HTA on cooler outlet | System Shut Down |
| Tube Burn Out   | Flow Stopped           | HTA on tube surface  | Heating Off      |
| Thermocouple Damage   | Tube Too Hot           | HTA on tube surface  | Heating Off      |
| Power Surges  | Power Failure/Restored | Reset Relays         | Power Stays Off  |
| PSW: Pressure Switch    PRV: Pressure Relief Valve    LAL: Low-Level Alarm<br>HTA: High Temperature Alarm |                        |                      |                  |

fluctuations in electrical resistance) and down the length of the test section. Because the flow hadn't stopped, the tube temperature was within the acceptable range and the HTA (high temperature alarm) did not respond. In this case a manual over-ride was required to terminate the experiment. From this realization it was established that, before installing the test section, the electrical contactors had to be examined carefully to make sure both contacting surface areas were smooth and clean; otherwise, due to the presence of an air gap between the electrical connections and the tube surface, the electrical resistance would be high, causing tube burn-out.

The test section was electrical resistance heated by alternating current (up to 20 V, 300 A). The tube lengths constructed of drawn 304L stainless steel were supplied by Greenvilles Tube Corp., Clarksville, Arkansas (Wilson, 1994). The tube had a nominal thickness of 10 thousandths of an inch, but actual values and weights would vary from tube

to tube. The tube was connected to the fouling rig by two Swagelok dielectric fittings (with an electrical resistance of  $10 \text{ M}\Omega$  @  $10 \text{ V DC}$  and a leakage current of  $1 \mu\text{A}$  (SS-6-DE-6)), which ensured electrical isolation from the rest of the apparatus, and were capable of a holding capacity of  $13884 \text{ kPa}$  ( $2000 \text{ psig}$ ), which was higher than the bursting pressure. These fittings are typically installed on impulse lines ahead of monitoring stations in natural gas pipelines with the fitting interrupting the cathodic flow while still permitting fluid flow. A thermoplastic insulator provided the high dielectric strength over a range of conditions and a viton o-ring provided the primary fluid seal.

Current was applied to the test section from a mains  $208 \text{ V AC}$  supply via a power variac and a  $208\text{-}19 \text{ V}$  step-down transformer. The step-down transformer was connected to the test section by a pair of number three welding cables bolted to  $10 \text{ mm}$  thick copper busbars. The first busbar was located  $546 \text{ mm}$  ( $60$  tube diameters) from the upstream fitting to ensure a fully developed velocity profile in the heated section under turbulent conditions. The second busbar marked the end of the heated section and was positioned  $771 \text{ mm}$  downstream. For turbulent flow the required entry length is given by  $10 \leq x/D \leq 60$ , while for laminar flow,  $x/D = 0.05\text{Re}$ . Incopera and Dewitt (1990) mentioned that under laminar conditions, when both temperature and velocity profiles develop simultaneously, the above criterion may not be sufficient.

The voltage across the test section,  $V$ , was measured using an AC panel meter and displayed on the control panel. The current,  $I$ , was measured using a current transformer on one set of welding cables and was calibrated (Appendix 1) using an Amprobe ACD-9 Current meter:

$$I(\text{Amps}) = 148.77 (\text{ammeter reading}) + 0.2227, \quad R^2 = 0.99 \quad (3.1.1.1)$$

The power to the heated section was calculated, assuming a power factor of unity (Watkinson, 1968), as equal to  $VI$ , and then converted to heat flux using the nominal tube thickness of 10 thousandth of an inch:

$$\dot{Q} / \pi d_i L = \dot{q} (W / m^2) = VI / (\pi (0.009017 \times 0.771)) = 45.79 VI \quad (3.1.1.2)$$

where  $d_i$  is the inner diameter and  $L$  is the length of the heated section, both in meters. As previously discussed by Wilson (1994), there were variations in the tube thickness from tube to tube; however, the nominal thickness of 10 thousandths of an inch was considered the best overall estimate.

Bulk inlet and outlet temperatures were measured by thermocouples. The bulk inlet temperature was maintained constant during each experiment ( $50^\circ\text{C}$  for all of the experiments), while clean tube surface temperatures were varied roughly from  $73$  to  $83^\circ\text{C}$ , as measured by ten thermocouples spaced longitudinally on the outside of the vertical tube. The rate of rise in surface temperature at a given position gives a measure of the local fouling resistance at that temperature. Test sections are used only once, and then sectioned to allow in situ deposit examination and further analysis of the nature of the deposit material, either by optical microscopy, scanning electron microscopy, elemental analysis or deposit coverage studies.

The condition of uniform heat flux implies an axial temperature gradient along the surface of the tube. The highest rates of fouling occurred at the locations of the highest temperature thermocouples, and thus limited the duration of an experiment. Because clean surface temperatures were as high as  $83^\circ\text{C}$ , it was necessary to maintain some over-pressure (typically about 80 psig) on the test section to prevent the onset of boiling as the surface temperature rose due to fouling. Because of the high temperature limitation, some of the

thermocouples from the low temperature regions of the tube gave barely measurable fouling deposits. Reynolds numbers based on local fluid properties were varied from 1950 to 36000 to provide adequate data for a study of the velocity effect on the initial fouling rate and delay time.

### 3.1.2 Wall Temperature Measurements

To enable a test section to be removed and sectioned after each experiment, it was necessary to use removable wall thermocouples. This differs from Watkinson's (1968) setup, where silver soldered thermocouples were permanently fixed to the test section and were used to measure the tube outer wall temperatures.

The method employed by Wilson (1994) involved type K ribbon thermocouples mounted in a polyimide (Kapton™) carrier compressed against the side of the tube inside a clamping block that was screwed against the outside of the tube. The lead from the thermocouple had to be mounted and maintained normal to the direction of the tube, since the alternating current's magnetic field could cause significant noise and hence contribute to fluctuations in the thermocouple signal.

Ten thermocouples were located along the length of the heated section at 48, 125, 203, 286, 361, 443, 521, 600, 668, and 716 mm from the start of the 771 mm heated length. For experimental systems that exhibit characteristics which are strong functions of the wall temperature, the axial temperature profile provides an excellent description of the system behaviour.

The entire test section was enclosed by a steel cover that prevented accidental contact with live surfaces and prevented the release of chemicals into the path of the operator in the event of an emergency shutdown.

## 3.2 Modifications Made to Improve the TFU Performance

### 3.2.1 Initial TFU Operating Problems

The first set of the TFU experiments, performed with saturated calcium sulphate solution as the test fluid, achieved only limited success, due to the following problems:

- Long experimental duration (about 100 hours) followed by rapid fouling at the top of the test section which limited the continuation of the experiment.
- The presence of an in-line mesh strainer (700  $\mu\text{m}$ ) did not guarantee elimination of particles, so that the fouling was probably a combination of particulate deposition and surface crystallization.
- Lack of fouling results at low temperatures, due to low surface crystallization rates, made it too difficult to study the effect of wall temperature on the crystallization fouling.
- Deposit formation was not uniform circumferentially at any axial location along the test section.
- The solution concentration declined during each experiment, so it was difficult to analyze the results.
- At low fluid velocities, fluctuations in cooling water flow rate and poor heat transfer in the cooling stage after the test section caused variations in the bulk inlet temperature.

To improve performance, modifications were made on the TFU at each stage where needed.

### 3.2.2 Filter

To approach purely surface crystallization in the test section, a filter was installed upstream of the pump to eliminate particles. All the components, except the filter medium,

are made of stainless steel (316 SS). The filter has a 25 cm long housing (Cuno Incorporated, USA) resistant to high pressures (up to 300 psig) and temperatures (up to 80°C). Polypropylene cartridges (Cuno PolyNet), covering pore sizes from 1 to 5  $\mu\text{m}$ , were employed. Pressure drop across the filter was an important factor affecting the solution flow rate and hence determining the life time of a filter cartridge. Clean pressure drop for filters of 5 and 1  $\mu\text{m}$  pore sizes were about 4 and 25 psi, respectively, and during the experimental progress the aforementioned values increased. When the pressure drop across the filter increased to 40 psi (usually after about four experiments), the filter cartridge had to be replaced with a new one.

### 3.2.3 Concentration Equalizer

A concentration equalizer was designed and installed at the top of the holding tank, which allowed chemicals to be added during the experiment to maintain concentration constant without stopping an experiment. It consisted of a stainless steel pipe (80 cm long, 1 inch nominal diameter, schedule 80) connected to two 1 inch stainless steel ball valves (Figure 3.2.3.1). The concentration equalizer can be isolated from the rest of the apparatus, which is running at high pressures (about 80 psig), using valve  $V_1$ . Valve  $V_2$  is used for adding the required chemicals to the holding tank. Periodic sample withdrawal from the holding tank followed by concentration measurement using the EDTA technique (3500-Ca-D standard), indicates whether the concentration has changed or not. If the concentration drops, then it has to be adjusted to the required level by completing the following procedures:

1. Calculate the amount of the required chemicals (sodium sulphate and calcium nitrate) and weigh them precisely up to four decimal points ( $\pm 0.0001$  g).

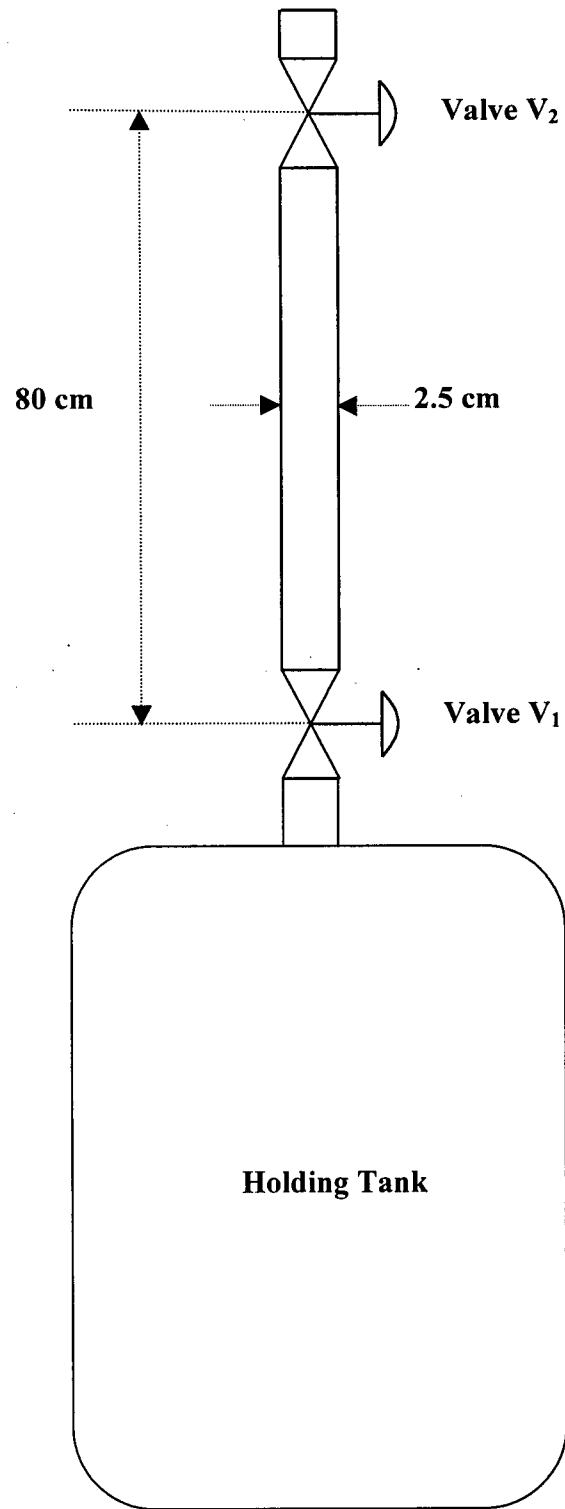


**Figure 3.2.3.1: Schematic of the Concentration Equalizer Assembled on the Holding Tank**

2. Add sodium sulphate and calcium nitrate to the required deionised water separately and heat them up to the bulk temperature level inside the holding tank.
3. Open valve  $V_2$  and add sodium sulphate solution into the concentration equalizer while valve  $V_1$  is kept closed, and then close valve  $V_2$  and open valve  $V_1$  slowly so that the system pressure does not change significantly.
4. Adjust the system pressure using the valve located in the gas line below the holding tank (Figure 3.1.1.1).
5. Add calcium nitrate solution into the holding tank following steps 3 to 5.
6. Withdraw samples from the holding tank about 15 minutes after completing the previous step, and measure the concentration to make sure that it has reached the required level.

#### 3.2.4 Cooling System Valve Modification

To improve the performance of the cooling stage after the test section, a new configuration of the valve arrangements was designed and installed as shown in Figure 3.2.4.1. Both stainless steel needle valves,  $V_{low}$  and  $V_{high}$ , can be used to adjust the cooling water flow rate at the required level with minimum fluctuations.  $V_{low}$  is used when the heat flux is low, i.e. for low solution flow rate inside the Tube Fouling Unit, and it can control the flow at a minimum value of 0.24 L/min.  $V_{high}$  is used when the heat flux is high, i.e. for high solution flow rate inside the Tube Fouling Unit. It can handle the maximum controllable flow up to about 30 L/min.

#### 3.2.5 New Thermocouple Holder Design

A new thermocouple holder was designed, and is shown in Figure 3.2.5.1. In the

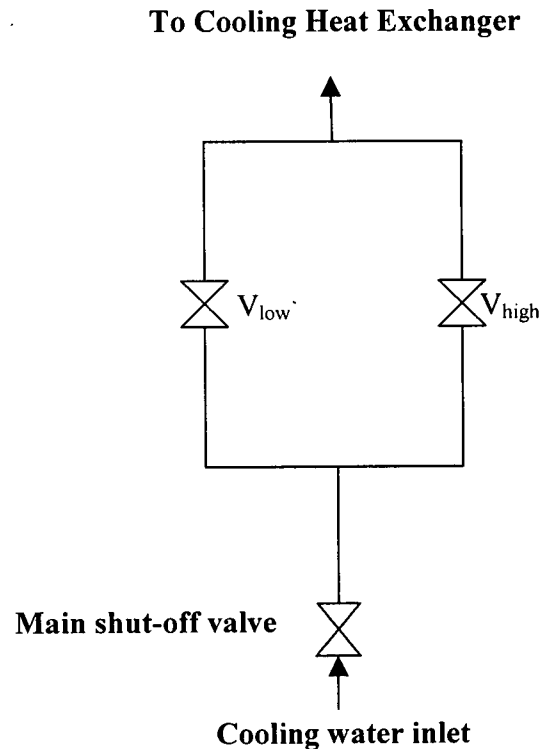
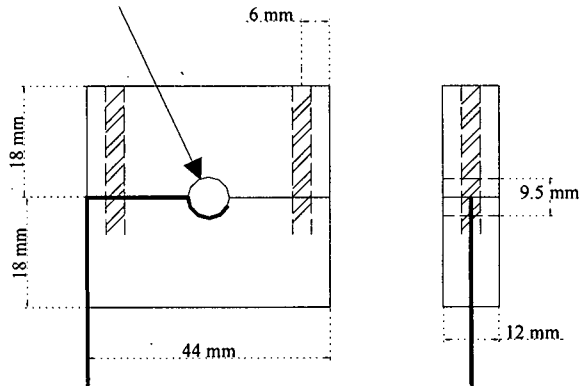


**Figure 3.2.4.1: New Cooling Water Valve Configuration Setup**

original design (Wilson, 1994), the thermocouple holders were fixed along the test section. Based on the Wilson design (1994), one side of the thermocouple holder was fixed at the apparatus main frame and the other side was clamped around the test section, so it was very difficult to align all ten thermocouples simultaneously. Due to the aforementioned problem, it was impossible to eliminate the air gaps between the thermocouple sensors and the test section surface completely and therefore, most of the time two or three of the thermocouples did not function properly. Moreover, although the thermocouple holder was fabricated from Lava<sup>TM</sup> (an insulating ceramic material), which was resistant to temperatures up to 1000°C, it was difficult and time-consuming to align it properly due to its higher weight. The new design has smaller dimensions and is fabricated from Tufnol (polymeric composite). It is much lighter than the original design and resistant to temperatures up to 300°C, which is

### Test Section



### Thermocouple Wire (to data logger)

**Figure 3.2.5.1: Schematic Diagram of the New Thermocouple Holder Construction Showing Tufnol Blocks Drilled for Set Screws**

appropriate for our operating temperature ranges. Also, the new design allows the location of the thermocouples to be changed from one experiment to another.

To minimize the heat loss from the test section during each experiment, an insulation collar (fabricated from Tufnol) was placed around the tube between each two thermocouples, and held in place by a wrap of glass fiber tightly covered by two layers of an aluminum backed fiberglass blanket fastened by removable straps. The entry and exit lengths were also insulated using a wrap of glass fiber and then covered with a cylinder of fiberglass insulation, again fastened by removable straps.

A high temperature alarm thermocouple of similar construction to the previously mentioned thermocouples was positioned close to the hotter end of the test section and served only as an alarm at the control panel rather than being data logged on the computer.

### 3.3 Data Acquisition System

Experimental data were collected using a DAS-8 analog/digital interface board, supported by in-house built software. The system is capable of saving real time data as well

as averaged data for a specified time interval. All data were saved by the PC and later transferred to Excel where a spreadsheet enabled easy data analysis.

Fluid bulk and wall temperature measurements showed an approximate variation of  $\pm 1^\circ\text{C}$ . The tank bulk temperature was considerably more stable and estimated errors were in the range of  $\pm 0.5^\circ\text{C}$ . All the thermocouples were periodically replaced with new ones, which before use were tested with boiling water.

The current through the heated section, and the voltage applied to the test section were measured at the control panel and the signals were connected to DAS-8 for automatic data logging on the PC as well. Panel measurements were periodically recorded manually during each experiment and the averaged values were compared with those of the data logger. The difference was not more than 0.2% for all the performed experiments. Both the voltage and current measurements were calibrated periodically (Appendix 1).

All significant temperature and pressure drop data were logged and displayed on the PC screen such that the progress of the experiment was easily monitored. For all of the experiments, data sampling was done within a second along with calculating a moving point average over a specific time interval, from one minute for experiments lasting up to 16 hours to 10 minutes for those lasting up to 100 hours. The calculated average was then logged as the value over the mid-point of the averaging time period. During the experiments thermocouple fluctuations were estimated to be around  $\pm 1^\circ\text{C}$ .

The heat flux applied to the test section was assumed to be uniform since the electrical properties of the stainless steel tube are not a strong function of temperature. The electrical resistance,  $R = \frac{\sigma L}{A}$ , where  $\sigma = 71.7(1+0.00094 T(^{\circ}\text{C})) \mu\Omega\text{cm}$ . Therefore given that the electrical resistivity is a very weak function of temperature, and assuming that the

cross-sectional area remains constant, the resistance will remain essentially constant (providing a uniform heat flux to the test section) and was calculated using Equation (3.1.1.2). The heat transfer to the fluid was calculated using

$$\dot{Q} = \dot{m}C_p(T_{b,out} - T_{b,in}) \quad (3.3.1)$$

and the results from Equations (3.1.1.2) and (3.3.1) were compared to estimate the heat loss. The specific heat capacity  $C_p$  for calcium sulphate solutions was assumed to equal that of water and was evaluated at the average bulk temperature,  $T_b = (T_{b,in} + T_{b,out})/2$ . These two estimates from the heat balance were on average within 3.2 % of each other (Equation (3.1.1.2) gave consistently greater values of  $\dot{Q}$  than Equation (3.3.1)) and considered to be in reasonable agreement. The difference in  $\dot{Q}$  by these two equations was on average 51 W, which can be accounted for by the range of uncertainty of the thermocouple readings ( $\pm 1^\circ\text{C}$ ). At high heat fluxes this difference would be 0.5 – 1 %, while at low heat fluxes, generally the case at the lower fluid velocities, there could be up to 6 % variation in heat flux estimates. The value of the heat flux and thus heat transferred to the liquid was calculated from Equation (3.1.1.2), since Equation (3.3.1) involved assumptions about the fluid heat capacity  $C_p$ . However, given that these equations were generally in good agreement, the small heat losses were neglected except for the lowest velocity, where Equation (3.3.1) was used.

Except at low fluid flow rates (using the LFR rotameter), the mass flow rate of process fluid was typically very stable (within  $\pm 1\%$ ) once steady state had been achieved. During each experiment, the values of instantaneous mass flow rates were monitored, recorded manually, and averaged throughout the experiment. Using Equations (3.1.1.2) and (3.3.1) as a check on the heat balance (and hence the rotameter calibration), this method proved satisfactory. The rotameter calibration plots are presented in Appendix 1.

### 3.4 TFU Experimental Procedures

The main advantage of this fouling loop compared to other fouling rigs is the presence of a removable test section in which the local deposits can be examined by cutting the tube once the thermocouples are removed after each experiment. Therefore particular care should be taken in the preparation, cleanliness and treatment of the test section before and after each experiment. The following procedure shows the stringent methods employed to ensure reproducible conditions from one experiment to another:

1. For all of the experiments the test section was first examined carefully by measuring its length, diameter, thickness, and checking the presence of any deformation or irregularity to assure that it could be used without causing any problem during the experiment.
2. The test section was soaked in a bath of hot water and detergent overnight to remove any grease or residual dirt that might be present.
3. The test section was then rinsed with cold water to remove the grease and detergent.
4. The inside and outside of the test section were cleaned using acetone with several bottle cleaning brushes. The test section was then allowed to dry.
5. The test section and fittings were weighed to obtain a clean weight.
6. The union to the heated section at the top of the test section was removed and the tube installed. The union was then re-assembled.
7. The top and bottom of the tube were secured to the equipment and then tightened at the electrical connections.
8. All thermocouples were attached to the tube one by one, assuring that they do not have any deficiencies.

9. The TFU was pressure-tested with nitrogen to above the required operating pressure for the experiment and joints examined for leaks with Snoop.
10. Tufnol insulators were attached between thermocouples. Thermocouples were then aligned and tightened without leaving any air gap between the tube surface and thermocouple sensor.
11. Thin white fiberglass, which acted as the second layer of insulation, was wrapped over Tufnol insulators.
12. Two lengths of insulation were installed over the entrance and exit lengths of the tube.
13. The third layer of insulation, two layers of aluminum-backed fiberglass, was used at each thermocouple location. Two long cylinders of insulation were used at the entrance and exit lengths.
14. Metal guards were installed around the tube to protect the operator from electric current or a chemical leak.
15. The concentration equalizer was assembled such that there were no leaks from its lower and upper valves.
16. For the disassembly, steps 5-15 were performed in reverse order. Special attention was paid to avoid dislodging any material deposit on the inside of the tube.
17. The test section was then carefully removed and allowed to drip dry in the laboratory.

To commence a run, the pump was started, the flow rate and operating pressure adjusted to the desired set point, and the variac set to the required power setting. The data logger was started, and once thermal pseudo-steady state was achieved (approximately 15 minutes), the critical control parameters were monitored and followed for the duration of the

experiment, i.e. cooling water flow rate and temperature, test fluid flow rate, surface temperatures, voltage and current, and bulk fluid temperatures. Cyclic variations in heat flux throughout an experiment required the occasional adjustment of the variac to ensure operation at a constant heat flux.

Several liquid samples were taken from the test section inlet to follow the concentration changes throughout each experiment. Solution calcium concentration was measured by titration using EDTA. If the concentration declined more than 50 ppm, then the solution concentration was adjusted by following the procedures listed in Section 3.2.3.

Bulk temperatures were maintained as low as practicable (50°C bulk inlet temperature) to avoid significant bulk crystallization. For experiments performed at bulk inlet 50°C, the bulk temperature typically rose to 62°C at the outlet.

The duration of each experiment was limited by the time to reach a maximum surface temperature of 165°C at 790 kPa (100 psig), i.e. the anticipated onset of boiling of the aqueous fluid. Unfortunately, some experiments (at high heat flux) were prematurely terminated due to tube burn-out.

To terminate an experiment, the power to the test section was slowly reduced to zero over five minutes to allow the test section to cool to the bulk temperature, thereby preventing the deposit from suffering thermal shock and becoming dislodged. Then the pump was stopped and the system pressure slowly reduced to atmospheric pressure. The holding tank contents were emptied through the drainage port and the test section removed to dry in the laboratory. Finally, some samples were taken for performing some analysis, such as concentration measurements and crystal size distribution analysis.

### 3.4.1 TFU Cleaning Procedure

The following procedure was employed to clean the whole recirculation path including the holding tank after each experiment. To perform the cleaning operation, the test section was replaced by a dummy tube.

1. As soon as practicable after each experiment, the solution was drained from the TFU, the insulation removed and the test section disconnected.
2. 68 liters of distilled water were recirculated through the TFU for approximately one hour to dissolve calcium sulphate crystals and remove any trapped solution. The contents were then drained.
3. 68 liters of 0.01 N HCl were added and recirculated through the TFU for approximately 4 hours until the bulk temperature reached 50°C (by heat generated in the pump). At this time the contents were drained immediately.
4. 68 liters of distilled water were recirculated through the TFU for approximately one hour as a final rinse solution and the TFU was air dried overnight after draining the contents.

### 3.5 Solution Preparation for TFU Experiments

For the first set of experiments, calcium sulphate solution was prepared by dissolving solid calcium sulphate reagent in deionised water directly, but the following problems arose:

- Fouling experiment duration was more than 100 hours followed by the occurrence of rapid fouling at the top thermocouple location, which limited the continuation of each experiment.
- Deposit formation was not uniform circumferentially even at a given axial location.

- Even by increasing the mixing time (more than 24 hours) during the solution preparation, the solution concentration was below the saturation level.
- The low solubility resulted in a significant amount of undissolved material left in the solution, which was not desirable.

To overcome the aforementioned problems, an indirect method was employed for solution preparation, i.e., by dissolving calcium nitrate tetrahydrate,  $\text{Ca}(\text{NO}_3)_2 \cdot 4\text{H}_2\text{O}$  and sodium sulphate,  $\text{Na}_2\text{SO}_4$ . This resulted in the formation of calcium and sulphate ions as illustrated in the following reaction:



This technique allowed us to prepare calcium sulphate solutions with the concentration ranging from 3100 to 3600 ppm. The calculated sodium nitrate content was from 3875 to 4500 ppm by weight. This method of generating the calcium sulphate solution has been widely used (Table 2.7.3) without any reports of interference by the foreign ions.

Batches of calcium sulphate solution, about 65 liters, were prepared by dissolving calcium nitrate,  $\text{Ca}(\text{NO}_3)_2 \cdot 4\text{H}_2\text{O}$  (Fisher Scientific, Industrial Grade 99%), and sodium sulphate,  $\text{Na}_2\text{SO}_4$  (Fisher Scientific, Industrial Grade 99%), in deionised water using the following procedure:

1. Calculate the amount of sodium sulphate and calcium nitrate based on the desired concentration of calcium sulphate with sodium sulphate in about 1 % excess.
2. Dissolve sodium sulphate and calcium nitrate separately in about 33 L of deionised water.
3. Pour sodium sulphate solution into the holding tank followed by calcium nitrate solution.

4. Circulate the solution in the TFU using the in-line 1- $\mu\text{m}$  filter for about three hours to aid complete mixing and to remove micron-size particles.
5. Measure solution concentration using EDTA titration. If the concentration is lower than the desired value, calculate the chemicals needed to achieve the desired value, prepare separate solutions of sodium sulphate and calcium nitrate and then pour them into the holding tank. Similarly, if the concentration is higher than the desired value, dilute the solution appropriately using deionised water.

After ensuring a thoroughly well mixed chemical system, the power to the test section was applied to achieve the operating conditions required. Heating up the test section to steady state took approximately 30 minutes.

### **3.6 Jacketed Glass Reactor (JGR) Experiments**

#### **3.6.1 Jacketed Glass Reactor (JGR) Constituents**

After completing the TFU experiments, in order to separate the contribution of surface reaction from that of mass transfer and to evaluate calcium sulphate solubilities under the TFU operating conditions, a Jacketed Glass Reactor (JGR) system, Figure 3.6.1.1, was designed. The reactor was constructed from glass with a working volume of 0.7 liter and a diameter of 10 cm. A magnetic stirrer, under constant stirring rate, was used to keep the temperature and concentration uniform throughout the reactor. The JGR was employed for performing batch experiments, in which the same solutions were used as for the TFU experiments. The bulk temperature was varied in the range of 60 to 84°C, while the initial concentrations of  $\text{CaSO}_4$  were 3100 and 3400 ppm by weight.

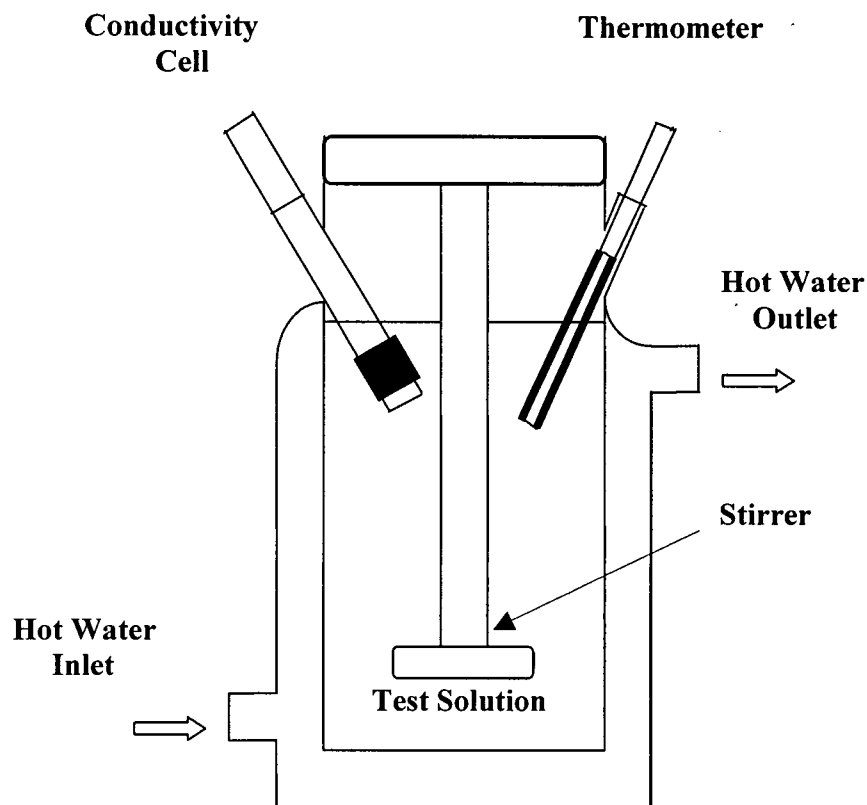


**Figure 3.6.1.1: Schematic Diagram of the Jacketed Glass Reactor (JGR)**

A constant temperature bath (Lauda – Thermostat, type NB-S15), which uses distilled water as a heating medium, was employed to circulate hot water through the JGR jacket and to keep the test solution temperature inside the JGR constant during the experiment. A thermometer is aligned inside the test solution, in the center of the JGR, to monitor the bulk temperature during the experiment. Also, an off-take port, placed at the JGR side, allows the removal of samples from the JGR to measure the solution concentration using an EDTA technique during the experiment. The aforementioned technique could be used for only a limited number of times (six to eight times in each experiment), so to overcome this problem a conductance meter (Jen Way 4042) was employed to measure the solution concentration

without consuming any solution. The concentration was measured by immersing the conductivity cell in the solution through the last port in the JGR. The idea behind using conductivity for measuring concentration in the JGR setup is that, as the calcium sulphate precipitates according to the following reaction:



the solution conductivity, which is a measure of the concentration of ions such as  $\text{Ca}^{2+}$ ,  $\text{SO}_4^{2-}$ ,  $\text{H}^+$ ,  $\text{OH}^-$ ,  $\text{Na}^+$ , and  $\text{NO}_3^-$ , decreases. Therefore it is possible to monitor the solution concentration during the experiment. Initially there were some problems with keeping the conductivity cell continuously inside the JGR during each experiment, since examination of the conductivity cell revealed that some crystals form on the cell surface and cause errors in measuring the solution concentration. To overcome this problem, the conductivity cell was immersed in the JGR for a short time (about 2 to 3 minutes) during the measurement, and quickly taken out of the solution after the measurement. Also, in order to make the measurement faster and more accurate, after each measurement the conductivity cell was kept inside distilled water that was almost at the same temperature as that of the JGR contents.

### 3.6.2 JGR Operating Procedures

To initiate an experiment, the following procedure was employed:

- I. Clean the JGR with detergent to make sure that there are no impurities left inside it.
- II. Connect the hot water hose to the JGR properly to avoid any leaks during the experiment and turn on the hot water constant bath temperature recirculator, adjusting the required temperature level.

- III. Weigh the required chemicals, sodium sulphate ( $\text{Na}_2\text{SO}_4$ ) and calcium nitrate tetrahydrate ( $\text{Ca}(\text{NO}_3)_2 \cdot 4\text{H}_2\text{O}$ ), and dissolve them separately in the same amount of deionised water (0.35 L).
- IV. Filter both sodium sulphate and calcium nitrate solutions separately using a  $0.22 \mu\text{m}$  filter.
- V. Add sodium sulphate solution into the JGR and keep the calcium nitrate solution inside the constant temperature bath, which has almost the same temperature as that of the JGR.
- VI. Place and align the JGR on the plate stirrer, adjusting the stirring rate to the required level (300 rpm).
- VII. Check the temperature of both solutions as they are heated up until the temperature reaches the required level.
- VIII. Add the calcium nitrate solution to the sodium sulphate solution that already exists inside the JGR at almost the same temperature.
- IX. Seal the JGR lid and ports using plastic covers and aluminum foil to avoid the solution vaporization.
- X. Record the time (using a stopwatch), bulk temperature, and solution conductivity, at the same time measuring the solution concentration using EDTA, and consider the measured values as the initial measurements (recorded at time zero).
- XI. Continue the above measurements with a proper time interval until the concentration stays constant, but measure the concentration (using EDTA) only six to eight times during each experiment.

- XII. Terminate the experiment once the concentration does not change significantly and record the final solution concentration, conductivity, and bulk temperature measurements.

In all of the performed experiments, system pressure was almost atmospheric and the stirring rate was kept at the highest operating level (300 rpm) to ensure as complete mixing as feasible of the contents and to eliminate the mass transfer resistance. Once the kinetic measurement data collection was terminated, the experiment was continued for about one week to obtain the saturation concentration at the operating temperature (Appendix 2). After terminating the experiment, the water bath and the stirrer were turned off and then the JGR was removed from the setup and rinsed thoroughly with detergent and scrubbed to remove any residue. Once the entire reactor was clean, it was placed inside the fume hood and allowed to dry.

### 3.7 Physical Properties

Three solutions with different concentrations (pure water, 2100 ppm and 3400 ppm as  $\text{CaSO}_4$ ) were prepared using the required chemicals (sodium sulphate and calcium nitrate). The physical properties ( $\nu, \rho$ ) of these solutions were investigated over the typical operating temperature range. An Ubbelohde viscometer was used to measure kinematic viscosity, and specific gravity bottles were used to determine the density. The data were collected over the range 25-80°C. Figures (3.7.1) and (3.7.2) show the variation of kinematic viscosity and density with temperature. The ratios of the densities of both 2100 ppm and 3400 ppm calcium sulphate solutions to that of water were found to be almost constant at average values of 1.0037 and 1.0053, respectively. Also, the same calculations for kinematic viscosities gave values of 1.007 and 1.011, respectively. Therefore the solution density and

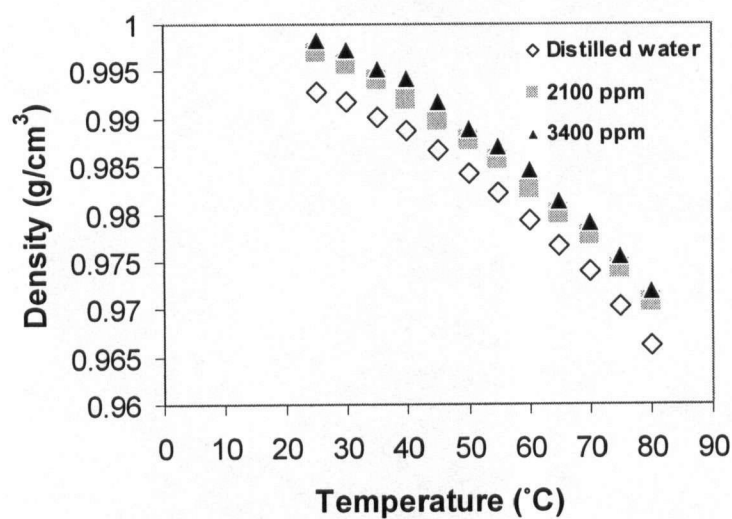


Figure 3.7.1: Densities of Solutions with Different Concentrations

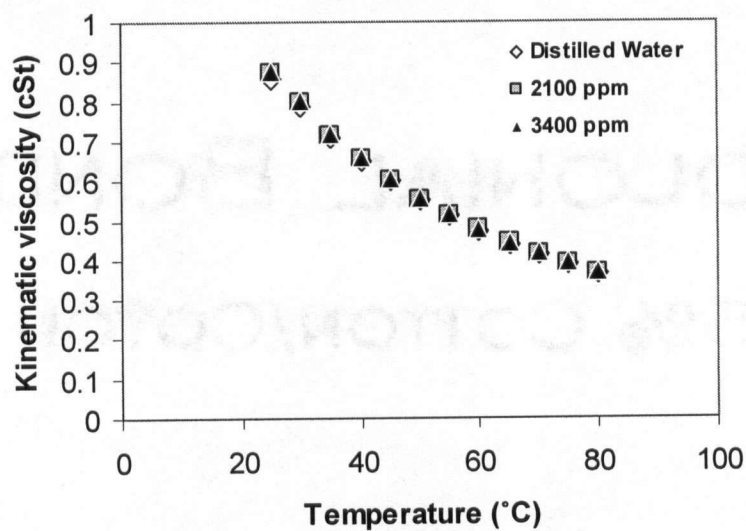


Figure 3.7.2: Kinematic Viscosities of Solutions with Different Concentrations

**Table 3.7.1: Property Measurement Results for Different Concentrations as a Function of Temperature**

| Solution Concentration | Property                    | Fitted Expressions as a Function of Temperature            | R <sup>2</sup> |
|------------------------|-----------------------------|--|----------------|
| Pure water             | $\rho$ (g/cm <sup>3</sup> ) | $-4.76E-6T^2(^{\circ}C) + 2.12T(^{\circ}C) + 0.995$        | 1.00           |
|                        | $\nu$ (mm <sup>2</sup> /s)  | $1.078E-4 T^2(^{\circ}C) - 2.012E-2 T(^{\circ}C) + 1.289$  | 0.99           |
| 2100 ppm               | $\rho$ (g/cm <sup>3</sup> ) | $-3.47 E-6T^2(^{\circ}C) - 1.136 T(^{\circ}C) + 1.002$     | 1.00           |
|                        | $\nu$ (mm <sup>2</sup> /s)  | $1.180 E-4T^2(^{\circ}C) - 2.135 E-2 T(^{\circ}C) + 1.327$ | 0.99           |
| 3400 ppm               | $\rho$ (g/cm <sup>3</sup> ) | $-3.98E-6 T^2(^{\circ}C) - 6.380E-5 T(^{\circ}C) + 1.002$  | 1.00           |
|                        | $\nu$ (mm <sup>2</sup> /s)  | $1.1811 E-4T^2(^{\circ}C) - 2.139E-2 T(^{\circ}C) + 1.331$ | 0.99           |

kinematic viscosity can be calculated as the density and kinematic viscosity of water multiplied by the aforementioned factors. Table 3.7.1 shows the fitted expressions for different concentrations as a function of temperature. It is clear that the kinematic viscosities are stronger functions of temperature than the densities. Solution density and viscosity measurements are presented in Appendix 6 as well.

### 3.8 Deposit Property Estimation Procedures

To evaluate deposit properties such as thermal conductivity and density and see how they change with temperature and velocity, test sections from nine performed experiments were studied taking advantage of the range of fluid velocities, as shown in Table 3.8.1. Also, several of the samples were examined using the Scanning Electron Microscope (SEM) to compare the deposit morphology under different operating conditions.

**Table 3.8.1: Experiments Used for Deposit Analysis**

| Run No. | V (m/s) |
|---------|---------|
| 812     | 0.1     |
| 811     | 0.2     |
| 817     | 0.3     |
| 804     | 0.5     |
| 803     | 0.7     |
| 806     | 1.0     |
| 809     | 1.2     |
| 807     | 1.4     |
| 808     | 1.6     |

As previously discussed, up to 10 individual thermocouples are used in one experiment, and therefore up to 10 mass deposition and thickness results can be utilized. This procedure will elucidate approximate values of deposit thermal conductivity,  $\lambda_f$ , and density,  $\rho_f$ . The following procedure was employed to determine these two physical properties of the calcium sulphate deposits:

1. Section and cut the fouled tube into approximately 20 mm sections.
2. Put each section of interest into a desiccator and dry until constant weight. This process will typically take 48 hours.
3. Determine dry weight (fouled weight) of each section ( $\pm 0.0001$  g).
4. Measure the exact length of each 20 mm section using a caliper ( $\pm 0.0001$  m).
5. Performing duplicates and averaging, estimate with calipers the thickness of the deposit at the tube section inlet and outlet.
6. Heat 1 liter of 10% HCl solution to 50°C using a hot plate and magnetic stirrer.
7. Place each section into the HCl solution for approximately 15 minutes to remove the deposit. Visually check each section for signs of remaining deposit.

8. Soak each section in hot water for 5 minutes and rinse with distilled water.
9. Dry for up to 48 hours in a desiccator until the clean sections reach constant weight.
10. Measure the weight of each section (clean weight) and record the deposit mass for each section.
11. Place any sample required (collected deposit from each section) in a sealed container for SEM analysis.

**Table 3.8.2: TFU Thermocouple Locations**

| Thermocouple No. | Axial location (mm) downstream of 547-mm entrance length |
|------------------|--|
| 1                | 48   |
| 2                | 125  |
| 3                | 203  |
| 4                | 286  |
| 5                | 361  |
| 6                | 443  |
| 7                | 521  |
| 8                | 600  |
| 9                | 668  |
| 10               | 716  |
| Heated length    | 771  |
| Exit length      | 512  |

Table 3.8.2 shows the thermocouple locations along the heated length of the tube.

After determining the deposit coverage ( $m_f$ ) at a given fouling resistance, the product  $\lambda_f \rho_f$  can be determined from

$$R_f = \frac{m_f}{\lambda_f \rho_f} = \frac{x_f}{\lambda_f} \quad (3.8.1)$$

Also, by estimating deposit thickness ( $x_f$ ) and plotting this against the fouling resistance, the value of  $\lambda_f$  can be determined, enabling an estimate of both  $\lambda_f$  and  $\rho_f$  of the fouling deposit.

#### 4. Experimental Results and Discussions

Fouling experiments were performed under different operating conditions using calcium sulphate solution as the model fluid to investigate the effects of important process variables on delay time and initial fouling rate under surface crystallization conditions. Also, a deposit coverage analysis provided useful information on deposit physical properties such as density and thermal conductivity. Moreover, in one experiment a test was made to see, once a deposit had formed, whether or not deposit removal occurs. The effect of filter pore size on fouling behavior was investigated as well. Finally, a jacketed-glass reactor was used to study the kinetics of calcium sulphate precipitation and extract purely chemical (i.e. surface-integration) activation energies.

##### 4.1 Data Processing Steps for Fouling Experiments

Up to 10 thermocouples located at various axial positions along the length of the tube were utilized to measure the thermal fouling resistances. During the experiments, it was found that calcium sulphate fouling rates were strongly dependent upon both surface temperature and solution concentration. In each experiment, concentration was held constant. To take into account the temperature gradient along the test section, local fouling results were used. For each thermocouple, fouling results were obtained employing the following procedure.

After an experiment was completed, a plot of outside wall temperature ( $T_{w,o}$ ) versus thermocouple axial location for clean conditions was constructed to determine the individual performance of each thermocouple. The aforementioned plot was compared with a constructed bulk temperature gradient plot along the test section. Slight misalignment of a thermocouple during assembly, or simply age, might render that

thermocouple unreliable for a given experiment, and therefore to be discarded from calculations. Figure 4.1.1 shows an example plot in which both lines are almost parallel (within 4%), and therefore all thermocouples were considered to function properly. Also, Figure 4.1.2 clearly shows the strong wall temperature effect of calcium sulphate scaling along the length of the test section. The lower thermocouples,  $T_1$ ,  $T_2$ , and  $T_3$ , are in the roughness control period while thermocouples  $T_4$  to  $T_{10}$  are in the fouling period.

To determine the delay time and initial fouling rate, the following steps were taken:

1. Initially, all thermocouple temperatures were plotted and an approximate time to arrive at steady state was determined. This allows one to evaluate the steady state conditions.
2. For a given thermocouple, the time period before commencement of fouling, i.e. the delay time  $\tau_D$ , when the inside wall temperature  $T_{w,i}$  was constant, was determined by subtracting the heat-up time from the time when  $1/U$  started to decline, using the following criterion:

$$\frac{\frac{1}{U_c} - \frac{1}{U}}{\frac{1}{U_c}} > 0.05 \quad (4.1.1)$$

where  $U_c$  is the local clean heat transfer coefficient, evaluated at initial steady state conditions using the following equation:

$$U_c(x) = \frac{\dot{q}}{(T_{w,i})_c(x) - T_b(x)} \quad (4.1.2)$$

and  $U$  is the instantaneous local heat transfer coefficient, evaluated at subsequent times,  $t$ , from the following equation:

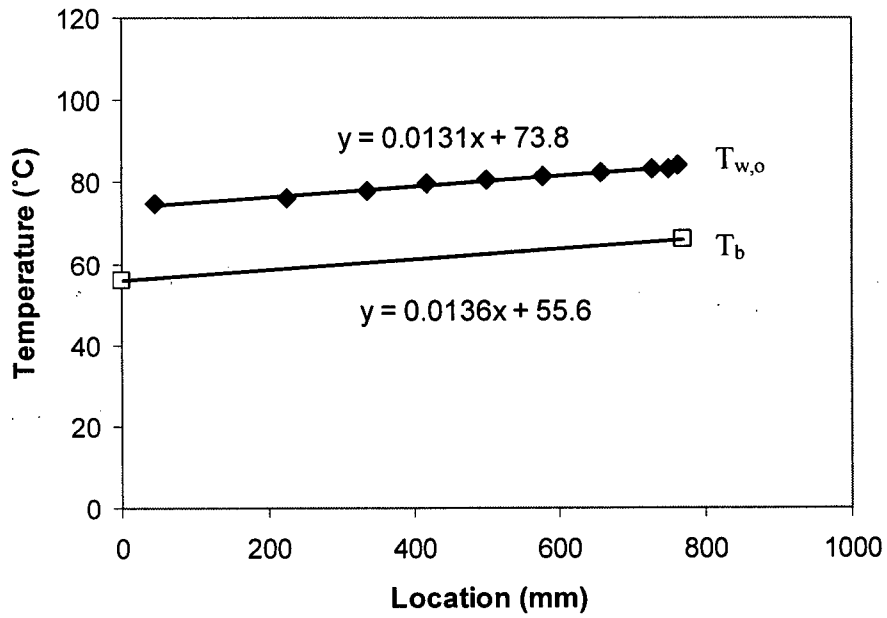


Figure 4.1.1: Temperature Profile for Clean Condition (TFU 703)

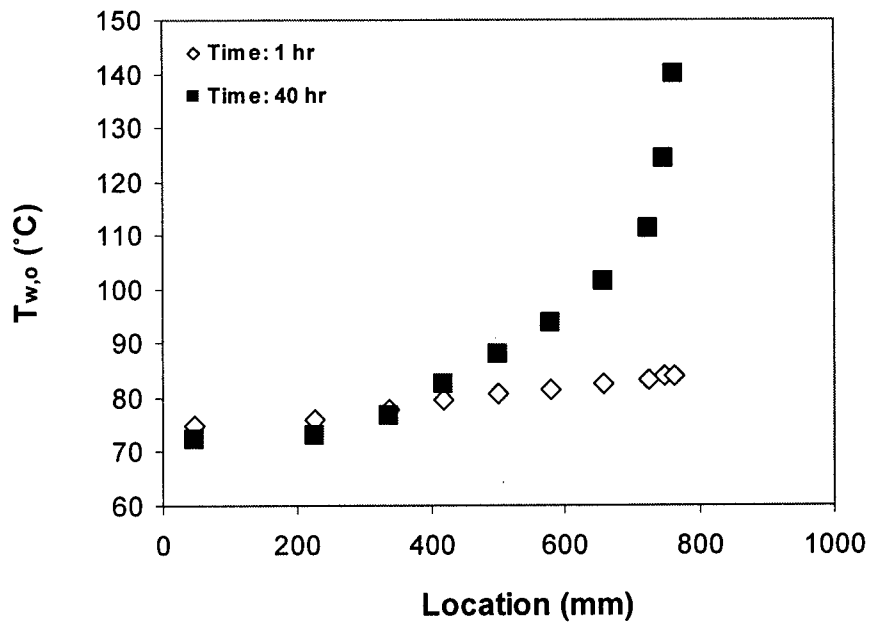


Figure 4.1.2: Initial and Final Wall Temperature Profiles (TFU 703)

$$U(x,t) = \frac{\dot{q}}{T_{w,i}(x) - T_b(x)} \quad (4.1.3)$$

where the heat flux  $\dot{q}$  is based on the inside area of the tube. The aforementioned procedure for delay time evaluation was employed for all of the thermocouples. A typical plot is illustrated in Figure 4.1.3, which throws more light on the initial stages of fouling progress. For all the experiments, an initial steady state period was always present, which made the estimation of the clean inside wall temperature and heat transfer coefficient straight-forward. The bulk temperature at position  $x$  was determined by assuming that the bulk temperature increases linearly under condition of a uniform heat flux along the length of the tube, and was therefore calculated as:

$$T_b(x) = T_{b,in} + [T_{b,out} - T_{b,in}] \frac{x}{L} \quad (4.1.4)$$

where  $L$  is the length of the heated section and  $x$  is the location of the thermocouple of interest. The inside wall temperature was calculated using the analytical solution of the steady state heat conduction equation for a long, hollow cylinder with uniform heat generation and an adiabatic outer wall:

$$T_{w,i}(x) = T_{w,o}(x) + \left( \frac{\dot{Q}}{2\pi L \lambda_{tube}} \right) \left[ \frac{1}{2} - \left( \frac{r_o^2}{r_o^2 - r_i^2} \right) \ln \left( \frac{r_o}{r_i} \right) \right] \quad (4.1.5)$$

Depending upon the exact operating conditions, the variation between the inside and outside wall temperature was between 0.5°C and 2°C.

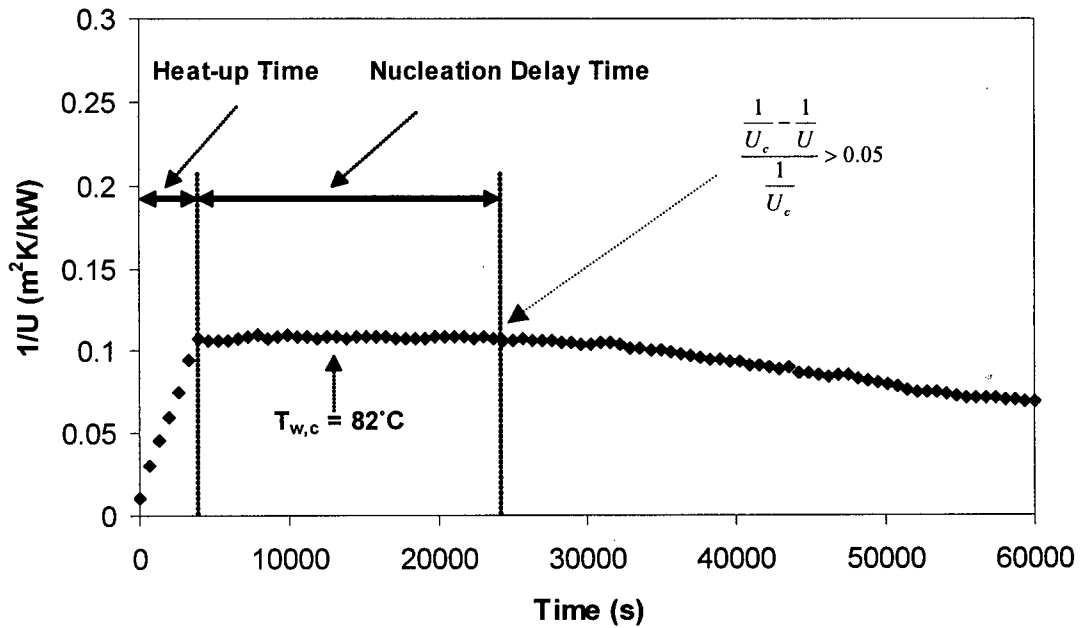


**Figure 4.1.3: Initial Fouling Stages at  $x = 715$  mm for TFU 703 ( $V = 1.2$  m/s), Showing Heat-up, Nucleation and Roughness Stages**

For the time period in which fouling clearly occurred, the fouling resistance,  $R_f$ , was determined from

$$R_f = \frac{1}{U(x,t)} - \frac{1}{U_c(x)} \quad (4.1.6)$$

After a roughness control period, the fouling resistance increased linearly and therefore a linear regression analysis easily determined the initial fouling rate,  $\dot{R}_{fo}$ , employing the following equation:

$$\dot{R}_{fo} = \frac{d}{dt} \left( \frac{1}{U(x,t)} \right) \quad (4.1.7)$$

This equation assumes that the convective heat transfer coefficient does not change with respect to time, e.g. as a result of surface

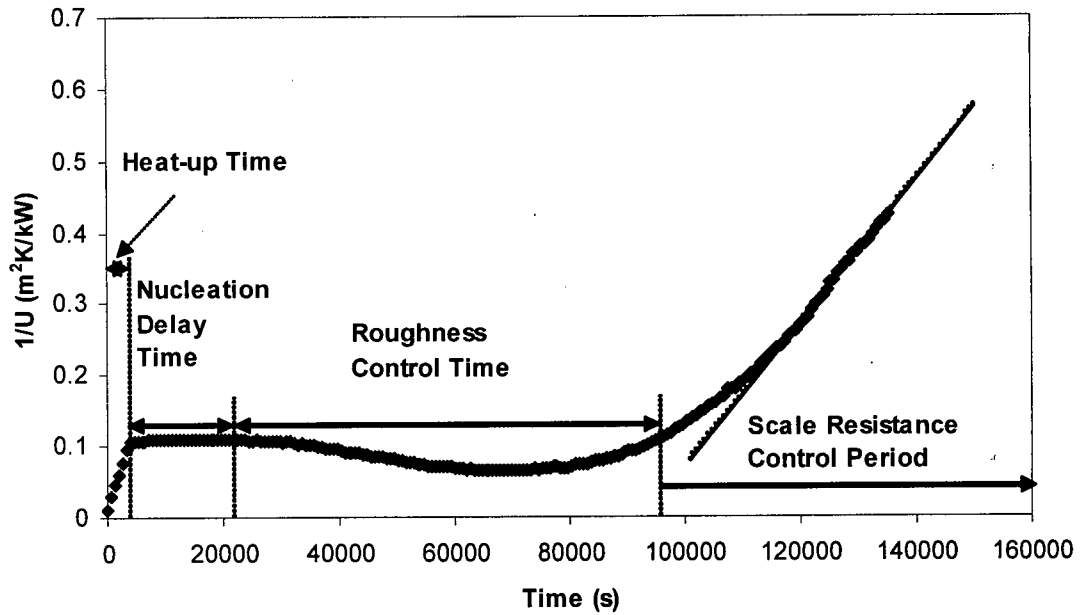


Figure 4.1.4: Different Fouling Stages at  $x = 715$  mm for TFU 703 ( $V = 1.2$  m/s,  $C = 3128$  ppm)

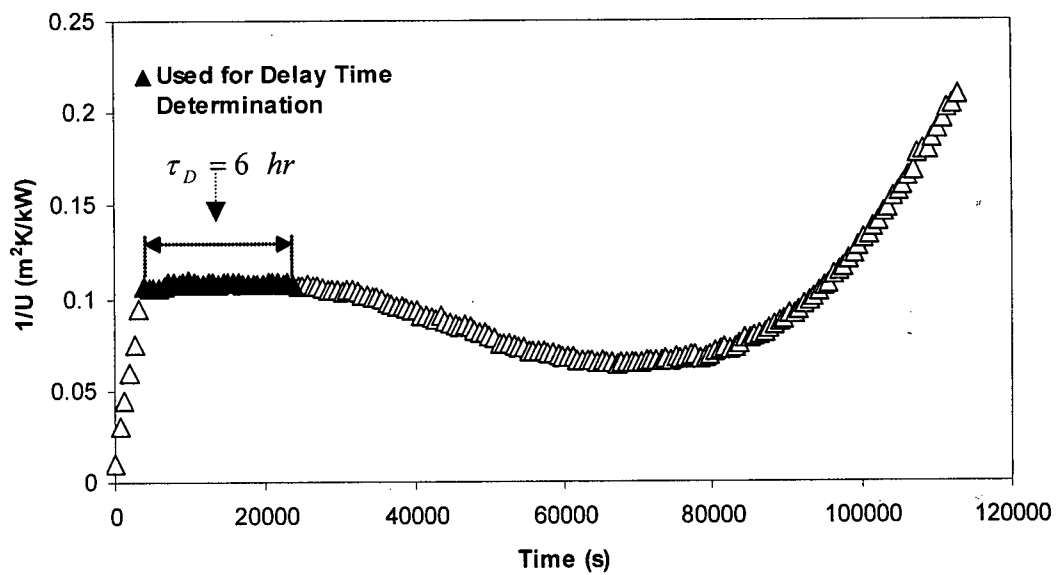


Figure 4.1.5: Delay Time Evaluation at  $x = 715$  mm for TFU 703 ( $V = 1.2$  m/s,  $C = 3128$  ppm)

roughness effects due to fouling, as in the roughness control period. In the initial fouling rate determination, the first point was chosen such that there was no systematic deviation from the regression at time values below this initial point. The small amount of fouling that occurs before the linear rate has been ignored in this calculation. Since there was no subsequent deviation from linearity during the fouling progression, all the points following the initial point were used in the regression analysis. Figure 4.1.4 illustrates a complete view of the fouling progress stages observed for one thermocouple. It consists of four different regions: a short heat-up time (about half an hour), a nucleation delay time (horizontal region), a roughness control period in which the heat transfer enhancement of the scale roughness over-rides the heat transfer resistance of the scale, and a final region in which scale resistance over-rides scale roughness. Figure 4.1.5 illustrates the delay time evaluation, determined as  $6 \pm 0.1$  hours at  $x = 715$  mm.

#### 4.2 Fouling Experiments

Thirteen fouling experiments over a range of fluid mass fluxes and wall temperatures were performed to investigate delay times and initial fouling rates. Four experiments were performed to study the concentration and wall temperature effect on the delay time at a velocity of 1.2 m/s covering inside wall temperatures from 72 to 82°C with a concentration range from 3128 to 3600 ppm (wt.). The remaining nine experiments were performed at a concentration of 3400 ppm to study the effect of velocity on both delay time and initial fouling rates.

Batches of aqueous supersaturated calcium sulphate solutions were prepared and added to the holding tank. Prior to the addition of heat to the test section, the solution was circulated for 30 minutes to ensure a thoroughly well mixed chemical system. The power to the test section was then applied to achieve the operating conditions required. Heating up the test section to steady state took approximately 10 - 15 minutes.

#### 4.2.1 Effect of Concentration and Wall Temperature on Delay Time

In all the performed experiments an in-line 1- $\mu\text{m}$  pore size filter was employed to eliminate micron sized particles. Delay times were detected and measured for all ten thermocouples in each experiment. In general, for each experiment the delay time decreased from  $T_1$  (the lowest or bottom thermocouple on the test section) to  $T_{10}$  (the highest or top thermocouple), respectively, the delay time being a strong function of surface temperature. Thus, for example, in one experiment, in which clean wall temperatures at two different locations were  $76^\circ\text{C}$  and  $82^\circ\text{C}$ , respectively, the corresponding delay times,  $\tau_D$ , were 14 hours and 6 hours. In addition to the wall temperature, solution concentration plays an important role as well. In the performed experiments, the supersaturation ratio,  $S$ , at each wall temperature was evaluated. The results for experiments performed under different concentrations at a fixed velocity are presented in Table 4.2.1.1 which illustrates how delay time changes with concentration and surface temperature. For a given concentration in Table 4.2.1.1, the first column presents the inside wall temperatures from the lowest thermocouple,  $T_1$ , to the top one,  $T_{10}$ , and the second and third columns present the corresponding supersaturation ratio and the measured delay time. Two important conclusions can be made from these results: firstly, for a given concentration, delay time decreases with increasing wall temperature;

and secondly, for a given wall temperature, delay time decreases with increasing concentration.

#### 4.2.2 Surface Energy and Delay Time Activation Energies

Based on the classical nucleation theory (Equation 2.3.2) and the results in Table 4.2.1.1, a plot of  $\ln \tau_D$  versus  $(\ln S)^2$  was constructed for each surface temperature. For instance, in Figure 4.2.2.1 the surface temperature is 82°C and the slope of the line determines the effective crystal surface energy,  $\gamma_{\text{eff}}$ , as 9.6 mJ/m<sup>2</sup>. The effective surface energy values were calculated at other surface temperatures and the results are presented in Table 4.2.2.1. Surface energy values in Table 4.2.2.1 range from 7.5 to 9.9 mJ/m<sup>2</sup>. These values are at the low end of the range 8-50 mJ/m<sup>2</sup>, determined as surface energy for CaSO<sub>4</sub>·2H<sub>2</sub>O in the same manner by several authors mainly in bulk precipitation (Section 2.4). Also, for the surface nucleation under laminar flow conditions, values of 7.9 and 14.6 mJ/m<sup>2</sup> have been reported by Linnikov (1999) for flow on a metal surface and by Hasson et al. (2003) on a polymeric membrane surface, respectively.

**Table 4.2.1.1: Delay Time Values for Different Operating Conditions (V=1.2 m/s)**

| Run             | 703            |      |               | 707            |      |               | 706            |      |               | 708            |      |               |
|-----------------|----------------|------|---------------|----------------|------|---------------|----------------|------|---------------|----------------|------|---------------|
| C (ppm)         | 3128           |      |               | 3291           |      |               | 3400           |      |               | 3600           |      |               |
| Locatio         | $T_{w,c}$ (°C) | S    | $\tau_D$ (hr) |
| T <sub>1</sub>  | 73.3           | 1.29 | 13.73         | 73.1           | 1.35 | 7.36          | 72.4           | 1.40 | 4.71          | 73.2           | 1.48 | 1.28          |
| T <sub>2</sub>  | 74.5           | 1.29 | 13.92         | 73.8           | 1.36 | 5.93          | 73.7           | 1.41 | 4.17          | 73.8           | 1.49 | 1.09          |
| T <sub>3</sub>  | 75.1           | 1.30 | 13.73         | 75.1           | 1.37 | 5.39          | 74.2           | 1.41 | 3.08          | 74.5           | 1.50 | 0.91          |
| T <sub>4</sub>  | 76.5           | 1.31 | 12.08         | 76.4           | 1.38 | 5.39          | 76.4           | 1.43 | 2.17          | 75.9           | 1.51 | 0.72          |
| T <sub>5</sub>  | 77.5           | 1.32 | 8.61          | 77.2           | 1.39 | 4.13          | 78.1           | 1.43 | 2.17          | 76.6           | 1.52 | 0.54          |
| T <sub>6</sub>  | 78.2           | 1.33 | 9.34          | 78.7           | 1.40 | 2.87          | 78.5           | 1.44 | 2.17          | 78.3           | 1.53 | 0.54          |
| T <sub>7</sub>  | 79.2           | 1.33 | 6.77          | 79.2           | 1.40 | 2.87          | 80.3           | 1.45 | 2.17          | 78.8           | 1.54 | 0.36          |
| T <sub>8</sub>  | 80.6           | 1.34 | 9.33          | 81             | 1.41 | 1.61          | 81.1           | 1.46 | 1.27          | 80.9           | 1.55 | 0.36          |
| T <sub>9</sub>  | 81.7           | 1.35 | 8.60          | 81.2           | 1.42 | 1.61          | 81.5           | 1.46 | 1.27          | 81.1           | 1.55 | 0.36          |
| T <sub>10</sub> | 82.1           | 1.35 | 6.04          | 81.8           | 1.42 | 1.61          | 82.2           | 1.47 | 0.72          | 81.7           | 1.55 | 0.36          |

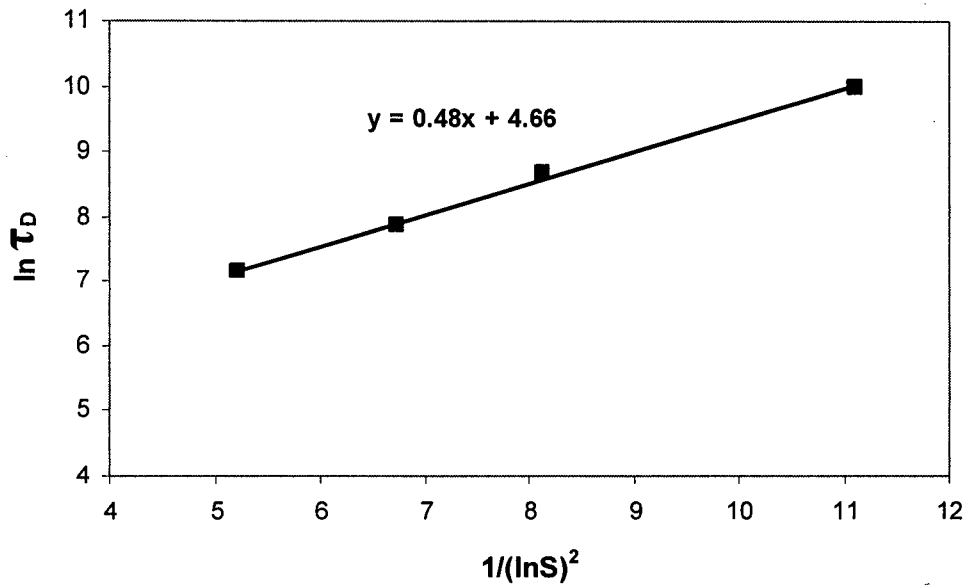


Figure 4.2.2.1: Plot of Delay Time versus Supersaturation According to Classical Nucleation Theory ( $V = 1.2$  m/s,  $T_{w,c} = 82^\circ\text{C}$ )

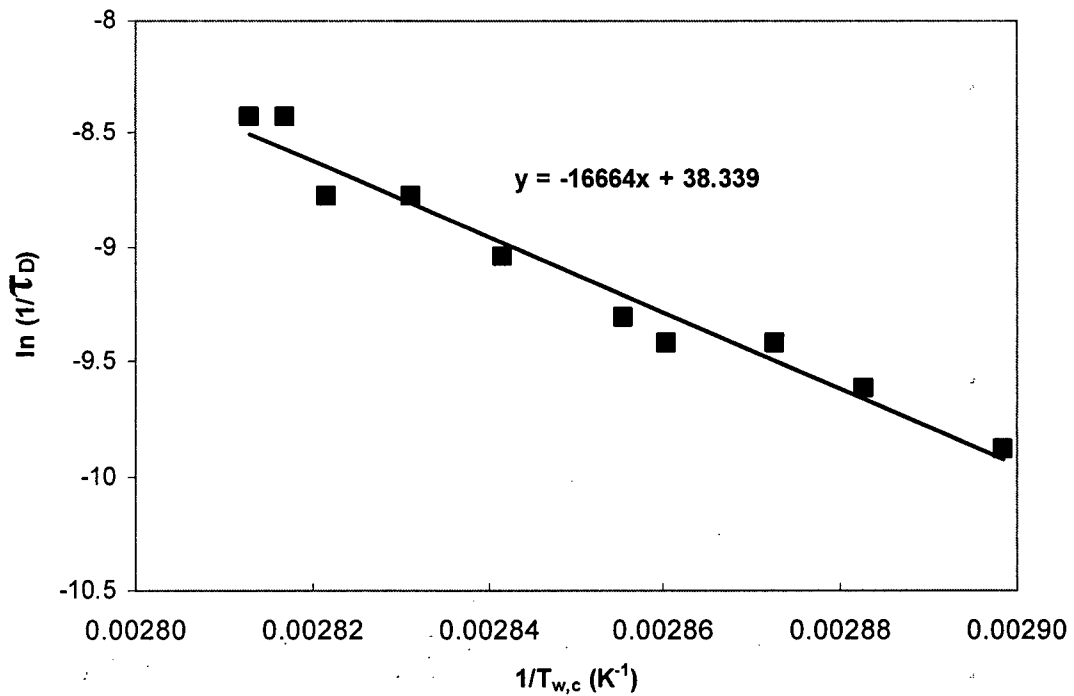


Figure 4.2.2.2: Arrhenius Type Plot of Delay Time versus Local Inside Wall Temperature for TFU 804 ( $C=3400$  ppm,  $V = 0.5$  m/s)

Table 4.2.2.1: Surface Energy Values for Different inside Wall Temperatures

|                                     | T <sub>1</sub> | T <sub>2</sub> | T <sub>3</sub> | T <sub>4</sub> | T <sub>5</sub> | T <sub>6</sub> | T <sub>7</sub> | T <sub>8</sub> | T <sub>9</sub> | T <sub>10</sub> |
|-------------------------------------|----------------|----------------|----------------|----------------|----------------|----------------|----------------|----------------|----------------|-----------------|
| Location, x (mm)                    | 48             | 125            | 203            | 286            | 361            | 443            | 521            | 600            | 668            | 716             |
| Temperature (°C)                    | 73.0           | 74.0           | 74.7           | 76.3           | 77.4           | 78.4           | 79.4           | 80.9           | 81.4           | 82.0            |
| $\gamma_{eff}$ (mJ/m <sup>2</sup> ) | 7.5            | 7.6            | 8.1            | 8.5            | 8.6            | 8.9            | 8.9            | 9.6            | 9.9            | 9.6             |

Table 4.2.2.2: Delay Time Activation Energies

| C = 3400 ppm |                       |                     |         |                         |                             |
|--------------|-----------------------|---------------------|---------|-------------------------|-----------------------------|
| Run No.      | T <sub>w,c</sub> (°C) | T <sub>b</sub> (°C) | V (m/s) | E <sub>D</sub> (kJ/mol) | $\Omega$ (s <sup>-1</sup> ) |
| 812          | 71-87                 | 51-62               | 0.1     | 79                      | 5.99E+6                     |
| 811          | 66-83                 | 51-61               | 0.2     | 78                      | 4.10E+7                     |
| 817          | 71-83                 | 51-62               | 0.3     | 119                     | 6.21E+13                    |
| 804          | 72-83                 | 51-63               | 0.5     | 139                     | 4.47E+16                    |
| 803          | 72-83                 | 51-63               | 0.7     | 163                     | 1.94E+20                    |
| 806          | 72-83                 | 51-62               | 1.0     | 163                     | 2.78E+20                    |
| 809          | 73-82                 | 51-62               | 1.2     | 163                     | 2.30E+20                    |
| 807          | 73-83                 | 51-62               | 1.4     | 172                     | 6.39E+21                    |
| 808          | 73-83                 | 51-62               | 1.6     | 165                     | 4.22E+20                    |

For experiments performed at the same concentration and at a given velocity, plotting the logarithm of reciprocal delay time vs. the reciprocal of inside surface temperature, based on an Arrhenius equation (after Branch, 1991), determines the delay time activation energy at that velocity. Figure 4.2.2.2 is a delay time plot for a given experiment according to the equation:

$$\ln(1/\tau_D) = \ln\Omega - E_D/RT_{w,c} \quad (4.2.2.1)$$

where individual thermocouple results were used to determine the surface temperature at a velocity of 0.5 m/s. Delay time activation energy E<sub>D</sub> for this experiment was determined as 139 kJ/mol, and the pre-exponential factor  $\Omega$  as 4.47 x 10<sup>16</sup> s<sup>-1</sup>. The results

for all runs performed are presented in Table 4.2.2.2. Delay time activation energy values in Table 4.2.2.2 are in the range 78 – 172 kJ/mol, which is higher than the values of 50-72 kJ/mol measured for bulk precipitation of calcium sulphate by Alimi et al. (2003). The main reasons why their results differ from those in this study are probably that, firstly, there was a different species such as  $\text{Cl}^-$  in their test fluid, that secondly their solutions were more highly supersaturated and that thirdly they employed a different technique, viz. a quartz microbalance (QMC), for detection of crystal formation.

### 4.2.3 Effect of Velocity on the Delay Time

Effect of velocity on the delay time is illustrated in Figures 4.2.3.1 and 4.2.3.2 for two different wall temperatures. Figure 4.2.3.1 shows the effect of velocity on the delay time at a fixed clean wall temperature of 82°C. It is seen that as the velocity increases, the delay time first decreases and then remains almost constant for velocities exceeding 0.5 m/s (which corresponds to  $\text{Re} = 11200$ ). The observed trend is explainable as due to the mechanism governing the initiation process, i.e. up to 0.5 m/s the process is mass transfer controlled and for higher velocities it is reaction controlled. At lower wall temperatures the velocity at which the controlling mechanism changes shifts towards lower velocities. For instance, at the wall temperature of 74°C, shown in Figure 4.2.3.2, it occurs around 0.2 m/s.

## 4.3 Initial Fouling Rate Analysis

### 4.3.1 Initial Fouling Rate Measurement

Due to the longitudinal temperature gradient on the surface of the tube (caused by the solution being heated as it passes through the tube), the downstream thermocouples showed the highest temperatures; they therefore exhibited the highest rate of fouling and

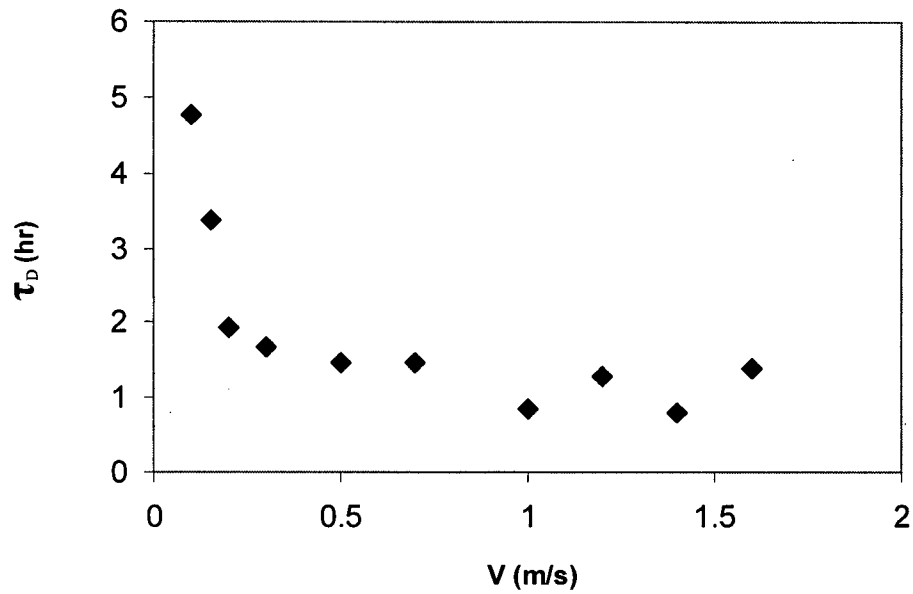


Figure 4.2.3.1: Effect of Velocity on the Delay Time  
( $T_{w,c} = 82^\circ\text{C}$ ,  $C = 3400$  ppm)

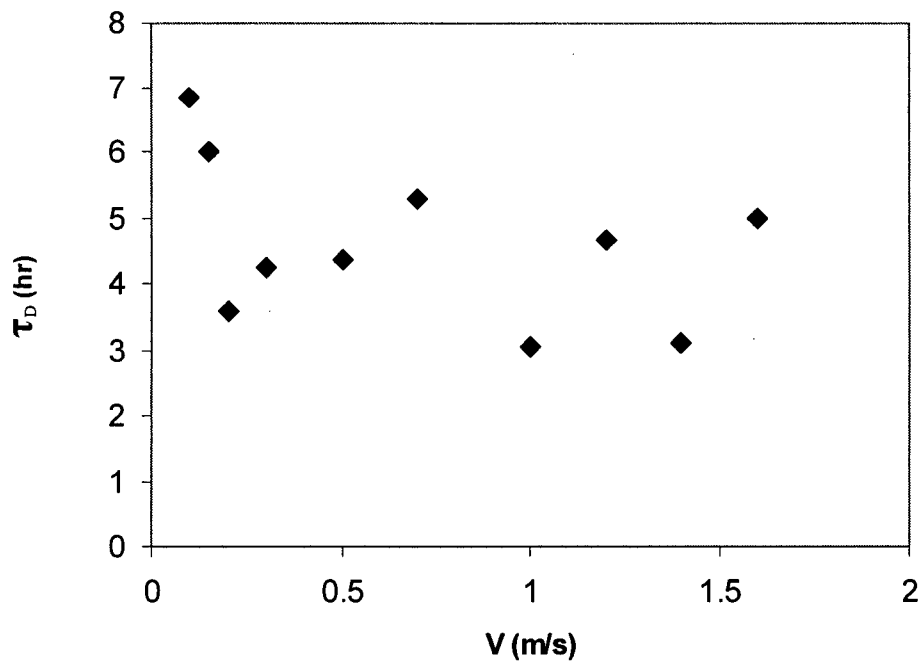


Figure 4.2.3.2: Effect of Velocity on the Delay Time  
( $T_{w,c} = 74^\circ\text{C}$ ,  $C = 3400$  ppm)

thus limited the duration of an experiment. Because clean inside wall temperatures were as high as 85°C, it was necessary to maintain some over-pressure on the test section to prevent the onset of boiling as the wall temperature rose due to fouling. When the test section pressure was maintained at 791 kPa (100 psig), measured wall temperatures were allowed to rise to 170°C before terminating the experiment. Because of this temperature restriction, the low temperature regions of the tube gave very low, and sometimes barely measurable, initial fouling rates. For this reason, and to simplify data analysis, a criterion was established in which the local fouling resistance, after completing the roughness control period, had to increase by 5%, i.e.  $R_f U_c \geq 0.05$  in order to be considered significant. Thus any data where the local heat transfer coefficient did not decrease by more than 5% compared to the clean heat transfer coefficient were neglected. Reynolds numbers based on local fluid properties were varied from 2100 to 36000 to provide adequate data for a complete study of the velocity effect on initial fouling rates.

As previously discussed, fouling was measured thermally, and the local heat transfer coefficient at a given thermocouple location was determined from Equation (4.1.3), the fouling resistance from Equation (4.1.6), and the initial fouling rate from Equation (4.1.7).

Figure 4.3.1.1 shows a plot of inside wall temperatures obtained from three thermocouple locations: the lowest,  $T_1$ , the middle,  $T_5$ , and the highest,  $T_{10}$  from TFU 703, which indicates a strong temperature effect on the initial fouling rate. For each of the three thermocouples the clean inside wall temperatures were evaluated from the horizontal (initiation) regions as 73, 78, and 82°C, respectively. The lowest thermocouple illustrates that the fouling progress is in the roughness control period and therefore no

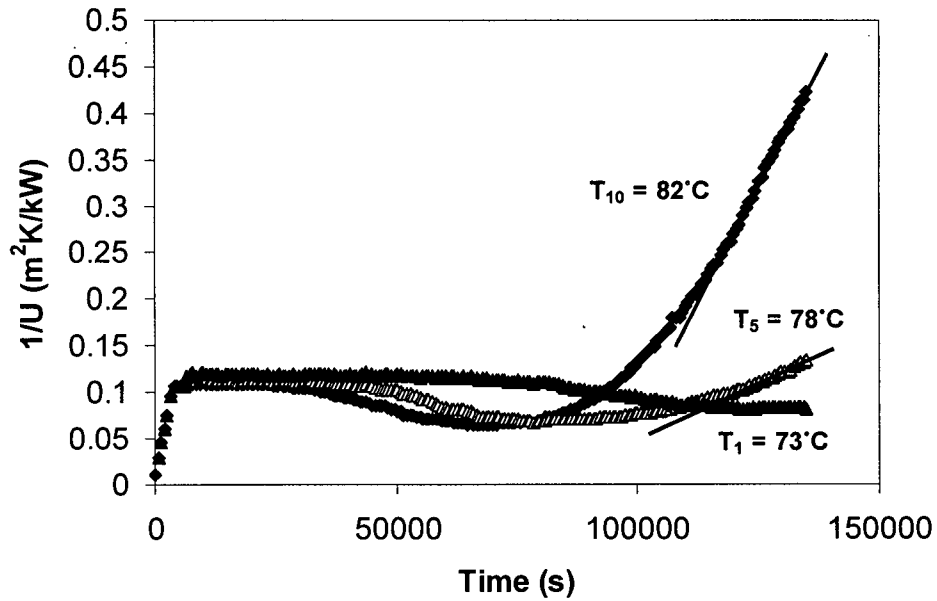


Figure 4.3.1.1: Inside Wall Temperature Profiles for Different Locations (TFU 703,  $V = 1.2$  m/s,  $C = 3128$  ppm)

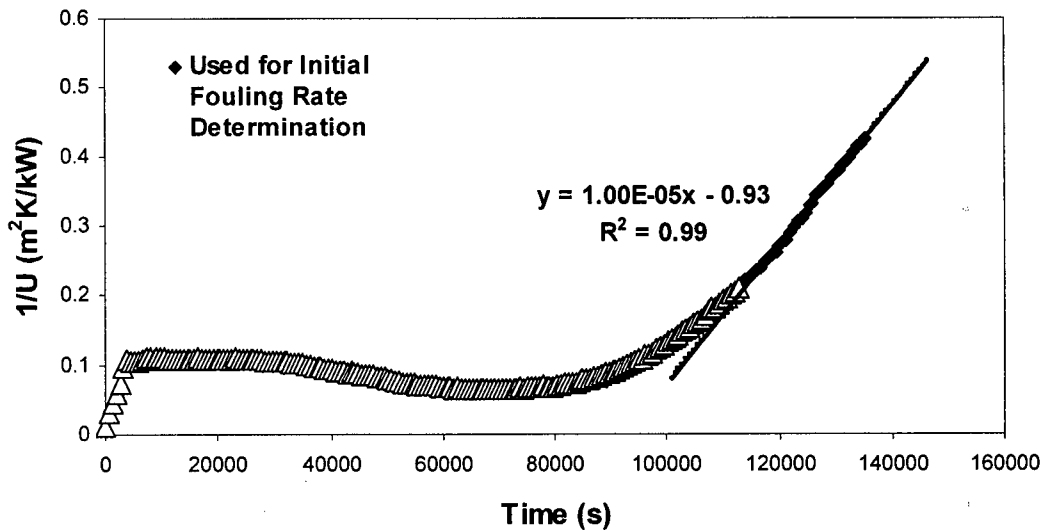


Figure 4.3.1.2: Initial Fouling Rate Determination for the Top Thermocouple (TFU 703,  $V = 1.2$  m/s,  $T_{w,c} = 82^\circ\text{C}$ ,  $C = 3128$  ppm)

initial fouling rate can be measured. On the other hand, the middle and the top ones show a linear increase in wall temperature for at least a short period of time after the roughness control period. Figure 4.3.1.2 illustrates the points employed for evaluating the initial fouling rate. The slope of the line determines the initial fouling rate as  $1.00 \times 10^{-5} \text{ m}^2\text{K/kJ}$ .

### 4.3.2 Effect of Velocity on the Initial Fouling Rate

In each experiment, performed at a given velocity, it was possible for 10 thermocouples to describe the system behaviour over a range of wall temperatures. Figure 4.3.2.1 shows the linear least squares regression for TFU 809 fitted to the Arrhenius type equation  $\dot{R}_{fo} = A \exp\left(-\frac{\Delta E_f}{R(T_{w,i})_c}\right)$ . A linear least squares regression linearises the experimental data as  $\ln(\dot{R}_{fo})$  versus  $1/(T_{w,i})_c$ . However, a non-linear least squares regression, which minimizes the sum of the squares of the residuals of  $\dot{R}_{fo}$  rather than of  $\ln(\dot{R}_{fo})$ , was used to see whether or not the results are the same. Figure 4.3.2.2 shows the same data, where a non-linear least squares regression is used. Both methods give the same value for fouling activation energy, 387 kJ/mol, and only slightly different values for pre-exponential factor,  $6.656 \text{ E}+52$  for linear regression and  $6.6891 \text{ E}+52$  for non-linear regression. Therefore, for all the experimental results, the simpler linear method was used to extract fouling activation energy values. The Arrhenius parameters for performed experiments at a concentration of 3400 ppm (wt.) are presented in Table 4.3.2.1. It is seen that as the velocity is increased fouling activation energy increases as well. In general, these fouling activation energies are considerably larger than the values reported for purely chemical activation energies for calcium sulphate bulk precipitation.

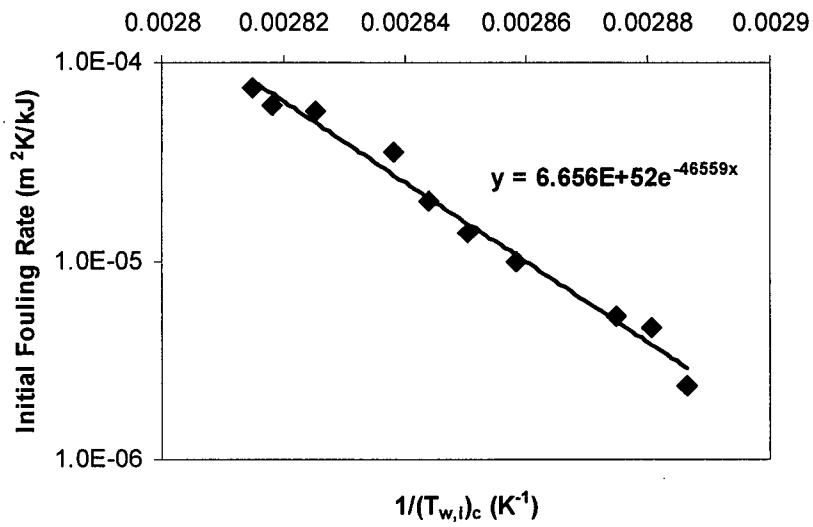


Figure 4.3.2.1: Linear Least Squares Regression for TFU 809

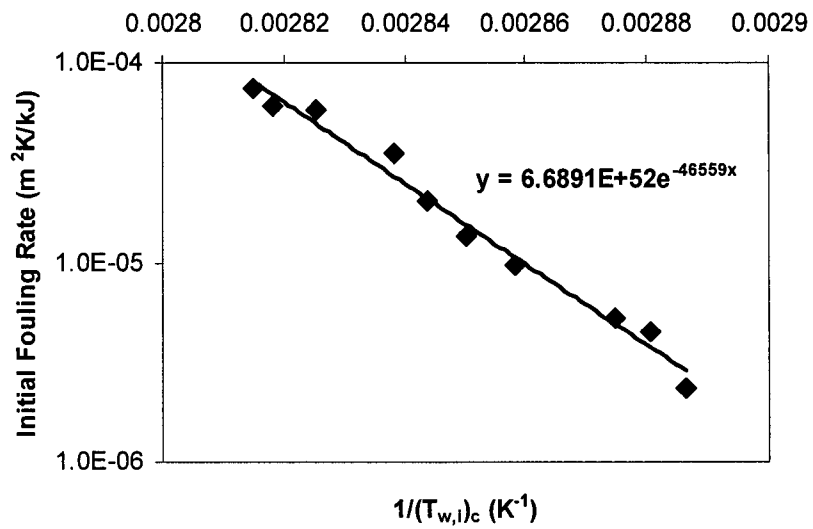
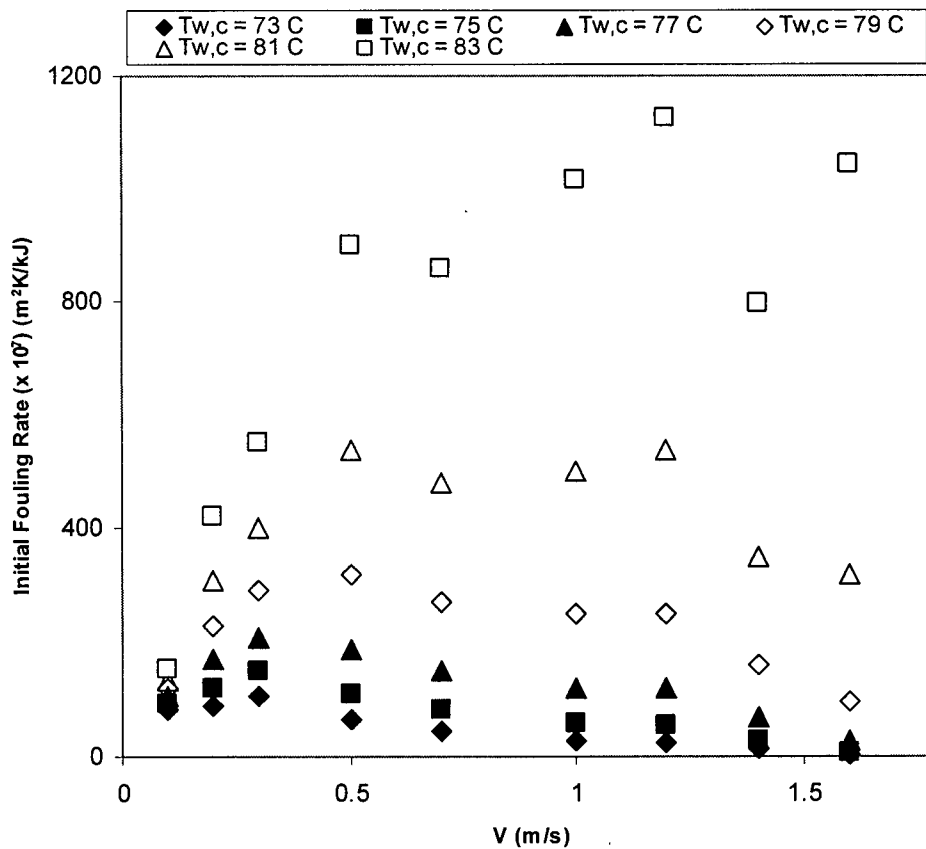


Figure 4.3.2.2: Non-linear Least Squares Regression for TFU 809

**Table 4.3.2.1: Arrhenius parameters for Calcium Sulphate Fouling Experiments  
(C = 3400 ppm)**

| Run No. | $T_{w,c}$ (°C) | $T_b$ (°C) | V (m/s) | Re ( $T_f$ ) | $\Delta E_f$<br>(kJ/mol) | A ( $m^2K/kJ$ ) |
|---------|----------------|------------|---------|--------------|--------------------------|-----------------|
| 812     | 71-87          | 51-62      | 0.1     | 2200         | 66                       | 8.9E+4          |
| 811     | 66-83          | 51-61      | 0.2     | 4200         | 159                      | 8.2E+18         |
| 817     | 71-83          | 51-62      | 0.3     | 6200         | 170                      | 3.68E+22        |
| 804     | 72-83          | 51-63      | 0.5     | 10600        | 268                      | 1.65E+35        |
| 803     | 72-83          | 51-63      | 0.7     | 14700        | 304                      | 3.62E+40        |
| 806     | 72-83          | 51-62      | 1.0     | 20800        | 367                      | 3.67E+49        |
| 809     | 73-82          | 51-62      | 1.2     | 25100        | 387                      | 6.65E+52        |
| 807     | 73-83          | 51-62      | 1.4     | 29400        | 425                      | 1.71E+58        |
| 808     | 73-83          | 51-62      | 1.6     | 33800        | 620                      | 1.84E+78        |



**Figure 4.3.2.3: Effect of Velocity on Initial Fouling Rate (C = 3400 ppm,  
( $T_{w,i}$ )<sub>c</sub> = 73 – 83°C,  $T_b$  = 50 – 61°C)**

Only at the lowest velocity, 0.1 m/s, is the activation energy close to the reported values for bulk precipitation, which in the temperature range of 15 – 90°C is 44 – 65 kJ/mol (Liu and Nancollas, 1975; Schierholtz, 1958; Konak, 1974; Smith and Sweett, 1971; He et al., 1994). For surface crystallization and without reporting the velocity, a range of 105-219 kJ/mol was reported by Bansal et al. (2005), which is closer to our experimental results. Since the fouling activation energy was not constant over a range of velocities, a single wall process does not always govern calcium sulphate scaling, and both bulk and wall processes must be important. In this work, these processes are considered to be mass transfer from the bulk to, and surface integration in, the vicinity of the wall. From Table 4.3.2.1 it is possible to use the Arrhenius expression to determine  $\dot{R}_{fo}$  at a given value of  $(T_{w,i})_c$  for each experiment and hence investigate the effect of velocity on the initial fouling rate. Thus Figure 4.3.2.3 shows the calculated results at six different surface temperatures where the initial fouling rate is strongly dependent upon the velocity. In all cases one can see the presence of a maximum deposition rate at a critical velocity as predicted by the model (Equation 2.8.1.16). Also, as the clean inside wall temperature decreases, the value of the maximum  $\dot{R}_{fo}$  decreases, and the location of the maximum for the four highest temperatures shifts towards a decreasing velocity, both trends being consistent with the model. Figure 4.3.2.3 indicates how strong the dependence of the fouling rate is on wall temperature, with appreciable differences observed for even 2°C wall temperature changes. At a wall temperature of 83°C it seems that the maximum initial fouling rate occurs around 1.2 m/s. At lower wall temperatures, below 73°C, there is very little distinction between initial fouling rates at different velocities, with experimental scatter probably playing a more significant role.

## 4.4 Deposit Distribution along the Test Section and its Physical Properties

### 4.4.1 Deposit Coverage Analysis

A deposit morphology study enables us to answer several questions:

- What is the dominant crystal shape for the buildup deposit and is the deposit layer uniform and homogeneous?
- What is the nature of the deposit? Does deposit aging occur and is its appearance the typical white deposit that has been reported by other researchers?
- Do the deposit characteristics change from one experiment to another, and if so, does this variation explain the existence of the increasing fouling rate with velocity at low fluid velocities?
- How do the crystals grow under different operating conditions along the test section? Is the amount of deposit at a given fluid velocity only wall temperature dependent?
- Does the deposit consist only of calcium, sulphur, and oxygen, or are other elements also present in the deposit?

Figure 4.4.1.1 is a photograph of an opened test section, cut into approximately 20 mm lengths, showing the nature of the white deposit along the sections of the fouled tube. Of the twelve sections presented in Figure 4.4.1.1, section 1 illustrates the fouling situation in the unheated entry region closest to the lower cable connection, sections 2 to 11 correspond to different thermocouple locations from  $T_1$  to  $T_{10}$ , and section 12 corresponds to the unheated exit region closest to the upper cable connection. The fluid flow direction in the photograph is indicated by increasing section number. Clearly, in the

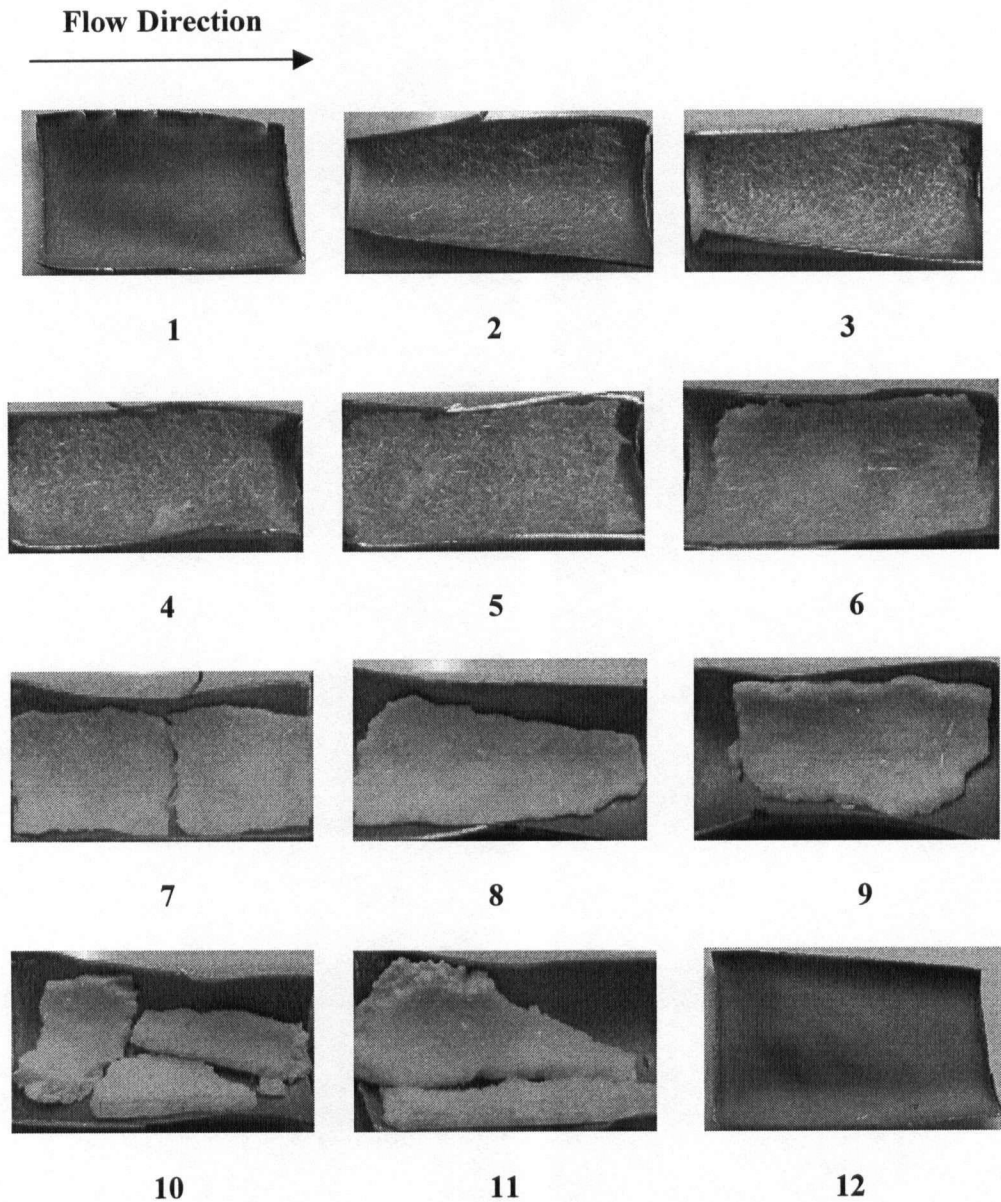


**Figure 4.4.1.1: Photograph of Fouled Tube Sections from TFU 809  
( $V = 1.2$  m/s)**

top of the unheated entry region, section 1, and in the region following the heated area, section 12, there is no deposition, while the hottest sections (2-11) show visible amounts of deposit. This shows that the amount of calcium sulphate deposition is a strong function of wall temperature, and the fact that there is no deposition in section 1 and that there is a

sudden termination of deposition in section 12 suggests that the contribution of bulk deposition is very small. Note that in the low temperature region needle crystals are scattered without covering the whole surface area, but as the wall temperature increases in the direction of fluid flow along the length of the tube, the buildup deposit gets more integrated with increased thickness to about 1 mm. Also, at lower temperatures the deposit was more tenacious, whereas at higher temperatures the deposit flaked off easily. Clearly, the deposit layer is not homogeneous or uniform along the entire length of the heated section. This is to be expected, since at low wall temperatures surface crystallization occurs at a low rate and hence individual crystals are distinguishable on the surface. However, at higher temperatures the degree of supersaturation is greater (by about 20-30 %) and disturbances in growth arise, resulting in the formation of a scale film that consists of many single crystals growing in different directions and increasingly wedging into each other. This non-homogeneity should be considered when the effective deposit thickness is used to evaluate the deposit physical properties ( $\lambda_f$  and  $\rho_f$ ).

To help gain an understanding of the deposit morphology, samples from different locations were prepared for scanning electron microscope (SEM) analysis. To avoid damaging the deposit structure, samples were prepared and mounted in cross-section and thus analyzed in-situ. Figures 4.4.1.2 – 4.4.1.4 show some of the scanning electron micrographs from samples in TFU 809.

Each sample taken of the fouled tube was a 20 mm stainless steel length of 9.017 mm OD with approximate wall thickness of 0.254 – 0.271 mm. A stainless steel tube cutter, which had the least impact on the tube and deposit, was used to cut test sections into approximately 20 mm sections. Figure 4.4.1.2, selected from lower temperature

regions, shows that from one nucleation centre (nucleus) formed on the surface of a crystallization cell, several crystals were growing simultaneously. This phenomenon is called splitting of crystals in which, after the formation of a crystal nucleus at the metal surface, it converts into a crystallization centre from which crystals grow simultaneously. Figure 4.4.1.3 shows a clearer picture of the splitting phenomenon. It illustrates that the deposit contains many needle-like crystals packed closely together, which is typical for gypsum ( $\text{CaSO}_4 \cdot 2\text{H}_2\text{O}$ ). The large crystals are surrounded by many smaller, randomly oriented crystals. Figure 4.4.1.4 shows an even clearer picture and confirms that calcium sulphate crystallizes preferentially in the form of needles.

Energy Dispersive X-ray (EDX) analyses were made of some of the deposits and Figure 4.4.1.5 is a typical result. It shows that the deposit consisted mostly of calcium, oxygen and sulphur. Another feature of the analyses was the absence of any sodium peak in the results. This shows that the by-product ( $\text{NaNO}_3$ ) of the chemical reaction from which the  $\text{CaSO}_4$  is obtained is not present in the deposit. This is to be expected, as sodium salts are normally highly soluble.

In addition to the qualitative results, shown in Figure 4.4.1.5, the corresponding quantitative values are presented in Table 4.4.1.1. Individual weight percent values for main elements, extracted from four different trials, prove that the deposits consist mainly of calcium, sulphur, and oxygen. Also, for three different calcium sulphate phases: gypsum ( $\text{CaSO}_4 \cdot 2\text{H}_2\text{O}$ ), hemihydrate ( $\text{CaSO}_4 \cdot 1/2\text{H}_2\text{O}$ ), and anhydrite ( $\text{CaSO}_4$ ), elemental weight percent was calculated and presented in Table 4.4.1.1. Since EDX technique does not detect hydrogen, in the aforementioned calculations hydrogen was not

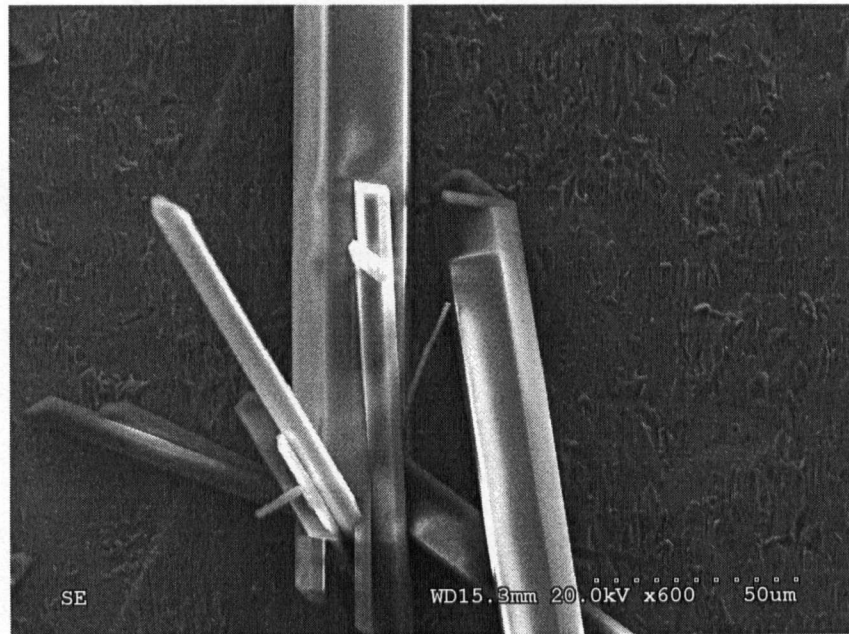


Figure 4.4.1.2: SEM of TFU 809,  $x \approx 48$  mm, Magnification 600x



Figure 4.4.1.3: SEM of TFU 809,  $x \approx 710$  mm, Magnification 60x



Figure 4.4.1.4: SEM of TFU 809,  $x \approx 710$  mm, Magnification 90x

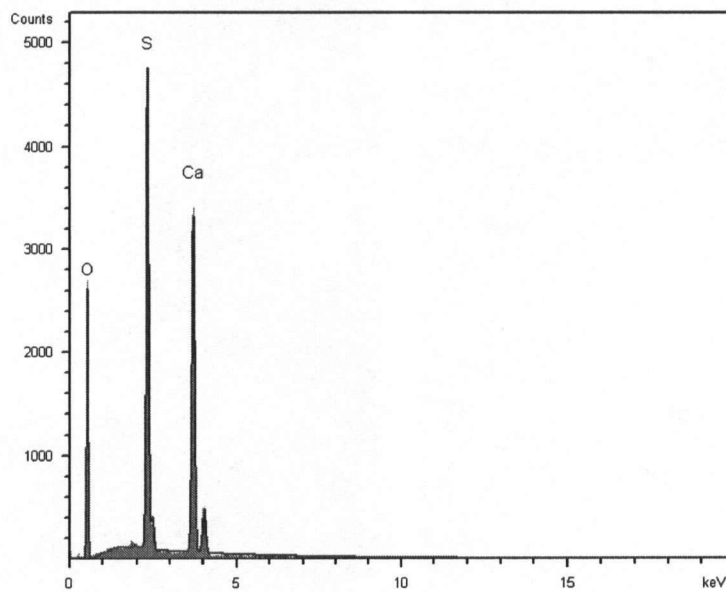


Figure 4.4.1.5: EDX Analysis of the Fouling Deposits for TFU 809

**Table 4.4.1.1: EDX Analysis of the Fouling Deposits for TFU 809**

| <b>EDX Results</b>                                       |                  |                 |                 |                |
|--|------------------|-----------------|-----------------|----------------|
| <b>Trial #</b>   | <b>Ca (wt %)</b> | <b>S (wt %)</b> | <b>O (wt %)</b> | <b>Total %</b> |
| 1  | 21.30            | 16.69           | 61.34           | 99.33          |
| 2  | 24.58            | 19.43           | 55.54           | 99.55          |
| 3  | 26.71            | 22.13           | 50.96           | 99.80          |
| 4  | 24.59            | 19.41           | 55.40           | 99.40          |
| Average  | 24.30            | 19.42           | 55.81           | 99.52          |
| <b>Calculated Results (without considering hydrogen)</b> |                  |                 |                 |                |
| CaSO <sub>4</sub> · 2H <sub>2</sub> O                    | 23.81            | 19.05           | 57.14           | 100            |
| CaSO <sub>4</sub> · 0.5H <sub>2</sub> O                  | 27.59            | 22.07           | 50.34           | 100            |
| CaSO <sub>4</sub>  | 29.41            | 23.53           | 47.06           | 100            |

considered. Although EDX technique is not recommended for accurate measurements, comparing its averaged elemental weight percent values with the corresponding calculated values for each phase illustrates that the deposit consists mainly of gypsum. This is to be expected, since the samples were analyzed from the solution-side deposit where the temperature was about 83°C. This temperature is below 98°C, the temperature at which the phase transformation to hemihydrate occurs.

It should be mentioned that there are limitations associated with the aforementioned techniques. For instance, since electrons do not pass through air, the experiments must be run in vacuum. This means that water may evaporate from wet samples easily and affect the results. However, since water of hydration is strongly bonded in the crystal structure, it is not easily released under vacuum. Therefore, it is not affected by the sample procedure in SEM/EDX.

To confirm the EDX results, thermogravimetric analysis (TGA), which measures weight changes as a function of time, was performed on the dry samples. Figure 4.4.1.6 shows the results over the whole time interval. First, the sample was heated up from room

temperature to about 99°C within 5 minutes and held at that temperature for about one hour. Then it was heated up to 900°C within 20 minutes and held at that temperature for about 2 hours. The weight loss curve indicates that at 99°C the magnitude of the weight loss (about 20 % of the original sample weight) agrees well with what is stoichiometrically expected for complete dehydration of the gypsum to the anhydrite form. No significant weight loss occurred at 900°C, showing that the complete phase transformation occurs at 99°C.

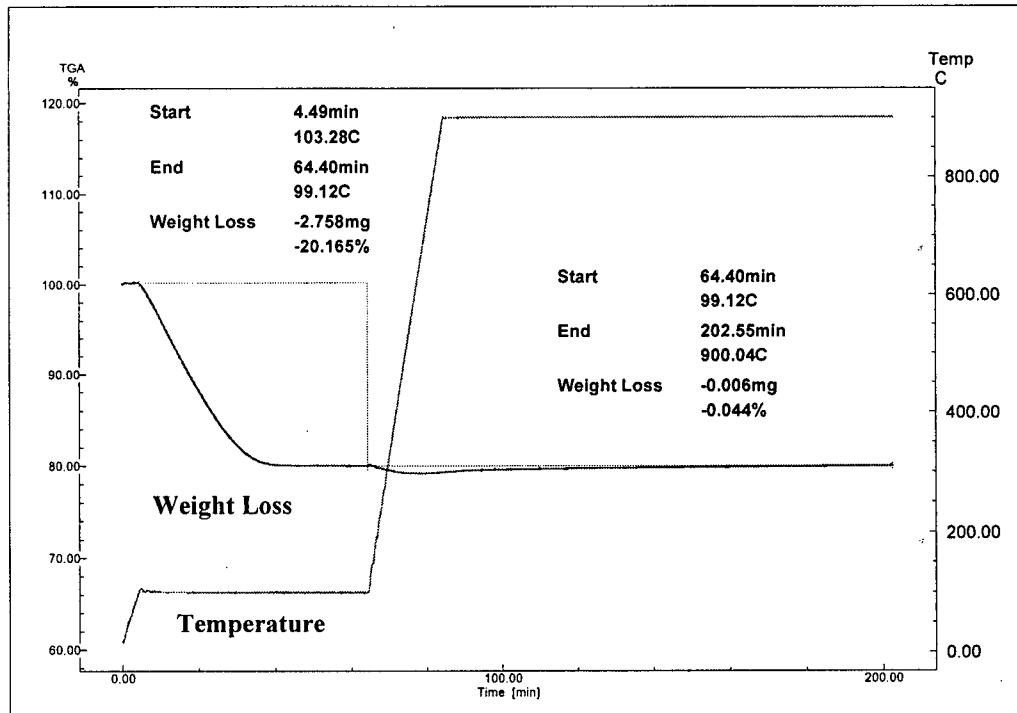


Figure 4.4.1.6: Weight Loss Profile for Dry Sample in TFU 809,  $x \approx 710$  mm

#### 4.4.2 Deposit Physical Properties

Following the measurement procedures described in Section 3.8, Figure 4.4.2.1 shows a typical plot of deposit coverage and deposit thickness along the length of the fouled tube. The heated section started at 547 mm from the tube inlet, and deposition is clearly visible after that. Similarly the heated section ends at 1318 mm and the amount of deposit reduces rapidly. Note that the deposit coverage method is more accurate than the deposit thickness method, where reading the caliper thickness is considerably more subjective, and therefore very much an approximate technique, especially with the presence of needle crystals. However, the same trends are clearly observed using both

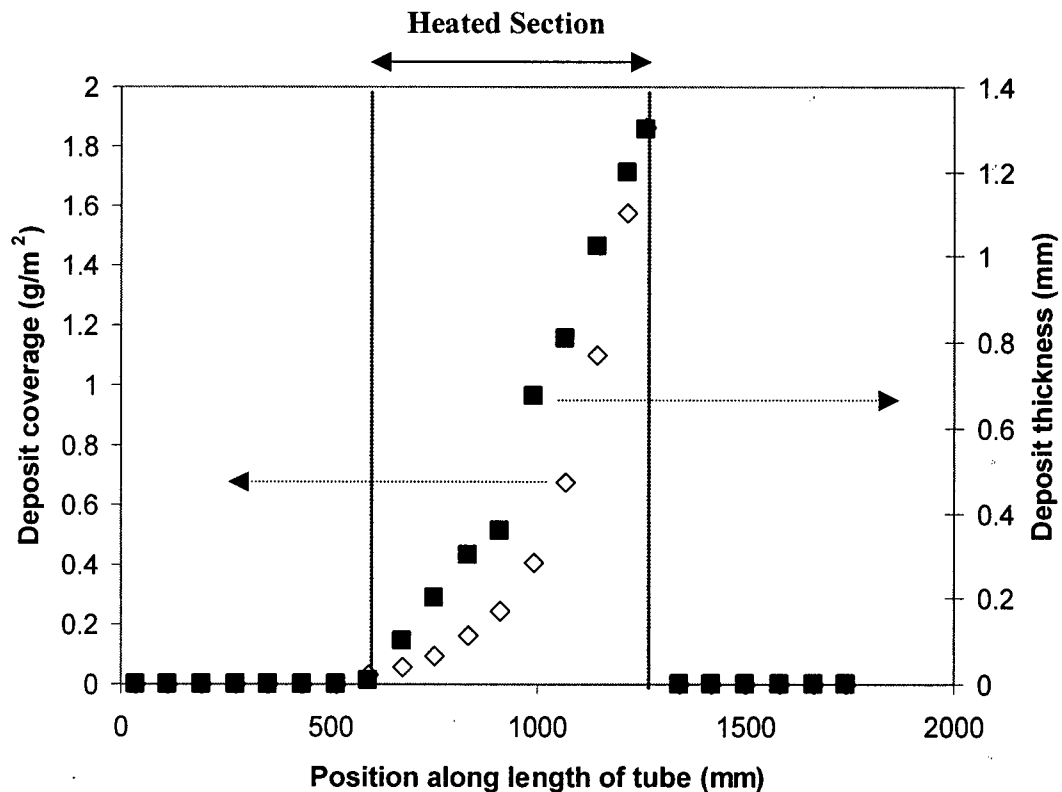


Figure 4.4.2.1: Deposit Distribution along Length of Tube for TFU 809

methods. A summary of the deposit coverage and thickness results along the heated section is shown in Table 4.4.2.1.

Figure 4.4.2.2 plots the deposit coverage  $m_f$  and deposit thickness  $x_f$  results for each experiment against  $R_f$ , giving unique values for  $\lambda_f$  (= slope of  $x_f$  vs.  $R_f$ ) and  $\rho_f \lambda_f$  (= slope of  $m_f$  vs.  $R_f$ ). All linear regressions fit the experimental data well with the exception of those for lower velocities ( $V < 0.3$  m/s). At low velocities, where mass transfer controls, crystallization rate was low and therefore the corresponding fouling resistance to each thermocouple was negative, i.e. the fouling process was in the roughness control period. Only positive fouling resistances were employed to construct the plots in Figure 4.4.2.2. Without roughness effects both plots,  $m_f$  vs.  $R_f$  and  $x_f$  vs.  $R_f$ , have to pass through the origin. However, due to the roughness effect on convective heat transfer (which gives rise to the roughness control period), the measured  $R_f$  is less than the true  $R_f$ . Therefore the plots of  $m_f$  vs.  $R_f$  should show a positive intercept on the  $m_f$  axis, and the plots of  $x_f$  vs.  $R_f$  a positive intercept on the  $x_f$  axis. In general, the  $x_f$  plots did consistently show a positive intercept, but, presumably due to experimental shortcomings, the  $m_f$  plots did not always do so.

All of the deposit density and thermal conductivity results from Fig. 4.4.2.2 are shown in Table 4.4.2.2. Thermal conductivity values, presented in Table 4.4.2.2, showed a range from 0.84 to 1.89 W/m·K and averaged  $1.34 \pm 0.15$  W/m·K, which is less than the value of 2.2 W/m·K reported by Najibi et al. (1997), but larger than 1.15 W/m·K reported by Krause (1993) and 0.58 W/m·K by Hasson and Zahavi (1970).

Figure 4.4.2.3 throws more light on the data. Deposit coverage and deposit thickness results for each thermocouple were each divided by the corresponding final

#### 4: Experimental Results and Discussions

**Table 4.4.2.1: Deposit Coverage and Thickness Results**

|         | Section length (mm) | Section surface area (mm <sup>2</sup> ) | Fouled weight (g) | Clean weight (g) | Deposit weight (g) | $R_f$ (m <sup>2</sup> K/W) | $m_f$ (kg/m <sup>2</sup> ) | $x_f$ (mm) | $T_{w,initial}$ (°C) | $T_{w,final}$ (°C) | V (m/s) | $\rho_f \lambda_f = m_f/R_f$ (kgW/m <sup>4</sup> K) | $\lambda_f = x_f/R_f$ (W/m·K) |
|---------|---------------------|---|-------------------|------------------|--------------------|----------------------------|----------------------------|------------|----------------------|--------------------|---------|---|-------------------------------|
| TFU 812 | 20.06               | 568.25                                  | 1.2808            | 1.2772           | 0.0036             | -0.000050                  | 0.0063                     | -          | 70.5                 | 66.3               | 0.10    | -   | -                             |
|         | 20.16               | 571.09                                  | 1.422             | 1.2702           | 0.1518             | 0.000552                   | 0.2658                     | 0.55       | 71.6                 | 81.1               | 0.10    | 481.88  | 1.00                          |
|         | 20.16               | 571.09                                  | 1.5768            | 1.2898           | 0.287              | 0.000417                   | 0.5026                     | 0.89       | 74.3                 | 81.6               | 0.10    | 1204.29   | 2.13                          |
|         | 20.425              | 578.59                                  | 1.5796            | 1.294            | 0.2856             | 0.000472                   | 0.4936                     | 0.83       | 76.5                 | 81.5               | 0.10    | 1044.82   | 1.76                          |
|         | 20.11               | 569.67                                  | 1.4796            | 1.2909           | 0.1887             | -0.000368                  | 0.3312                     | 0.68       | 78.8                 | 74.6               | 0.10    | -   | -                             |
|         | 20.16               | 571.09                                  | 1.4937            | 1.2965           | 0.1972             | -0.000539                  | 0.3453                     | 0.87       | 81.4                 | 74.1               | 0.10    | -   | -                             |
|         | 20.225              | 572.93                                  | 1.4299            | 1.299            | 0.1309             | -0.000834                  | 0.2285                     | 0.71       | 83.6                 | 69.9               | 0.10    | -   | -                             |
|         | 20.1                | 569.39                                  | 1.4772            | 1.2764           | 0.2008             | -0.000813                  | 0.3527                     | 0.96       | 84.2                 | 71                 | 0.10    | -   | -                             |
|         | 20                  | 566.55                                  | 1.5657            | 1.2709           | 0.2948             | -0.000419                  | 0.5203                     | 1.08       | 84.7                 | 76.8               | 0.10    | -   | -                             |
| 19.55   | 553.81              | 1.5493                                  | 1.2421            | 0.3072           | 0.001039           | 0.5547                     | 1.3                        | 87.3       | 79.1                 | 0.10               | 534.04  | 1.25  |                               |
| TFU 811 | 20.66               | 585.25                                  | 1.4161            | 1.3302           | 0.0859             | -                          | 0.1468                     | -          | 66.1                 | 81.3               | 0.20    | -   | -                             |
|         | 20.11               | 569.67                                  | 1.3852            | 1.3024           | 0.0828             | -0.000050                  | 0.1453                     | 0.43       | 68.7                 | 70.3               | 0.20    | -   | -                             |
|         | 19.81               | 561.17                                  | 1.3621            | 1.2763           | 0.0858             | -0.000042                  | 0.1529                     | 0.48       | 71.3                 | 72.2               | 0.20    | -   | -                             |
|         | 20.1                | 569.39                                  | 1.4008            | 1.2908           | 0.11               | -0.000005                  | 0.1932                     | 0.54       | 75.3                 | 75.9               | 0.20    | -   | -                             |
|         | 20.29               | 574.77                                  | 1.4596            | 1.3095           | 0.1501             | -0.000061                  | 0.2611                     | 0.8        | 76.8                 | 75.3               | 0.20    | -   | -                             |
|         | 20.63               | 584.40                                  | 1.529             | 1.3242           | 0.2048             | 0.000213                   | 0.3504                     | 0.79       | 78.2                 | 81.6               | 0.20    | 664.98  | 1.50                          |
|         | 20.17               | 571.37                                  | 1.5374            | 1.2875           | 0.2499             | 0.000246                   | 0.4374                     | 0.95       | 80.5                 | 88.7               | 0.20    | 1778.55   | 3.86                          |
|         | 20.18               | 571.65                                  | 1.6398            | 1.2976           | 0.3422             | 0.000344                   | 0.5986                     | 1.08       | 82.0                 | 93.3               | 0.20    | 1739.17   | 3.14                          |
|         | 20.2                | 572.22                                  | 1.7767            | 1.2969           | 0.4798             | 0.000592                   | 0.8385                     | 1.13       | 82.5                 | 101.7              | 0.20    | 1415.93   | 1.91                          |
|         | 20.31               | 575.34                                  | 1.7991            | 1.3023           | 0.4968             | 0.000647                   | 0.8635                     | 1.3        | 83.4                 | 104.3              | 0.20    | 1335.02   | 2.01                          |
| TFU 817 | 20.28               | 574.49                                  | 1.359             | 1.2899           | 0.0691             | 0.000243                   | 0.1203                     | 0.1        | 70.7                 | 80.8               | 0.30    | 495.80  | 0.41                          |
|         | 20.19               | 571.94                                  | 1.4219            | 1.2848           | 0.1371             | 0.000180                   | 0.2397                     | 0.2        | 72.3                 | 81.8               | 0.30    | 1334.63   | 1.11                          |
|         | 20.45               | 579.30                                  | 1.4327            | 1.3031           | 0.1296             | 0.000104                   | 0.2237                     | 0.21       | 74.4                 | 78.7               | 0.30    | 2151.13   | 2.02                          |
|         | 20.04               | 567.69                                  | 1.4393            | 1.2835           | 0.1558             | 0.000134                   | 0.2744                     | 0.34       | 75.0                 | 82                 | 0.30    | 2048.11   | 2.54                          |
|         | 20.26               | 573.92                                  | 1.5094            | 1.2909           | 0.2185             | 0.000163                   | 0.3807                     | 0.48       | 76.4                 | 87                 | 0.30    | 2340.20   | 2.95                          |
|         | 20.4                | 577.89                                  | 1.5581            | 1.2963           | 0.2618             | 0.000321                   | 0.4530                     | 0.55       | 78.4                 | 96.2               | 0.30    | 1410.23   | 1.71                          |
|         | 20.45               | 579.30                                  | 1.5663            | 1.2993           | 0.267              | 0.000266                   | 0.4609                     | 0.65       | 78.8                 | 94.6               | 0.30    | 1731.40   | 2.44                          |
|         | 20                  | 566.55                                  | 1.6365            | 1.276            | 0.3605             | 0.000446                   | 0.6363                     | 0.82       | 81.8                 | 102.8              | 0.30    | 1425.35   | 1.84                          |
|         | 19.88               | 563.16                                  | 1.6946            | 1.2716           | 0.423              | 0.000698                   | 0.7511                     | 0.92       | 82.0                 | 116.2              | 0.30    | 1076.07   | 1.32                          |
|         | 20.26               | 573.92                                  | 1.8656            | 1.3003           | 0.5653             | 0.001133                   | 0.9850                     | 1.13       | 82.9                 | 115.5              | 0.30    | 869.41  | 1.00                          |

**4: Experimental Results and Discussions**

**Table 4.4.2.1: Deposit Coverage and Thickness Results (cont'd)**

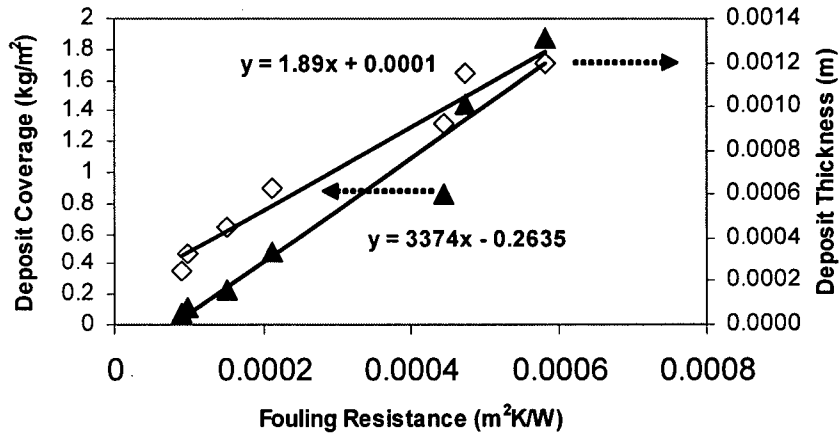
|         | Section length (mm) | Section surface area (mm <sup>2</sup> ) | Fouled weight (g) | Clean weight (g) | Deposit weight (g) | R <sub>f</sub> (m <sup>2</sup> K/W) | m <sub>f</sub> (kg/m <sup>2</sup> ) | x <sub>f</sub> (mm) | T <sub>w,initial</sub> (°C) | T <sub>w,final</sub> (°C) | V (m/s) | ρ <sub>f</sub> λ <sub>f</sub> = m <sub>f</sub> /R <sub>f</sub> (kgW/m <sup>4</sup> K) | λ <sub>f</sub> = x <sub>f</sub> /R <sub>f</sub> (W/m·K) |
|---------|---------------------|---|-------------------|------------------|--------------------|-------------------------------------|-------------------------------------|---------------------|-----------------------------|---------------------------|---------|---|---|
| TFU 804 | 20.83               | 590.07                                  | 1.367             | 1.3328           | 0.0342             | 0.000190                            | 0.0580                              | 0.2                 | 72.1                        | 74                        | 0.50    | 305.26  | 1.05  |
|         | 20.74               | 587.52                                  | 1.3962            | 1.337            | 0.0592             | 0.000133                            | 0.1008                              | 0.3                 | 74.0                        | 76.9                      | 0.50    | 760.33  | 2.26  |
|         | 19.92               | 564.29                                  | 1.3698            | 1.2707           | 0.0991             | 0.000202                            | 0.1756                              | 0.38                | 75.2                        | 83.6                      | 0.50    | 869.40  | 1.88  |
|         | 20.4                | 577.89                                  | 1.494             | 1.3058           | 0.1882             | 0.000487                            | 0.3257                              | 0.75                | 76.7                        | 95.9                      | 0.50    | 668.58  | 1.54  |
|         | 20.43               | 578.74                                  | 1.5968            | 1.3111           | 0.2857             | 0.000336                            | 0.4937                              | 0.85                | 77.3                        | 104.5                     | 0.50    | 1467.96   | 2.53  |
|         | 20.26               | 573.92                                  | 1.7703            | 1.3047           | 0.4656             | 0.000474                            | 0.8113                              | 0.9                 | 79.0                        | 116.8                     | 0.50    | 1711.74   | 1.90  |
|         | 19.39               | 549.27                                  | 1.8885            | 1.2392           | 0.6493             | 0.000653                            | 1.1821                              | 1                   | 80.3                        | 132.1                     | 0.50    | 1811.19   | 1.53  |
|         | 20.27               | 574.20                                  | 2.2503            | 1.3064           | 0.9439             | 0.000823                            | 1.6438                              | 1.35                | 81.5                        | 146.3                     | 0.50    | 1996.77   | 1.64  |
|         | 20.44               | 579.02                                  | 2.5081            | 1.3159           | 1.1922             | 0.001054                            | 2.0590                              | 1.35                | 82.1                        | 165.5                     | 0.50    | 1952.81   | 1.28  |
|         | 20.19               | 571.94                                  | 2.671             | 1.2934           | 1.3776             | 0.001356                            | 2.4087                              | 1.4                 | 82.6                        | 170.5                     | 0.50    | 1776.76   | 1.03  |
| TFU 803 | 19.56               | 554.09                                  | 1.279             | 1.2572           | 0.0218             | 0.000103                            | 0.0393                              | 0.18                | 72.6                        | 75                        | 0.70    | 381.98  | 1.75  |
|         | 20.35               | 576.47                                  | 1.3596            | 1.3105           | 0.0491             | 0.000259                            | 0.0852                              | 0.25                | 74.2                        | 78.4                      | 0.70    | 328.89  | 0.97  |
|         | 20.24               | 573.35                                  | 1.3885            | 1.2907           | 0.0978             | 0.000178                            | 0.1706                              | 0.35                | 75.0                        | 78.4                      | 0.70    | 958.34  | 1.97  |
|         | 20.2                | 572.22                                  | 1.4707            | 1.2938           | 0.1769             | 0.000197                            | 0.3091                              | 0.5                 | 76.3                        | 101.3                     | 0.70    | 1570.52   | 2.54  |
|         | 20.54               | 581.85                                  | 1.6269            | 1.3237           | 0.3032             | 0.000262                            | 0.5211                              | 0.85                | 77.5                        | 107.9                     | 0.70    | 1986.64   | 3.24  |
|         | 20.23               | 573.07                                  | 1.7112            | 1.31             | 0.4012             | 0.000402                            | 0.7001                              | 0.9                 | 78.6                        | 125.4                     | 0.70    | 1739.96   | 2.24  |
|         | 20.54               | 581.85                                  | 2.1561            | 1.3182           | 0.8379             | 0.000742                            | 1.4401                              | 1.25                | 80.1                        | 165.2                     | 0.70    | 1940.43   | 1.68  |
|         | 19.84               | 562.02                                  | 2.3766            | 1.2763           | 1.1003             | 0.000823                            | 1.9578                              | 1.4                 | 81.3                        | 175.6                     | 0.70    | 2378.21   | 1.70  |
|         | 20.1                | 569.39                                  | 2.6182            | 1.2905           | 1.3277             | 0.000823                            | 2.3318                              | 1.45                | 82.1                        | 176.4                     | 0.70    | 2834.35   | 1.76  |
|         | 20.41               | 578.17                                  | 2.9792            | 1.3189           | 1.6603             | 0.000893                            | 2.8717                              | 1.55                | 82.5                        | 184.7                     | 0.70    | 3216.35   | 1.74  |
| TFU 806 | 20.54               | 581.85                                  | 1.3417            | 1.3256           | 0.0161             | -0.000015                           | 0.0277                              | -                   | 71.9                        | 70.9                      | 1.00    | -   | -   |
|         | 19.93               | 564.57                                  | 1.3125            | 1.2831           | 0.0294             | 0.000076                            | 0.0521                              | 0.15                | 73.2                        | 75.5                      | 1.00    | 682.50  | 1.97  |
|         | 20.23               | 573.07                                  | 1.3607            | 1.3089           | 0.0518             | 0.000158                            | 0.0904                              | 0.2                 | 74.2                        | 77.8                      | 1.00    | 573.32  | 1.27  |
|         | 19.58               | 554.66                                  | 1.3787            | 1.2697           | 0.109              | 0.000116                            | 0.1965                              | 0.4                 | 76.0                        | 85.8                      | 1.00    | 1694.12   | 3.45  |
|         | 20.23               | 573.07                                  | 1.4918            | 1.3015           | 0.1903             | 0.000170                            | 0.3321                              | 0.5                 | 76.4                        | 103.3                     | 1.00    | 1947.81   | 2.93  |
|         | 19.9                | 563.72                                  | 1.5897            | 1.2887           | 0.301              | 0.000322                            | 0.5340                              | 0.8                 | 78.5                        | 128                       | 1.00    | 1660.12   | 2.49  |
|         | 19.87               | 562.87                                  | 1.8777            | 1.2593           | 0.6184             | 0.000577                            | 1.0987                              | 1.1                 | 79.0                        | 167                       | 1.00    | 1904.50   | 1.91  |
|         | 19.76               | 559.76                                  | 2.2402            | 1.2568           | 0.9834             | 0.000688                            | 1.7568                              | 1.25                | 81.7                        | 186.5                     | 1.00    | 2552.02   | 1.82  |
|         | 20.65               | 584.97                                  | 2.6858            | 1.313            | 1.3728             | 0.000737                            | 2.3468                              | 1.4                 | 82.0                        | 194                       | 1.00    | 3182.60   | 1.90  |
|         | 20.15               | 570.80                                  | 2.7729            | 1.2859           | 1.487              | 0.000793                            | 2.6051                              | 1.4                 | 82.6                        | 203.3                     | 1.00    | 3283.20   | 1.76  |

#### 4: Experimental Results and Discussions

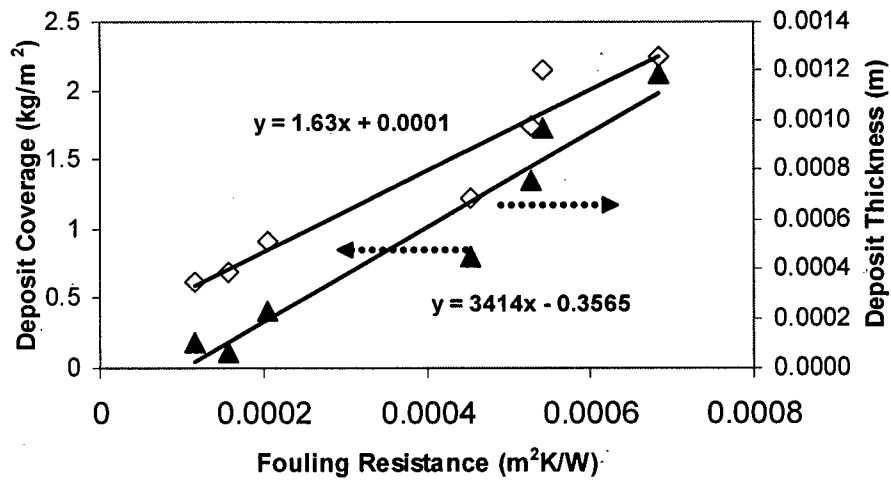
**Table 4.4.2.1: Deposit Coverage and Thickness Results (cont'd)**

|         | Section length (mm) | Section surface area (mm <sup>2</sup> ) | Fouled weight (g) | Clean weight (g) | Deposit weight (g) | $R_f$ (m <sup>2</sup> K/W) | $m_f$ (kg/m <sup>2</sup> ) | $x_f$ (mm) | $T_{w,initial}$ (°C) | $T_{w,final}$ (°C) | V (m/s) | $\rho_f \lambda_f = m_f/R_f$ (kgW/m <sup>4</sup> K) | $\lambda_f = x_f/R_f$ (W/m·K) |
|---------|---------------------|---|-------------------|------------------|--------------------|----------------------------|----------------------------|------------|----------------------|--------------------|---------|---|-------------------------------|
| TFU 809 | 20.65               | 584.97                                  | 1.3492            | 1.3304           | 0.0188             | 0.000004                   | 0.0321                     | -          | 73.3                 | 75.6               | 1.20    | 9022.60   | -                             |
|         | 20.14               | 570.52                                  | 1.3391            | 1.3059           | 0.0332             | 0.000026                   | 0.0582                     | -          | 74.0                 | 80.2               | 1.20    | 2232.25   | -                             |
|         | 20.025              | 567.26                                  | 1.3376            | 1.2838           | 0.0538             | 0.000072                   | 0.0948                     | 0.2        | 74.7                 | 80.9               | 1.20    | 1317.24   | 2.78                          |
|         | 19.85               | 562.31                                  | 1.3738            | 1.2841           | 0.0897             | 0.000095                   | 0.1595                     | 0.3        | 76.7                 | 92                 | 1.20    | 1679.18   | 3.16                          |
|         | 20.05               | 567.97                                  | 1.4326            | 1.2955           | 0.1371             | 0.000164                   | 0.2414                     | 0.36       | 77.7                 | 107.8              | 1.20    | 1469.82   | 2.19                          |
|         | 20.13               | 570.24                                  | 1.5323            | 1.3001           | 0.2322             | 0.000233                   | 0.4072                     | 0.68       | 78.5                 | 120.7              | 1.20    | 1744.19   | 2.91                          |
|         | 20.33               | 575.90                                  | 1.7071            | 1.3196           | 0.3875             | 0.000454                   | 0.6729                     | 0.81       | 79.2                 | 159.9              | 1.20    | 1480.82   | 1.78                          |
|         | 19.76               | 559.76                                  | 1.8837            | 1.2667           | 0.617              | 0.000580                   | 1.1023                     | 1.03       | 80.8                 | 183.1              | 1.20    | 1901.83   | 1.78                          |
|         | 20.11               | 569.67                                  | 2.1887            | 1.2924           | 0.8963             | 0.000643                   | 1.5734                     | 1.2        | 81.7                 | 195.1              | 1.20    | 2446.54   | 1.87                          |
|         | 20.1                | 569.39                                  | 2.3676            | 1.3064           | 1.0612             | 0.000684                   | 1.8638                     | 1.3        | 82.1                 | 202.2              | 1.20    | 2725.79   | 1.90                          |
| TFU 807 | 20.13               | 570.10                                  | 1.3008            | 1.2887           | 0.0121             | -0.000019                  | 0.0212                     | -          | 73.0                 | 70.5               | 1.40    | -   | -                             |
|         | 20.03               | 567.26                                  | 1.3032            | 1.2807           | 0.0225             | -0.000011                  | 0.0397                     | -          | 74.2                 | 73.1               | 1.40    | -   | -                             |
|         | 20.13               | 570.10                                  | 1.3221            | 1.2852           | 0.0369             | -0.000001                  | 0.0647                     | 0.18       | 75.9                 | 76.7               | 1.40    | -   | -                             |
|         | 19.68               | 557.49                                  | 1.3177            | 1.2581           | 0.0596             | 0.000156                   | 0.1069                     | 0.38       | 76.7                 | 93.5               | 1.40    | 685.31  | 2.44                          |
|         | 19.80               | 560.89                                  | 1.3784            | 1.2738           | 0.1046             | 0.000116                   | 0.1865                     | 0.35       | 77.6                 | 90.4               | 1.40    | 1607.67   | 3.02                          |
|         | 19.62               | 555.79                                  | 1.4778            | 1.2549           | 0.2229             | 0.000205                   | 0.4011                     | 0.51       | 79.1                 | 121.4              | 1.40    | 1953.45   | 2.48                          |
|         | 20.22               | 572.79                                  | 1.7449            | 1.2854           | 0.4595             | 0.000455                   | 0.8022                     | 0.69       | 80.1                 | 172.4              | 1.41    | 1764.48   | 1.52                          |
|         | 20.43               | 578.74                                  | 2.0694            | 1.2908           | 0.7786             | 0.000529                   | 1.3453                     | 0.98       | 81.3                 | 188.5              | 1.41    | 2542.94   | 1.85                          |
|         | 20.34               | 576.19                                  | 2.2965            | 1.303            | 0.9935             | 0.000542                   | 1.7243                     | 1.2        | 82.4                 | 192.2              | 1.41    | 3181.28   | 2.21                          |
|         | 19.88               | 563.16                                  | 2.4711            | 1.278            | 1.1931             | 0.000686                   | 2.1186                     | 1.26       | 82.9                 | 221.3              | 1.41    | 3089.11   | 1.84                          |
| TFU 808 | 20.30               | 575.05                                  | 1.3119            | 1.2985           | 0.0134             | -0.000020                  | 0.0233                     | -          | 73.8                 | 71.3               | 1.61    | -   | -                             |
|         | 20.30               | 575.05                                  | 1.3075            | 1.2951           | 0.0124             | -0.000023                  | 0.0216                     | -          | 74.6                 | 71.2               | 1.61    | -   | -                             |
|         | 19.95               | 565.14                                  | 1.3061            | 1.2848           | 0.0213             | -0.000015                  | 0.0377                     | 0.11       | 75.7                 | 74.3               | 1.61    | -   | -                             |
|         | 20.35               | 576.47                                  | 1.3374            | 1.2964           | 0.041              | 0.000090                   | 0.0711                     | 0.25       | 76.9                 | 80.4               | 1.61    | 790.25  | 2.78                          |
|         | 20.40               | 577.89                                  | 1.3673            | 1.3043           | 0.063              | 0.000099                   | 0.1090                     | 0.33       | 77.8                 | 87.2               | 1.61    | 1101.19   | 3.33                          |
|         | 19.55               | 553.81                                  | 1.3832            | 1.2569           | 0.1263             | 0.000150                   | 0.2281                     | 0.45       | 78.9                 | 100.5              | 1.61    | 1520.38   | 3.00                          |
|         | 20.25               | 573.64                                  | 1.5799            | 1.3025           | 0.2774             | 0.000212                   | 0.4836                     | 0.63       | 80.4                 | 118.8              | 1.61    | 2281.04   | 2.97                          |
|         | 19.88               | 563.01                                  | 1.7624            | 1.2757           | 0.4867             | 0.000444                   | 0.8645                     | 0.93       | 81.0                 | 134.9              | 1.61    | 1946.97   | 2.09                          |
|         | 20.12               | 569.95                                  | 2.1198            | 1.2946           | 0.8252             | 0.000474                   | 1.4478                     | 1.15       | 81.8                 | 193.3              | 1.62    | 3052.35   | 2.42                          |
|         | 20.12               | 569.95                                  | 2.3627            | 1.2932           | 1.0695             | 0.000583                   | 1.8765                     | 1.2        | 82.4                 | 220.1              | 1.62    | 3217.05   | 2.06                          |

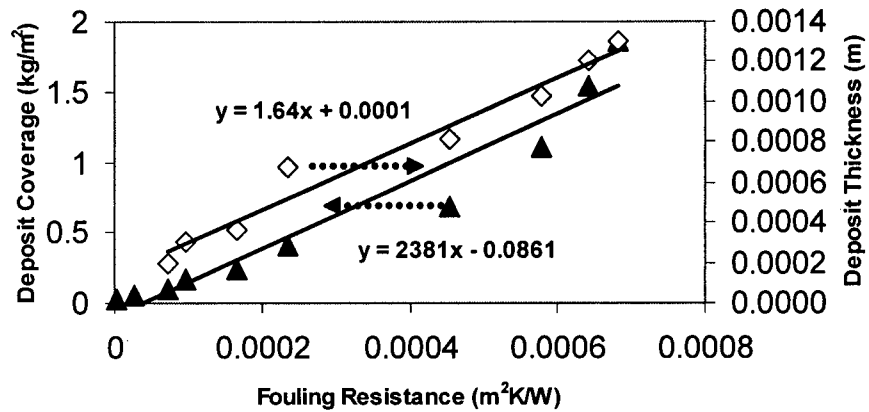
Evaluation of Deposit Physical Properties for TFU 808



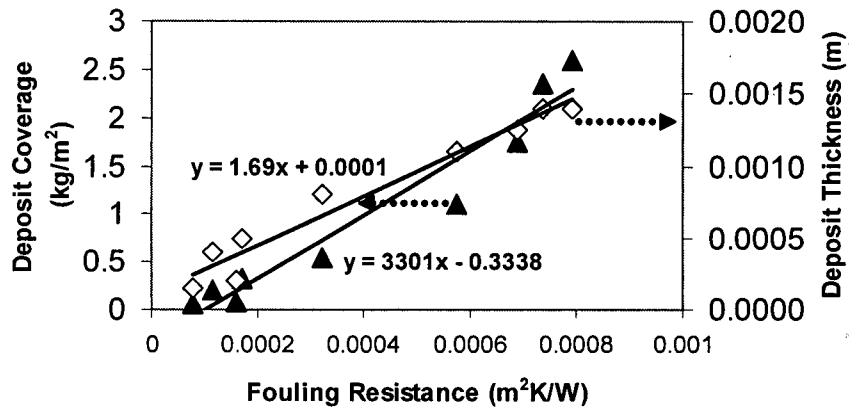
Evaluation of Deposit Physical Properties for TFU 807



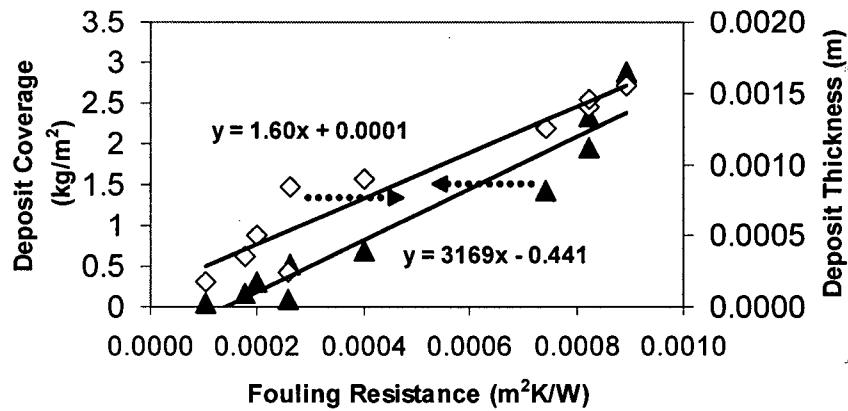
Evaluation of Deposit Physical Properties for TFU 809



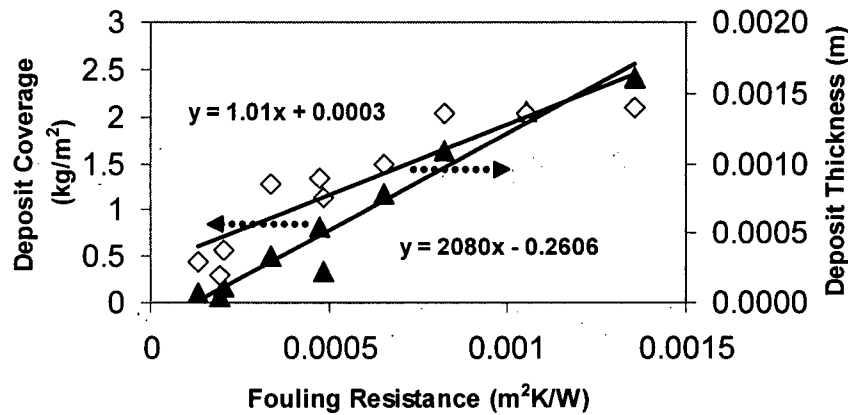
Evaluation of Deposit Physical Properties for TFU 806



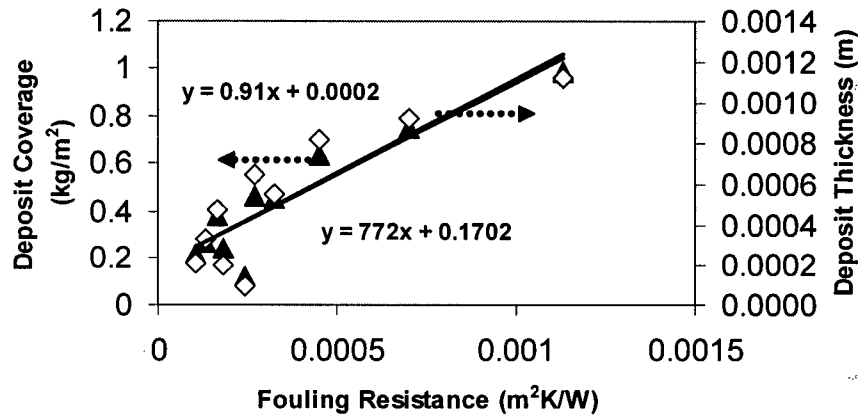
Evaluation of Deposit Physical Properties for TFU 803



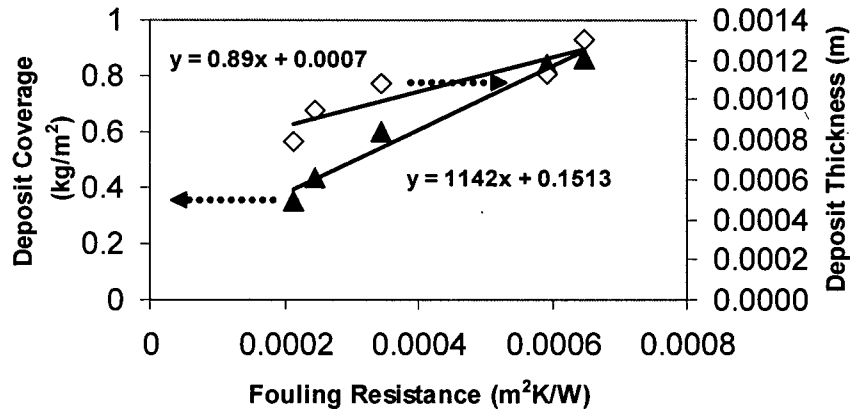
Evaluation of Deposit Physical Properties for TFU 804



Evaluation of Deposit Physical Properties for TFU 817



Evaluation of Deposit Physical Properties for TFU 811



Evaluation of Deposit Physical Properties for TFU 812

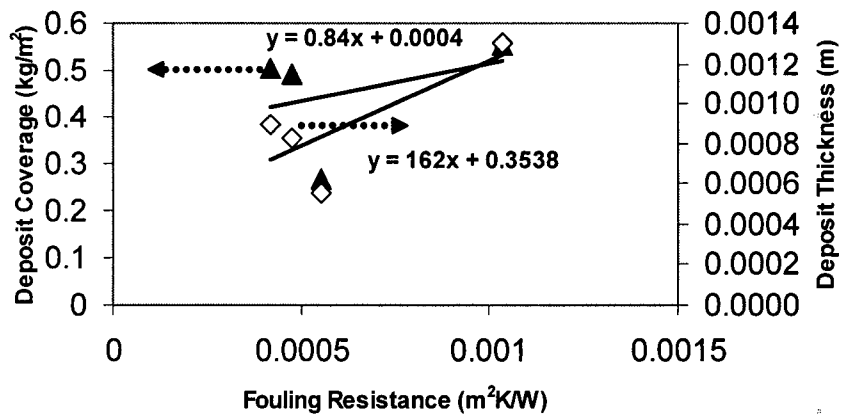


Figure 4.4.2.2 Deposit Coverage for Each Experiment

Table 4.4.2.2: Summary of Deposit Coverage and Thickness Results from Fig. 4.4.2.2.

| TFU | V (m/s) | Re ( $T_b$ ) | $\rho_f \lambda_f$ (kg·W/m <sup>4</sup> ·K) | $\lambda_f$ (W/m·K) | $\rho_f$ (kg/m <sup>3</sup> ) |
|-----|---------|--------------|---|---------------------|-------------------------------|
| 812 | 0.1     | 2200         | 162   | 0.84                | 193                           |
| 811 | 0.2     | 4200         | 1142  | 0.89                | 1283                          |
| 817 | 0.3     | 6200         | 772   | 0.91                | 848                           |
| 804 | 0.5     | 10600        | 2080  | 1.01                | 2059                          |
| 803 | 0.7     | 14700        | 3169  | 1.60                | 1981                          |
| 806 | 1       | 20800        | 3301  | 1.69                | 1953                          |
| 809 | 1.2     | 25100        | 2381  | 1.64                | 1451                          |
| 807 | 1.4     | 29400        | 3414  | 1.63                | 2094                          |
| 808 | 1.6     | 33800        | 3374  | 1.89                | 1785                          |

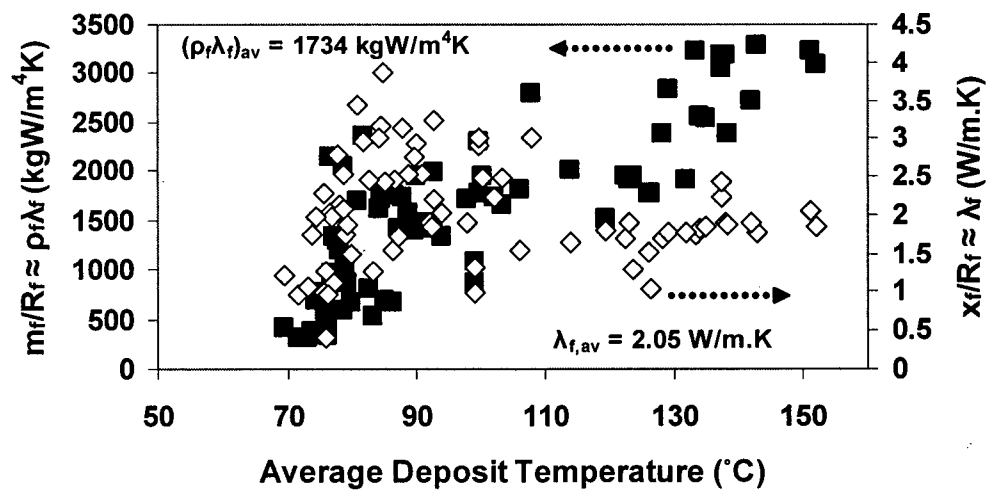
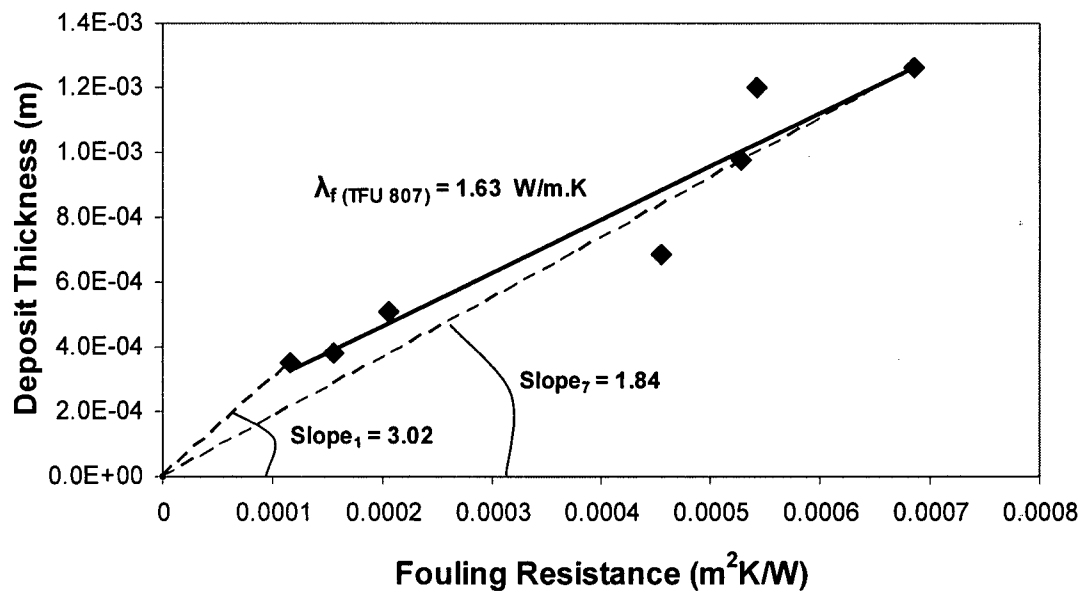


Figure 4.4.2.3: Dependence of Physical Properties on Temperature for All Data

fouling resistance and plotted against the average deposit temperature. This deposit temperature was determined by averaging the inside wall temperature at time zero and at the end of the experiment. The wall temperature at time zero was assumed to be the deposit-fluid interface temperature throughout the experiment since the process was at constant heat flux. Figure 4.4.2.3 shows the results for all the experimental data points. It illustrates that the term  $\rho_f \lambda_f$  increase with temperature. A possible explanation for this

increase is that phase transformation occurs at the high temperatures, i.e. above 98°C. This indicates that there is likely to be an aging effect. Thermal conductivity is sensitive to temperature as well. Despite considerable scatter in Figure 4.4.2.3 ( $\lambda_f = 0.41\text{-}3.86$  W/m.K), the average deposit thermal conductivity for these experiments, from the values determined in Table 4.4.2.1, was  $2.05 \pm 0.61$  W/m.K, corresponding very closely to the value of 2.2 W/m.K of Najibi et al. (1997). The corresponding average for  $\rho_f \lambda_f$  was  $1734 \pm 1169$  kgW/m<sup>4</sup>K. The reason for variety in reported values for deposit physical properties in the literature stems from the techniques used for measurement and the operating conditions under which fouling occurs. For instance, Krause (1993) used porosity measurement rather than thermal resistance to evaluate deposit physical properties, and Müller-Steinhagen et al. (1995) reported the thermal conductivity values of deposit formed under boiling conditions.



**Figure 4.4.2.4: Comparison of Different Deposit Thermal Conductivity Measurement Methods**

Figure 4.4.2.4, constructed for run 807, illustrates why the average deposit thermal conductivity of 2.05 W/m.K is higher than all the values of  $\lambda_f$  in Table 4.4.2.2. The slope of the solid line determines the deposit thermal conductivity as 1.63 W/m.K which is presented in Table 4.4.2.2. But in fact for each data point, the slope of the line connecting points (0,0) and ( $R_f$ ,  $x_f$ ) determines the corresponding thermal conductivity values presented in Table 4.4.2.1. In Figure 4.4.2.4 slope<sub>1</sub> and slope<sub>7</sub> designate the slope of the corresponding lines made for the first and the last points. It is clear that the slope of the solid line is smaller than that of almost any other dashed line. The same analysis can be used to explain why the average  $\rho_f \lambda_f$  of 1734 kgW/m<sup>4</sup>K is less than most of the values of  $\rho_f \lambda_f$  in Table 4.4.2.2.

In addition to the above, all of the measured deposit coverage results were plotted against the deposit thickness results to determine a more direct estimate of the average deposit density for this set of experiments. These results are shown in Figure 4.4.2.5. From the slope of the best fit line, the average deposit density was determined to be 1524 kg/m<sup>3</sup>. This is less than the average value of 2100 reported by Muller-Steinhagen et al. (1995) or the values of 2400 to 2700 kg/m<sup>3</sup> reported by other researchers for pure gypsum. It seems that the whole set of data points exhibits two different slopes, so Figure 4.4.2.6 was constructed to determine both the low and high deposit densities. Values of 633.5 and 3005 kg/m<sup>3</sup> were extracted from Figure 4.4.2.6. A concern may arise about using the averaging method shown in Figure 4.4.2.3, as it involves the effect of data points that deviate significantly from the average value. When all data points are given equal weight, these highly scattered points tended to artificially alter the average value, so the methods used in Figures 4.4.2.5 - 4.4.2.6 are believed to generate more acceptable

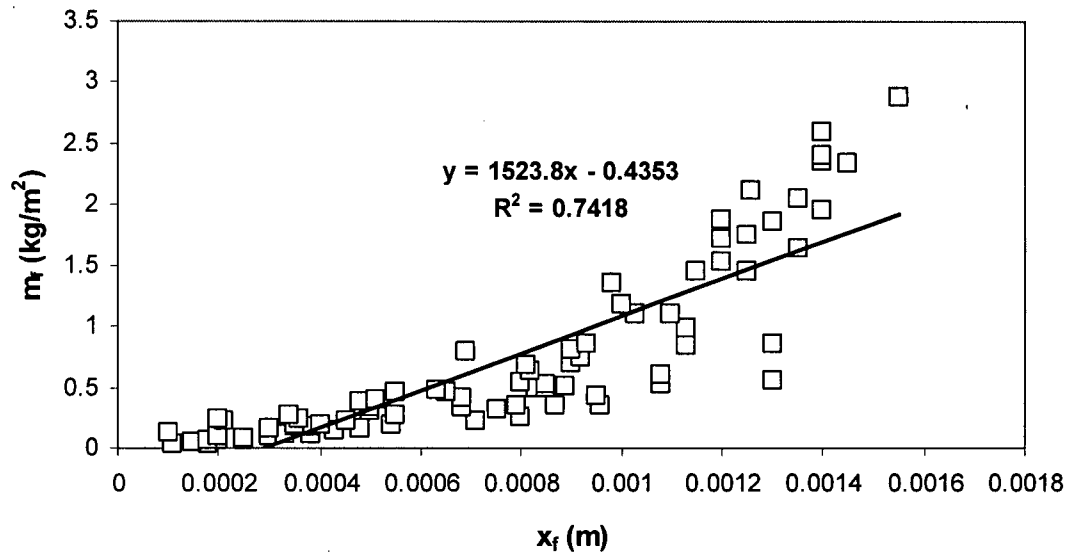


Figure 4.4.2.5: Estimation of an Average Deposit Density for TFU 800 Experiments

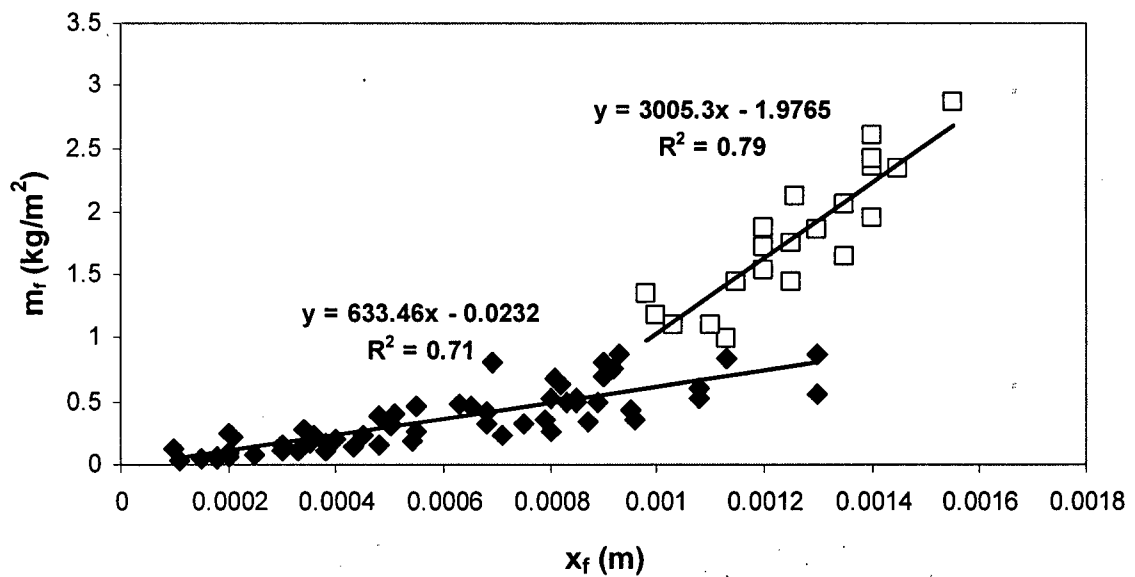


Figure 4.4.2.6: Estimation of Low and High Deposit Density for TFU 800 Experiments

results for deposit density.

It is worth mentioning that, in general, employing fouling resistance measurements to evaluate deposit density as above involves an approximation. Thus, true and calculated deposit densities can be expressed as follows:

$$\rho_{f,true} = \frac{m_{dep}}{\frac{\pi}{4}(D_t^2 - D_i^2)L} = \frac{4m_{dep}}{\pi(D_t - D_i)(D_t + D_i)L} = \frac{2m_{dep}}{\pi x_f(D_t + D_i)L} \quad (4.4.2.1)$$

$$\rho_{f,calc'd} = \frac{m_{dep}}{\pi D_t L x_f} \quad (4.4.2.2)$$

where  $m_{dep}$ ,  $x_f$ ,  $D_t$ ,  $D_i$ , and  $L$  are deposit mass, deposit thickness, inside tube diameter, inner deposit diameter, and tube length, respectively. Combining Equations (4.4.2.1) and (4.4.2.2) with the fact that  $D_i = D_t - 2x_f$  yields:

$$\frac{\rho_{f,true}}{\rho_{f,calc'd}} = \frac{D_t}{D_t - x_f} \quad (4.4.2.3)$$

Equation (4.4.2.3) shows that  $\rho_{f,true}$  approaches  $\rho_{f,calc'd}$  when  $x_f$  approaches zero, i.e. the thinner the deposit thickness, the more theoretically accurate the calculated deposit density. But for lower deposit thicknesses the presence of needle crystals makes it difficult to *measure* the thickness accurately. Therefore the deposit density evaluated at smaller thicknesses in Figure 4.4.2.5 is actually *less* accurate than that at higher thicknesses.

The question that remains unanswered is why there appears to be a velocity effect on the thermal conductivity and density of the fouling deposit, shown previously in Table 4.4.2.2. There are three possible explanations. The first is that perhaps there is a deposit

aging effect. If the deposit was to age with time and/or temperature, then calcium sulphate deposit, which originally forms as gypsum ( $\text{CaSO}_4 \cdot 2\text{H}_2\text{O}$ ) would be converted to other phases such as hemihydrate or anhydrite with a corresponding increase in thermal conductivity and density (Fand, 1969). An increase has been observed (Table 4.4.2.2) but with a corresponding increase in velocity rather than time or wall temperature. From the experimental data there was generally a decrease in deposit thickness as the fluid velocity increased. Therefore a thinner deposit, formed at higher velocities, would be more prone to aging as compared with a thicker one for which more time is needed to become aged. A second possibility could be the effect of void spaces within the deposit. As the fluid velocity increases, the replenishment of liquid in the void spaces will also increase, causing a corresponding increase in heat transfer coefficient, and decrease in the observed fouling resistance. Therefore, for a given deposit coverage and thickness, an increased value of both the deposit thermal conductivity and the density would result from the calculations. A third possibility could be the direction of crystal growth. At lower velocities the crystals grow radially outward from the nucleation sites along the test section and therefore the deposit is more porous, which has lower density and thermal conductivity. On the other hand, at higher velocities the crystals grow axially, leading to more compact deposit buildup having lower porosity. Of the aforementioned possibilities, the third is likely to play the dominant role since it is consistent with other researchers' observations. For instance, Krause (1993) measured the deposit porosity and showed that as the Reynolds number was increased from 12000 to 32000 the deposit porosity decreased from 0.23 to 0.12.

#### 4.5 Deposit Removal

Removal effects were studied by increasing the fluid velocity while simultaneously eliminating the concentration driving force. First, an experiment was started as described in Section 3.4 until a significant amount of deposit was formed for the top thermocouples and there were no longer significant changes in the wall temperature, i.e. an asymptotic fouling resistance was reached. The experiment was then stopped and the test fluid concentration was decreased to saturation level by removing part of the test fluid and diluting the rest of it using deionized water. The experiment was re-started with higher fluid velocity, since if no removal occurs at higher velocity then obviously there would be no deposit removal at the original velocity as well. Other operating conditions such as bulk and wall temperatures were kept the same as before.

In TFU 804, performed at the initial fluid velocity of 0.5 m/s, after about 12 hours experimental duration the velocity was increased to 0.7 m/s. Ten thermocouples reflected the same velocity effect and here the trends are explained for the lowest, middle, and highest thermocouples. Figures 4.5.1 - 4.5.3 illustrate the local reciprocal heat transfer coefficient before and after the velocity change for thermocouples  $T_{10}$ ,  $T_5$ , and  $T_1$ , respectively. Figure 4.5.1 illustrates that for thermocouple  $T_{10}$ , after reaching the asymptotic fouling resistance at 0.5 m/s, increasing the velocity to 0.7 m/s increases the local heat transfer coefficient, which then stays constant. Due to the absence of a concentration driving force, the deposition rate would be negligible. If removal were operative, the value of  $1/U$  should decrease. The fact that  $1/U$  remains constant with time proves there is no removal effect at a velocity of 0.7 m/s, which implies that there is no removal effect at 0.5 m/s as well. Figure 4.5.2, in which the fouling resistance has not

reached the asymptotic fouling value before the velocity increase, follows the same trend as in Figure 4.5.1. In Figure 4.5.3, thermocouple  $T_1$  is in the linear region before the velocity change and it is clear that no deposit removal occurs after the velocity increase.

To see whether or not the decrease in  $1/U$  after the velocity increase is due to an increase in convective heat transfer, reciprocal heat transfer coefficient before and after the velocity change can be written as follows:

$$\frac{1}{U_1} = R_{f1} + \frac{1}{h_1} \quad (4.5.1)$$

$$\frac{1}{U_2} = R_{f2} + \frac{1}{h_2} \quad (4.5.2)$$

where indices 1 and 2 correspond to conditions before and after the velocity increase, respectively. Combining Equations (4.5.1) and (4.5.2) yields the following equation:

$$-\Delta R_f = \left( \frac{1}{U_1} - \frac{1}{U_2} \right) - \left( \frac{1}{h_1} - \frac{1}{h_2} \right) \quad (4.5.3)$$

where

$$\Delta R_f = R_{f2} - R_{f1} \quad (4.5.4)$$

The terms  $\left( \frac{1}{U_1} - \frac{1}{U_2} \right)$  and  $\left( \frac{1}{h_1} - \frac{1}{h_2} \right)$  can be evaluated from the TFU 804 thermal fouling

results and the Dittus-Boelter (1930) equation,

$$Nu = 0.023 Re^{0.8} Pr^{0.4} \quad (4.5.5)$$

respectively. Equation (4.5.5) is applicable for heating conditions under turbulent flow regimes and was earlier shown to correctly predict the heat transfer performance of the TFU under clean conditions. To use Equation (4.5.5), it was assumed that before and after the velocity increase the physical properties of the test fluid remain the same since

Figure 4.5.1: Local Reciprocal Heat Transfer Coefficient Before and After the Velocity Increase for  $T_{10}$

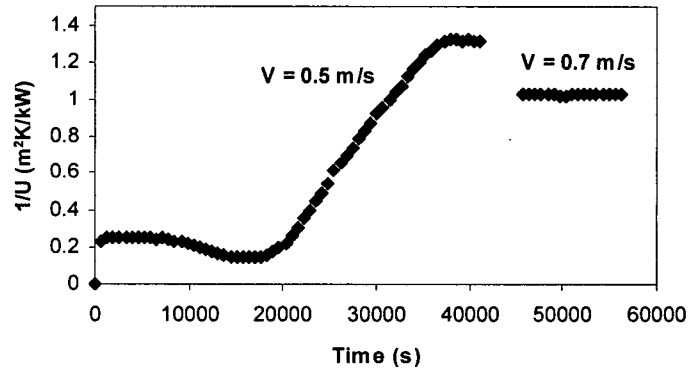


Figure 4.5.2: Local Reciprocal Heat Transfer Coefficient Before and After the Velocity Increase for  $T_5$

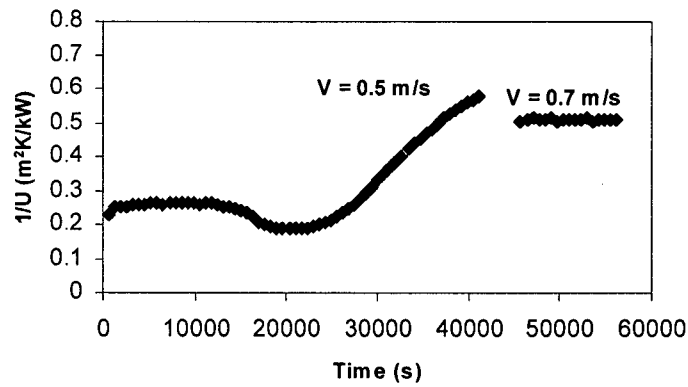
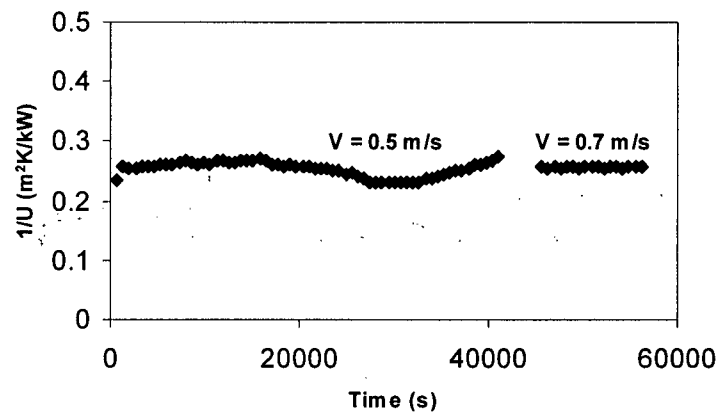


Figure 4.5.3: Local Reciprocal Heat Transfer Coefficient Before and After the Velocity Increase for  $T_1$



**Table 4.5.1: Comparison of Local Reciprocal Heat Transfer Coefficients Before and After the Velocity Increase**

| Thermocouple          | From TFU 804             |                          |                                |                        | From Eq.<br>(4.5.5)            |
|-----------------------|--------------------------|--------------------------|--------------------------------|------------------------|--------------------------------|
|                       | $1/U_1$<br>( $m^2K/kW$ ) | $1/U_2$<br>( $m^2K/kW$ ) | $1/U_1-1/U_2$<br>( $m^2K/kW$ ) | $-\Delta R_f / R_{f1}$ | $1/h_1-1/h_2$<br>( $m^2K/kW$ ) |
| <b>T<sub>1</sub></b>  | 0.279                    | 0.215                    | $6.4 \times 10^{-2}$           | 0.05                   | $5.54 \times 10^{-2}$          |
| <b>T<sub>5</sub></b>  | 0.596                    | 0.509                    | $8.7 \times 10^{-2}$           | 0.09                   | $5.76 \times 10^{-2}$          |
| <b>T<sub>10</sub></b> | 1.317                    | 1.031                    | $2.86 \times 10^{-1}$          | 0.21                   | $5.96 \times 10^{-2}$          |

their changes with solution dilution are negligible. The results extracted from the aforementioned calculations allowed evaluation of the term  $\Delta R_f$  by employing Equation (4.5.3) and from there an estimate of the fraction of the removed deposit,  $-\Delta R_f / R_{f1}$ , due to velocity surge was calculated. The results, for thermocouples T<sub>1</sub>, T<sub>5</sub>, and T<sub>10</sub>, are presented in Table 4.5.1. It shows that T<sub>10</sub> has the highest value of calculated deposit removal due to velocity surge and the reason for this is that T<sub>10</sub> has the highest deposit thickness.

Some researchers believe that a linear fouling behavior could imply that the difference between deposition and removal rate is constant, i.e. that even in the linear region removal could be important, but Figure 4.5.3 proves that at higher velocity the removal is negligible. The aforementioned experimental results contradict the findings of Mwaba et al. (2001). They performed three different experiments — at velocities of 0.3, 0.6, and 1.0 m/s — and after adjusting the concentration, the experiments were re-started

with the same velocities as before they were stopped. They reported an average decrease of 30% in the fouling resistance in each experiment and concluded that the observed decrease occurred because of removal effects in the top layer of the deposit, which was weak and porous and could therefore easily be removed. The fact is that the operating conditions play an important role in the experimental results, so care should be taken when interpreting the results. For instance, in the absence of an in-line filter in the experimental setup the fouling mechanism is a combination of particulate and crystallization fouling, which alters the fouling behavior from the situation when particles are absent. Particles in the test fluid can cause deposit removal by erosion as well as changing the deposit strength, which in turn affects the removal rate. Bansal et al. (2005) calculated the total deposit removal rate using the turbulent burst concept. In their calculations, it was assumed that the particles were deposited in a single layer on the surface and therefore the calculated removal rate was for particulate material on the surface. They argued that, since the crystals attach strongly to the heat transfer surface compared with the particles, the efficiency of a turbulent burst to remove crystals would be much lower than that to remove the particles, and hence concluded that the deposit removal for purely surface crystallization was negligible.

#### **4.6 Filter Pore Size Effect**

Three extra experiments, TFU 814, TFU 815, and TFU 816, were carried out to determine the effect of filter pore size on the fouling behavior. The operating conditions were similar except for the different filter pore sizes used. In TFU 815 no filter was employed during the experiment, but in runs TFU 814 and TFU 816 in-line 1- $\mu\text{m}$  and 5- $\mu\text{m}$  filter pore sizes, respectively, were used. In all the aforementioned experiments,

initially a 1- $\mu\text{m}$  filter cartridge was used to eliminate any particles present in the test fluid and then, before applying heat to the test section, the filter cartridge was replaced by the required one. For the three experiments the bulk velocity was 1.2 m/s and the wall temperature covered a range from 73°C at the lowest thermocouple to 83°C at the highest. Table 4.6.1 represents the important measured parameters such as initial fouling rate and delay time. The fouling curves for  $T_{10}$ ,  $T_5$ , and  $T_1$  are shown in Figures 4.6.1, 4.6.2, and 4.6.3, respectively. Figure 4.6.1 illustrates that at the top of the test section, the filter pore size has little impact on the initial fouling rate and delay time (Table 4.6.1), since initially there are no particles in the solution (they have been filtered out with a 1- $\mu\text{m}$  filter before starting the experiment). Due to higher wall temperature at  $T_{10}$ , crystal formation and growth are faster and occur before the appearance of any particles in the bulk solution. Therefore surface crystallization dominates. However, Figure 4.6.3 shows that at the test

**Table 4.6.1: The Effect of Filtration on the Delay Time and Initial Fouling Rate**

|  | TFU                            | $T_1$       | $T_2$       | $T_3$       | $T_4$       | $T_5$       | $T_6$       | $T_7$       | $T_8$       | $T_9$       | $T_{10}$    |
|--|--------------------------------|-------------|-------------|-------------|-------------|-------------|-------------|-------------|-------------|-------------|-------------|
| $\dot{R}_{fo}$<br>( $\text{m}^2\text{K}/\text{kJ}$ ) | 815<br>no filter               | 5.74<br>E-6 | 9.19<br>E-6 | 1.12<br>E-5 | 1.84<br>E-5 | 2.56<br>E-5 | 3.49<br>E-5 | 4.71<br>E-5 | 5.23<br>E-5 | 6.23<br>E-5 | 6.95<br>E-5 |
|  | 816<br>5- $\mu\text{m}$ filter | 2.34<br>E-6 | 4.25<br>E-6 | 1.01<br>E-5 | 1.47<br>E-5 | 2.41<br>E-5 | 3.22<br>E-5 | 4.01<br>E-5 | 5.13<br>E-5 | 6.17<br>E-5 | 7.45<br>E-5 |
|  | 814<br>1- $\mu\text{m}$ filter | 1.73<br>E-6 | 3.38<br>E-6 | 6.33<br>E-6 | 1.05<br>E-5 | 1.52<br>E-5 | 2.45<br>E-5 | 3.53<br>E-5 | 5.02<br>E-5 | 6.31<br>E-5 | 7.27<br>E-5 |
| $\tau_D$ (hr)  | 815<br>no filter               | 2.72        | 1.45        | 1.45        | 1.45        | 1.27        | 0.72        | 0.72        | 0.72        | 0.72        | 0.72        |
|  | 816<br>5- $\mu\text{m}$ filter | 3.78        | 2.70        | 2.70        | 1.98        | 1.26        | 1.08        | 1.08        | 1.08        | 1.08        | 1.08        |
|  | 814<br>1- $\mu\text{m}$ filter | 3.85        | 2.75        | 2.38        | 2.38        | 2.38        | 2.01        | 2.38        | 1.27        | 1.09        | 1.27        |

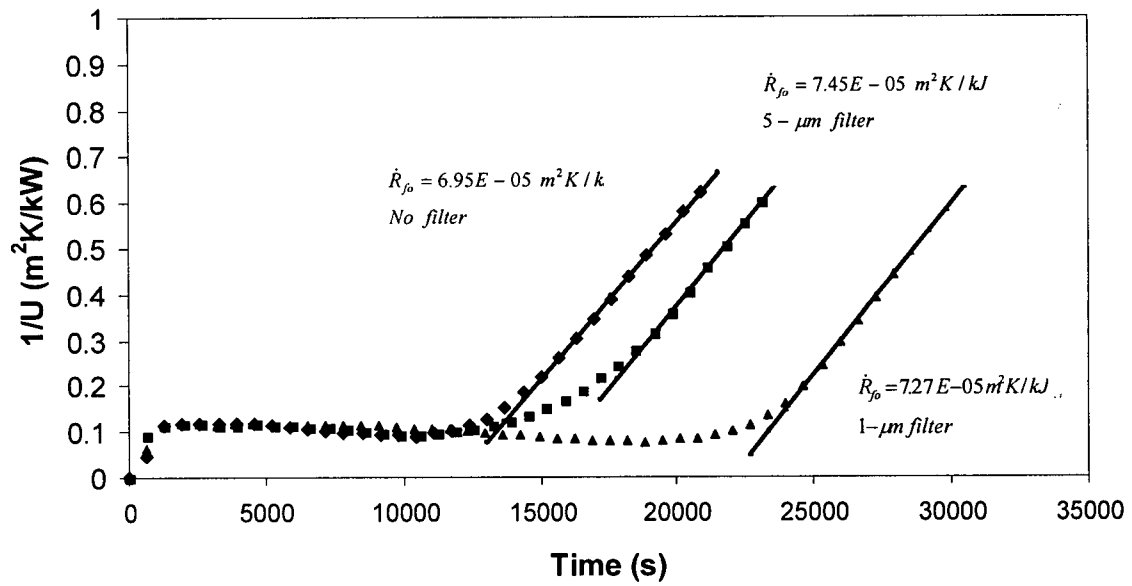


Figure 4.6.1: The Effect of Filtration on Fouling Behavior at Thermocouple  $T_{10}$

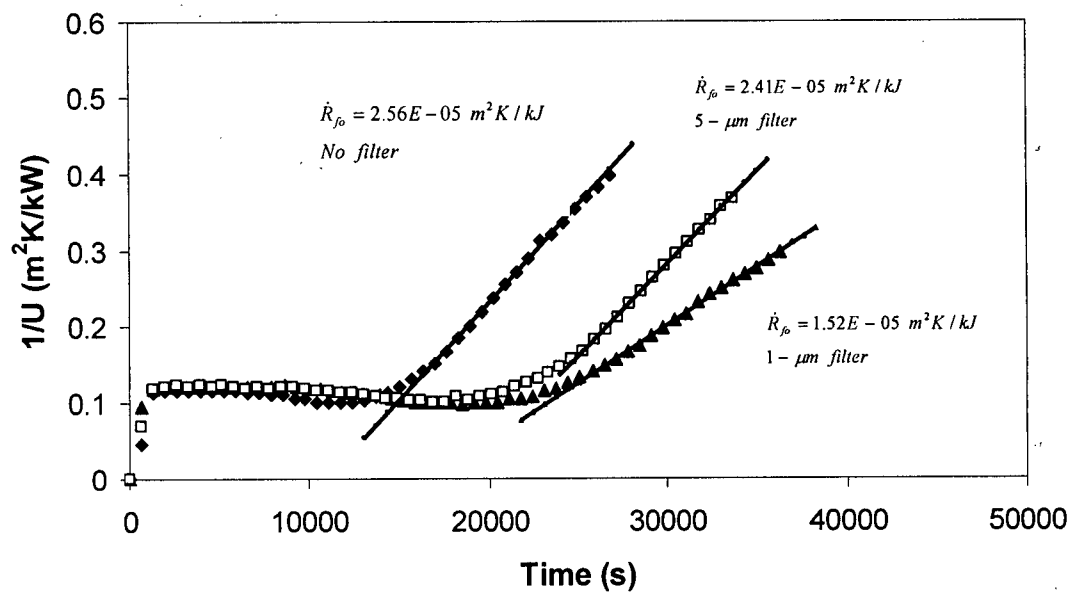
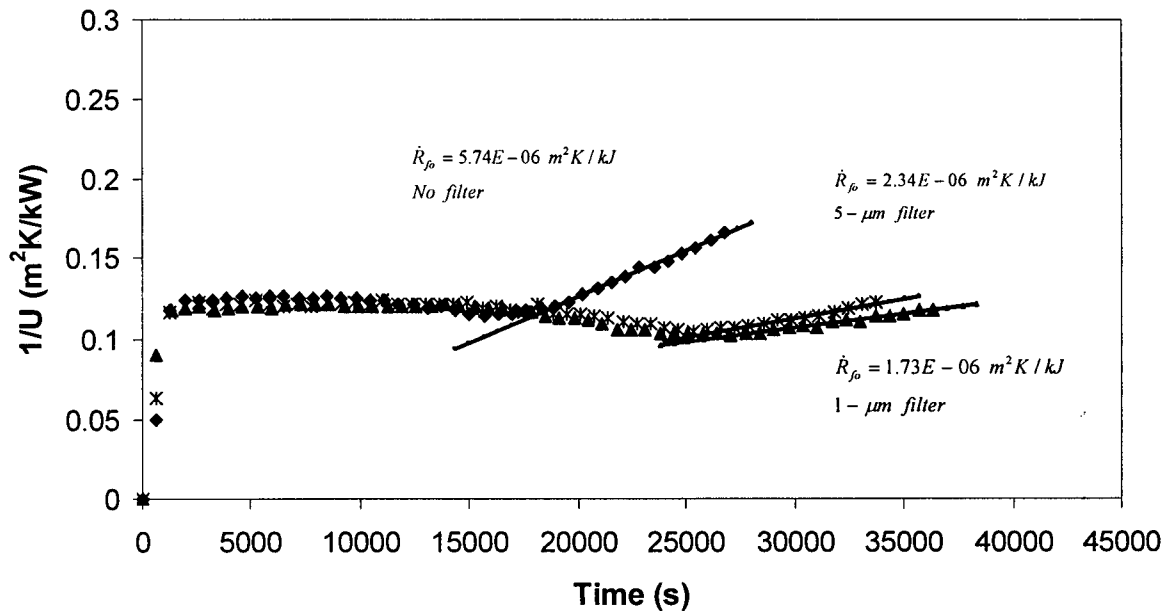


Figure 4.6.2: The Effect of Filtration on Fouling Behavior at Thermocouple  $T_5$



**Figure 4.6.3: The Effect of Filtration on Fouling Behavior at Thermocouple  $T_1$**

section inlet, filter pore size has more impact on the initial fouling rate. A possible reason is that at lower temperature the initiation period takes longer and therefore, as the time goes by, bulk crystallization occurs and particulate fouling may dominate the whole fouling process. For  $T_1$ , when no filter is used, the delay time is smaller and the initial fouling rate is larger than with either filter. Almost the same trend is seen in Figure 4.6.2 for  $T_5$ .

#### 4.7 Kinetic Studies

In order to separate the contribution of surface reaction (integration) from that of mass transfer, purely chemical activation energy values were generated through kinetic studies of calcium sulphate precipitation. A jacketed-glass reactor (JGR) which contained a magnetic stirrer was operated at a high stirring rate of 300 revolutions/minute, to assure a uniform temperature and concentration throughout the reactor, and hence surface

integration control. Bulk temperatures were kept constant during each experiment employing a constant temperature bath. Two sets of experiments were performed with different initial solution concentrations, i.e. 3100 and 3400 ppm, and the bulk temperature was varied in the range of 60 to 84°C. The experimental results for activation energy are compared to other reported activation energies in the literature, as well as to the fouling activation energies.

#### 4.7.1 A General Approach to Kinetics of Calcium Sulphate Precipitation

Crystallization kinetics of calcium sulphate was studied in batch experiments. Following the measurement procedures described in Section 3.6.2, during each experiment calcium sulphate concentration was measured and recorded with time. Figure 4.7.1.1 illustrates calcium sulphate concentration variation with time at  $T_b = 80^\circ\text{C}$  and  $C_{A0} = 3100$  ppm. A proper rate equation is needed to interpret the trend observed in Figure 4.7.1.1. Although several expressions have been proposed for kinetics of calcium

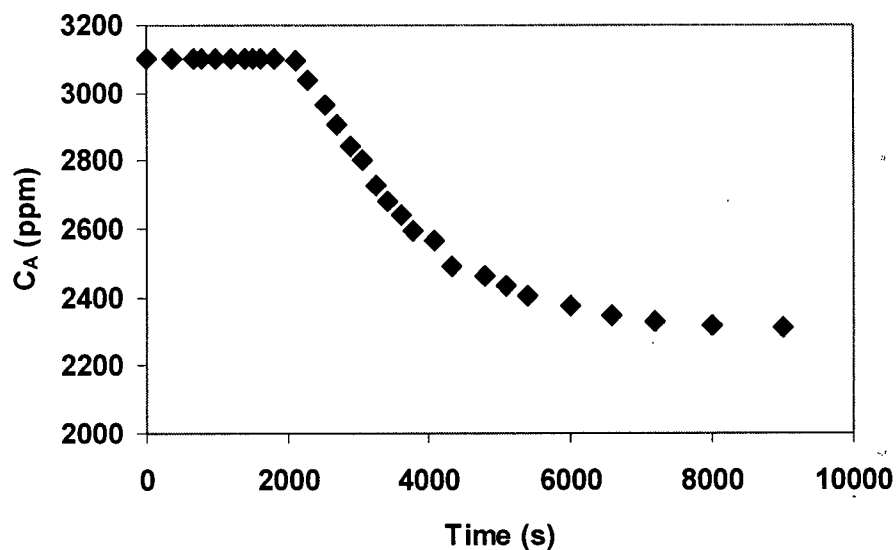


Figure 4.7.1.1: Plot of Calcium Sulphate Concentration vs. time ( $T_b = 80^\circ\text{C}$ ,  $C_{A0} = 3100$  ppm)

sulphate crystallization, Smith and Sweett (1971) suggested that the following equation, given by Nancollas (1968) and Konak (1974), describes calcium sulphate precipitation best:

$$-\frac{dC_A}{dt} = k_r A_c (C_A - C_{As})^2 \quad (4.7.1.1)$$

A simple approach to Equation (4.7.1.1) is to lump the term  $k_r$  with  $A_c$ , and introduce a new term as follows:

$$k = k_r A_c \quad (4.7.1.2)$$

Integrating Equation (4.7.1.1) yields the following expression:

$$\frac{1}{C_A - C_{As}} - \frac{1}{C_{A_0} - C_{As}} = kt \quad (4.7.1.3)$$

where  $C_{A_0}$  and  $C_A$  are the calcium sulphate concentrations at the start of the experiment ( $t = 0$ ) and time  $t$ , respectively. For all the experimental results, Equation 4.7.1.3 was

employed to extract the reaction rate constant,  $k$ , by plotting  $\frac{1}{C_A - C_{As}} - \frac{1}{C_{A_0} - C_{As}}$  vs.

time. Figure 4.7.1.2 illustrates a typical result, which is similar to that of Bansal et al. (2005). In each experiment, three different regions are recognized after the delay period.

The first region presents a low rate, which is probably associated with nuclei formation.

The second region corresponds to an intermediate rate, which is presumably related to both nuclei formation and crystal growth. The third region shows the highest rate, in

which crystal growth is dominant. The same trends were observed for all the experiments. For each experiment three different reaction rate constants were evaluated:

$k_l$  for the low rate region,  $k_{int}$  for the intermediate rate region, and  $k_h$  for the high rate

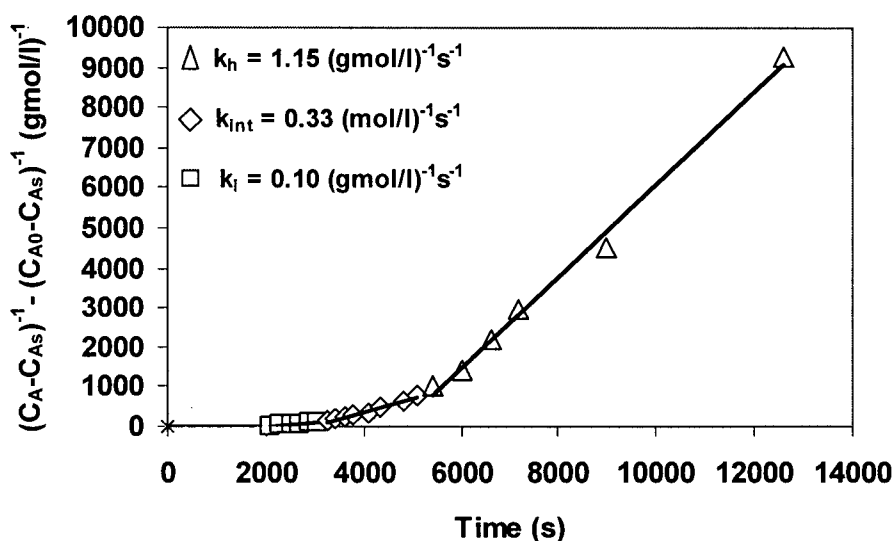


Figure 4.7.1.2: Reaction Rate Constants for Different Reaction Steps  
( $T_b = 80^\circ\text{C}$ ,  $C_{A0} = 3100$  ppm)

region. Therefore it was possible to construct an Arrhenius plot,  $\ln k$  vs.  $1/T$ , for a set of experiments operated over a range of bulk temperatures. In the aforementioned analysis individual rate regions were considered separately and therefore three activation energies,  $E_i$ ,  $E_{int}$ , and  $E_h$ , corresponding to each region were extracted. Figure 4.7.1.3 illustrates a typical Arrhenius plot for individual regions, where the values of purely chemical activation energies were determined as  $249 \pm 15$  kJ/mol for the low rate region,  $238 \pm 18$  kJ/mol for the intermediate rate region, and  $226 \pm 20$  kJ/mol for the high rate region. Individual reaction rate constants for each region along with purely chemical activation energies under different bulk temperatures and initial concentrations are presented in Table 4.7.1.1. At  $60^\circ\text{C}$  with an initial concentration of 3100 ppm the crystallization rate was extremely slow, and after performing the experiment for 48 hours, no significant variation in concentration was detected. On the other hand at  $84^\circ\text{C}$  with an initial concentration of 3400 ppm the precipitation rate was very fast, so that it was difficult to monitor concentration with time.

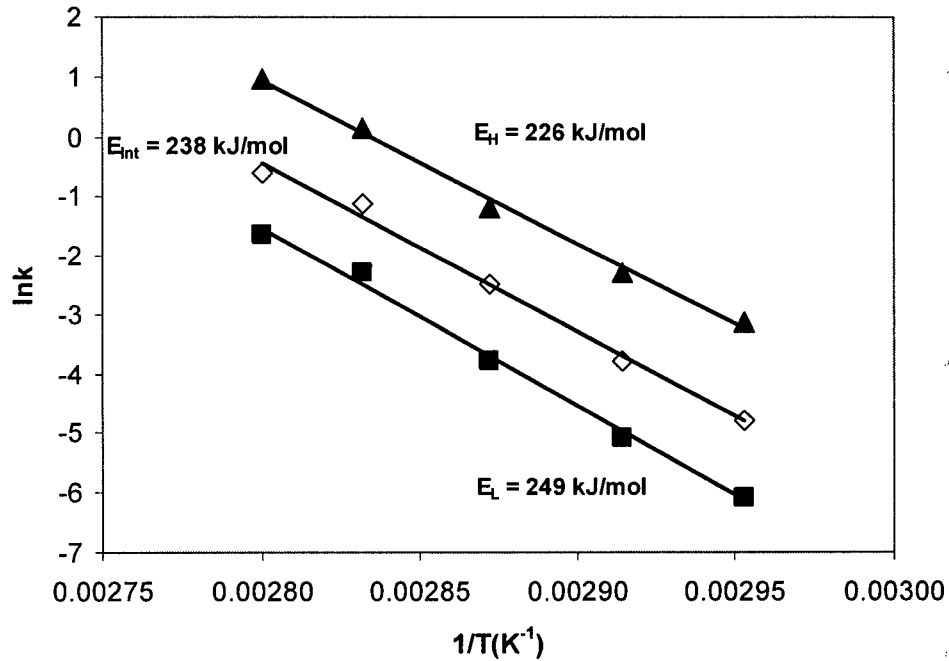


Figure 4.7.1.3 Arrhenius plot for three different stages ( $C_{A0} = 3100$  ppm)

Table 4.7.1.1: Kinetic Results for Individual Crystallization Stages (Stirring Rate = 300 RPM)

| $T_b$ (°C) | $k_1$ (gmol/l) <sup>-1</sup> .s <sup>-1</sup> |             | $k_{int}$ (gmol/l) <sup>-1</sup> .s <sup>-1</sup> |             | $k_2$ (gmol/l) <sup>-1</sup> .s <sup>-1</sup> |             |
|------------|---|-------------|---|-------------|---|-------------|
|            | * $C_{A01}$                                   | * $C_{A02}$ | * $C_{A01}$                                       | * $C_{A02}$ | * $C_{A01}$                                   | * $C_{A02}$ |
| 60         | –   | 0.002       | –   | 0.013       | –   | 0.029       |
| 65         | 0.002   | 0.014       | 0.016   | 0.030       | 0.044   | 0.057       |
| 70         | 0.006   | 0.039       | 0.023   | 0.144       | 0.102   | 0.701       |
| 75         | 0.022   | 0.129       | 0.084   | 0.313       | 0.308   | 1.06        |
| 80         | 0.101   | 0.264       | 0.332   | 0.595       | 1.151   | 2.13        |
| 84         | 0.193   | –           | 0.547   | –           | 2.578   | –           |
| E (kJ/mol) | 249   | 240         | 238   | 193         | 226   | 225         |

\* $C_{A01} = 3100$  ppm, \* $C_{A02} = 3400$  ppm

Activation energies, presented in Table 4.7.1.1, cover a range of 193 to 249 kJ/mol for all the three regions and for two different initial concentrations. These values overlap at the high end of the range 105 - 219 kJ/mol reported by Bansal et al. (2005), and are higher than the values reported by other researchers in Table 2.5.1.1. However,

these values are smaller than the maximum fouling activation energy of 620 kJ/mol evaluated from the present fouling experiments. The differences between reported values for activation energies in the literature may be justified by determining the operating conditions under which the concentration is monitored. For instance, Bansal et al. (2005) measured the concentration during the fouling experiment employing samples withdrawn from the fouling loop at timed intervals, and they believed that the concentration drop was due to surface crystallization. For bulk crystallization, most of the researchers have focused on the seeded crystallization technique, where the initial total surface area of crystals is known, and the main assumption is that no further nucleation occurs during the experiment.

#### 4.7.2 A Modified Kinetic Approach

In the previous section, it was shown that the lumped reaction rate constant was not constant in each batch experiment. But a proper kinetic model has to be validated by producing constant  $k_r$  values for each bulk temperature. In order to overcome this problem, one approach would be to separate reaction rate constant from crystal surface area, and to do so O'Rourke and Johnson's (1955) approach was adopted. In his method, which is applicable to cases where the surface area of the crystal changes significantly with time but the shape of the growing crystals remain invariant during the growth process, crystal surface area is given by:

$$A_c = A_o (m / m_o)^{2/3} \quad (4.7.2.1)$$

where  $A_c$  is the surface area of crystals at any time  $t$ ,  $A_o$  and  $m_o$  are the surface area and the mass of crystals at time  $t_o$  and  $m$  is the mass of crystals at any time  $t$ . In the present

study, from Equation (4.7.2.1), an expression was derived for the term  $A_c$  as a function of concentration rather than of crystal mass, namely

$$A_c = A_{o1} \left( \frac{C_{Ao} - C_A}{C_{Ao} - C_{Ao1}} \right)^{2/3} \quad (4.7.2.2)$$

where  $C_{Ao}$  is the initial concentration (at the start of the experiment),  $C_{Ao1}$  is the first concentration measurement after precipitation has started,  $A_{o1}$  is the total surface area of crystals corresponding to concentration  $C_{Ao1}$ , and  $C_A$  is the concentration at any time  $t$ . Therefore it was possible to incorporate Equation (4.7.2.2) with any proper kinetic model proposed by other researchers. For instance, combining Konak's (1974) model with Equation (4.7.2.2), we arrive at the following differential equation:

$$-\frac{dC_A}{dt} = kA_{o1} \left( \frac{C_{Ao} - C_A}{C_{Ao} - C_{Ao1}} \right)^{2/3} (C_A - C_{As})^2 \quad (4.7.2.3)$$

the integral form from time  $t_o$  being

$$-\int_{C_{Ao1}}^{C_A} \frac{dC_A}{\left( \frac{C_{Ao} - C_A}{C_{Ao} - C_{Ao1}} \right)^{2/3} (C_A - C_{As})^2} = k'(t - t_o) \quad (4.7.2.4)$$

where  $k' = kA_{o1}$ .

For all the performed experiments, Equation (4.7.2.4) was numerically integrated using an adaptive Simpson quadrature technique (Appendix 4) and the results were plotted vs. time to evaluate  $k'$ . Figure 4.7.2.1 shows a typical plot for a bulk temperature of 65°C and the initial concentration of 3400 ppm. It introduces a unique reaction rate constant which was determined as 401.43 (gmol/l)<sup>-1</sup>.s<sup>-1</sup>. This method was employed for other batch experiments to extract reaction rate constant values corresponding to each temperature (Appendix 3) and then a pure chemical activation energy was evaluated.

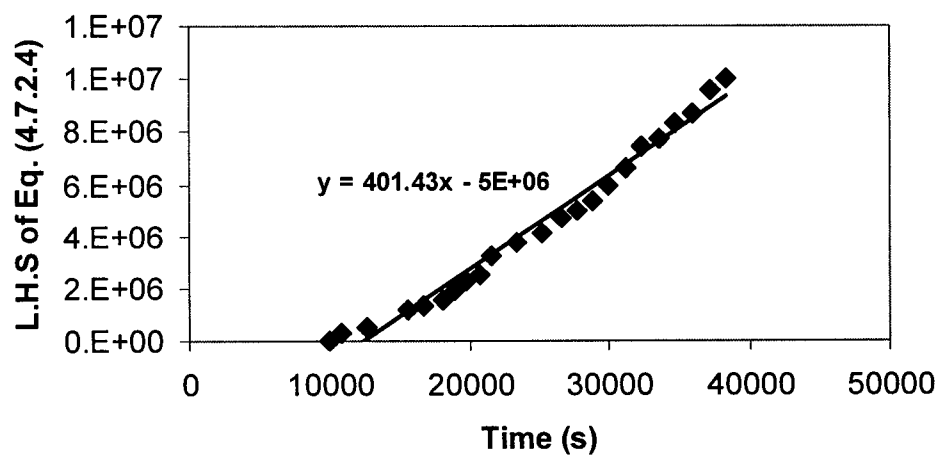


Figure 4.7.2.1: Reaction Rate Constant Evaluation Based on the Modified Kinetic Model ( $T_b = 65^\circ\text{C}$ ,  $C_{A0} = 3400$  ppm)

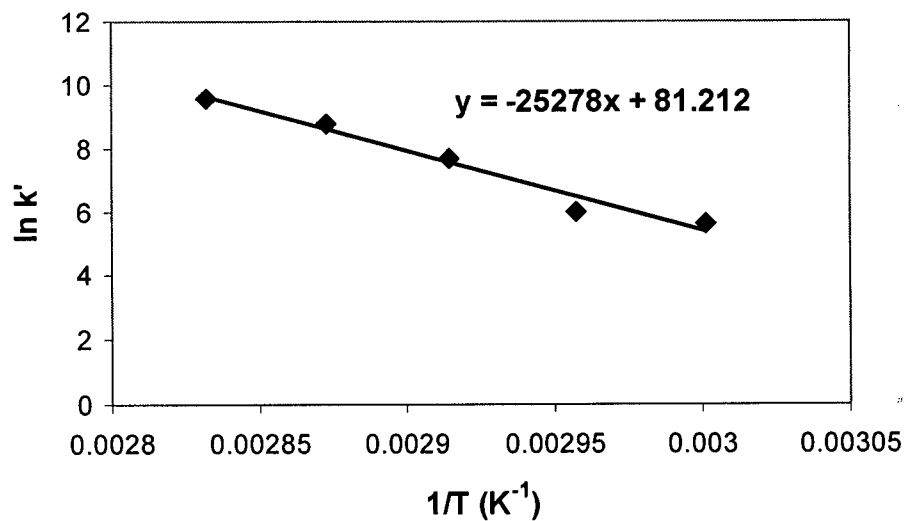


Figure 4.7.2.2: Arrhenius Plot for Modified Kinetic Approach ( $C_{A0} = 3400$  ppm)

**Table 4.7.2.1: Kinetic Results Based on the New Kinetic Model**

| T <sub>b</sub> (°C) | k' (gmol/l) <sup>-1</sup> .s <sup>-1</sup> |                            |
|---------------------|--|----------------------------|
|                     | C <sub>A0</sub> = 3100 ppm                 | C <sub>A0</sub> = 3400 ppm |
| 60                  | -  | 267                        |
| 65                  | 379  | 401                        |
| 70                  | 471  | 2139                       |
| 75                  | 3103                                       | 6305                       |
| 80                  | 17872                                      | 14520                      |
| 84                  | 26271                                      | -                          |
| E (kJ/mol)          | 254  | 210                        |

Figure 4.7.2.2 is an Arrhenius plot in which the slope of the line yields the chemical activation energy as  $210 \pm 21$  kJ/mol. The final results at two values of C<sub>A0</sub> are presented in Table 4.7.2.1. As in the case of Table 4.7.1.1, the values of the measured rate constants change with initial concentration. This effect could possibly be attributed to the variation of A<sub>o1</sub> from one experiment to another.

A question that remains unanswered is why the maximum fouling activation energy shown in Table 4.3.2.1 is still larger than the chemical activation energies presented in Table 4.7.2.1. A possible reason relates to the number of nucleation sites along the test section. The following equation was used to evaluate fouling activation energies:

$$\dot{R}_{fo} = A \exp\left(\frac{-\Delta E_f}{R(T_{w,i})_c}\right) \quad (4.7.2.1)$$

Equation (4.7.2.1) is valid only when the local surface nucleation sites are the same along the length of the test section. However, as discussed in Section 4.4.2, the deposit was more compact at the top of the test section as compared with lower sections where the deposit was more porous and did not cover the whole tube surface area. These findings are consistent with others reported by Hasson and Zahavi (1970) and Bansal and Muller-

Steinhagen. (1993). For instance, in an annular test section heated electrically, Hasson and Zahavi (1970) found that the first appearance of a fine scale coating could be visually detected at the downstream edge of the tube some 10 to 30 minutes from initial operation. This nucleate layer then propagated toward the upstream edge of the tube, initially at a fast rate and subsequently at a rapidly diminishing rate which became very slow as the upstream edge of the tube was approached. Also, in a plate heat exchanger where the calcium sulphate solution was heated by hot water, Bansal and Muller-Steinhagen (1993) found that the deposit was more severe in the upper downstream part of the plate than in the upstream part. These observations indicate that the number of nucleation sites either on the surface or in the boundary layer plays an important role.

## 5. Mathematical Modeling and Discussions

### 5.1 Initial Fouling Rate Model

To explore the applicability of Epstein's mathematical model (1994) of the initial fouling rate to the present data, the first step is to define proper constants and parameters in the following equation, derived from the model (Section 2.8.1):

$$\phi_{do} = k_m \left( \Delta C + \frac{k_m}{2k_a} - \sqrt{\frac{1}{4} \left( \frac{k_m}{k_a} \right)^2 + \frac{k_m}{k_a} \Delta C} \right) \quad (2.8.1.6)$$

Combining Equation (2.8.1.6) with

$$\dot{R}_{fo} = \frac{r \phi_{do}}{\lambda_f \rho_f} \quad (2.8.1.8)$$

we arrive at:

$$\dot{R}_{fo} = \frac{r}{\rho_f \lambda_f} k_m \left( \Delta C + \frac{k_m}{2k_a} - \sqrt{\frac{1}{4} \left( \frac{k_m}{k_a} \right)^2 + \frac{k_m}{k_a} \Delta C} \right) \quad (5.1.1)$$

where the mass transfer coefficient  $k_m$  and the attachment coefficient  $k_a$  are determined using Equations (2.8.1.9) and (2.8.1.13):

$$k_m = v_* / k' Sc^{2/3} \quad (2.8.1.9)$$

$$k_a = \frac{\nu e^{-\Delta E / RT_w}}{k'' v_*^2} \quad (2.8.1.13)$$

But for evaluating  $k_m$ , the precursor diffusivity required to calculate the Schmidt number is unknown. In general, Einstein's approach (1905), which is based on the kinetic theory of liquids and a modification of Stokes' law for the movement of a particle in a viscous fluid, is applicable for a dilute suspension of spheres. It is expressed concisely in the form

$$D = \frac{k_b T}{\phi r_p \eta} \quad (5.1.2)$$

where  $D$  is the diffusivity ( $\text{m}^2\text{s}^{-1}$ ),  $T$  the absolute temperature (K),  $\eta$  the fluid viscosity ( $\text{kg m}^{-1}\text{s}^{-1}$ ),  $r_p$  the molecular radius (m),  $k_b$  the Boltzman's constant and the dimensionless factor  $\phi$  has a numerical value between  $4\pi$  and  $6\pi$  depending on the solute : solvent molecular size ratio. It is difficult to obtain  $r_p$ , so the most directly useful relationship that emerges is

$$D\eta/T = \text{constant}$$

and hence the precursor diffusivity is proportional to the solution temperature divided by the viscosity:

$$\text{i.e. } D = D_o \frac{T}{\eta} \quad (5.1.3)$$

In electrolyte solutions, diffusivity is a complicated function of temperature, viscosity, and solute concentration, but for dilute solutions simpler expressions, similar to Equation (5.1.3), have been developed. In this study the solution concentration was always less than 0.02 gmol/ l, and therefore the assumption of a dilute solution allows us to neglect the effect of concentration on the diffusivity and use Equation (5.1.3). Combining Equations (5.1.3), (2.8.1.9), (2.8.1.13), and (5.1.1) yields

$$\dot{R}_{fo} = P_1 C_1 \left( \Delta C + \frac{P_2 C_2 e^{\Delta E / RT_w}}{2} - \sqrt{\frac{1}{4} (P_2 C_2 e^{\Delta E / RT_w})^2 + P_2 C_2 e^{\Delta E / RT_w} \Delta C} \right) \quad (5.1.4)$$

where

$$P_1 = \frac{r D_o^{2/3}}{\rho_f \lambda_f k'} \quad (5.1.5)$$

$$C_1 = \left[ \left( \frac{\rho T}{\eta^2} \right)^{2/3} v_* \right]_f \quad (5.1.6)$$

$$P_2 = \frac{D_o^{2/3} k''}{k'} \quad (5.1.7)$$

$$C_2 = \left[ v_* \left( \frac{\rho T}{\eta^2} \right)^{2/3} \right]_f \left[ v_*^2 \left( \frac{\rho}{\eta} \right) \right]_s \quad (5.1.8)$$

Indices f and s designate film and surface operating conditions, i.e., the corresponding terms are evaluated at film and surface temperatures. The experimental results from the calcium sulphate fouling experiments were used to evaluate best fit values of the parameters  $P_1$ ,  $P_2$ , and  $\Delta E$  in Equation (5.1.4). For each experimental data point i.e.,  $T_b$ ,  $T_w$ ,  $\Delta C$ , and  $v_*$ , expressions for  $C_1$  and  $C_2$  are unique to each data point and are used as the input data for the mathematical program to solve Equation (5.1.4) for the unknowns,  $P_1$ ,  $P_2$ , and  $\Delta E$ . These input data are shown in Table 5.1.1. Solution of Equation (5.1.4) for  $N$  sets of data and  $j$  variables ( $P_1$ ,  $P_2$ , and  $\Delta E$ ) can be achieved using a non-linear least squares regression, by minimizing  $\sigma^2$  in

$$\sigma^2 = \frac{\sum_{i=1}^N \left( \left[ \dot{R}_{fo}(\text{expt}) - \dot{R}_{fo}(\text{model}) \right]^2 \right)}{(N - j)} \quad (5.1.9)$$

The Levenberg-Marquardt method uses a combination of Newton's method and a steepest-descent method to perform non-linear curve-fitting to the experimental data. This procedure was employed here using Matlab 7.4 (Appendix 5).

Once the best solution of  $P_1$ ,  $P_2$ , and  $\Delta E$  (i.e. from the minimum sum of the squares of the residuals) has been evaluated, the model is then capable of predicting initial fouling rates at given wall and bulk temperatures, over a range of fluid velocities, and therefore can be quantitatively compared to the experimental data.

Table 5.1.1: Spreadsheet for Initial Fouling Rate Modeling

| Run             | $\dot{R}_p (m^2 K/kJ)$ | $T_{w,i} (^{\circ}C)$ | $T_b (^{\circ}C)$ | $T_r (^{\circ}C)$ | $V (m/s)$ | $Re (T_s)$ | $f_s$   | $v_s (m/s)$ | $\rho_r (kg/m^3)$ | $\eta_r (kg/m.s)$ | $Re (T_r)$ | $f_r$   | $v_r (m/s)$ | $\Delta C (kg/m^3)$ | $C_1$    | $C_2$    |
|-----------------|------------------------|-----------------------|-------------------|-------------------|-----------|------------|---------|-------------|-------------------|-------------------|------------|---------|-------------|---------------------|----------|----------|
| 812             |                        |                       |                   |                   |           |            |         |             |                   |                   |            |         |             |                     |          |          |
| T <sub>1</sub>  | -                      | 70.5                  | 51.4              | 61.0              | 0.1011    | 2189       | 0.01269 | 0.00805     | 983.33            | 4.644E-04         | 1930       | 0.01328 | 0.00823     | 0.912               | 1.09E+06 | 1.70E+08 |
| T <sub>2</sub>  | -                      | 71.6                  | 52.6              | 62.1              | 0.1011    | 2217       | 0.01263 | 0.00804     | 982.69            | 4.564E-04         | 1964       | 0.01319 | 0.00821     | 0.931               | 1.12E+06 | 1.75E+08 |
| T <sub>3</sub>  | -                      | 74.3                  | 53.7              | 64.0              | 0.1013    | 2281       | 0.01250 | 0.00801     | 981.61            | 4.438E-04         | 2019       | 0.01306 | 0.00818     | 0.978               | 1.16E+06 | 1.85E+08 |
| T <sub>4</sub>  | 5.82E-06               | 76.5                  | 55.0              | 65.8              | 0.1014    | 2328       | 0.01241 | 0.00798     | 980.60            | 4.329E-04         | 2070       | 0.01294 | 0.00815     | 1.016               | 1.19E+06 | 1.94E+08 |
| T <sub>5</sub>  | 1.19E-05               | 78.8                  | 56.1              | 67.5              | 0.1015    | 2372       | 0.01233 | 0.00797     | 979.59            | 4.231E-04         | 2118       | 0.01284 | 0.00813     | 1.056               | 1.23E+06 | 2.03E+08 |
| T <sub>6</sub>  | 1.39E-05               | 81.4                  | 57.3              | 69.4              | 0.1016    | 2414       | 0.01226 | 0.00795     | 978.43            | 4.129E-04         | 2170       | 0.01272 | 0.00810     | 1.102               | 1.27E+06 | 2.12E+08 |
| T <sub>7</sub>  | 7.03E-06               | 83.6                  | 58.4              | 71.0              | 0.1017    | 2442       | 0.01221 | 0.00794     | 977.41            | 4.048E-04         | 2214       | 0.01263 | 0.00808     | 1.140               | 1.31E+06 | 2.19E+08 |
| T <sub>8</sub>  | 9.76E-06               | 84.2                  | 59.7              | 72.0              | 0.1018    | 2449       | 0.01219 | 0.00795     | 976.81            | 4.004E-04         | 2239       | 0.01259 | 0.00807     | 1.150               | 1.32E+06 | 2.23E+08 |
| T <sub>9</sub>  | 1.64E-05               | 84.7                  | 60.7              | 72.7              | 0.1018    | 2454       | 0.01218 | 0.00795     | 976.33            | 3.970E-04         | 2257       | 0.01255 | 0.00806     | 1.159               | 1.34E+06 | 2.26E+08 |
| T <sub>10</sub> | 2.06E-05               | 87.3                  | 61.4              | 74.4              | 0.1019    | 2473       | 0.01215 | 0.00794     | 975.26            | 3.902E-04         | 2297       | 0.01247 | 0.00805     | 1.204               | 1.37E+06 | 2.33E+08 |
| 811             |                        |                       |                   |                   |           |            |         |             |                   |                   |            |         |             |                     |          |          |
| T <sub>1</sub>  | -                      | 66.1                  | 51.4              | 58.8              | 0.2011    | 4125       | 0.01024 | 0.01439     | 984.51            | 4.807E-04         | 3713       | 0.01060 | 0.01464     | 0.835               | 1.84E+06 | 8.69E+08 |
| T <sub>2</sub>  | -                      | 68.7                  | 52.5              | 60.6              | 0.2013    | 4267       | 0.01013 | 0.01433     | 983.52            | 4.669E-04         | 3822       | 0.01050 | 0.01458     | 0.880               | 1.92E+06 | 9.24E+08 |
| T <sub>3</sub>  | 8.72E-06               | 71.3                  | 53.6              | 62.5              | 0.2015    | 4401       | 0.01003 | 0.01427     | 982.49            | 4.540E-04         | 3931       | 0.01040 | 0.01453     | 0.926               | 1.99E+06 | 9.81E+08 |
| T <sub>4</sub>  | 1.15E-05               | 75.3                  | 54.8              | 65.1              | 0.2018    | 4587       | 0.00990 | 0.01420     | 981.01            | 4.372E-04         | 4082       | 0.01028 | 0.01446     | 0.995               | 2.09E+06 | 1.06E+09 |
| T <sub>5</sub>  | 1.22E-05               | 76.8                  | 55.9              | 66.4              | 0.2019    | 4650       | 0.00986 | 0.01418     | 980.25            | 4.294E-04         | 4157       | 0.01022 | 0.01443     | 1.021               | 2.14E+06 | 1.10E+09 |
| T <sub>6</sub>  | 1.91E-05               | 78.2                  | 57.1              | 67.7              | 0.2021    | 4704       | 0.00983 | 0.01417     | 979.47            | 4.220E-04         | 4230       | 0.01016 | 0.01441     | 1.046               | 2.19E+06 | 1.13E+09 |
| T <sub>7</sub>  | 2.94E-05               | 80.5                  | 58.2              | 69.4              | 0.2023    | 4782       | 0.00978 | 0.01414     | 978.43            | 4.129E-04         | 4322       | 0.01009 | 0.01437     | 1.086               | 2.25E+06 | 1.18E+09 |
| T <sub>8</sub>  | 3.59E-05               | 82.0                  | 59.3              | 70.7              | 0.2025    | 4826       | 0.00975 | 0.01414     | 977.63            | 4.064E-04         | 4391       | 0.01004 | 0.01435     | 1.112               | 2.30E+06 | 1.22E+09 |
| T <sub>9</sub>  | 4.26E-05               | 82.5                  | 60.3              | 71.4              | 0.2026    | 4840       | 0.00974 | 0.01414     | 977.15            | 4.029E-04         | 4430       | 0.01001 | 0.01433     | 1.121               | 2.33E+06 | 1.23E+09 |
| T <sub>10</sub> | 5.05E-05               | 83.4                  | 61.0              | 72.2              | 0.2027    | 4862       | 0.00973 | 0.01413     | 976.65            | 3.992E-04         | 4471       | 0.00999 | 0.01432     | 1.136               | 2.36E+06 | 1.25E+09 |
| 817             |                        |                       |                   |                   |           |            |         |             |                   |                   |            |         |             |                     |          |          |
| T <sub>1</sub>  | 9.05E-06               | 70.7                  | 51.3              | 61.0              | 0.2967    | 6439       | 0.00893 | 0.01982     | 983.30            | 4.641E-04         | 5668       | 0.00928 | 0.02021     | 0.915               | 2.68E+06 | 2.53E+09 |
| T <sub>2</sub>  | 9.21E-06               | 72.3                  | 52.6              | 62.5              | 0.2969    | 6557       | 0.00888 | 0.01978     | 982.49            | 4.540E-04         | 5794       | 0.00921 | 0.02016     | 0.943               | 2.76E+06 | 2.64E+09 |
| T <sub>3</sub>  | 8.52E-06               | 74.4                  | 53.8              | 64.1              | 0.2972    | 6702       | 0.00882 | 0.01974     | 981.56            | 4.432E-04         | 5936       | 0.00915 | 0.02010     | 0.980               | 2.85E+06 | 2.77E+09 |
| T <sub>4</sub>  | 1.63E-05               | 75.0                  | 55.2              | 65.1              | 0.2974    | 6743       | 0.00881 | 0.01973     | 980.98            | 4.369E-04         | 6021       | 0.00911 | 0.02007     | 0.990               | 2.90E+06 | 2.84E+09 |
| T <sub>5</sub>  | 1.77E-05               | 76.4                  | 56.5              | 66.5              | 0.2976    | 6831       | 0.00877 | 0.01971     | 980.19            | 4.288E-04         | 6135       | 0.00906 | 0.02003     | 1.014               | 2.98E+06 | 2.94E+09 |
| T <sub>6</sub>  | 2.27E-05               | 78.4                  | 57.8              | 68.1              | 0.2979    | 6946       | 0.00873 | 0.01968     | 979.20            | 4.195E-04         | 6271       | 0.00900 | 0.01998     | 1.049               | 3.06E+06 | 3.07E+09 |
| T <sub>7</sub>  | 3.51E-05               | 78.8                  | 59.1              | 69.0              | 0.2981    | 6969       | 0.00872 | 0.01968     | 978.68            | 4.150E-04         | 6339       | 0.00897 | 0.01996     | 1.056               | 3.11E+06 | 3.12E+09 |
| T <sub>8</sub>  | 4.86E-05               | 81.8                  | 60.4              | 71.1              | 0.2985    | 7108       | 0.00867 | 0.01965     | 977.34            | 4.043E-04         | 6507       | 0.00890 | 0.01991     | 1.108               | 3.22E+06 | 3.29E+09 |
| T <sub>9</sub>  | 6.16E-05               | 82.0                  | 61.5              | 71.8              | 0.2986    | 7118       | 0.00867 | 0.01966     | 976.93            | 4.013E-04         | 6556       | 0.00888 | 0.01990     | 1.112               | 3.26E+06 | 3.32E+09 |
| T <sub>10</sub> | 6.12E-05               | 82.9                  | 62.3              | 72.6              | 0.2988    | 7153       | 0.00865 | 0.01965     | 976.39            | 3.975E-04         | 6618       | 0.00885 | 0.01988     | 1.128               | 3.30E+06 | 3.38E+09 |

Table 5.1.1: Spreadsheet for Initial Fouling Rate Modeling (cont'd)

| Run             | $\dot{R}_f (m^2 K/kJ)$ | $T_{wi} (°C)$ | $T_b (°C)$ | $T_f (°C)$ | V (m/s) | Re ( $T_s$ ) | $f_s$   | $v_s$ (m/s) | $\rho_f$ (kg/m <sup>3</sup> ) | $\eta_f$ (kg/m.s) | Re ( $T_f$ ) | $f_f$   | $v_f^*$ (m/s) | $\Delta C$ (kg/m <sup>3</sup> ) | $C_1$    | $C_2$    |
|-----------------|------------------------|---------------|------------|------------|---------|--------------|---------|-------------|-------------------------------|-------------------|--------------|---------|---------------|---------------------------------|----------|----------|
| 804             |                        |               |            |            |         |              |         |             |                               |                   |              |         |               |                                 |          |          |
| T <sub>1</sub>  | 4.91E-06               | 72.1          | 51.4       | 61.8       | 0.4969  | 10950        | 0.00766 | 0.03076     | 982.88                        | 4.588E-04         | 9599         | 0.00795 | 0.03133       | 0.940                           | 4.22E+06 | 9.76E+09 |
| T <sub>2</sub>  | 6.68E-06               | 74.0          | 52.7       | 63.4       | 0.4974  | 11172        | 0.00762 | 0.03070     | 981.99                        | 4.480E-04         | 9831         | 0.00790 | 0.03125       | 0.973                           | 4.36E+06 | 1.02E+10 |
| T <sub>3</sub>  | 1.15E-05               | 75.2          | 54.1       | 64.7       | 0.4978  | 11306        | 0.00760 | 0.03068     | 981.24                        | 4.397E-04         | 10017        | 0.00786 | 0.03120       | 0.994                           | 4.47E+06 | 1.06E+10 |
| T <sub>4</sub>  | 2.10E-05               | 76.7          | 55.5       | 66.1       | 0.4982  | 11463        | 0.00757 | 0.03064     | 980.39                        | 4.309E-04         | 10222        | 0.00781 | 0.03113       | 1.020                           | 4.59E+06 | 1.10E+10 |
| T <sub>5</sub>  | 2.77E-05               | 77.3          | 56.8       | 67.1       | 0.4985  | 11525        | 0.00756 | 0.03064     | 979.83                        | 4.254E-04         | 10354        | 0.00778 | 0.03110       | 1.030                           | 4.67E+06 | 1.12E+10 |
| T <sub>6</sub>  | 3.69E-05               | 79.0          | 58.2       | 68.6       | 0.4990  | 11682        | 0.00753 | 0.03061     | 978.89                        | 4.168E-04         | 10566        | 0.00774 | 0.03104       | 1.060                           | 4.80E+06 | 1.17E+10 |
| T <sub>7</sub>  | 4.74E-05               | 80.3          | 59.6       | 70.0       | 0.4994  | 11791        | 0.00751 | 0.03060     | 978.06                        | 4.099E-04         | 10745        | 0.00770 | 0.03099       | 1.082                           | 4.92E+06 | 1.21E+10 |
| T <sub>8</sub>  | 5.40E-05               | 81.5          | 61.0       | 71.3       | 0.4998  | 11882        | 0.00749 | 0.03059     | 977.25                        | 4.036E-04         | 10913        | 0.00767 | 0.03095       | 1.103                           | 5.02E+06 | 1.24E+10 |
| T <sub>9</sub>  | 6.49E-05               | 82.1          | 62.1       | 72.1       | 0.5001  | 11926        | 0.00749 | 0.03059     | 976.71                        | 3.997E-04         | 11019        | 0.00765 | 0.03093       | 1.114                           | 5.09E+06 | 1.26E+10 |
| T <sub>10</sub> | 7.39E-05               | 82.6          | 63.0       | 72.8       | 0.5003  | 11961        | 0.00748 | 0.03059     | 976.26                        | 3.966E-04         | 11104        | 0.00763 | 0.03091       | 1.122                           | 5.14E+06 | 1.28E+10 |
| 803             |                        |               |            |            |         |              |         |             |                               |                   |              |         |               |                                 |          |          |
| T <sub>1</sub>  | 3.67E-06               | 72.6          | 51.4       | 62.0       | 0.6973  | 15445        | 0.00698 | 0.04120     | 982.75                        | 4.571E-04         | 13519        | 0.00723 | 0.04194       | 0.948                           | 5.68E+06 | 2.37E+10 |
| T <sub>2</sub>  | 5.98E-06               | 74.2          | 52.7       | 63.5       | 0.6979  | 15706        | 0.00695 | 0.04115     | 981.93                        | 4.474E-04         | 13813        | 0.00719 | 0.04185       | 0.976                           | 5.85E+06 | 2.47E+10 |
| T <sub>3</sub>  | 7.17E-06               | 75.0          | 54.1       | 64.6       | 0.6983  | 15833        | 0.00694 | 0.04113     | 981.30                        | 4.403E-04         | 14034        | 0.00716 | 0.04179       | 0.990                           | 5.97E+06 | 2.54E+10 |
| T <sub>4</sub>  | 1.39E-05               | 76.3          | 55.5       | 65.9       | 0.6989  | 16028        | 0.00691 | 0.04109     | 980.51                        | 4.321E-04         | 14302        | 0.00713 | 0.04172       | 1.013                           | 6.13E+06 | 2.63E+10 |
| T <sub>5</sub>  | 1.97E-05               | 77.5          | 56.7       | 67.1       | 0.6994  | 16196        | 0.00690 | 0.04107     | 979.80                        | 4.251E-04         | 14536        | 0.00710 | 0.04166       | 1.034                           | 6.27E+06 | 2.71E+10 |
| T <sub>6</sub>  | 2.33E-05               | 78.6          | 58.1       | 68.4       | 0.6999  | 16341        | 0.00688 | 0.04105     | 979.05                        | 4.182E-04         | 14776        | 0.00706 | 0.04160       | 1.053                           | 6.41E+06 | 2.80E+10 |
| T <sub>7</sub>  | 4.33E-05               | 80.1          | 59.5       | 69.8       | 0.7006  | 16521        | 0.00686 | 0.04103     | 978.16                        | 4.106E-04         | 15048        | 0.00703 | 0.04154       | 1.079                           | 6.57E+06 | 2.89E+10 |
| T <sub>8</sub>  | 5.64E-05               | 81.3          | 60.8       | 71.1       | 0.7011  | 16651        | 0.00685 | 0.04102     | 977.38                        | 4.045E-04         | 15275        | 0.00700 | 0.04149       | 1.100                           | 6.71E+06 | 2.97E+10 |
| T <sub>9</sub>  | 5.16E-05               | 82.1          | 62.0       | 72.1       | 0.7016  | 16732        | 0.00684 | 0.04102     | 976.74                        | 3.999E-04         | 15451        | 0.00698 | 0.04145       | 1.114                           | 6.82E+06 | 3.03E+10 |
| T <sub>10</sub> | 7.16E-05               | 82.5          | 62.8       | 72.7       | 0.7019  | 16771        | 0.00683 | 0.04102     | 976.36                        | 3.973E-04         | 15554        | 0.00697 | 0.04143       | 1.121                           | 6.88E+06 | 3.07E+10 |
| 806             |                        |               |            |            |         |              |         |             |                               |                   |              |         |               |                                 |          |          |
| T <sub>1</sub>  | 1.34E-06               | 71.9          | 51.3       | 61.6       | 0.9973  | 21928        | 0.00638 | 0.05632     | 982.97                        | 4.599E-04         | 19222        | 0.00660 | 0.05727       | 0.936                           | 7.69E+06 | 5.95E+10 |
| T <sub>2</sub>  | 3.00E-06               | 73.2          | 52.5       | 62.9       | 0.9980  | 22241        | 0.00636 | 0.05626     | 982.27                        | 4.513E-04         | 19586        | 0.00656 | 0.05718       | 0.959                           | 7.89E+06 | 6.17E+10 |
| T <sub>3</sub>  | 4.77E-06               | 74.2          | 53.8       | 64.0       | 0.9987  | 22474        | 0.00634 | 0.05622     | 981.61                        | 4.438E-04         | 19918        | 0.00654 | 0.05709       | 0.976                           | 8.07E+06 | 6.37E+10 |
| T <sub>4</sub>  | 7.44E-06               | 76.0          | 55.1       | 65.6       | 0.9996  | 22865        | 0.00631 | 0.05615     | 980.72                        | 4.342E-04         | 20360        | 0.00650 | 0.05698       | 1.008                           | 8.31E+06 | 6.65E+10 |
| T <sub>5</sub>  | 1.48E-05               | 76.4          | 56.3       | 66.4       | 1.0001  | 22953        | 0.00631 | 0.05615     | 980.25                        | 4.294E-04         | 20586        | 0.00648 | 0.05693       | 1.014                           | 8.44E+06 | 6.77E+10 |
| T <sub>6</sub>  | 2.12E-05               | 78.5          | 57.6       | 68.1       | 1.0011  | 23355        | 0.00628 | 0.05609     | 979.23                        | 4.198E-04         | 21056        | 0.00644 | 0.05683       | 1.051                           | 8.70E+06 | 7.09E+10 |
| T <sub>7</sub>  | 3.88E-05               | 79.0          | 58.9       | 69.0       | 1.0017  | 23451        | 0.00627 | 0.05609     | 978.68                        | 4.150E-04         | 21300        | 0.00643 | 0.05677       | 1.060                           | 8.84E+06 | 7.22E+10 |
| T <sub>8</sub>  | 5.46E-05               | 81.7          | 60.2       | 71.0       | 1.0029  | 23869        | 0.00624 | 0.05604     | 977.44                        | 4.050E-04         | 21825        | 0.00639 | 0.05667       | 1.107                           | 9.15E+06 | 7.58E+10 |
| T <sub>9</sub>  | 6.60E-05               | 82.0          | 61.3       | 71.7       | 1.0034  | 23917        | 0.00624 | 0.05605     | 977.00                        | 4.017E-04         | 22003        | 0.00637 | 0.05664       | 1.112                           | 9.25E+06 | 7.68E+10 |
| T <sub>10</sub> | 7.16E-05               | 82.6          | 62.0       | 72.3       | 1.0038  | 23998        | 0.00624 | 0.05605     | 976.58                        | 3.988E-04         | 22165        | 0.00636 | 0.05661       | 1.122                           | 9.35E+06 | 7.78E+10 |

Table 5.1.1: Spreadsheet for Initial Fouling Rate Modeling (cont'd)

| Run             | $\dot{R}_o (m^2 K/kJ)$ | $T_{w,i} (°C)$ | $T_b (°C)$ | $T_f (°C)$ | V (m/s) | Re ( $T_s$ ) | $f_s$   | $v_{s_2}$ (m/s) | $\rho_f$ (kg/m <sup>3</sup> ) | $\eta_f$ (kg/m.s) | Re ( $T_f$ ) | $f_f$   | $v_f^*$ (m/s) | $\Delta C$ (kg/m <sup>3</sup> ) | $C_1$    | $C_2$    |
|-----------------|------------------------|----------------|------------|------------|---------|--------------|---------|-----------------|-------------------------------|-------------------|--------------|---------|---------------|---------------------------------|----------|----------|
| 809             |                        |                |            |            |         |              |         |                 |                               |                   |              |         |               |                                 |          |          |
| T <sub>1</sub>  | 2.37E-06               | 73.3           | 51.2       | 62.3       | 1.1943  | 26643        | 0.00608 | 0.06583         | 982.61                        | 4.554E-04         | 23238        | 0.00629 | 0.06696       | 0.961                           | 9.12E+06 | 9.78E+10 |
| T <sub>2</sub>  | 4.56E-06               | 74.0           | 52.4       | 63.2       | 1.1950  | 26841        | 0.00606 | 0.06580         | 982.07                        | 4.490E-04         | 23568        | 0.00626 | 0.06687       | 0.973                           | 9.29E+06 | 1.00E+11 |
| T <sub>3</sub>  | 5.27E-06               | 74.7           | 53.6       | 64.2       | 1.1956  | 27034        | 0.00605 | 0.06578         | 981.53                        | 4.428E-04         | 23896        | 0.00624 | 0.06680       | 0.985                           | 9.47E+06 | 1.03E+11 |
| T <sub>4</sub>  | 9.83E-06               | 76.7           | 54.9       | 65.8       | 1.1968  | 27537        | 0.00603 | 0.06570         | 980.57                        | 4.326E-04         | 24458        | 0.00621 | 0.06667       | 1.020                           | 9.78E+06 | 1.08E+11 |
| T <sub>5</sub>  | 1.38E-05               | 77.7           | 56.0       | 66.9       | 1.1976  | 27774        | 0.00601 | 0.06567         | 979.95                        | 4.265E-04         | 24811        | 0.00618 | 0.06659       | 1.037                           | 9.97E+06 | 1.11E+11 |
| T <sub>6</sub>  | 2.05E-05               | 78.5           | 57.3       | 67.9       | 1.1983  | 27957        | 0.00600 | 0.06566         | 979.32                        | 4.206E-04         | 25158        | 0.00616 | 0.06652       | 1.051                           | 1.02E+07 | 1.13E+11 |
| T <sub>7</sub>  | 3.56E-05               | 79.2           | 58.5       | 68.9       | 1.1990  | 28110        | 0.00600 | 0.06565         | 978.74                        | 4.155E-04         | 25467        | 0.00614 | 0.06646       | 1.063                           | 1.03E+07 | 1.16E+11 |
| T <sub>8</sub>  | 5.76E-05               | 80.8           | 59.7       | 70.3       | 1.2001  | 28420        | 0.00598 | 0.06562         | 977.88                        | 4.084E-04         | 25911        | 0.00612 | 0.06637       | 1.091                           | 1.06E+07 | 1.20E+11 |
| T <sub>9</sub>  | 6.06E-05               | 81.7           | 60.7       | 71.2       | 1.2008  | 28579        | 0.00597 | 0.06562         | 977.28                        | 4.038E-04         | 26204        | 0.00610 | 0.06632       | 1.107                           | 1.08E+07 | 1.22E+11 |
| T <sub>10</sub> | 7.44E-05               | 82.1           | 61.5       | 71.8       | 1.2013  | 28649        | 0.00597 | 0.06563         | 976.90                        | 4.010E-04         | 26386        | 0.00609 | 0.06629       | 1.114                           | 1.09E+07 | 1.24E+11 |
| 807             |                        |                |            |            |         |              |         |                 |                               |                   |              |         |               |                                 |          |          |
| T <sub>1</sub>  | 1.66E-06               | 73.0           | 51.2       | 62.1       | 1.3980  | 31093        | 0.00585 | 0.07562         | 982.69                        | 4.564E-04         | 27143        | 0.00605 | 0.07688       | 0.955                           | 1.04E+07 | 1.47E+11 |
| T <sub>2</sub>  | 1.74E-06               | 74.2           | 52.4       | 63.3       | 1.3990  | 31484        | 0.00583 | 0.07555         | 982.01                        | 4.483E-04         | 27631        | 0.00602 | 0.07676       | 0.976                           | 1.07E+07 | 1.52E+11 |
| T <sub>3</sub>  | 3.66E-06               | 75.9           | 53.7       | 64.8       | 1.4002  | 32002        | 0.00581 | 0.07547         | 981.15                        | 4.387E-04         | 28235        | 0.00599 | 0.07663       | 1.006                           | 1.10E+07 | 1.59E+11 |
| T <sub>4</sub>  | 6.02E-06               | 76.7           | 55.0       | 65.9       | 1.4011  | 32238        | 0.00580 | 0.07545         | 980.54                        | 4.323E-04         | 28652        | 0.00597 | 0.07654       | 1.020                           | 1.12E+07 | 1.63E+11 |
| T <sub>5</sub>  | 6.63E-06               | 77.6           | 56.1       | 66.9       | 1.4019  | 32489        | 0.00579 | 0.07543         | 979.95                        | 4.265E-04         | 29045        | 0.00595 | 0.07646       | 1.035                           | 1.14E+07 | 1.67E+11 |
| T <sub>6</sub>  | 1.68E-05               | 79.1           | 57.4       | 68.3       | 1.4032  | 32873        | 0.00577 | 0.07539         | 979.11                        | 4.187E-04         | 29586        | 0.00592 | 0.07635       | 1.061                           | 1.17E+07 | 1.73E+11 |
| T <sub>7</sub>  | 3.46E-05               | 80.1           | 58.6       | 69.4       | 1.4041  | 33111        | 0.00576 | 0.07537         | 978.43                        | 4.129E-04         | 30001        | 0.00590 | 0.07628       | 1.079                           | 1.20E+07 | 1.78E+11 |
| T <sub>8</sub>  | 4.86E-05               | 81.3           | 59.8       | 70.6       | 1.4052  | 33371        | 0.00575 | 0.07536         | 977.69                        | 4.069E-04         | 30443        | 0.00588 | 0.07620       | 1.100                           | 1.22E+07 | 1.83E+11 |
| T <sub>9</sub>  | 5.74E-05               | 82.4           | 60.9       | 71.7       | 1.4062  | 33585        | 0.00574 | 0.07535         | 977.00                        | 4.017E-04         | 30836        | 0.00586 | 0.07613       | 1.119                           | 1.24E+07 | 1.87E+11 |
| T <sub>10</sub> | 6.47E-05               | 82.9           | 61.7       | 72.3       | 1.4068  | 33678        | 0.00574 | 0.07536         | 976.58                        | 3.988E-04         | 31063        | 0.00585 | 0.07610       | 1.128                           | 1.26E+07 | 1.89E+11 |
| 808             |                        |                |            |            |         |              |         |                 |                               |                   |              |         |               |                                 |          |          |
| T <sub>1</sub>  | -                      | 73.8           | 51.3       | 62.6       | 1.6058  | 35998        | 0.00565 | 0.08534         | 982.44                        | 4.533E-04         | 31378        | 0.00584 | 0.08676       | 0.969                           | 1.19E+07 | 2.15E+11 |
| T <sub>2</sub>  | 4.05E-07               | 74.6           | 52.5       | 63.6       | 1.6067  | 36294        | 0.00564 | 0.08531         | 981.87                        | 4.467E-04         | 31844        | 0.00582 | 0.08665       | 0.983                           | 1.21E+07 | 2.21E+11 |
| T <sub>3</sub>  | 1.29E-06               | 75.7           | 53.7       | 64.7       | 1.6078  | 36681        | 0.00562 | 0.08526         | 981.21                        | 4.394E-04         | 32376        | 0.00579 | 0.08654       | 1.002                           | 1.24E+07 | 2.28E+11 |
| T <sub>4</sub>  | 3.95E-06               | 76.9           | 55.0       | 66.0       | 1.6090  | 37081        | 0.00561 | 0.08521         | 980.48                        | 4.318E-04         | 32947        | 0.00577 | 0.08642       | 1.023                           | 1.27E+07 | 2.36E+11 |
| T <sub>5</sub>  | 5.65E-06               | 77.8           | 56.1       | 67.0       | 1.6099  | 37366        | 0.00560 | 0.08519         | 979.89                        | 4.259E-04         | 33397        | 0.00575 | 0.08633       | 1.039                           | 1.29E+07 | 2.42E+11 |
| T <sub>6</sub>  | 1.20E-05               | 78.9           | 57.4       | 68.2       | 1.6111  | 37694        | 0.00559 | 0.08516         | 979.17                        | 4.193E-04         | 33929        | 0.00573 | 0.08623       | 1.058                           | 1.32E+07 | 2.49E+11 |
| T <sub>7</sub>  | 2.25E-05               | 80.4           | 58.6       | 69.5       | 1.6125  | 38095        | 0.00557 | 0.08513         | 978.34                        | 4.122E-04         | 34514        | 0.00571 | 0.08613       | 1.084                           | 1.36E+07 | 2.57E+11 |
| T <sub>8</sub>  | 3.08E-05               | 81.0           | 59.8       | 70.4       | 1.6134  | 38252        | 0.00557 | 0.08513         | 977.78                        | 4.077E-04         | 34894        | 0.00569 | 0.08607       | 1.095                           | 1.38E+07 | 2.62E+11 |
| T <sub>9</sub>  | 5.20E-05               | 81.8           | 60.8       | 71.3       | 1.6143  | 38441        | 0.00556 | 0.08513         | 977.22                        | 4.034E-04         | 35267        | 0.00568 | 0.08601       | 1.108                           | 1.40E+07 | 2.67E+11 |
| T <sub>10</sub> | 5.23E-05               | 82.4           | 61.6       | 72.0       | 1.6151  | 38574        | 0.00556 | 0.08514         | 976.77                        | 4.001E-04         | 35550        | 0.00567 | 0.08596       | 1.119                           | 1.41E+07 | 2.71E+11 |

## 5.2 Input Data

Potentially 90 data points from nine fouling experiments using ten surface thermocouples were available for modeling. A number of data points either failed to meet the fouling criterion ( $R_f U_c \geq 0.05$ ) or produced obviously erroneous results (due to malfunctioning thermocouples), and therefore 84 data points were employed in the modeling. To run the program, an input file was prepared by converting raw experimental data from text delimited files, generated by data-acquisition system and saved in the computer, to Microsoft Excel spreadsheets for data manipulation. A sample spreadsheet used to evaluate the constants  $C_1$  and  $C_2$  for Equations (5.1.4), (5.1.6), and (5.1.8) is shown in Table 5.1.1. Input data, produced in Excel, were imported to Matlab and were used as program input. In preparation of all 84 experimental data points, the film temperature was used for the mass transfer term while the surface temperature was used for the chemical attachment term. A summary of experimental data used in the analysis is shown in Figure 5.2.1. It shows the range of fluid velocity and of initial fouling rate spanned by the experiments. The range of initial fouling rates at a given velocity arises because of temperature effects. At temperatures below  $73^\circ\text{C}$  no  $\dot{R}_{fo}$  was detected. The Reynolds number based on the local bulk properties ranged from 2100 to 35550, and clean inside wall temperatures varied from  $66$  to  $87^\circ\text{C}$ . The bulk inlet temperature was kept approximately at  $50^\circ\text{C}$ . In Figure 5.2.1, some points are completely overlapping each other.

## 5.3 Physical Properties and Temperature Effect

Before using experimental data in any modeling problem involving heat, mass, or momentum transfer, it is essential to determine which properties change with temperature

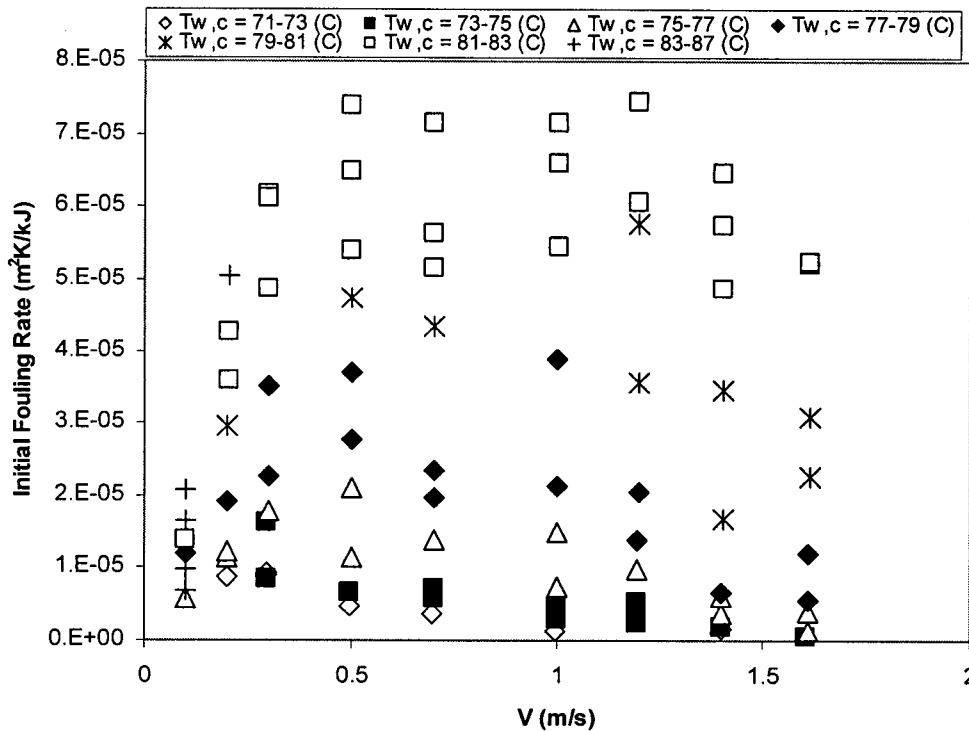


**Figure 5.2.1: Experimental Data Used for Modeling (C = 3400 ppm)**

and what temperature is appropriate for physical properties evaluation. The effect of temperature on fluid properties such as density and viscosity was presented in Section 3.7. The effect of non-isothermal flow on the friction factor, which is required to evaluate  $v_{*}$ , must also be considered.

Friction factors are typically correlated for isothermal flow; therefore applying the Petukhov (1970) equation,

$$f = (1.58 \ln Re - 3.28)^{-2} \quad (5.3.1)$$

to non-isothermal data caused concern about its applicability. For  $Re < 2100$ , McAdams (1954) recommended evaluation of the friction factor in non-isothermal flow at  $T' = T_b + (T_w - T_b)/4$ . For  $Re > 2100$ , evaluation of the friction factor was recommended at  $T'' = T_b + (T_w - T_b)/2$ . In essence, using such film temperatures in  $Re$  accounts for the non-isothermality of the fluid flow. Since all experimental data in the present work were

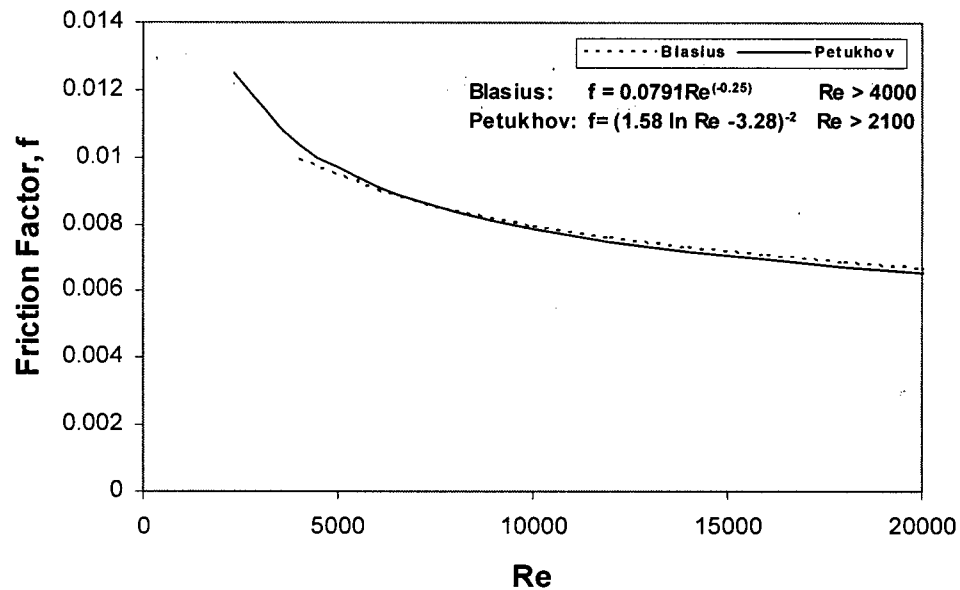


**Figure 5.3.1: Friction Factor Correlations**

at  $Re > 2100$ , the film temperature was calculated as the arithmetic mean of  $T_w$  and  $T_b$ .

The Petukhov friction factor correlation shown in Figure 5.3.1 was employed in this work since this correlation, unlike the more conventional Blasius equation, also shown in Figure 5.3.1, is reported to be valid to the low end of the transition Reynolds numbers. This was used to evaluate the fluid friction velocity in Equations (5.1.6) and (5.1.8).

Another important consideration in Equation (5.1.4) is whether the bulk temperature, wall temperature or some mathematical average of these two temperatures should be used to evaluate the fluid physical properties in terms other than  $Re$ .

Since mass transfer of the fouling precursor to the vicinity of the heat transfer surface occurs in the momentum boundary layer, between the bulk solution and the surface, the logical temperature to use in terms arising from Equation (2.8.1.9) was the

**Table 5.4.1: Adjusted Parameters at the Optimal Solution**

|                | $\Delta E$ (kJ/mol) | $P_1 \left( \frac{m^8 K s^5}{kg^4} \right)^{1/3}$ | $P_2 \left( \frac{kg^5 s^2}{m^{10} K^2} \right)^{1/3}$ |
|----------------|---------------------|---|--|
| Optimum Values | 262.5               | $1.59 \times 10^{-14}$                            | $5.21 \times 10^{-50}$                                 |

film temperature. In this case the arithmetic average film temperature,  $T_f = (T_b + T_w)/2$  was employed to evaluate film density and viscosity. Obviously the chemical attachment coefficient, introduced as  $k_a$  in Equation (2.8.1.13), is associated with surface phenomena and therefore physical properties in terms arising from this equation were evaluated at the wall temperature.

#### 5.4 Model Predictions

Using all the experimental data of Table 5.1.1 in the computer program, the optimal solution occurred at the values presented in Table 5.4.1. The optimal value of 262.5 kJ/mol for activation energy is larger than the values ranging from 210 to 254 kJ/mol, found from kinetic studies (Sections 4.7.1 and 4.7.2). Also, it is larger than the range of 105-219 kJ/mol reported by Bansal et al. (2005) for wall surface crystallization (fouling) for an unreported range of velocity.

The program was run for fixed values of activation energy and the sum of the squares of the residuals was found for each optimal solution of  $P_1$  and  $P_2$ . Figure 5.4.1 shows the final optimum value of 262.5 kJ/mol for activation energy, which corresponds to the minimum value of the sum of the squares of the residuals equal to  $7.86 \times 10^{-15}$   $(m^2 K/J)^2$ .

A plot comparing the experimental and model predictions for initial fouling rate is

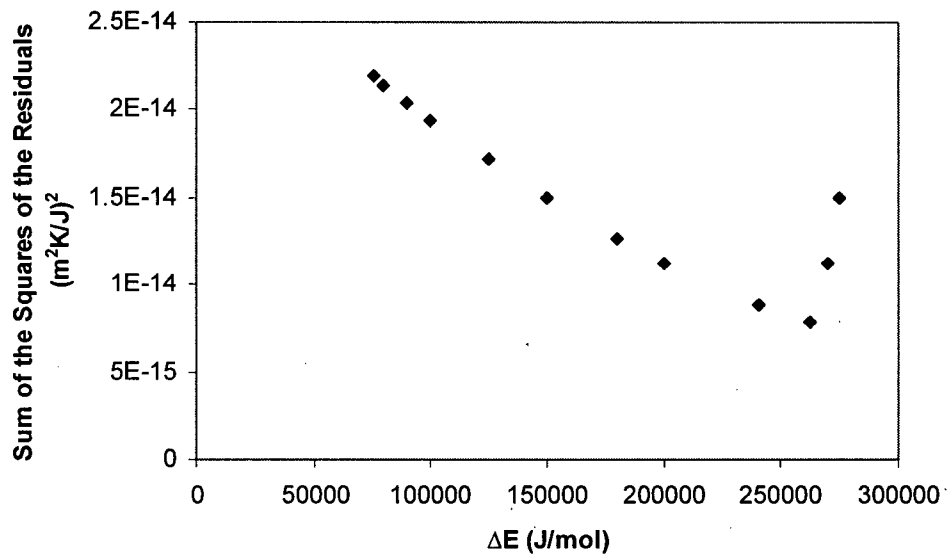


Figure 5.4.1: Sum of the Squares of the Residuals Over a Range of Activation Energies

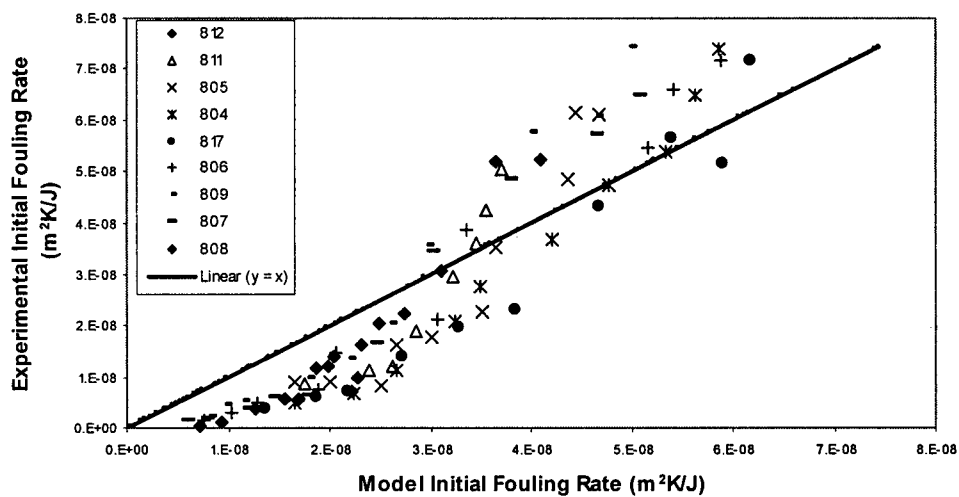


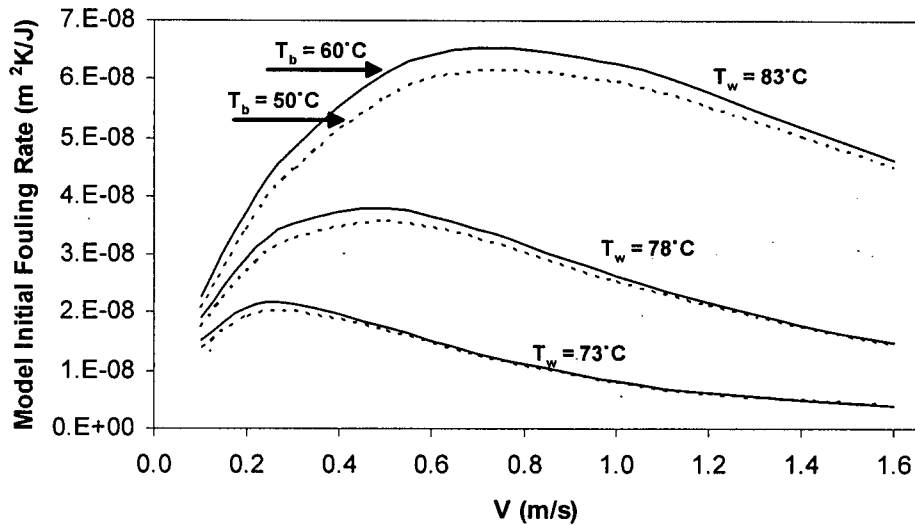
Figure 5.4.2: Comparing Experimental and Model Initial Fouling Rate Results Listed in Table 5.4.1.a (Run numbers are identified in legend)

Table 5.4.1a: Statistical Analysis of the Results

| $(\dot{R}_{fo})_{\text{expt}}$<br>( $m^2 K / J$ ) | $(\dot{R}_{fo})_{\text{model}}$<br>( $m^2 K / J$ ) | $\left( (\dot{R}_{fo})_{\text{model}} - (\dot{R}_{fo})_{\text{expt}} \right)^2$<br>( $m^2 K / J$ ) <sup>2</sup> | $\frac{\left  (\dot{R}_{fo})_{\text{model}} - (\dot{R}_{fo})_{\text{expt}} \right }{(\dot{R}_{fo})_{\text{expt}}}$ | $\left( \frac{(\dot{R}_{fo})_{\text{model}} - (\dot{R}_{fo})_{\text{expt}}}{(\dot{R}_{fo})_{\text{expt}}} \right)^2$ |
|---|--|---|--|--|
| 5.82E-09  | 1.70E-08   | 1.25E-16  | 1.918  | 3.678  |
| 1.19E-08  | 1.88E-08   | 4.75E-17  | 0.579  | 0.335  |
| 1.39E-08  | 2.08E-08   | 4.74E-17  | 0.495  | 0.245  |
| 7.03E-09  | 2.25E-08   | 2.38E-16  | 2.194  | 4.815  |
| 9.76E-09  | 2.31E-08   | 1.77E-16  | 1.365  | 1.862  |
| 1.64E-08  | 2.36E-08   | 5.16E-17  | 0.438  | 0.192  |
| 2.06E-08  | 2.54E-08   | 2.31E-17  | 0.233  | 0.054  |
| 8.72E-09  | 1.63E-08   | 5.68E-17  | 0.864  | 0.747  |
| 1.15E-08  | 2.33E-08   | 1.38E-16  | 1.023  | 1.046  |
| 1.22E-08  | 2.60E-08   | 1.90E-16  | 1.129  | 1.274  |
| 1.91E-08  | 2.85E-08   | 8.86E-17  | 0.493  | 0.243  |
| 2.94E-08  | 3.24E-08   | 9.09E-18  | 0.103  | 0.011  |
| 3.59E-08  | 3.50E-08   | 8.45E-19  | 0.026  | 0.001  |
| 4.26E-08  | 3.60E-08   | 4.37E-17  | 0.155  | 0.024  |
| 5.05E-08  | 3.75E-08   | 1.69E-16  | 0.257  | 0.066  |
| 9.05E-09  | 1.43E-08   | 2.78E-17  | 0.582  | 0.339  |
| 9.21E-09  | 1.81E-08   | 7.92E-17  | 0.966  | 0.934  |
| 8.52E-09  | 2.35E-08   | 2.23E-16  | 1.754  | 3.076  |
| 1.63E-08  | 2.52E-08   | 7.96E-17  | 0.547  | 0.300  |
| 1.77E-08  | 2.91E-08   | 1.30E-16  | 0.644  | 0.415  |
| 2.27E-08  | 3.46E-08   | 1.42E-16  | 0.525  | 0.275  |
| 3.51E-08  | 3.60E-08   | 7.56E-19  | 0.025  | 0.001  |
| 4.86E-08  | 4.39E-08   | 2.16E-17  | 0.096  | 0.009  |
| 6.16E-08  | 4.48E-08   | 2.83E-16  | 0.273  | 0.075  |
| 6.12E-08  | 4.72E-08   | 1.95E-16  | 0.228  | 0.052  |
| 4.91E-09  | 1.37E-08   | 7.75E-17  | 1.793  | 3.213  |
| 6.68E-09  | 1.96E-08   | 1.67E-16  | 1.934  | 3.741  |
| 1.15E-08  | 2.40E-08   | 1.56E-16  | 1.087  | 1.182  |
| 2.10E-08  | 3.01E-08   | 8.25E-17  | 0.432  | 0.187  |
| 2.77E-08  | 3.28E-08   | 2.60E-17  | 0.184  | 0.034  |
| 3.69E-08  | 4.05E-08   | 1.31E-17  | 0.098  | 0.010  |
| 4.74E-08  | 4.68E-08   | 4.06E-19  | 0.013  | 0.000  |
| 5.40E-08  | 5.27E-08   | 1.70E-18  | 0.024  | 0.001  |
| 6.49E-08  | 5.58E-08   | 8.24E-17  | 0.140  | 0.020  |
| 7.39E-08  | 5.84E-08   | 2.39E-16  | 0.209  | 0.044  |
| 3.67E-09  | 1.10E-08   | 5.33E-17  | 1.990  | 3.959  |
| 5.98E-09  | 1.57E-08   | 9.48E-17  | 1.628  | 2.651  |
| 7.17E-09  | 1.86E-08   | 1.31E-16  | 1.597  | 2.551  |
| 1.39E-08  | 2.40E-08   | 1.03E-16  | 0.730  | 0.533  |
| 1.97E-08  | 2.98E-08   | 1.03E-16  | 0.515  | 0.265  |
| 2.33E-08  | 3.58E-08   | 1.57E-16  | 0.537  | 0.288  |
| 4.33E-08  | 4.47E-08   | 2.06E-18  | 0.033  | 0.001  |

Table 5.4.1a: Statistical Analysis of the Results (cont'd)

| $(\dot{R}_{fo})_{\text{exp } t}$<br>( $m^2 K / J$ ) | $(\dot{R}_{fo})_{\text{model}}$<br>( $m^2 K / J$ ) | $\left( (\dot{R}_{fo})_{\text{model}} - (\dot{R}_{fo})_{\text{exp } t} \right)^2$<br>( $m^2 K / J$ ) <sup>2</sup> | $\frac{\left  (\dot{R}_{fo})_{\text{model}} - (\dot{R}_{fo})_{\text{exp } t} \right }{(\dot{R}_{fo})_{\text{exp } t}}$ | $\left( \frac{(\dot{R}_{fo})_{\text{model}} - (\dot{R}_{fo})_{\text{exp } t}}{(\dot{R}_{fo})_{\text{exp } t}} \right)^2$ |
|---|--|---|--|--|
| 5.64E-08  | 5.25E-08   | 1.54E-17  | 0.070  | 0.005  |
| 5.16E-08  | 5.79E-08   | 4.03E-17  | 0.123  | 0.015  |
| 7.16E-08  | 6.08E-08   | 1.17E-16  | 0.151  | 0.023  |
| 1.34E-09  | 1.59E-09   | 1.00E-18  | 0.187  | 0.034  |
| 3.00E-09  | 8.02E-09   | 2.52E-17  | 1.675  | 2.804  |
| 4.77E-09  | 1.04E-08   | 3.12E-17  | 1.172  | 1.373  |
| 7.44E-09  | 1.60E-08   | 7.33E-17  | 1.150  | 1.323  |
| 1.48E-08  | 1.76E-08   | 7.66E-18  | 0.187  | 0.035  |
| 2.12E-08  | 2.76E-08   | 4.09E-17  | 0.302  | 0.091  |
| 3.88E-08  | 3.06E-08   | 6.78E-17  | 0.212  | 0.045  |
| 5.46E-08  | 4.94E-08   | 2.70E-17  | 0.095  | 0.009  |
| 6.60E-08  | 5.20E-08   | 1.96E-16  | 0.212  | 0.045  |
| 7.16E-08  | 5.71E-08   | 2.11E-16  | 0.203  | 0.041  |
| 2.37E-09  | 6.31E-09   | 1.55E-17  | 1.664  | 2.768  |
| 4.56E-09  | 7.63E-09   | 9.41E-18  | 0.673  | 0.452  |
| 5.27E-09  | 9.12E-09   | 1.48E-17  | 0.731  | 0.535  |
| 9.83E-09  | 1.50E-08   | 2.72E-17  | 0.531  | 0.281  |
| 1.38E-08  | 1.91E-08   | 2.76E-17  | 0.381  | 0.145  |
| 2.05E-08  | 2.30E-08   | 6.23E-18  | 0.122  | 0.015  |
| 3.56E-08  | 2.67E-08   | 7.85E-17  | 0.249  | 0.062  |
| 5.76E-08  | 3.71E-08   | 4.20E-16  | 0.356  | 0.127  |
| 6.06E-08  | 4.41E-08   | 2.71E-16  | 0.271  | 0.074  |
| 7.44E-08  | 4.74E-08   | 7.29E-16  | 0.363  | 0.132  |
| 1.66E-09  | 4.55E-09   | 8.33E-18  | 1.739  | 3.023  |
| 1.74E-09  | 6.32E-09   | 2.10E-17  | 2.633  | 6.932  |
| 3.66E-09  | 9.90E-09   | 3.90E-17  | 1.705  | 2.908  |
| 6.02E-09  | 1.22E-08   | 3.79E-17  | 1.023  | 1.046  |
| 6.63E-09  | 1.53E-08   | 7.46E-17  | 1.302  | 1.696  |
| 1.68E-08  | 2.18E-08   | 2.55E-17  | 0.300  | 0.090  |
| 3.46E-08  | 2.74E-08   | 5.25E-17  | 0.210  | 0.044  |
| 4.86E-08  | 3.54E-08   | 1.75E-16  | 0.272  | 0.074  |
| 5.74E-08  | 4.42E-08   | 1.74E-16  | 0.230  | 0.053  |
| 6.47E-08  | 4.88E-08   | 2.54E-16  | 0.247  | 0.061  |
| 4.05E-10  | 5.25E-10   | 1.44E-20  | 0.296  | 0.087  |
| 1.29E-09  | 1.79E-09   | 2.54E-19  | 0.387  | 0.150  |
| 3.95E-09  | 1.04E-08   | 4.22E-17  | 1.644  | 2.703  |
| 5.65E-09  | 1.32E-08   | 5.65E-17  | 1.331  | 1.771  |
| 1.20E-08  | 1.73E-08   | 2.86E-17  | 0.446  | 0.199  |
| 2.25E-08  | 2.48E-08   | 5.46E-18  | 0.104  | 0.011  |
| 3.08E-08  | 2.85E-08   | 5.27E-18  | 0.075  | 0.006  |
| 5.20E-08  | 3.41E-08   | 3.22E-16  | 0.345  | 0.119  |
| 5.23E-08  | 3.87E-08   | 1.85E-16  | 0.260  | 0.067  |
|   |  | $9.92 \times 10^{-17}$  | 67.4 %   | 86.4 %   |
|   |  | VAR   | AAD  | RMS  |



**Figure 5.4.3: Effect of Wall and Bulk Temperatures on Model Predictions**

shown in Figure 5.4.2 as a pronounced “S” shape, in which more than half the points lie below the  $45^\circ$  line and the rest above it. Examining all the points in the scatter diagram reveals that points above the  $45^\circ$  line generally correspond to higher wall temperatures than those below it. In an attempt to segregate the two data sets, the points above the  $45^\circ$  line were separated from those below it and the same program was run for each of them separately. After constructing the two plots in the manner of Figure 5.4.2, the same “S” shape was observed for each but with less intensity. It is argued here that this non-random deviation indicates that surface nucleation plays a significant role which was not considered in the model, so that any model improvement needs to take this role into account.

To determine the goodness of the fit, the variance, the average absolute percent deviation (AAD), and the root mean square percent deviation (RMS) were evaluated for all the data points. The variance, AAD, and RMS have values of  $9.92 \times 10^{-17}$ , 67.4 %, and 86.4 %, respectively.

Figure 5.4.3 shows the strong effect of wall temperature on the initial fouling rate over a range of fluid velocities, according to the model predictions at wall temperatures of 73, 78, and 83°C. Also, note the effect of bulk temperature: shown at each wall temperature are predictions for bulk temperatures of 50 and 60°C. Recall that in this analysis the physical properties for the mass transfer term are evaluated at the film temperature, while those for the chemical attachment term are based on the clean inside wall temperature. From Figure 5.4.3, results at constant wall temperature show that the bulk temperature has a greater effect in the mass transfer controlled region than in the attachment region. Hence, although bulk temperatures were kept low to eliminate bulk crystallization, the bulk temperature influences the film temperature, and as a consequence, the balance between mass transfer and chemical attachment. Also, at lower wall temperatures, since physical properties at both bulk and wall temperatures approach the same values, the bulk temperature has less impact on the initial fouling rate.

The initial fouling rate predictions in Figure 5.4.3 follow the expected model trends, i.e. a maximum in predicted initial fouling rate with velocity, and a shift of the location of the maximum to higher velocities as the wall temperature is increased. These trends are consistent with previous descriptions of the model (Epstein, 1994). The rate of decrease of the initial fouling rate in the “attachment controlled” region of the model is less than expected. For instance, doubling of velocity from 0.8 to 1.6 m/s on average results in approximately 52 % fall-off of the fouling rate. This is presumably due to the persistence of a significant mass transfer influence well beyond the maximum.

Figure 5.4.4 is a comparison plot of the nine experimental data points at each of three wall temperatures to the corresponding optimum model predictions based on all 84

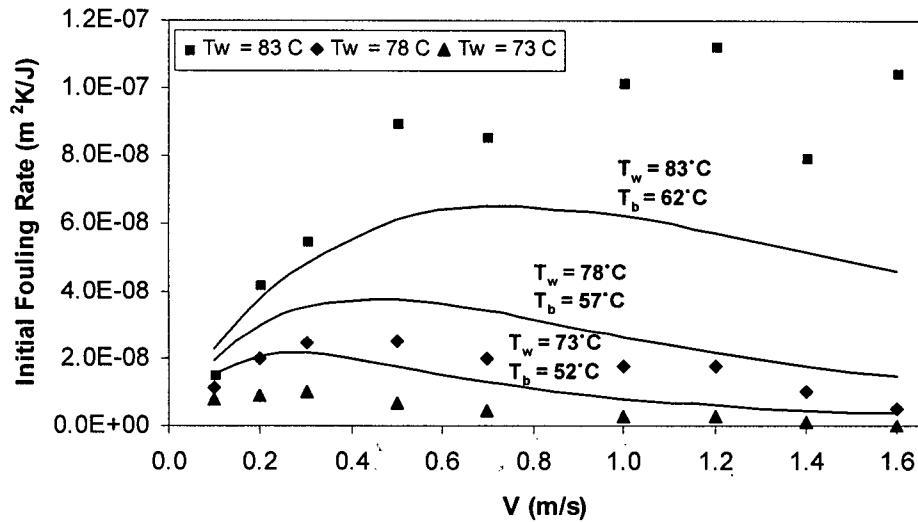


**Figure 5.4.4: Comparison of Model Predictions to Experimental Data Obtained from the Arrhenius Type Equations. Points above  $\dot{R}_{fo} = 8 \times 10^{-8} \text{ m}^2\text{K/J}$  Are Extrapolations.**

data points. The greatest deviations between experimental and predictions occur at the highest wall temperature, where the predictions are mainly lower than the experimental results. On the other hand, at the lower wall temperatures the model-generated values are higher than the experimental results. However, despite these discrepancies, the model and the data points follow similar trends.

It is worth mentioning that the mathematical model (Epstein, 1994) tested assumes a constant concentration driving force  $\Delta C$ . In the present work,  $\Delta C$  increases somewhat along the test section. However, referring to Table 5.1.1, the changes in  $\Delta C$  are relatively small.

### 5.5 Estimation of Constants from Model Solutions

From the solutions to the model it is possible to compare values of constants from this study to those reported by Epstein (1994), and to accepted isothermal values

(Metzner and Friend, 1958). The following discussion first illustrates how values of  $k'$  and  $k''$  are extracted from the modeling results.

In the Stokes-Einstein equation, Equation (5.1.3), it is assumed that the diffusivity is proportional to the absolute solution temperature divided by viscosity at the relevant film conditions. Therefore, the proportionality constant,  $D_o$ , was lumped into the parameter  $P_1$  along with mass transfer constant  $k'$  and the physical properties (Equation (5.1.5)). Once the constant  $D_o$  and the physical properties are estimated for each system,  $k'$  can be evaluated.

To estimate  $D_o$ , the values of diffusivity that have been reported by Bohnet (1987) were employed. Table 5.5.1 shows these diffusivities under different wall and bulk temperatures. In the present study, these values were employed to find the best fitted value for  $D_o$  in Equation (5.1.3). In Figure 5.5.1 the slope of the line determines the value of  $D_o$  as  $1.43 \times 10^{-15} \text{ kg}\cdot\text{m}/\text{s}^2\text{K}$ .

Both  $k'$  and  $k''$  are obtained through Equations (5.1.5) and (5.1.7), which define the parameters  $P_1$  and  $P_2$ . From a study of the calcium sulphate fouling deposit properties

**Table 5.5.1: Diffusivities of Calcium Sulphate in Water at Different Temperatures (Bohnet, 1987)**

| $D \text{ (m}^2/\text{s)}$ | $T_s \text{ (}^\circ\text{C)}$ | $T_b \text{ (}^\circ\text{C)}$ | $T_f \text{ (}^\circ\text{C)}$ |
|----------------------------|--------------------------------|--------------------------------|--------------------------------|
| $1.057 \times 10^{-9}$     | 88                             | 43.5                           | 65.75                          |
| $1.042 \times 10^{-9}$     | 77                             | 42.8                           | 63.3                           |
| $1.054 \times 10^{-9}$     | 75                             | 43.4                           | 59.9                           |
| $1.082 \times 10^{-9}$     | 87                             | 44.7                           | 59.2                           |
| $1.088 \times 10^{-9}$     | 85                             | 45                             | 65.9                           |

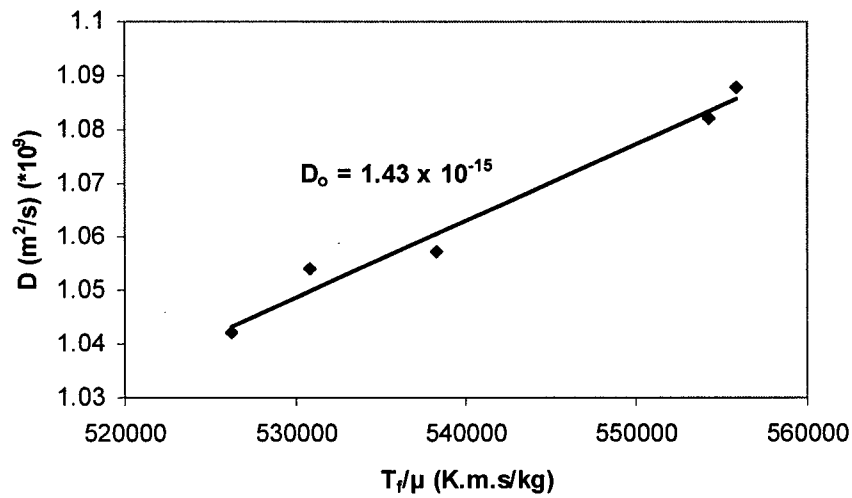


**Figure 5.5.1: Extracting Best Value of  $D_0$  Based on the Data of Bohnet (1987), with  $T_f$  = Absolute Film Temperature**

**Table 5.5.2: Summary of Transport and Attachment Properties Used in or Evaluated from Model**

| Property  | Value                           |
|---|---------------------------------|
| $D_0$ in Equation (5.1.1)                               | $1.43 \times 10^{-15}$          |
| $D \text{ (m}^2\text{/s)}$                              | $(1.022 - 1.22) \times 10^{-9}$ |
| Sc  | 462 - 334                       |
| $\rho_f \lambda_f \text{ (kg}^2\text{/m}^2\text{Ks}^3)$ | 1734                            |
| $k'$ from Equation (5.1.5)                              | 4.5                             |
| $k''$ from Equation (5.1.7)                             | $1.78 \times 10^{-39}$          |

(Section 4.4.2), the product  $\rho_f \lambda_f$  was estimated as  $1734 \text{ kg}^2/\text{m}^2\text{Ks}^3$ . If the stoichiometric ratio  $r$ , the mass of fouling deposit per mass of precursor required to produce it, is taken as 1, a solution for  $k'$  can be obtained from Equation (5.1.5), and  $k''$  can then be determined from Equation (5.1.7). The calculated values are presented in Table 5.5.2.

After developing a mathematical model for initial chemical reaction fouling, Epstein (1994) used a reference point method to evaluate  $k'$  as 502.3 for the data of Crittenden et al. (1987a) on the solution polymerization of styrene. It was argued that the magnitude of this value (compared to 11.8 determined by Metzner and Friend (1958) for isothermal systems with high Schmidt numbers) could be due in part to the non-isothermality of Crittenden et al.'s (1987a) experimental system and the fact that some of their data points were in the laminar flow range. In addition, Epstein (1994) indicated that an underestimation of  $Sc$  in Equation (2.8.1.9) due to the use of wall temperatures instead of film temperatures to evaluate the fluid physical properties could contribute to the high value of  $k'$  as compensation for the lowered value of  $Sc$  in the same equation.

Two years later, Vasak and Epstein (1996) re-analyzed Crittenden et al.'s (1987a) experimental data by minimizing the variance using a multi-parameter non-linear least squares regression. This analysis achieved similar results and the best estimate of  $k'$  was revised to 481.

In spite of employing a non-isothermal fouling apparatus in the present study, it is shown that the value of 4.5 obtained for  $k'$  is considerably smaller than suggested above for styrene polymerization fouling and much closer to the 11.8 of Metzner and Friend (1958). In our work, the physical properties in  $Sc$  were accounted for by consideration of

the film temperature. The main concern about the validity of the estimated  $k'$  is the fact that nucleation sites were not incorporated in the model.

Since  $k''$  includes the pre-exponential factor, which is radically different from case to case, it is not logical to compare its value from this work to that of any other study and expect to get the same values.

### 5.6 Problems Associated with Surface Crystallization Modeling

As discussed, there were deviations between experimental results and modeling predictions at both high and low wall temperatures. To explain them, there is a need for mathematical model improvement for precipitating solutions with solutes such as calcium sulphate. This can be done by refining the surface integration term by incorporating new parameters. Bansal et al. (2005) proposed the following equation for the deposition rate in crystallizing systems:

$$\dot{m}_d = k_r (C_b - C_{sat})^n N \left( \frac{M}{M_g} \right)^{n'} \quad (5.6.1)$$

where  $N$  is a “function of the nucleation sites provided by the particles present in the solution”,  $M$  the crystal mass formed on the surface at time  $t$ ,  $M_g$  the crystal mass on the surface when crystal growth starts, and  $n'$  is an exponent. Equation (5.6.1) is similar to those developed for seeded crystallization in the bulk fluid where a known number of nucleation seeds with known surface areas are added to the system. Although Equation (5.6.1) is designed for surface crystallization, it is not clear how it can be applied to solutions without any particles in the bulk fluid. Even if Equation (5.6.1) can be used for surface crystallization by considering  $N$  as the number of surface nucleation seeds, it would be difficult to generate nucleation sites on a surface in a reproducible manner, let

alone count them. Another difficulty is that nuclei can form in the boundary layer close to the surface rather than on the surface itself, which makes the surface crystallization even more complicated. Therefore, any improved model that is developed in the future should take the above facts into account.

### 5.7 Considering Nucleation Sites in a Crude Model

To take into account the nucleation sites, a crude approach can be made to at least reduce the deviations between model predictions and experimental results. The idea is to modify Equation (2.8.1.2) for calcium sulphate surface integration as follows:

$$\phi_{do} = k_a (C_w - C_{sat})^2 N_c \quad (5.7.1)$$

where  $k_a$  can be evaluated from Equation (2.8.1.13) and the number of nucleation sites,  $N_c$ , is assumed to be a function of wall temperature  $T_w$ , i.e.

$$\phi_{do} = k_a (C_w - C_{sat})^2 f(T_w) \quad (5.7.2)$$

Following the steps described in Sections 2.8.1 and 5.1 for the initial fouling rate model development, we arrive at:

$$\dot{R}_{fo} = P_1 C_1 \left( \Delta C + \frac{P_2 C_2 e^{\Delta E / RT_w}}{2f(T_w)} - \sqrt{\frac{1}{4} \left( \frac{P_2 C_2 e^{\Delta E / RT_w}}{f(T_w)} \right)^2 + \frac{P_2 C_2 e^{\Delta E / RT_w} \Delta C}{f(T_w)}} \right) \quad (5.7.3)$$

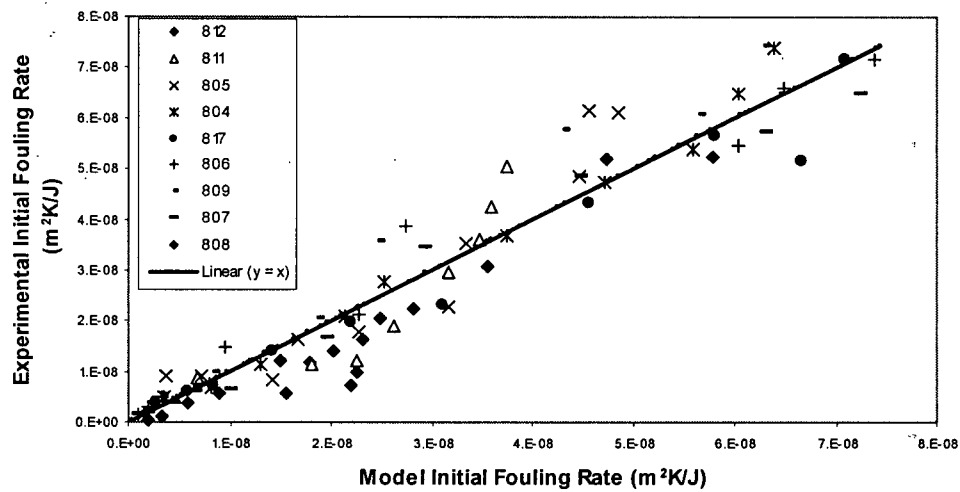
The computer program was modified according to Equation (5.7.3), assuming the following form of  $f(T_w)$ :

$$f(T_w) = a' T_w^{b'} \quad (5.7.4)$$

Using Equation (5.7.4) thus added two more parameters,  $a'$  and  $b'$ , to the previous ones,  $P_1$ ,  $P_2$ , and  $\Delta E$ , but  $a'$  was lumped into the parameter  $P_2$ , and therefore the total number of parameters was reduced to 4, i.e.  $P_1$ ,  $P_2$ ,  $\Delta E$ , and  $b'$ .

**Table 5.7.1: Adjusted Parameters for Refined Model**

|                | $\Delta E$ (kJ/mol) | $P_1 \left( \frac{m^8 K s^5}{kg^4} \right)^{1/3}$ | $P_2 \left( \frac{kg^5 s^2}{m^{10} K^2} \right)^{1/3}$ | $b'$  |
|----------------|---------------------|---|--|-------|
| Optimum Values | 458.5               | $1.52 \times 10^{-14}$                            | $8.00 \times 10^{-47}$                                 | 12.65 |

**Figure 5.7.1: Comparing Experimental and Model Initial Fouling Rate Results for the Refined Model**

After running the program using all 84 data points, the optimal solution occurred at the values shown in Table 5.7.1. It can be seen that  $P_1$  has not changed significantly compared with that in the original model. This is to be expected since in the new model it is only the surface reaction term that has been modified, which has little impact on mass transfer. However, activation energy and  $P_2$  have changed since both are coupled in the surface integration term.

Figure 5.7.1 illustrates that in contrast to the comparison plot in the original model, the experimental and model predictions are scattered around the 45° line for initial

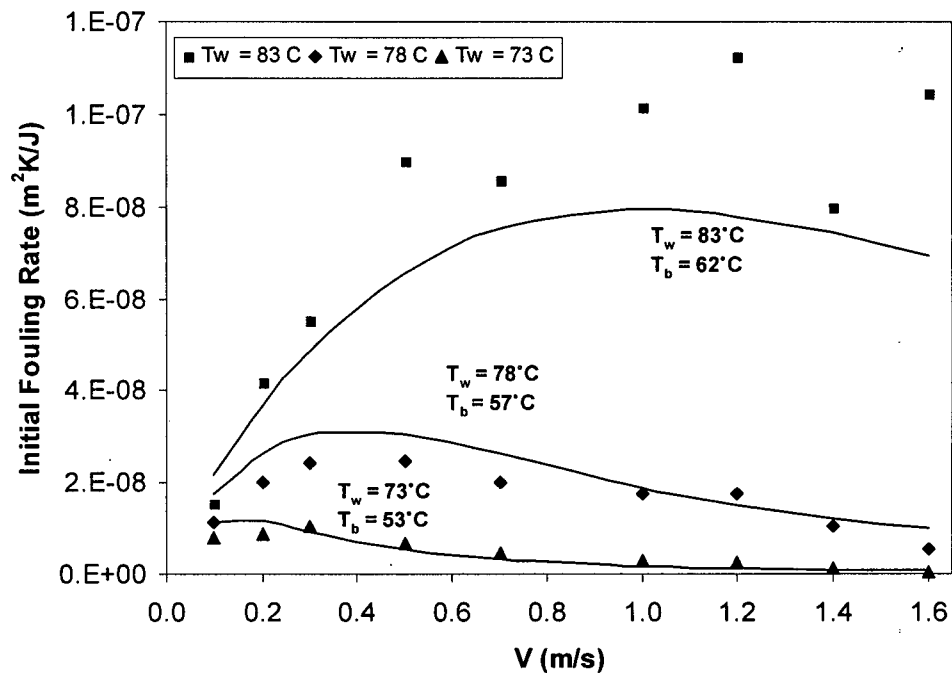


Figure 5.7.2: Comparison of Model Predictions to Experimental Data for the Refined Model

Table 5.7.2: Comparing Original Model with Refined Model

|                | $k'$ | $k''$                  | VAR                    | AAD (%) | RMS (%) |
|----------------|------|------------------------|------------------------|---------|---------|
| Original Model | 4.5  | $1.78 \times 10^{-39}$ | $9.92 \times 10^{-17}$ | 67.4    | 86.4    |
| Refined Model  | 4.8  | $3.03 \times 10^{-36}$ | $3.66 \times 10^{-17}$ | 28.6    | 45.84   |

fouling rate with smaller discrepancies between them. Also, Figure 5.7.2 illustrates that, although at the highest wall temperature the experimental results remain higher than the model predictions, the discrepancies are again smaller than before. At lower wall temperatures, the new model predictions and experimental results are more closely matched than in the original model and more matched than at the highest temperature for either model.

Table 5.7.2 is a comparison between the results of the original model and the refined one. The mass transfer term,  $k'$ , has increased from 4.5 to 4.8 and the attachment term  $k''$  has increased from  $1.78 \times 10^{-39}$  to  $3.03 \times 10^{-36}$ . Also, the statistical parameters have improved in the new model as compared with those in the original one.

This section has shown that mathematical modeling of the calcium sulphate solution fouling data, using Epstein's (1994) theoretical model, has been reasonably successful. Although the experimental data display a poorer model fit than the previously mentioned styrene in kerosene polymerization data (Crittenden et al., 1987a & b), the fundamental features of a velocity dependence, a maximum initial fouling rate, and a wall temperature dependence, were all displayed by both the model and the data. In addition, the bulk temperature was shown to have a moderate effect on the model-predicted initial fouling rate. This temperature effect was particularly significant at higher wall temperatures. The effect of bulk temperature was examined for bulk temperatures of 50°C and 60°C, and it was shown that the initial fouling rate could increase up to 6 % for a 10°C increase in  $T_b$  at constant  $T_w$ . In addition, it was shown that in the original model for higher wall temperatures the experimental results are higher than the model predictions and the opposite is true for lower wall temperatures. The discrepancies between the model predictions and the experimental results were improved by refining the model by introducing a new term for number of surface nucleation sites as a function of wall temperature.

Although the important features of the initial fouling rate model (Epstein, 1994) have been demonstrated, there are two important experimental observations worthy of note. Firstly, the fouling activation energies were considerably larger than the chemical

(surface integration) activation energies extracted from the pure kinetic studies. Secondly, while the deviations between the experimental results and the model predictions at lower wall temperatures were improved by refining the model, the experimental results are still higher than the model predictions at the highest wall temperature. These observations suggest that the number of nucleation sites on the surface and/or in the boundary layer play an important role in the fouling phenomenon. Therefore, there is a need for more experimental information on nucleation sites and for mathematical model improvement in the surface integration term.

## 6. Summary

The effect of fluid velocity and wall temperature on the initial fouling rate of aqueous calcium sulphate solutions was investigated and used to test a mathematical model for initial fouling rate (Epstein, 1994). In order to approach purely wall surface crystallization, bulk fluid temperature was kept at a minimum possible value, micron-size particles were eliminated using an in-line 1- $\mu\text{m}$  filter, and the wall temperature was kept as high as possible. Therefore the dominant deposition mechanisms were mass transfer in solution and surface integration to the test section wall, i.e. non-particulate fouling. Fouling experiments were performed over the following range of experimental conditions:  $\text{Re} = 2200 - 35600$ ,  $T_{w,i} = 66 - 87^\circ\text{C}$ .

For any given experiment, local fouling results were in most cases well represented by an Arrhenius type equation ( $\dot{R}_{fo} = A \exp\left(-\frac{\Delta E_f}{R(T_{w,i})_c}\right)$ ) at a given solute concentration and velocity, and over a range of clean inside wall temperatures. Hence from each experiment a fouling activation energy was determined. The criterion  $R_f U_c \geq 0.05$  was used to decide which experimental data to include in the data analysis. From nine fouling experiments, fouling activation energies of 66 to 620 kJ/mol resulted. Only at the lowest velocity, 0.1 m/s, is the activation energy close to the reported values for bulk precipitation, which in the temperature range of 15 – 90°C is 44 – 65 kJ/mol (Liu and Nancollas, 1975; Schierholtz, 1958; Konak, 1974; Smith and Sweett, 1971; He et al., 1994). The only other values that have been reported for fouling activation energies come from Bansal et al. (2005). Without specifying the velocity range, they reported a range of 105-219 kJ/mol, which is closer to our experimental results. Fouling activation energy, generated from fouling experiments in this study, increased with velocity, but its

maximum value was significantly larger than the kinetic activation energies. It was argued that this behaviour is due to the effect of surface nucleation sites. Since the activation energy was not constant over a range of velocities, a single wall process does not govern calcium sulphate scaling, but both bulk and wall processes must be important.

Experimentally, it was shown that at constant wall (and bulk) temperature there was a maximum initial fouling rate over a range of velocities. This maximum rate increased with increasing wall temperature, and the velocity at which the maximum occurred also increased with increasing wall temperature. These observations were consistent with the mathematical model (Epstein, 1994).

To evaluate the constants in Equation (5.1.4) for modeling purposes, the film temperature was used to evaluate the physical properties associated with mass transfer term, and the wall temperature was used to evaluate the physical properties associated with the chemical attachment term. The best modeling results generated the optimum activation energy as 262.5 kJ/mol. The average absolute percent deviation between the optimum solution and the experimental results was 67.4 %. The parameter  $P_1$  containing the mass transfer term,  $k'$ , was  $1.59 \times 10^{-14} \left( \frac{m^8 K s^5}{kg^4} \right)^{1/3}$  and the parameter  $P_2$  containing the attachment term,  $k''$ , was  $5.2 \times 10^{-50} \left( \frac{kg^5 s^2}{m^{10} K^2} \right)^{1/3}$ . Using the results from the deposit property study and the literature values for diffusivity,  $k'$ , the dimensionless mass transfer constant, was estimated as 4.5. This is close to 11.8 from Metzner and Friend (1958) for isothermal conditions, and much lower than the value of 481 reported by Vasak and Epstein (1996) for the non-isothermal styrene polymerization data (Crittenden et al., 1987a), where all the physical properties were calculated at the wall temperature.

A comparison between experimental results and the model predictions was made. It illustrated that although both model predictions and experimental results follow the expected model (Epstein, 1994) trends, at higher wall temperatures the model predictions were lower than the experimental results, and the opposite was true for lower wall temperatures. It was argued that the discrepancies between the model predictions and the experimental results were due to surface nucleation sites that were not considered in the model.

In order to lower the discrepancies between the model predictions and the experimental results, the model was refined by introducing a new term in the surface integration term. A simple function of wall temperature was employed in the refined model for the number of nucleation sites. This increased the number of adjustable parameters to 4. The program was modified according to the new model and was run with all experimental data points, and again a comparison plot was made. It indicated that the model predictions and experimental results were better matched as compared with the original model. The evaluated optimized parameters showed that the mass transfer term,  $k'$ , did not change significantly, but both activation energy and  $k''$  were increased. The activation energy was increased from 262.5 to 458.5 kJ/mol and the attachment term,  $k''$ , from  $1.78 \times 10^{-39}$  to  $3.03 \times 10^{-36}$ . The statistical analysis revealed that the average absolute percent deviation between the optimum solution and the experimental results was decreased from 67.4 to 28.6 %.

In order to separate the contribution of surface reaction (integration) from that of mass transfer, purely chemical activation energy values were generated through kinetic studies of calcium sulphate precipitation in a jacketed-glass reactor operated at a high

stirring rate. Two sets of experiments were performed with different initial solution concentrations, i.e. 3100 and 3400 ppm, and the bulk temperature was varied in the range of 60 to 84°C. The assumption of a second order reaction, as reported by Nancollas (1968) and Konak (1974), was employed to interpret the results by two different approaches. In the first approach, the surface area of crystals was assumed to be constant and this assumption led to generating three different regions with different reaction rate constants. A range of activation energies from 193 to 249 kJ/mol was extracted from Arrhenius plots. In order to produce a single reaction rate constant for each bulk temperature, the second approach was employed. It took the crystal surface area changes into account during each experiment and the activation energies were determined as 210 and 254 kJ/mol for initial concentrations of 3400 and 3100 ppm, respectively. These values were smaller than the maximum fouling activation energy of 620 kJ/mol extracted from fouling experiments.

Four fouling experiments were performed to study concentration and wall temperature effects on the delay time at a velocity of 1.2 m/s, covering inside wall temperatures from 72 to 83°C with a concentration range from 3100 to 3600 ppm (wt.). From classical nucleation theory, the effective surface energy values were calculated at different surface temperatures ranging from 7.5 to 9.9 mJ/m<sup>2</sup>. These values are at the low end of the range 8-50 mJ/m<sup>2</sup>, measured as surface energy for CaSO<sub>4</sub>·2H<sub>2</sub>O by several authors mainly in bulk precipitation. However, these values are close to 7.9 and 14.6 mJ/m<sup>2</sup> reported respectively by Linnikov (1999) for surface nucleation on a metal surface and by Hasson et al. (2003) on a polymeric membrane surface under laminar flow conditions.

Also, nine fouling experiments were performed at a concentration of 3400 ppm to study the effect of velocity on delay time. It was shown that for a given wall temperature, as the velocity increases, the delay time first decreases and then remains almost constant. This trend is explainable as due to the mechanism governing the initiation process, i.e. up to a specific velocity the process is mass transfer controlled and for higher velocities it is surface reaction controlled. Moreover, it was shown that at lower wall temperatures the velocity at which the controlling mechanism changes shifts towards lower velocities.

Using the approach applied by Branch (1991) to black liquor fouling, calcium sulphate delay time activation energies for wall surface crystallization were determined for the first time over a range of fluid velocities. It was shown that as the velocity increased, delay time activation energies increased and approached a value around 172 kJ/mol.

Removal effects were studied by increasing the fluid velocity while simultaneously eliminating the concentration driving force. In one experiment, after significant deposit buildup, fluid velocity was increased from 0.5 to 0.7 m/s. Calculations showed that some deposit was apparently removed due to the velocity surge, but at the raised velocity no continuous deposit removal was detected for all ten thermocouples.

Three fouling experiments were carried out to determine the effect of filter pore size on the fouling behavior. It was shown that at the top of the test section (higher wall temperatures), the filter pore size has little impact on the initial fouling rate and delay time. However, at the test section inlet (lower wall temperatures), the initial fouling rate is increased with filter pore size. These observations indicate that at higher wall temperatures, surface crystallization occurs quickly and therefore it dominates the fouling

process. However, at lower wall temperatures, wall surface crystallization is slow and the initiation period takes longer, so that as the time goes by, the possibility of bulk precipitation, which contributes to particulate fouling, is higher and therefore filter pore size become more important.

Examination of the morphology of the deposit revealed that the deposit at the test section inlet was tenacious and similar to typical needle crystals scattering on the surface without covering the whole surface. However, at higher wall temperatures the deposit covered the whole surface area but flaked off easily. The deposit appeared white as found by other researchers.

The deposit morphology (SEM) confirmed the needle crystal shape that caused a roughness control period. The EDX analysis showed that the deposit was mainly gypsum. Also, the TGA analysis showed that a deposit weight loss occurred mainly at a temperature of about 99°C. This confirmed that the deposit was gypsum and that the phase transformation, from gypsum to anhydrite, occurred at 99°C. Also, increasing the temperature to 900°C did not cause any further significant weight loss, showing that the anhydrite is the stable phase at higher temperatures.

A deposit property study allowed evaluation of the deposit density and thermal conductivity. The deposit density as determined from deposit coverage and thickness measurements was dependent on the deposit thickness, i.e. at lower and higher thicknesses its values were determined as 633 and 3005 kg/m<sup>3</sup>, respectively. The higher value is closer to values reported in other studies. On average, thermal conductivity and  $\rho_f \lambda_f$  obtained using  $R_f$  measurements were approximated as 2.05 W/m·K and 1734 kgW/m<sup>4</sup>K, respectively.

## 7. Conclusions

An experimental investigation of calcium sulphate scaling was carried out covering a broad range of flow conditions ( $Re = 2100 - 35600$ ) and temperatures ( $T_{w,i} = 66 - 87^\circ\text{C}$ ,  $T_b = 50 - 62^\circ\text{C}$ ). The aforementioned fouling experiments were supported by kinetic batch experiments. The results obtained from the experiments led to the following conclusions:

- Initial fouling rate experimental results for calcium sulphate solutions of 3400 ppm were generally consistent with the model (Epstein, 1994). Fouling rates increased as the Reynolds number was raised from about 2100 to about 8000. At higher wall temperature of  $87^\circ\text{C}$ , the fouling rate remained constant as Reynolds number was further increased to 25000, whereas at lower wall temperatures the rate declined from the maximum by a factor of 3 to 4.
- Both model calculated and experimental results followed the same trends but with discrepancies. To lower the aforementioned deviations, the kinetic term in the model was refined by introducing a simple function of wall temperature for number of nucleation sites. This decreased the differences significantly to a level of 50 to 90 %.
- No continuous deposit removal was detected at velocities of 0.5 and 0.7 m/s, under the operating conditions of  $T_{w,i} = 72 - 83^\circ\text{C}$ ,  $T_b = 50 - 62^\circ\text{C}$ , and  $C = 3400$  ppm.
- Delay times were found to be of the order of 1-7 hours, and decreased with increasing velocity up to 0.2-0.4 m/s and then remained almost constant at higher velocities.

- Delay time activation energies for calcium sulphate scaling were generated for the first time. They changed from 62 kJ/mol and approached to a value of 172 kJ/mol as the velocity was increased from 0.1 to 1.6 m/s.
- Delay time measurements were successfully correlated by a model based on the classical nucleation theory and from there calcium sulphate surface energy values were extracted. They were in good agreement with other literature results.
- Surface energy values for calcium sulphate turbulent flow conditions were reported for the first time. At  $Re = 25100$ ,  $T_{w,i} = 72 - 83^{\circ}C$ ,  $C = 3128-3600$  ppm, surface energy changed from 7.5 to 9.9 mJ/m<sup>2</sup>, indicating that surface energy increases slightly with temperature.
- Kinetic experiments employing a batch reactor, performed at temperatures ranging from 60 to 84°C, and initial concentrations of 3100 and 3400 ppm, showed that purely chemical activation energies are in the range of 193 to 254 kJ/mol.
- Various deposit analysis such as SEM, EDX, and TGA confirmed that the deposit was gypsum with typical needle shape.

## 8. Recommendations for Future Studies

This study explained some of the features observed in calcium sulphate scaling, but also generated questions which require further modeling or experimental work, or fouling equipment modification. These are:

- In this study, important features of the mathematical model (Epstein, 1994), applied to aqueous calcium sulphate solutions under sensible heating conditions were displayed by the experimental data. However, there were discrepancies between the model predictions and the experimental results. It was argued that this occurred because of neglect of surface nucleation sites in the model. Therefore there is a need for refining the model to take the number of nucleation sites into account. Also, in order to verify any proposed model, it is essential to find proper techniques for measuring the number of nucleation sites.
- Epstein's (1994) mathematical fouling model was developed and verified for Crittenden et al.'s (1987) styrene polymerization data (chemical reaction fouling). Also, it was further validated for isothermal colloidal particulate fouling under attractive double layer conditions (Vasak et al., 1995) and chemical reaction fouling (Rose, 1999) of two dilute protein solutions. This model should be tested for mixed salt crystallizing solutions such as calcium sulphate and calcium carbonate, which are a common problem in desalination units.
- Tube surface roughness plays an important role in scaling, especially in the initiation period. Some investigators believe that it provides additional

sites for nucleation, thereby promoting fouling. But during this study it was found that in some runs the wall temperature decreased significantly due to the crystal roughness effect, and then even after one week no further fouling was observed. Therefore it would be worthwhile to study the effect of tube surface roughness on the delay time, the roughness control period, and the initial fouling rate. To perform such a study, it would be essential to find a technique to roughen the tube surface in a reproducible manner.

- Experimentally, it was shown that the fluid velocity affects the delay time. As discussed, delay time is closely related to classical nucleation theory, which is usually applied to stagnant fluids. It would be worthwhile performing a study to incorporate both classical nucleation theory and hydrodynamics of the flow in a model.
- The TFU pump and connections to the heated section should be replaced. Also, there is a need for installing proper pressure sensors to accurately monitor pressure drop across the test section over a wide range of flow rates.

## Nomenclature

|              |   |                  |
|--------------|---|------------------|
| A            | Constant in Equation (2.3.2)  | $s^{-1}m^{-2}$   |
| A            | Frequency factor  | —                |
| $A_1$        | Frequency factor  | —                |
| A            | Debye-Hückel constant   | —                |
| $A_c$        | Surface area of crystals  | $m^2$            |
| $A_o$        | Surface area of crystals at time $t_o$  | $m^2$            |
| $A_{o1}$     | Crystal surface area when the precipitation starts  | $m^2$            |
| AAD          | Average absolute deviation = $100 \times \frac{\sum_{i=1}^N \left[ \frac{ (\dot{R}_{fo})_{calc} - (\dot{R}_{fo})_{exp i} }{(\dot{R}_{fo})_{exp i}} \right]_i}{N}$ | %                |
| $a'$         | Constants in Equation (5.7.4)   | —                |
| $a_i$        | Activity of component i   | —                |
| B            | Constant in Equation (2.3.1)  | —                |
| b            | Constant in Equation (2.7.8)  | $s^{-1}$         |
| b            | Constant in Equation (1.2.1)  | —                |
| $b'$         | Constants in Equation (5.7.4)   | —                |
| C            | Solute concentration  | $gmol/l, kg/m^3$ |
| $\Delta C$   | Concentration driving force   | $gmol/l, kg/m^3$ |
| $C_A$        | Concentration of component A  | $gmol/l, kg/m^3$ |
| $C_{A_o}$    | Concentration at the start of the experiment  | $gmol/l, kg/m^3$ |
| $C_{A_{o1}}$ | Concentration when the precipitation starts   | $gmol/l, kg/m^3$ |

|              |  |   |
|--------------|--|---|
| $C_{As}$     | Saturation concentration of component A                  | gmol/l , kg/m <sup>3</sup>  |
| $C_b$        | Bulk concentration of foulant                            | gmol/l , kg/m <sup>3</sup>  |
| $C_i$        | Concentration of component i                             | gmol/l , kg/m <sup>3</sup>  |
| $C_{M_aX_b}$ | Concentration of salt $M_aX_b$                           | gmol/l  |
| $C_p$        | Specific heat capacity                                   | kJ/molK   |
| $C_s$        | Solute saturation concentration at the given temperature | gmol/l , kg/m <sup>3</sup>  |
| $C_{sat}$    | Saturation concentration                                 | gmol/l , kg/m <sup>3</sup>  |
| $C_w$        | Concentration of foulant at wall                         | gmol/l , kg/m <sup>3</sup>  |
| $C_1$        | Constant in Equation (5.1.6)                             | (m <sup>-1</sup> K <sup>-2</sup> s <sup>-1</sup> ) <sup>1/3</sup> |
| $C_2$        | Constant in Equation (5.1.8)                             | (m <sup>-1</sup> K <sup>-2</sup> s <sup>2</sup> ) <sup>1/3</sup>  |
| $D$          | Diffusivity  | m <sup>2</sup> /s   |
| $D$          | Tube diameter  | m   |
| $D_o$        | Constant in Equation (5.1.3)                             | (kg·m/Ks <sup>2</sup> )   |
| $D_i$        | Inner deposit diameter                                   | m   |
| $D_t$        | Inside tube diameter                                     | m   |
| $d$          | Tube diameter  | m   |
| $d_i$        | Inside tube diameter                                     | m   |
| $d_p$        | Equivalent crystal diameter                              | m   |
| $d_p$        | Particle diameter  | m   |
| $E_D$        | Delay time activation energy                             | J/mol   |
| $\Delta E$   | Activation energy  | J/mol   |

|                    |   |                                   |
|--------------------|---|-----------------------------------|
| $\Delta E_f$       | Fouling activation energy                                   | J/mol                             |
| $f$                | Friction factor = $2\tau_w / \rho V^2$                      | –                                 |
| $G$                | Mass flux   | kg/ m <sup>2</sup> . s            |
| $\Delta G_{crit}$  | Critical Gibbs free energy                                  | J/mol                             |
| $\Delta G'_{crit}$ | Critical Gibbs free energy in Equation (2.2.6)              | J/mol                             |
| $h$                | Convection heat transfer coefficient                        | W/m <sup>2</sup> K                |
| $h_1$              | Convection heat transfer coefficient before velocity change | W/m <sup>2</sup> ·K               |
| $h_2$              | Convection heat transfer coefficient after velocity change  | W/m <sup>2</sup> ·K               |
| $I$                | Current   | Amps                              |
| $I$                | Ionic strength of the solution                              | mol/m <sup>3</sup>                |
| $J$                | Nucleation rate   | m <sup>-2</sup> s <sup>-1</sup>   |
| $J$                | Nucleation rate   | m <sup>-3</sup> s <sup>-1</sup>   |
| $j$                | Number of variables in Equation (5.1.9)                     | –                                 |
| $K$                | Parameter in Equation (2.3.3)                               | –                                 |
| $k_1$              | Constant in Equation (2.8.1.10)                             | –                                 |
| $k_2$              | Constant in Equation (2.8.1.14)                             | kg·s <sup>3</sup> /m <sup>6</sup> |
| $k_3$              | Constant in Equation (2.8.1.16)                             | m <sup>4</sup> K/kgW              |
| $k_4$              | Constant in Equation (2.8.1.16)                             | kg·s <sup>3</sup> /m <sup>6</sup> |
| $k_a$              | Chemical attachment coefficient,                            | m <sup>4</sup> /kg. s             |
| $k_B$              | Boltzmann constant  | J/K                               |
| $k_d$              | Reaction rate constant                                      | s <sup>-1</sup>                   |

|                  |   |                                       |
|------------------|---|---------------------------------------|
| $k_l$            | Mass transfer coefficient                                     | $\text{kg/m}^2\text{s}$               |
| $k_m$            | Mass transfer coefficient                                     | $\text{m/s}$                          |
| $k_r$            | Surface reaction rate constant                                | $\text{m}^4/\text{kg}\cdot\text{s}$   |
| $K'_S$           | Ionic solubility product                                      | $(\text{kmol/m}^3)^2$                 |
| $K_{sp}$         | Solubility product  | $(\text{kg/m}^3)^2$                   |
| $K'_{SP}$        | Ionic solubility product                                      | $(\text{kmol/m}^3)^2$                 |
| $k'$             | Constant in equation (2.8.1.11)                               | —                                     |
| $k''$            | Constant in equation (2.8.1.13)                               | $\text{kg}\cdot\text{s}^2/\text{m}^4$ |
| $k_R$            | Reaction coefficient in bulk crystallization surface reaction | $\text{m/mol}\cdot\text{s}$           |
| L                | Length of the heated section                                  | $\text{m}$                            |
| M                | Crystal mass  | $\text{kg}$                           |
| $M_g$            | Crystal mass when crystal growth starts                       | $\text{kg}$                           |
| m                | Mass of crystals at time t                                    | $\text{kg}$                           |
| $m_0$            | Mass of crystals at time $t_0$                                | $\text{kg}$                           |
| $\dot{m}_c$      | Crystallization deposition rate                               | $\text{kg/m}^2\cdot\text{s}$          |
| $\dot{m}_d$      | Deposition rate   | $\text{kg/m}^2\cdot\text{s}$          |
| $m_{\text{dep}}$ | Deposit mass  | $\text{kg}$                           |
| $m_f$            | Deposit coverage  | $\text{g/mm}^2, \text{kg/m}^2$        |
| $\dot{m}_p$      | Particulate fouling rate                                      | $\text{kg/m}^2\cdot\text{s}$          |
| $\dot{m}_r$      | Removal rate  | $\text{kg/m}^2\cdot\text{s}$          |
| N                | Number of nucleation sites                                    | —                                     |

|                |   |  |
|----------------|---|--|
| $N_A$          | Avogadro's number                           | $\text{mol}^{-1}$                                |
| $N_f$          | Number of fault points in the deposit layer | —  |
| $N_s$          | Number of nucleation sites                  | —  |
| $Nu$           | Nusselt number ( $hd/\lambda$ )             | —  |
| $n$            | Surface reaction order                      | —  |
| $n'$           | Constant in Equation (5.6.1)                | —  |
| $P$            | Inter-crystalline adhesion force            | N  |
| $\Delta P$     | Pressure drop across the test section       | kPa  |
| $Pr$           | Prandtl Number ( $\eta C_p/\lambda$ )       | —  |
| $P_1$          | Parameter in Equation (5.1.4)               | $\left(\frac{m^8 K s^5}{kg^4}\right)^{1/3}$      |
| $P_2$          | Parameter in Equation (5.1.4)               | $\left(\frac{kg^5 s^2}{m^{10} K^2}\right)^{1/3}$ |
| $\dot{q}$      | Heat flux                                   | $\text{W}/\text{m}^2$                            |
| $\dot{Q}$      | Heat rate                                   | W  |
| $R$            | Universal gas constant                      | $\text{J}/\text{mol}\cdot\text{K}$               |
| $Re$           | Reynolds number ( $Gd/\eta$ )               | —  |
| $\dot{R}_{fo}$ | Initial fouling rate                        | $\text{m}^2 \cdot \text{K}/\text{J}$             |
| $R_f^*$        | Asymptotic fouling resistance               | $\text{m}^2 \cdot \text{K}/\text{W}$             |
| $R_f$          | Fouling resistance                          | $\text{m}^2 \cdot \text{K}/\text{W}$             |

|             |   |         |
|-------------|---|---------|
| RMS         | Root mean square = $100 \times \sqrt{\frac{\sum_{i=1}^N \left[ \frac{(\dot{R}_{fo})_{\text{exp } i} - (\dot{R}_{fo})_{\text{calc}}}{(\dot{R}_{fo})_{\text{calc}}} \right]^2}{N}}$ | %       |
| r           | Stoichiometric ratio in Equation (2.8.1.8)  | —       |
| $r_A$       | Rate of reaction of component A   | mol/l·s |
| $r_i$       | Inner radius of the tube  | m       |
| $r_c$       | Radius of the nucleated crystallite   | m       |
| $r_p$       | Radius of the particle  | m       |
| S           | Supersaturation ratio   |         |
| Sc          | Schmidt number ( $\eta / \rho D$ )  | —       |
| T           | Temperature   | °C or K |
| $T_b$       | Bulk fluid temperature  | °C or K |
| $T_s$       | Surface temperature   | °C or K |
| $T_{b,in}$  | Bulk fluid inlet temperature  | °C or K |
| $T_{b,out}$ | Bulk fluid outlet temperature   | °C or K |
| $T_f$       | Film temperature  | °C or K |
| $T_{w,c}$   | Tube wall temperature at clean condition  | °C or K |
| $T_w$       | Tube wall temperature   | °C or K |
| $T_{w,i}$   | Inside wall temperature   | °C or K |
| $T_{w,o}$   | Outside wall temperature  | °C or K |
| t           | Time  | s       |

|               |   |                  |
|---------------|---|------------------|
| $U$           | Instantaneous local heat transfer coefficient   | $W/m^2K$         |
| $U_o$         | Clean heat transfer coefficient                 | $W/m^2K$         |
| $U_c$         | Local clean heat transfer coefficient           | $W/m^2K$         |
| $V$           | Voltage   | V                |
| $V$           | Bulk fluid velocity                             | m/s              |
| $v$           | Local fluid velocity                            | m/s              |
| $v_*$         | Friction velocity ( $=V\sqrt{f/2}$ )            | m/s              |
| $v_m$         | Molar volume of the crystalline phase           | $m^3/mol$        |
| $W_{precip.}$ | Rate of precipitation fouling                   | $kg/m^2 \cdot s$ |
| $x$           | Location of the thermocouple                    | mm               |
| $x_f$         | Deposit thickness                               | m, mm            |
| $z$           | Number of ions in a crystallizing salt molecule | —                |
| $z^+, z^-$    | Valencies of the cation and anion               | —                |
| $z_i$         | Valency of component i                          | —                |

### Greek Symbols

|                |                                     |                |
|----------------|-------------------------------------|----------------|
| $\beta$        | Shape factor                        | —              |
| $\gamma$       | Surface energy                      | $J/m^2$        |
| $\gamma_i$     | Activity coefficient of component i | —              |
| $\gamma_{eff}$ | Effective surface energy            | $J/m^2$        |
| $\eta$         | Dynamic viscosity                   | $kg/m \cdot s$ |
| $\theta$       | Fluid residence time                | s              |

---

|                   |                                      |                      |
|-------------------|--------------------------------------|----------------------|
| $\lambda_f$       | Deposit thermal conductivity         | W/m·K                |
| $\nu$             | Kinematic viscosity                  | m <sup>2</sup> /s    |
| $\rho$            | Density                              | kg/m <sup>3</sup>    |
| $\rho_f$          | Deposit density                      | kg/m <sup>3</sup>    |
| $\rho_{f,true}$   | True deposit density                 | kg/m <sup>3</sup>    |
| $\rho_{f,calc'd}$ | Calculated deposit density           | kg/m <sup>3</sup>    |
| $\sigma$          | Relative supersaturation             | —                    |
| $\sigma^2$        | Variance                             | —                    |
| $\tau_D$          | Delay time                           | s                    |
| $\tau_w$          | Wall shear stress                    | kg/m·s <sup>2</sup>  |
| $\phi_{do}$       | Initial mass flux of foulant         | kg/m <sup>2</sup> ·s |
| $\phi$            | Mass flux of foulant                 | kg/m <sup>2</sup> ·s |
| $\phi$            | Parameter in Equation (2.3.4)        | —                    |
| $\Psi$            | Deposit strength in Equation (1.2.1) | —                    |
| $\Omega$          | Constant in Equation (2.4.1)         | s <sup>-1</sup>      |

- Alimi, F., Elfil, H., Gardi, A.**, "Kinetics of the Precipitation of Calcium Sulfate Dihydrate in a Desalination Unit", *Desalination* **157**, (2003), pp. 9-16.
- Amjad, Z.**, "Calcium Sulfate Dihydrate (Gypsum) Scale Formation on Heat Exchanger Surfaces: The Influence of Scale Inhibitors", *Journal of Colloid and Interface Science*, **123**, (1988), pp. 523-536.
- Andritsos, N., Karabelas, A.J.** "The Influence of Particulates on CaCO<sub>3</sub> Scale Formation", *Journal of Heat Transfer* **121**(1), (1999), pp. 225-227.
- Augustin, W.**, "Verkrustung (Fouling) Von Wärmeübertragungsflächen", Ph.D. Thesis, Technical University of Braunschweig, (1992).
- Banchero, J.T., Gorden, K. F.**, "Scale Deposition on a Heated Surface", *Advances In Chemistry Series*, **27**, (1960), pp. 105-114.
- Bansal, B., Augustin, W., Muller-Steinhagen, H., Chen, X. D.**, "Fouling in Parallel and Series Flow Plate Heat Exchangers", *Proceedings of an international conference on Heat Exchanger Fouling: Fundamental Approaches & Technical Solutions*, Muller-Steinhagen, H., Watkinson, A.P., Malayeri, M.R., eds., Publico Publications, Davos, Switzerland, July, 2001a, pp. 81-87.
- Bansal, B., Muller-Steinhagen, H.**, "Crystallization Fouling in Plate Heat Exchangers", *Journal of Heat Transfer*, **115**, (1993), pp. 584-591.
- Bansal, B., Muller-Steinhagen, H., Chen, X. D.**, "Comparison of Crystallization Fouling in Plate and Double-Pipe Heat Exchangers", *Heat Transfer Engineering*, **22**, (2001b), pp. 13-25.
- Bansal, B., Chen, X. D., Mueller-Steinhagen, H.**, "Deposition and Removal mechanisms during Calcium Sulphate Fouling in Heat Exchangers." *International Journal of Transport Phenomena* **7**(1), (2005), pp. 1-22.
- Bansal, B., Muller-Steinhagen, H., Chen, X. D.**, "Effect of Suspended Particles on Crystallization Fouling in Plate Heat Exchangers", *Transactions of the ASME*, **119**, (1997), pp. 568-574.
- Bansal, B., Muller-Steinhagen, H., Chen, X. D.**, "Performance of Plate Heat Exchangers during Calcium Sulfate Fouling-Investigation with an In-line Filter", *Chemical Engineering and Processing*, **39**, (2000), pp. 507-519.
- Barba, D., Brandani, V., Digiacomo, G.**, "A Thermodynamic Model of CaSO<sub>4</sub> Solubility in Multicomponent Aqueous Solutions", *Chemical Engineering Journal*, **24**, (1982), pp. 191-200.

- Bohnet, M., Augustin, W., Hirsch, H.**, "Influence of Fouling Layer Shear Strength on Removal Behaviour", Proceedings of an international conference on Understanding Heat Exchanger Fouling and Its Mitigation, Muller-Steinhagen, H., Watkinson, A.P., Malayeri, M.R., eds., Il Ciocco Conference Centre, Castivecchio Pascoli, Italy, May, (1997), pp. 201-208.
- Bohnet, M.**, "Fouling of Heat-transfer Surfaces", *Chemical Engineering Technology*, **10**, (1987), pp. 113-125.
- Bott, T.R.**, *Fouling of Heat Exchangers*, Published by Elsevier, Amsterdam, The Netherlands (1995).
- Brahim, F., Augustin, W., Bohnet, M.**, "Numerical Simulation of Crystal Growth On Heat Transfer Surfaces", Proceedings of an international conference on Heat Exchanger Fouling: Fundamental Approaches & Technical Solutions, Muller-Steinhagen, H., Watkinson, A.P., Malayeri, M.R., eds., Publico Publications, Davos, Switzerland, July, 2001, pp. 137-144.
- Bramson, D., Hasson, D., Semiat, R.**, "The Roles of Gas Bubbling, Wall Crystallization and Particulate Deposition in CaSO<sub>4</sub> Scale Formation", *Desalination*, **100**, (1995), pp. 1-3.
- Branch, C. A.** "Heat Transfer and Heat Transfer Fouling in Evaporators with Kraft Pulp Black Liquor", Ph.D. thesis, University of Auckland, New Zealand, (1991).
- Branch, C. A.** "Heat Transfer and Heat Transfer Fouling in Kraft Black Liquor Evaporators", *Experimental Thermal and Fluid Science*, **14**, (1997) pp. 425-437.
- Bridgwater, J., Loo, C. E.**, "Removal of Crystalline Scale: Mechanisms and the Role of Thermal Stress", First National Heat Transfer Conference, UK (1984) pp. 455-463
- Brusilovsky, M., Borden, J., Hasson, D.**, "Flux Decline Due to Gypsum Precipitation on RO Membranes", *Desalination*, **86**(2), (1992), pp. 187-222.
- Chong, T. H., Sheikholeslami, R.**, "Thermodynamics and Kinetics for Mixed Calcium Carbonate and Calcium Sulphate Precipitation", *Chem. Eng. Sci.*, **56**, (2001), pp. 539-545.
- Crittenden, B.D., Alderman, N. J.**, "Mechanisms by Which Fouling Can Increase Overall Heat Transfer Coefficients", *Heat Transfer Engineering*, **13**, (1992), pp. 32-41.
- Crittenden, B.D., Hout S. A., Alderman, N.J.**, "Model Experiments of Chemical Reactin Fouling," *Chem. Eng. Res. Des.*, **65**, (1987a), pp. 165-170.
- Crittenden, B.D., Kolaczowski, S.T., Hout S. A.**, "Modeling Hydrocarbon Fouling", *Chem. Eng. Res. Des.*, **65**, (1987b), pp. 171-179.

- Davies, C. W.**, "Ion Association", London: Butterworth's (1962), pp. 34-35.
- Dittus, F.W., Boelter, L. M. K.**, "Publications on Engineering", University of California, Berkely, 2, (1930), pp. 443-451
- Einstein, A.**, Ann. Phys. (Leipzig) 17, 549 (1905). English Translation, Investigations on the Theory of Brownian Movement, Dover, New York, (1956).
- Epstein, N.**, "A Model of the Initial Chemical Reaction Fouling Rates for Flow within a Heated Tube, and its Verification", Heat Transfer 1994, Proceedings of The Tenth International Heat Transfer Conference, Brighton, UK , 4, (1994), pp. 225-229.
- Epstein, N.**, "Thinking about Heat Transfer Fouling: A 5 x 5 Matrix", Heat Transfer Engineering, 4, (1983), pp. 43-56.
- Epstein, N.**, "Towards Mitigation of Fouling by Consideration of Fouling Mechanisms", Proceedings of "Fouling Mitigation of Industrial Heat-Exchange Equipment", an International Conference, Muller-Steinhagen, H., Watkinson, A.P., Malayeri, M.R., eds., San Luis Obispo, Calif., June, 1995, pp. 13-26.
- Fahiminia, F., Watkinson, A. P. and Epstein, N.**, "Investigation of Initial Fouling Rates of Calcium Sulfate Solutions under Non-boiling Conditions (Work-in-progress)", Proc. 2003 ECI Conference on Heat Exchanger Fouling and Cleaning – Fundamental Applications, Muller-Steinhagen, H., Watkinson, A.P., Malayeri, M.R., eds., pp. 32-36, Engineering Conferences Internationals, New York (2003); <http://services.bepress.com/eci/heatexchanger/5>.
- Fand, R. M.**, "The Formation of Calcium-Sulfate Scale on a Heated Cylinder in Crossflow and Its Removal by Acoustically Induced Cavitation", Journal of Heat Transfer, 6, (1969), pp. 111-122.
- Furby, E., Glueckauf, E., McDonald, L.A.** "The Solubility of Calcium Sulfate in Sodium Chloride and Sea Salt Solutions", Desalination (1968), 4(2), pp. 264-76.
- Garside, J.** "Concept of Effectiveness Factors in Crystal Growth", Chemical Engineering Science, 26(9), (1971), pp. 1425-31.
- Gill, M., Sheikholeslami, R.** "A Preliminary Study to Estimate the Combined Effects of Precipitation and Particulate Fouling of CaSO<sub>4</sub>", Chemeca, New Zealand, The Society of Chemical Engineers, NZ, (1997).
- Glater, J.** "Scale Formation and Prevention", Principles of Desalination, Spiegler, K.S. and Larid, A.D.K. eds., Academic Press, London, (1980), pp. 627-678

- Gonionsky, V., TS., Golub, S. I. and Rozen, A. M.**, "Calculation of Heat Transfer Coefficients During Scale Formation", *Heat Transfer-Soviet Research*, **3**, No.3 (1970), pp. 116-121.
- Hasson, D.**, "Precipitation Fouling", *Fouling of Heat Transfer Equipment*, edited by E.F.C. Somerscales and J. G. Knudsen, Hemisphere, New York (1981), pp. 527-568.
- Hasson, D., Drak, A., and Semiat, R.**, "Induction Times Induced in an RO System by Antiscalants Delaying CaSO<sub>4</sub> Precipitation", *Desalination*, **157**, (2003), pp. 193-207.
- Hasson, D., Zahavi, J.**, "Mechanism of Calcium Sulfate Deposition on Heat-Transfer Surfaces", *I&EC Fundamentals*, **9**, (1970), pp. 1-10.
- He, S., Oddo, J.E., Tomson, M.b.**, "The Inhibition of Gypsum and Barite Nucleation in NaCl Brines at Temperatures from 25 to 90°C", *J. Colloid Interface Sci.*, **162**, (1994), pp. 297-303.
- Hewitt, G.F., Shires, G.L., Bott, T.R.**, "Process Heat Transfer", CRC Press, (1994), Ann Arbor, MI., pp. 857-877.
- Incopera, F.P. and Dewitt, D.P.**, "Fundamentals of Heat and Mass Transfer", 3<sup>rd</sup> Edition, (1990).
- Kazi, M. S. N., Muller-Steinhagen, H., Duffy, G. G., Chen, X. D.**, "Fibre-Modified Scaling Mechanisms in Heat Transfer Fouling Mitigation", *Chem. Eng. Comm.*, **189** (2002), pp. 742-758.
- Kazi, S. N., Duffy, G. G., Chen, X. D.**, "A Study of Fouling and Fouling Mitigation on Smooth and Roughened Metal Surfaces, and a Polymeric Material", *Proceedings of an International Conference on Heat Exchanger Fouling: Fundamental Approaches & Technical Solutions*, Muller-Steinhagen, H., Watkinson, A.P., Malayeri, M.R., eds., Publico Publications, Davos, Switzerland, July, (2001), pp. 65-72.
- Kazi, S. N., Duffy, G. G., Chen, X. D., , H.**, "Fibre-Modified Scaling Mechanisms In Heat Transfer Fouling Mitigation", *Proceedings of an international conference on Mitigation of Heat Exchanger Fouling and Its Economic and Environmental Implications* , Banff, Alberta, Canada, July, (1999), pp. 1-8.
- Keller, D. M., Massey, R.E., Hileman, O.E.**, "Kinetics of Calcium Sulphate Precipitation", *Can. J. Chem. Eng.*, **56**, (1978), pp. 831-838.
- Kern, D. Q., Seaton, R. E.**, "A Theoretical Analysis of Thermal Surface Fouling" *British Chemical Engineering*, **4**, (1959), pp. 258-262.

- Klepetsanis, P. G., Dalas, E. Koutsoukos, P. G.** *Langmuir*, **15**, (1999), pp. 1534-1540.
- Knudsen, J. G., McCluer, H. K.**, "Hard-Water Scaling of Finned Tubes at Moderate Temperatures", *Chemical Engineering Progress Symposium Series (Heat Transfer-Chicago)*, **55**, (1959), pp. 1-4.
- Konak, A. R.**, Ph.D. Thesis, The University of Birmingham, (1971).
- Konak, A. R.**, "A New Model for Surface Reaction-Controlled Growth of Crystals from Solution", *Chemical Engineering Science*, **29**, (1974), pp. 1537-1543.
- Krause, S.**, "Fouling of Heat-transfer Surfaces by Crystallization and Sedimentation", *International Chemical Engineering*, **33**, (1993), pp. 355-401.
- Lancia, A., Musmarra, D., Prisciandaro, M.**, "Measuring Induction Period for Calcium Sulfate Dihydrate Precipitation", *AIChE Journal*, **45**(2), (1999), pp. 390-397.
- Langelier, W.F., Caldwell, D.H., Lawrence, W.B.**, "Scale Control in Sea-Water Distillation Equipment", *Ind. Eng. Chem.*, **42**, (1950), pp. 126-132
- Li, X., Liu, L., Wang, H.**, "Investigation of Mixed Fouling Growth Progress—Microbial and CaCO<sub>3</sub> Fouling in Water Systems", *Proceedings of an International Conference on Heat Exchanger Fouling: Fundamental Approaches & Technical Solutions*, Muller-Steinhagen, H., Watkinson, A.P., Malayeri, M.R., eds., Publico Publications, Davos, Switzerland, July, 2001.
- Linnikov, Oleg D.**, "Investigation of the Initial Period of Sulphate Scale Formation part 1. Kinetics and Mechanism of Calcium Sulphate Surface Nucleation at its Crystallization on a Heat-exchange Surface", *Desalination*, **122**, (1999), pp. 1-14.
- Liu, S. T.; Nancollas, G. H.** "Kinetic and Morphological Study of the Seeded Growth of Calcium Sulfate Dihydrate in the Presence of Additives", *Journal of Colloid and Interface Science*, **52**(3), (1975), pp. 593-601.
- Liu, S. T.; Nancollas, G. H.** "The Kinetics of Crystal Growth of Calcium Sulphate Dihydrate", *Journal of Crystal Growth*, **6**, (1970), pp. 281-289.
- Loo, C.**, "Deposition and Removal of Calcium Sulphate and Calcium Carbonate Scales", Ph.D. Thesis, Department of Engineering Science, Oxford University, Uk (1979).
- Lu, C. H. and Fabuss, B. M.**, "CaSO<sub>4</sub> Scaling in Saline Water Distillation" *Ind. Eng. Chem. Des. and Develop.* **7**(2), (1968), pp. 206-214.
- McAdams, W. H.**, "Heat Transmission," 3rd edition, McGraw-Hill, New York, pp. 109-122 (1954).

- McCartney, E. R., Alexander, A. E.**, "The Effect of Additives on the Process of Crystallization. I. Crystallization of Calcium Sulfate", *Journal of Colloid Science*, **13**, (1958), pp. 383-396.
- Meek, R. L.**, "Mean Period of Fluctuations Near the Wall in Turbulent Flows", *AIChE J.*, **18**, (1972) pp. 854-855.
- Metzner, A. B.; Friend, W. L.**, "Theoretical Analogies between Heat, Mass, and Momentum Transfer, and Modifications for Fluids of High Prandtl or Schmidt Numbers". *Canadian Journal of Chemical Engineering*, **36**, (1958), pp. 235-240.
- Middis, J. , Muller-Steinhagen, H., Paul, S. T. , Duffy, G. G. ,** "Reduction of Heat Transfer Fouling by the Addition of Wood Pulp Fibers", *Heat Transfer Engineering*, **19**, (1998), pp. 36-44.
- Middis, J. , Muller-Steinhagen, H., Paul, S. T. , Duffy, G. G. ,** "Reduction of Heat Transfer Fouling by the Addition of Wood Pulp Fibers", *Heat Transfer Engineering*, **19**, (1994), pp. 36-44.
- Mori, H., Nakamura, M., Toyama, S.**, "Crystallization Fouling of Calcium Sulfate Dihydrate on Heat- Transfer Surfaces", *Journal of Chemical Engineering of Japan*, **29**, (1996), pp.166-173.
- Muller-Steinhagen, H.**, "Fouling: The Ultimate Challenge for Heat Exchanger Design", *Proceedings of the Sixth International Symposium on Transport Phenomena in Thermal Engineering*, Seoul, Korea, (1993), pp. 811-823.
- Muller-Steinhagen, H., Lamb, J., Jamialahmadi, M.**, "CaSO<sub>4</sub> Scale Formation on Surfaces During Boiling", *Proceedings of an international conference on Fouling Mitigation of Industrial Heat-Exchange Equipment* Muller-Steinhagen, H., Watkinson, A.P., Malayeri, M.R., eds., San Luis Obispo, California, USA, June, (1995), pp. 265-274.
- Mullin, J. W.**, *Crystallization*, 4<sup>th</sup> ed., Butterworth-Heinemann., Oxford, (2001).
- Mullin, J.W., Garside, J.**, "The Crystallization of Aluminium Potassium Sulphate: A Study in the Assessment of Crystallizer Design Data", *Trans. Instn Chem. Engrs*, **45**, (1967), pp. 285-90.
- Mwaba, M. G., Rindt, C. C. M., Vorstman, M. A. G., Van Steenhoven, A. A.**, "Calcium Sulfate Deposition and Removal Characteristics on a Heated Plate", *Proceedings of an Engineering Foundation Conference on Heat Exchanger Fouling: Fundamental Approaches & Technical Solutions*, Muller-Steinhagen, H., Watkinson, A.P., Malayeri, M.R., eds., Davos, Switzerland, July, 2001, pp. 57-63.

- Nancollas, G. H.**, "The Nucleation and Growth of Scale Crystals", in: Bryers, R.W. ed. *Fouling of Heat Exchanger Surfaces*. United Engineering Trustees Inc. New York, (1983).
- Nancollas, G. H.**, "Interactions in Electrolyte Solutions", Amsterdam: Elsevier, (1966), pp. 85-95.
- Nancollas, G. H.**, "Kinetics of Crystal Growth from Solution", *Journal of Crystal Growth*, **3-4**, (1968), pp. 335-339.
- Najibi, S. H., Muller-Steinhagen, H., Jamialahmadi, M.**, "Calcium Sulphate Scale Formation During Subcooled Flow Boiling", *Chemical Engineering Science*, **52**, (1997), pp. 1265-1283.
- O'Rourke, J.D., Johnson, R.A.**, "Kinetics and Mechanism in Formation of Slightly Soluble Ionic Precipitates", *Analytical Chemistry*, **27**, (1955), pp. 1699-1704.
- Ostroff, A. G.**, "Conversion of Gypsum to Anhydrite in Aqueous Salt Solutions", *Cosmochimica Acta*, **28(9)**, (1964), pp. 1363-72.
- Partridge, E.P., White, A. H.**, "Zeolite Water Treatment in a Large Central Heating Plant", *J. Am. Chem. Soc.* **51**, (1929), pp. 360-70.
- Petukhov, B. S.**, "Advances in Heat Transfer", Irvine, T. F. and Hartnett, J. P. Eds., Academic Press, New York, (1970).
- Randolph, A. D., Larson, M. A.**, "Analog Simulation of Dynamic Behavior in a Mixed Crystal Suspension", *Chemical Engineering Progress, Symposium Series*, **61(55)**, (1965), pp. 147-54.
- Ritter, R. B.**, "Crystalline Fouling Studies", *Transactions of the ASME*, **105**, (1983), pp. 374-379.
- Rose, I. C.**, "Model Investigation of Initial Fouling Rates of Protein Solutions In Heat Transfer Equipment", Ph.D. Thesis, The University of British Columbia, (1999).
- Rose, I. C., Watkinson, A.P., Epstein, N.**, "Testing a Mathematical Model for Initial Chemical Reaction Fouling using a Dilute Protein Solution", *Canadian Journal of Chemical Engineering* **78**, (2000), 5-11.
- Schierholtz, O. J.**, "The Crystallization of Calcium Sulfate Dihydrate", *Canadian Journal of Chemistry*, **36**, (1958), pp. 1057-1063.
- Sheikholeslami, R., Ong, H. W. K.**, "Kinetics and Thermodynamics of Calcium Carbonate and Calcium Sulphate at Salinities up to 1.5 M", *Desalination*, **157**, (2003), pp. 217-234.

- Sheikholeslami, R.**, "Calcium Sulfate Fouling-Precipitation or Particulate: A Proposed Composite Model", *Heat Transfer Engineering*, **21**, (2000), pp. 24-33.
- Smith, B. R., Sweett, F.**, "The Crystallization of Calcium Sulfate Dihydrate", *Journal of Colloid and Interface Science*, **37**(3), (1971), pp. 612-18.
- Sohnel, O, Mullin, J. W.**, "Interpretation of Crystallization Induction Periods", *Journal of Colloid and Interface Science* **123**, (1988), pp. 43-50.
- Taborek, J., Aoki, R. B., Ritter, R. B., Palen, J. W., Knudsen, J. G.**, "Fouling: The Unresolved Problem in Heat Transfer", *Chemical Engineering Progress*, **68**, (1972), pp. 59-67.
- TEMA, Standards of the Tubular Exchanger Manufacturers Association, 6<sup>th</sup> ed., (1978).
- Treybal, R.**, "Mass Transfer Operations", *Chemical Engineering Series*, 3<sup>rd</sup> Edition, McGraw-Hill, Montreal, (1980), pp. 72-75.
- Troup, D. H., Richardson, J. A.**, "Scale Nucleation on a Heat Transfer Surface and Its Prevention", *Chemical Engineering Communication*, **2**, (1978), pp. 167-180.
- Turner, D.I.**, "Calcium Sulphate Crystal Growth", Ph.D. Thesis, University of London, (1965).
- Turner, C. W.; Klimas, S. J.; Frattini, P. L.**, "The Effect of Surface Chemistry on Particulate Fouling Under Flow-Boiling Conditions", *Proceedings of an international conference on Heat Exchanger Fouling: Fundamental Approaches & Technical Solutions*, Muller-Steinhagen, H., Watkinson, A.P., Malayeri, M.R., eds., Publico Publications, Davos, Switzerland, July, 2001, pp. 19-23.
- Yu, H, Sheikholeslami, R. and Doherty, W. O. S.**, "Mechanism, Thermodynamics, and Kinetics of Composite Fouling of Calcium Oxalate and Amorphous Silica in Sugar Mill Evaporators-A Preliminary Study", *Chemical Engineering Science*, **57**, No. 1, (2002), pp. 1969-1978.
- Vasak, F., Bowen, B.D., Chen. C.Y., Kastanek, F., Epstein, N.**, "Fine Particle Deposition in Laminar and Turbulent Flows", *Can. J. Chem. Eng.*, **73**, (1995), pp. 785-792.
- Vasak, F. and Epstein, N.**, "Regression Analysis of a Chemical Reaction Fouling Model", *Can. J. Chem. Eng.*, **74**, (1996), pp. 173-175.
- Vasina, L. G., Boglovsky, A. V., Koldajeva, I. L., Noev, N. V.**, "Water-chemical Regimes of Distillation Plants Operating Beyond the Calcium Sulfate Dihydrate Scale Threshold", *Desalination* **105**(1-2), (1996), pp. 159-163.

**Walton, A.G.**, "The Formation and Properties of Precipitates", Chemical Analysis Monograph Series, Vol. 23. Interscience Publishers, 1967.

**Watkinson, A. P.**, "Particulate Fouling of Sensible Heat Exchangers", Ph.D. Thesis, The University of British Columbia, (1968).

**Wilson, D.I.**, "Model Experiments of Autoxidation Reaction Fouling", Ph.D. Thesis, The University of British Columbia, (1994).

**Wilson, D.I., Watkinson, A. P.**, "A Study of Autoxidation Reaction Fouling Heat Exchangers", Can. J. Chem. Eng., **74**, (1996), pp. 236-246

### 1. Power Calibration

Periodically, power applied to the test section was calibrated. In each calibration, voltage across the test section and current applied to it were measured directly using a clamp meter. The results were compared with the corresponding values on the panel and those on the data logger. A typical calibration result is shown in Table A1.1.

**Table A1.1: Test Section Power Calibration Results**

| Variac | Voltage (V) | Current (A) | Voltage (V) | Current (A) | Power (W)  | Voltage (V) | Current (A) | Power (W) |
|--------|-------------|-------------|-------------|-------------|------------|-------------|-------------|-----------|
| %      | Panel       |             | Clamp Meter |             | From Meter | Computer    |             |           |
| 0      | 0.04        | 0           | 0.0         | 0.5         | 0          | 0.1         | 3           | 0.3       |
| 5      | 0.92        | 0.08        | 0.9         | 12.6        | 12         | 0.9         | 11          | 9.9       |
| 10     | 1.89        | 0.18        | 1.9         | 26.25       | 51         | 1.9         | 24          | 45.6      |
| 15     | 2.95        | 0.28        | 3.0         | 41.8        | 126        | 3           | 40          | 120.0     |
| 20     | 3.92        | 0.38        | 4.0         | 56.1        | 223        | 4           | 54          | 216.0     |
| 25     | 5           | 0.49        | 5.1         | 72.1        | 365        | 5           | 70          | 350.0     |
| 30     | 6.04        | 0.59        | 6.1         | 88.6        | 544        | 6.1         | 86          | 524.6     |
| 35     | 7.03        | 0.69        | 7.1         | 103.3       | 735        | 7.1         | 101         | 717.1     |
| 40     | 8.03        | 0.79        | 8.1         | 118.5       | 962        | 8.1         | 115.5       | 935.6     |
| 45     | 9.07        | 0.9         | 9.2         | 134.4       | 1234       | 9.1         | 132         | 1201.2    |
| 50     | 10.15       | 1.01        | 10.3        | 150.6       | 1548       | 10.2        | 148         | 1509.6    |
| 55     | 11.09       | 1.11        | 11.2        | 165.5       | 1860       | 11.15       | 162.5       | 1811.9    |
| 60     | 12.13       | 1.21        | 12.3        | 180.5       | 2220       | 12.2        | 178         | 2171.6    |
| 65     | 13.23       | 1.32        | 13.4        | 196.3       | 2630       | 13.3        | 193.5       | 2573.6    |
| 70     | 14.17       | 1.41        | 14.4        | 210.2       | 3021       | 14.25       | 207.5       | 2956.9    |
| 75     | 15.2        | 1.51        | 15.4        | 224.6       | 3452       | 15.25       | 221.5       | 3377.9    |
| 80     | 16.25       | 1.61        | 16.4        | 239.2       | 3930       | 16.25       | 236.5       | 3843.1    |
| 85     | 17.41       | 1.72        | 17.6        | 256         | 4513       | 17.5        | 253.5       | 4436.3    |
| 90     | 18.36       | 1.81        | 18.6        | 269.1       | 5008       | 18.45       | 266.5       | 4916.9    |
| 95     | 19.22       | 1.88        | 19.5        | 280.7       | 5462       | 19.35       | 278.5       | 5389.0    |
| 98     | 19.9        | 1.95        | 20.1        | 289.3       | 5824       | 20          | 286.5       | 5730.0    |
| 100    | —           | 1.96        | 20.3        | 292.6       | 5951       | 20.2        | 290         | 5858.0    |

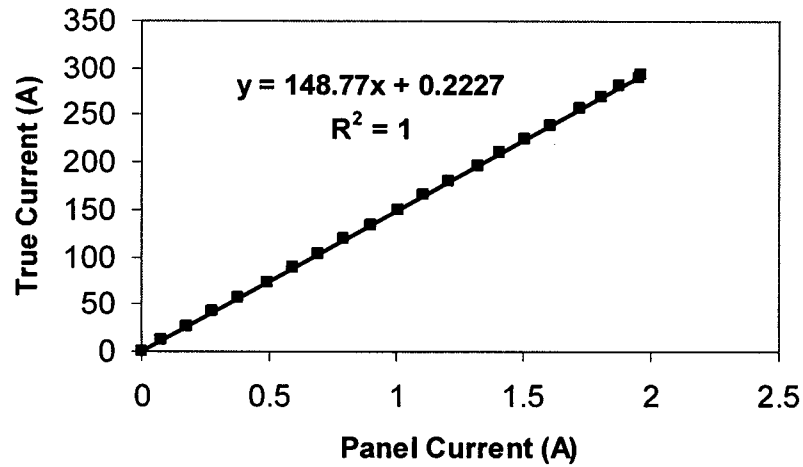


Figure A1.1: True Current Measurement vs. Panel Reading

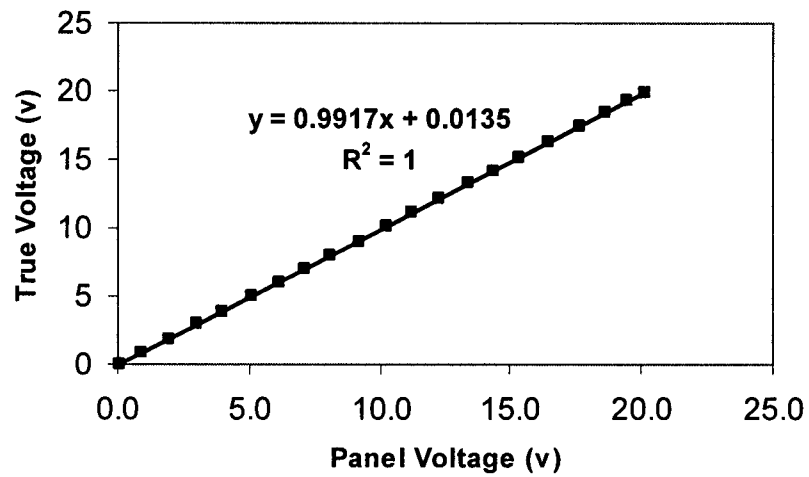


Figure A1.2: True Voltage Measurement vs. Panel Reading

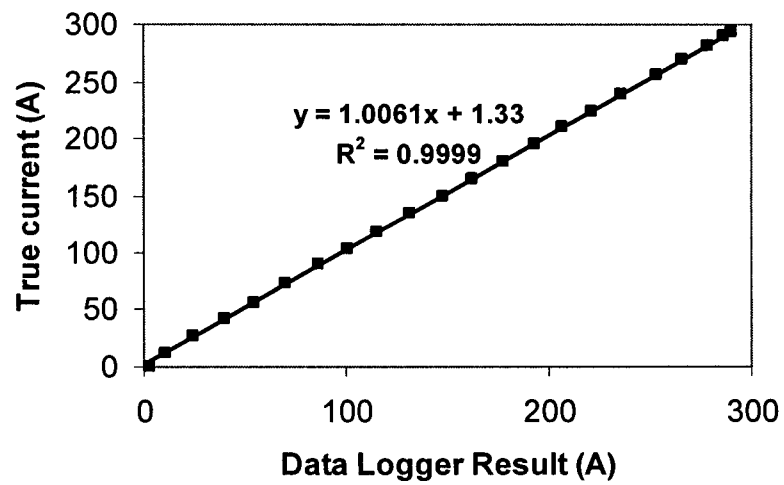


Figure A1.3: True Current Measurement vs. Data Logger Results

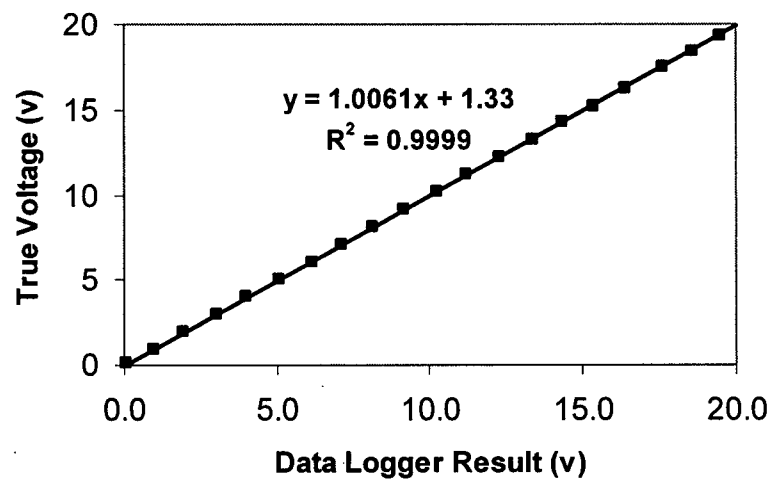


Figure A1.4: True Voltage Measurement vs. Data logger Result

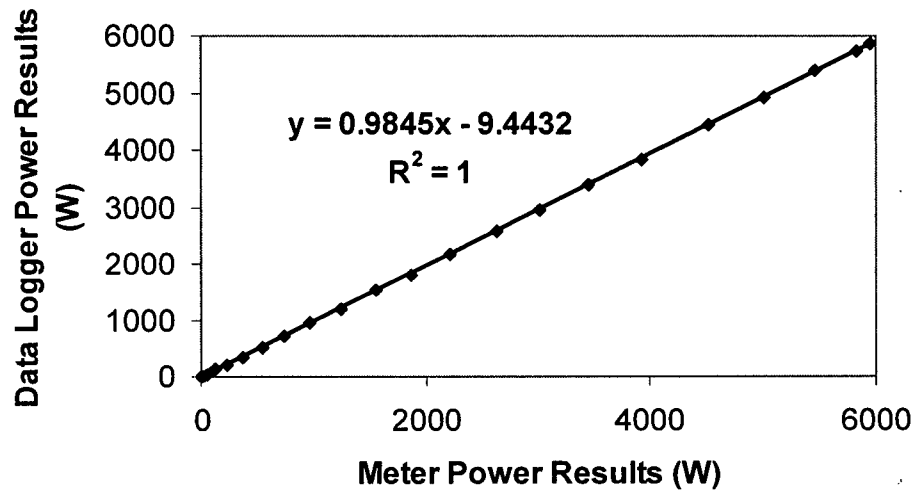


Figure A1.5: True Power Measurement vs. Data logger Result

## 2. Rotameter Calibration

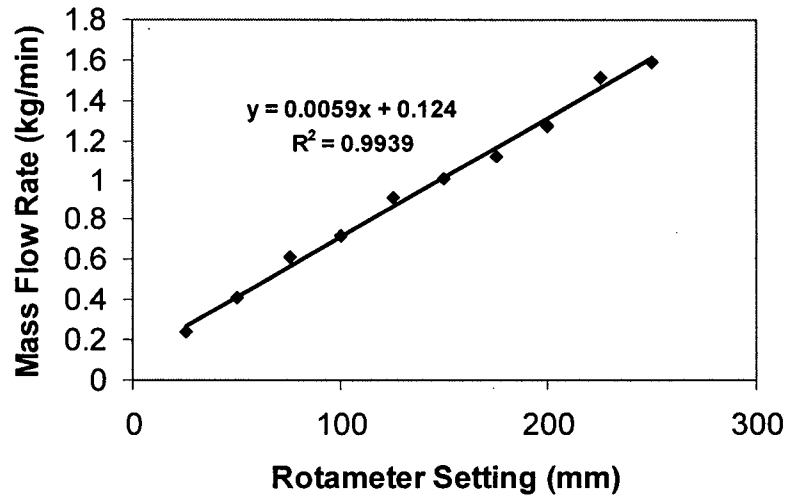


Figure A1.6: Low Flow Rate (LFR) Rotameter Calibration

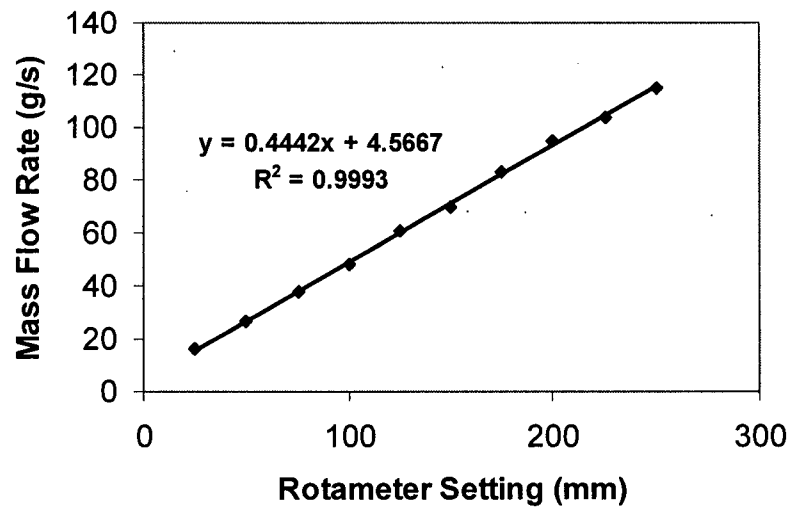


Figure A1.7: Mid Flow Rate (MFR) Rotameter Calibration

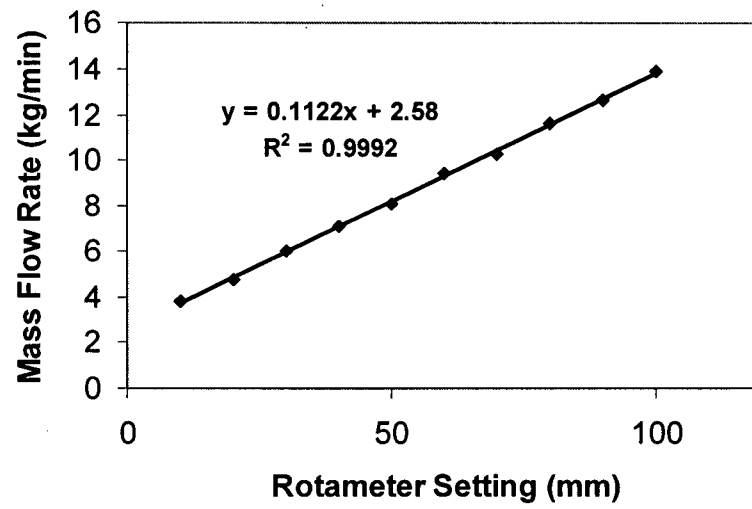
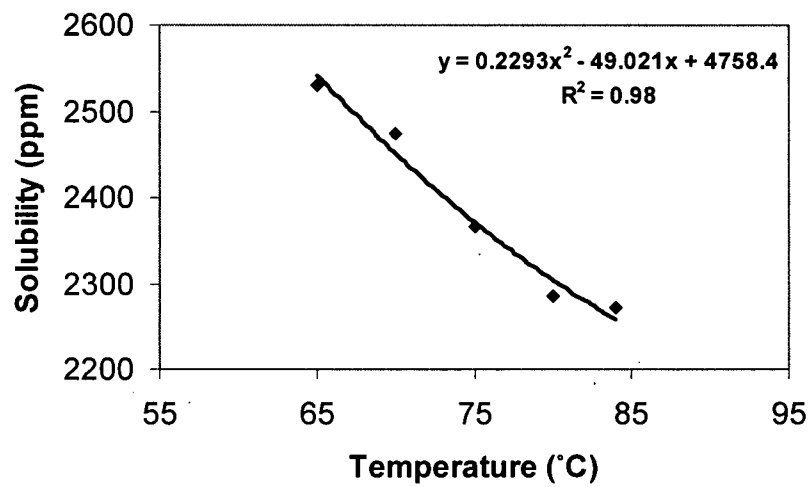
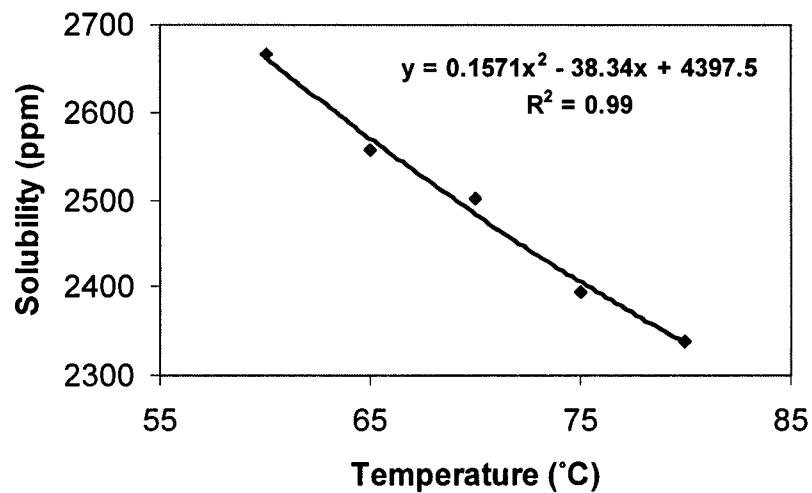


Figure A1.8: High Flow Rate (HFR) Rotameter Calibration

Table A2.1: Calcium Sulphate Solubility at Different Temperatures

| Temperature (°C) | Solubility (ppm)     |                      |
|------------------|----------------------|----------------------|
|                  | $C_{A_0} = 3100$ ppm | $C_{A_0} = 3400$ ppm |
| 60               | —                    | 2666                 |
| 65               | 2530                 | 2557                 |
| 70               | 2475                 | 2502                 |
| 75               | 2366                 | 2394                 |
| 80               | 2285                 | 2339                 |
| 84               | 2271                 | —                    |

Figure A2.1: Calcium Sulphate Solubility vs. Temperature ( $C_{A_0} = 3100$  ppm)Figure A2.2: Calcium Sulphate Solubility vs. Temperature ( $C_{A_0} = 3400$  ppm)

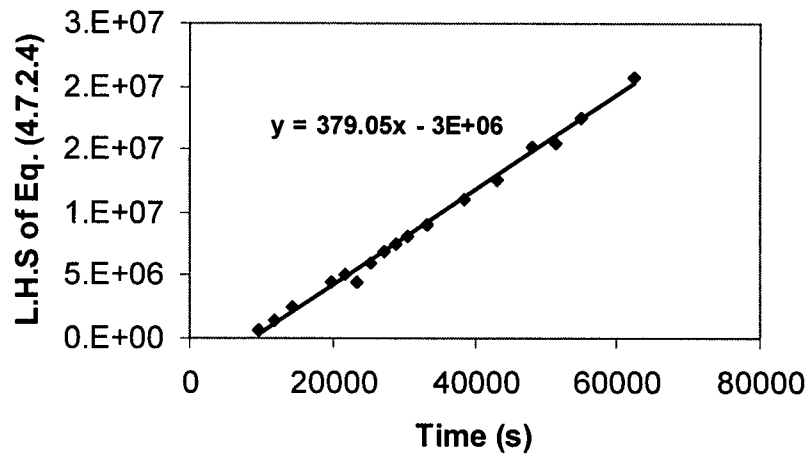


Figure A3.1: Reaction Rate Constant Evaluation Based on the Modified Kinetic Model ( $T_b = 65^\circ\text{C}$ ,  $C_{A0} = 3100$  ppm)

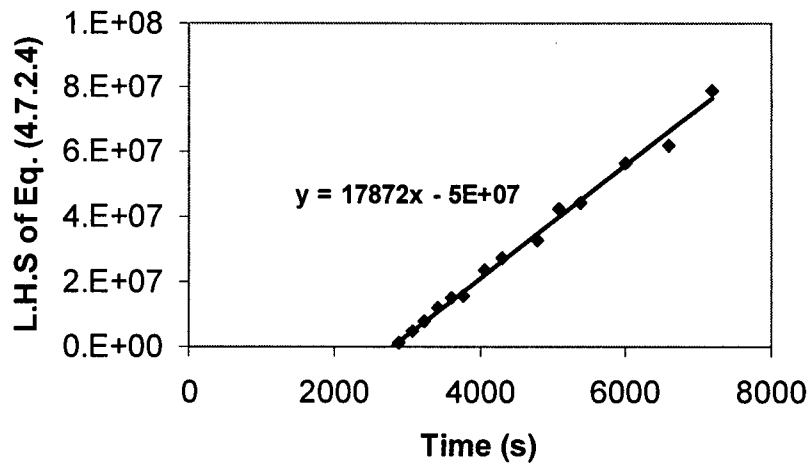


Figure A3.2: Reaction Rate Constant Evaluation Based on the Modified Kinetic Model ( $T_b = 80^\circ\text{C}$ ,  $C_{A0} = 3100$  ppm)

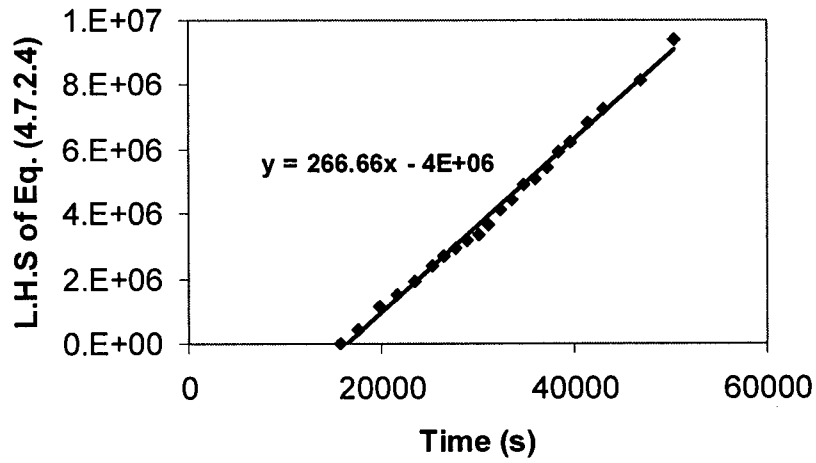


Figure A3.3: Reaction Rate Constant Evaluation Based on the Modified Kinetic Model ( $T_b = 60^\circ\text{C}$ ,  $C_{A0} = 3400$  ppm)

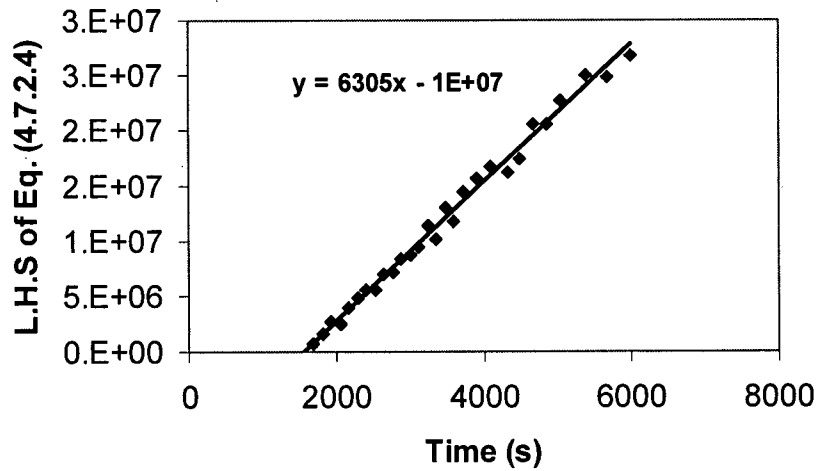


Figure A3.4: Reaction Rate Constant Evaluation Based on the Modified Kinetic Model ( $T_b = 75^\circ\text{C}$ ,  $C_{A0} = 3400$  ppm)

% This program applies Adaptive Simpson Quadrature Technique to integrate  
 % Equation (4.7.2.4), which was developed during kinetic studies. The following data  
 are the %program input, generated during a batch experiment performed under  $T_b = 65^\circ\text{C}$   
 % and  $CA_0 = 3400$  ppm. The first column is the time and the second is the corresponding  
 %concentration. The output is the "L.H.S of Eq. (4.7.2.4)" with the corresponding  
 time. These %data are easily imported to Excel for data manipulation.

```

data = [9900    3377.841
10800    3366.598
12600    3355.355
15600    3310.383
16680    3299.14
18000    3276.654
18900    3242.925
19800    3209.196
20700    3186.71
21600    3119.252
23400    3074.28
25200    3040.551
26580    2995.579
27780    2973.093
28800    2950.607
30000    2916.878
31200    2883.149
32400    2849.42
33600    2838.177
34800    2815.691
36000    2804.448
37200    2781.962
38400    2770.719
39600    2736.99
40800    2725.747
41400    2714.504
42780    2703.261
44040    2692.018];

t = data(:,1);
co= data(:,2);
p = length(t);
F = inline('-(136000^2)./(((153.44-ca/22.159).^(2/3)).*(ca-2556.8).^2)');
for i = 1:p
    myca = co(i);
    intc(i)=quad(F, 3377.841, myca);
    fprintf(' %n %6.4f', intc(i))
end

```

```
%This Matlab program uses Marquardt method to iteratively determine the
% best-fit parameter values in model (Epstein, 1994).

%a0 is the starting guess for the unknown parameters, P1,P2, and activation energy.
a0 is changed several times to obtain acceptable output with given tolerance.
a0 = [1e-15 ,1e-40 ,200000];

%The amount of C1, C2, Twall ,deltaC, and Rf, from Table 5.1.1, already imported
through excel
%file

data=[C1;C2;Twall;deltaC];

%Rf is the objective value the function , which usually in documents is
%referred as y(data).

zdata=Rf;

%Opts is a set of options for the function lsqcurvefit

opts = optimset('lsqcurvefit');

%Display the iteration, and then Change objective, and x Tolerance in each
%run.

opts.Display = 'iter';
opts.TolFun = 1e-0025;
opts.MaxFunEvals = 500;
opts.TolX = 1e-25;
opts.LevenbergMarquardt= 'on';
opts.MaxIter = 1000;

% Now the program returns matrix of variables and residual norms.

[a, resnorm] = lsqcurvefit(@mynewfun, a0, data, zdata, [], [], opts)
```

```
%This function m-file is part of the program for nonlinear curve fitting
```

```
function F = mynewfun(P, data)
```

```
%Reading data, Which already has been imported from excel
```

```
c1=data(1, :);
```

```
c2=data(2, :);
```

```
Tw=data(3, :);
```

```
dc=data(4, :);
```

```
%R is Universal Constant
```

```
R= 8.314;
```

```
%For simplicity the main function is broken to smaller functions.
```

```
F1 = 0.25 * (P(2)* c2 .* exp(P(3)./(R * (273.15+ Tw))))).^2;
```

```
F2 = P(2) * c2 .* exp(P(3)./(R * (273.15+ Tw))) .* dc;
```

```
F = P(1)*c1.*(dc + 0.5*P(2).*c2.*  
exp(P(3)./(R*(273.15+Tw)))-((F1+F2).^0.5));
```

**Appendix 6: Solution Physical Properties**

**Table A6: Solution Physical Properties Measurement for Different Concentrations**

| Pure water                  |       |       |       |       |       |       |       |       |       |       |       |       |
|-----------------------------|-------|-------|-------|-------|-------|-------|-------|-------|-------|-------|-------|-------|
| T(°C)                       | 25    | 30    | 35    | 40    | 45    | 50    | 55    | 60    | 65    | 70    | 75    | 80    |
| $\nu$ (cSt)                 | 0.857 | 0.786 | 0.711 | 0.652 | 0.599 | 0.552 | 0.510 | 0.474 | 0.439 | 0.414 | 0.387 | 0.363 |
| $\rho$ (g/cm <sup>3</sup> ) | 0.993 | 0.992 | 0.990 | 0.989 | 0.987 | 0.984 | 0.982 | 0.979 | 0.977 | 0.974 | 0.970 | 0.966 |
| $\eta$ (cp)                 | 0.851 | 0.780 | 0.704 | 0.644 | 0.591 | 0.543 | 0.501 | 0.464 | 0.429 | 0.404 | 0.376 | 0.351 |
| C = 2100 ppm                |       |       |       |       |       |       |       |       |       |       |       |       |
| T(°C)                       | 25    | 30    | 35    | 40    | 45    | 50    | 55    | 60    | 65    | 70    | 75    | 80    |
| $\nu$ (cSt)                 | 0.872 | 0.800 | 0.714 | 0.655 | 0.600 | 0.553 | 0.513 | 0.477 | 0.442 | 0.416 | 0.390 | 0.367 |
| $\rho$ (g/cm <sup>3</sup> ) | 0.997 | 0.996 | 0.994 | 0.992 | 0.990 | 0.988 | 0.986 | 0.983 | 0.980 | 0.978 | 0.974 | 0.971 |
| $\eta$ (cp)                 | 0.869 | 0.797 | 0.710 | 0.650 | 0.594 | 0.547 | 0.505 | 0.468 | 0.433 | 0.407 | 0.380 | 0.356 |
| C = 3400 ppm                |       |       |       |       |       |       |       |       |       |       |       |       |
| T(°C)                       | 25    | 30    | 35    | 40    | 45    | 50    | 55    | 60    | 65    | 70    | 75    | 80    |
| $\nu$ (cSt)                 | 0.875 | 0.802 | 0.717 | 0.659 | 0.604 | 0.554 | 0.515 | 0.478 | 0.444 | 0.418 | 0.392 | 0.368 |
| $\rho$ (g/cm <sup>3</sup> ) | 0.998 | 0.997 | 0.995 | 0.994 | 0.992 | 0.989 | 0.987 | 0.985 | 0.981 | 0.979 | 0.976 | 0.972 |
| $\eta$ (cp)                 | 0.874 | 0.800 | 0.714 | 0.655 | 0.599 | 0.548 | 0.508 | 0.471 | 0.436 | 0.409 | 0.383 | 0.358 |